SOLID PROPELLANT SUBSCALE BURNING RATE ANALYSIS METHODS FOR U.S. AND SELECTED NATO FACILITIES

R. S. Fry

CHEMICAL PROPULSION INFORMATION AGENCY

• THE JOHNS HOPKINS UNIVERSITY •

• WHITING SCHOOL OF ENGINEERING • COLUMBIA, MARYLAND 21044-3204 •

REPORT DOCUMENTATION PAGE

Form Approved
OMB No. 0704-0188

1. AGENCY USE ONLY *(Leave Blank)*	2. REPORT DATE January 2002	3. REPORT TYPE AND DATES COVERED Technical Report, Oct 1997-Mar 2001

4. TITLE AND SUBTITLE Solid Propellant Subscale Burning Rate Analysis Methods for U.S. and Selected NATO Facilities	5. FUNDING NUMBERS C:SP0700-97-D-4004

6. AUTHOR(S)

Fry, Ronald S.

7. PERFORMING ORGANIZATION NAME(S) AND ADDRESS(ES) The Johns Hopkins University Chemical Propulsion Information Agency 10630 Little Patuxent Parkway, Suite 202 Columbia, MD 21044-3204	8. PERFORMING ORGANIZATION REPORT NUMBER CPTR 75

9. SPONSORING/MONITORING AGENCY NAME (S) AND ADDRESS(ES) DTIC - AI Naval Air Warfare Center Weapons Division 8725 John J. Kingman Road Code 477000D Suite 0944 China Lake, CA 93555-6100 Ft. Belvoir, VA 22060-6218	10. SPONSORING/MONITORING AGENCY REPORT NUMBER

11. SUPPLEMENTARY NOTES

Hardcopies available from CPIA only.

12a. DISTRIBUTION/AVAILABILITY STATEMENT Approved For public release; distribution is unlimited	12b. DISTRIBUTION CODE

ABSTRACT (Maximum 200 words)

Current methods used within the NATO community for analyzing small motor burning rate test data are reviewed and recommendations are made to support improved prediction of internal ballistics of a full-scale solid propellant motor.

The NATO Research and Technology Organization (RTO), Advanced Vehicle Technology (AVT), Working Group (WG) 016 (formerly AGARD/PEP Working Group #27) undertook to evaluate methods used within the NATO propulsion community to measure burning rate in solid propellant rocket systems, with the purpose of identifying similarities and differences between the member nations. This WG was formed in 1996, consisting of representatives from 6 of the 15 member nations of NATO, with inputs accepted from 4 other member nations and a couple non-member nations. The NATO RTO/AVT WG 016 sought to contribute to improvements in the burning rate tools to address issues that have plagued the solid propulsion industry for over 40 years:

(1) Better understanding of burning rate data from various facilities to ease the comparison of propellants from various manufacturers and to improve international exchanges and cooperation.

(2) Better accuracy and reliability of measurements allowing a decrease in the number of tests (and associated time and cost) and an improved control of manufacturing and aging.

Simulated and real subscale rocket motor data were used to evaluate the two fundamentally different families of burning rate analysis methods. While organizational preferences generally dictate method usage, surveys indicate a trend toward methods that more effectively account for non-ideal tailoff, favoring improved accuracy. Consistency in these definitions would promote ease in correlating data internationally. Further development of the Hessler-Glick method shows promise. The NATO propulsion community is urged to review these findings as a means of advancing their own burning rate measurement and analysis methods.

13. SUBJECT TERMS				14. NUMBER OF PAGES
Burning rate	Firing tests (motor)	Qualitative analysis	Solid rocket propellants	266
Combustion	Instrumentation	Quantitative analysis	Test methods	
Combustion chambers	Measurement	Rocket motor	CPIA collection	16. PRICE CODE
Composite propellants	Parametric analysis	Solid propellants		

17. SECURITY CLASSIFICATION OF REPORT UNCLASSIFIED	18. SECURITY CLASSIFICATION OF THIS PAGE UNCLASSIFIED	19. SECURITY CLASSIFICATION OF ABSTRACT UNCLASSIFIED	20. LIMITATION OF ABSTRACT UA

The Chemical Propulsion Information Agency (CPIA) is a DoD Information Analysis Center operated by The Johns Hopkins University, Whiting School of Engineering, under Defense Supply Center Columbus (DSCC) contract SPO700-97-D-4004. The applicable DoD Instruction is 3200.12-R-2, "Centers for Analysis of Scientific and Technical Information." The CPIA's mailing address is The Johns Hopkins University, Chemical Propulsion Information Agency, Attn: Security Office, 10630 Little Patuxent Parkway, Suite 202, Columbia, Maryland, 21044-3204. The CPIA also provides technical and administrative support to the Joint Army-Navy-NASA-Air Force (JANNAF) Interagency Propulsion Committee.

The Government Administrative Manager for CPIA is the Defense Technical Information Center (DTIC), Code DTIC-AI, 8725 John J. Kingman Road, Suite 0944, Ft. Belvoir, VA 22060-6218. The Government Technical Manager (Contracting Officer's Technical Representative) is Mr. Stuart Blashill, Naval Air Warfare Center Weapons Division, Code 477000D, China Lake, CA 93555-6100.

PREFACE

This issue of the Chemical Propulsion Technology reviews (CPTR 75) continues CPIA's recurrent series of technical summaries and status reports on topics pertaining to missile, space, and gun propulsion technology. The general aim is to collect, analyze, and discuss technology advancements in a language understood by a broad range of propulsion technologists.

The results reported upon here are a part of the overall technical approach of:
(1) Surveying the NATO solid propulsion community for subscale and non-intrusive test methods, analysis, and scaling methods, and
(2) Analyzing "simulated" and "real" motor pressure-time data using multiple thickness/time and mass conservation burning rate analysis methods taken from the survey.

This CPTR reviews recommendations on current burning rate measurement methods used for analyzing small motor test data to allow accurate prediction of internal ballistics of a full-scale solid propellant motor. Findings and recommendations on performance scaling, and test techniques and subscale test hardware are reported in companion Chemical Propulsion Technology Reviews. JHU/CPIA CPTR 73, "Solid Propellant Test Motor Scaling," September 2001, reviews recommendations on current burning rate measurement test techniques and subscale test hardware for accurate scaling and prediction of internal ballistics of a full-scale solid propellant motor. Detailed recommendations on current burning rate measurement test techniques and subscale test hardware for accurate prediction of internal ballistics of a full-scale solid propellant motor are reported in JHU/CPIA CPTR 74, "Solid Propellant Subscale Burning Rate · Test Techniques and Hardware for U.S. and Selected NATO Facilities," July 2001. Recommendations on non-intrusive burning rate measurement methods are to be reported in a companion Chemical Propulsion Technology Review to be released at a future date. A complete report of the NATO RTO AVT WG 016 activities is available. The metric system of units is employed in this report except where industry convention dictates otherwise.

The author wishes to express his appreciation to Professor L.T. De Luca, Dipartimento di Energetica, Politecnico di Milan, Italy and Dr. Guy M.H.J.L. Gadiot, TNO Prins Marurits Laboratory, The Netherlands for their contributions to portions of this document.

CPIA solicits comments on the CPTR effort, including suggestions on topics for future issues. For technical comments or suggestions contact Mr. Tom Moore, CPIA Technical Services Supervisor, at 410-992-9951, ext 207, or the author Mr. Ronald Fry, CPIA Senior Research Engineer, at 410-992-9951, ext. 206. Individuals employed by organizations that subscribe to CPIA services may request personal copies of this document by contacting CPIA at 410-992-7300, cpia@jhu.edu, or http://www.cpia.jhu.edu.

ABSTRACT

Current methods used within the NATO community for analyzing small motor burning rate test data are reviewed and recommendations are made to support improved prediction of internal ballistics of a full-scale solid propellant motor.

The NATO Research and Technology Organization (RTO), Advanced Vehicle Technology (AVT), Working Group (WG) 016 (formerly AGARD/PEP Working Group #27) undertook to evaluate methods used within the NATO propulsion community to measure burning rate in solid propellant rocket systems, with the purpose of identifying similarities and differences between the member nations. This WG was formed in 1996, consisting of representatives from 6 of the 15 member nations of NATO, with inputs accepted from 4 other member nations and a couple non-member nations. The NATO RTO/AVT WG 016 sought to contribute to improvements in the burning rate tools to address issues that have plagued the solid propulsion industry for over 40 years:

(1) Better understanding of burning rate data from various facilities to ease the comparison of propellants from various manufacturers and to improve international exchanges and cooperation.

(2) Better accuracy and reliability of measurements allowing a decrease in the number of tests (and associated time and cost) and an improved control of manufacturing and aging.

Simulated and real subscale rocket motor data were used to evaluate the two fundamentally different families of burning rate analysis methods. While organizational preferences generally dictate method usage, surveys indicate a trend toward methods that more effectively account for non-ideal tailoff, favoring improved accuracy. Consistency in these definitions would promote ease in correlating data internationally. Further development of the Hessler-Glick method shows promise. The NATO propulsion community is urged to review these findings as a means of advancing their own burning rate measurement and analysis methods.

CONTENTS

NOMENCLATURE

a	pressure coefficient of ballistic steady burning rate, nondimemsional
A_b	area of the burning surface, cm^2
A_p	area of the grain port cross-section, cm^2
A_t	area of the nozzle throat, cm^2
CCP	circular center perforated grain
EB	end burner grain
g_0	standard acceleration gravity at sea level, 9.807 m/s^2
K	ratio of burning surface area A_b to nozzle throat area A_t, nondim.
L^*	ratio of the combustor cavity volume to nozzle throat area, m
m	mass burning rate, g/cm^2s
n	pressure exponent of ballistic steady burning rate, nondimemsional
p	pressure, MPa
p_c	combustion chamber, pressure, MPa
r_b	burning rate, cm/s
r_{MB}	mass balance burning rate, cm/s
r_{TOT}	thickness/time burning rate, cm/s
$\Re$	universal gas constant, 1.987 cal/mole, K
SCP	star center perforated grain
t	time, s
t_b	burning time, s
T	temperature, K
T_0	initial propellant temperature, K
T_c	combustion chamber gas temperature, K
T_{ref}	reference temperature (298 K)
V_c	combustion chamber free volume, cm^3
w_b	web thickness, mm

Greek Symbols

k	burned gas specific heat ratio
M	average molecular mass, g/mole
π_K	temperature sensitivity of steady chamber pressure, K^{-1}
ρ_c	combustion chamber gas density, g/cm^3
ρ_p	propellant density, g/cm^3
σ_p	temperature sensitivity of steady burning rate, K^{-1}

Subscripts

amb	ambient
avg	average
b	burning
c	chamber
max	maximum

Nomenclature unique to each analysis method is provided within Appendix B.

LIST OF FIGURES

LIST OF TABLES

1.0   INTRODUCTION

The rocket motor designer must have a good understanding of the variation of propellant burning rate with both pressure and temperature in order to produce an efficient design and minimize design iterations during development. Our understanding of burning rate analysis methods can be improved by examining practices employed by various facilities and countries engaged in the measurement and analysis of burning rate in solid propellant systems.

1.1   Objectives

This report reviews solid propellant burning rate analysis methods used by over 20 facilities from 7 NATO member countries. This represents a complete survey of all the international facilities involved in burning rate measurement, and is a thorough representation of the fundamental methods used in the solid propulsion community today. The historical basis and fundamental factors influencing these methods are reviewed, including the advantages and disadvantages encountered in their use. Survey results from the participants of a NATO Working Group are presented and discussed. Conclusions are drawn and recommendations are made for future applications.

1.1.1   NATO/RTO AVT Working Group Formation

The NATO Research and Technology Organization (RTO), Advanced Vehicle Technology (AVT), Working Group (WG) 016 (formerly AGARD/PEP Working Group #27) undertook to evaluate methods used within the NATO propulsion community to measure burning rate in solid propellant rocket systems. This report summarizes the objectives, approach, findings, and recommendations relative to test techniques and hardware used by the surveyed countries and facilities. A complete report of the NATO RTO AVT WG 016 activities is available[1], The WG was formed in 1996, consisting of representatives from 6 of the 15 member nations of NATO, with inputs accepted from 4 other member nations and a couple non-member nations. The WG conducted its activity from October 1997 to March 2001. The justification and relevance of this task to the Solid Rocket Industry includes the importance of solid propulsion to tactical and strategic rockets, missiles and space launch systems; the influence solid propellant burning rate has on performance; and the influence burning rate testing has on program costs.[2,3]

1.1.2   Justification for Studying Solid Propellant Burning Rate

Solid Rocket propulsion remains the major propulsion concept for the tactical and strategic missiles, and for many first stage launch systems. Among the parameters controlling the solid rocket motor operation, burning rate plays a very important role. The burning rate determines, with the burning area, the combustion processes, the mass flow rate, and therefore directly controls the pressure and thrust of the motor. Burning rate is a characteristic of the propellant that can be measured independently, at least for the more usual combustion regimes.

Accuracy of solid rocket thrust-time prediction has become increasingly more important in solid rocket design. One of the most significant variables in this prediction is the propellant burning rate. Accuracy of this value depends on empirical methods for calculating burning rate from subscale motor tests and for correlating this rate with predictions derived from full-scale motor tests. Thrust is very sensitive to the reference propellant burning rate. A variation in propellant burning rate of ±1%, for example, will result in a thrust variation of 1.5 – 2%. The methods of determining burning rate must be reliable and correlations dependable to predict thrust to an accuracy of ±3% using the Solid Performance Program (SPP).

Burning rate measurement is an important and significant activity in the solid propellant industry is devoted to, first during the development of a new propellant, then during the manufacturing (quality control), or for the service life (aging). All the countries with a tradition in the development and manufacturing of solid propellants are equipped with facilities for the burning rate measurement. These facilities are being continuously improved to increase the accuracy and reliability of the burning rate data.

The NATO RTO AVT WG 016 sought to contribute to improvements in the burning rate tools to provide:

- Better understanding of burning rate, $r_b(p,T_o)$, data from various facilities to ease the comparison of propellants from various manufacturers and to improve international exchanges and cooperation.
- Improved measurement accuracy and reliability to allow a decrease in the number of tests (and associated time and cost) and improved control of manufacturing and quality assurance and the assessment of aging.

1.2 Scope of the Working Group Activity

The working group has reviewed and compared methods for measuring steady-state burning rate of solid rocket propellant through current subscale motor practices with an emphasis on data analysis methods and non-intrusive techniques. The overall focus of the working group was approximately 70% small motors, 25% non-intrusive diagnostics and 5% other methods including strand burners. After three years of technical interchange meetings, the AVT WG 016 (formerly AGARD/PEP Working Group #27), whose charter was "Evaluation of Methods for Solid Propellant Burning Rate Measurements" completed its last meeting in Ottawa, Canada on 18-23 October 1999. Six NATO countries were actively participating, with a few others providing technical support. This report is the product of the six AVT WG 016 Meetings conducted between October 1996 and October 1999, supplemented with collaboration by WG members between the meetings and throughout CY2000-2001 during preparation of the final report. Specific objectives of WG 016 relevant to this report are to:

a) Review the small-scale motors used by the various NATO countries and the problems encountered.
b) Compare measurement methods and evaluate the differences
c) Produce an Advisory Report to the NATO community with the following features:
1) Provide information suitable as training for entry-level person and reference for the expert.
2) Collect, analyze and condense information into a language understandable to a wide range of technologists and managers.

1.3 Technical Approach

1.3.1 General Summary

WG activity included analyses, presentations, and discussions in support of completing a final RTO AVT advisory report. Topics addressed in this report include (1) introduction to the problem, justification for the WG and definition of the technical approach, (2) review of burning rate fundamentals, (3) review of basic analysis methods, (4) discussion of survey of methods used in the international community, (5) assessment of methods using simulated motor data, (6) assessment of methods using real motor data, (7) discussion of small motor data quality, and finally (8) summary, conclusions and recommendations.

The basic technical approach used to address the overall and specific objectives cited above has involved

a) Surveying the NATO solid propulsion community for subscale and non-intrusive test methods, analysis, and scaling methods, and
b) Analyzing "simulated" and "real" motor pressure-time data using multiple thickness/time and mass conservation burning rate analysis methods taken from the survey.

Time-consuming survey and analysis support was solicited from a wide range of facilities within the NATO solid propulsion community during the course of this effort. Four separate Analysis Round Robins were conducted with solicitations for support made to NATO propulsion industry contributors. The influence of various burning behaviors was examined in these round robins, such as progressive or regressive burning, constant and random bore offset variations, constant and random L* variations, and different rate equations. Results of the surveys on analysis methods and results of the round robins are reviewed in this report. Trends in observed differences in calculated burning rate for the different analysis methods were evaluated for these cases with a WG goal of making recommendations on preferred analysis methods. Detailed recommendations on solid propellant test motor scaling are reported in JHU/CPIA CPTR 73.[4] Detailed recommendations on current burning rate measurement test techniques

and subscale test hardware for accurate prediction of internal ballistics of a full-scale solid propellant motor are reported in JHU/CPIA CPTR 74.[5] A complete report of the NATO RTO AVT WG 016 activities is available.[1] Recommendations on non-intrusive burning rate measurement methods are to be reported in a companion Chemical Propulsion Technology Review to be released at a future date.

1.3.2 WG 016 as a Catalyst for Change

Analysis Round Robins were used in analyzing "simulated" and "real" motor pressure-time data for the purposes of involving the participants in the data analysis, review and discussion, and conclusion process. The WG considered this critical if either voluntary change was to be expected as an outcome of this study, or if resistance to changed procurement specifications was to be forestalled. One concern was, if the participants were not intimately involved in this process and were only acquainted with the finished comparisons/conclusions, that inertia and conservatism would likely dominate any subsequent actions. Steps to involve the participants in this process take time. Clearly participation and peer review was integral to activities as members of this WG. Peer review of the comparisons and the resulting conclusions was sought outside this WG on a selected basis throughout the period of this effort. Continuing efforts in this regard will be beneficial to understanding the merits of, or for taking further action on any conclusions drawn from this study.

1.4 NATO RTO AVT Working Group 016 Membership and Participants

Dr. P. Kuentzmann of ONERA, France, initiated the WG in 1997 under the former AGARD Propulsion and Energetics Panel (PEP), now the Applied Vehicle Technology (AVT) panel of the Research and Technology Organization (RTO), a Working Group 016 with the charter of "Evaluation of Methods for Solid Propellant Burning Rate Measurements." His early vision as advocate for this effort is appreciated.

The primary AVT Working Group 016 membership included:

Table 1 NATO RTO AVT WG 016 Membership		
Mr. Ronald Fry (Co-Chairman)	JHU/CPIA	U.S.
Dr. Robert Frederick	Univ Alabama in Huntsville	U.S.
Mr. Rene Couturier (Co- Chairman)	SNPE	France
Mr. Dominique Ribereau	SNPE	France
Mr. Jean-Paul Reynard	ONERA	France
Mr. Jean-Claude Traineau	ONERA	France
Dr. Hans-Ludwig Besser	Bayern-Chemie	Germany
Dr. Rudiger Strecker	Bayern-Chemie	Germany
Prof. Luigi DeLuca	Politecnico di Milano	Italy
Dr. Guy M.H.J.L. Gadiot	TNO PML	Netherlands
Mr. Tony Whitehouse	Royal Ordinance	UK

The WG016 members most gratefully acknowledge the significant contributions of Mr. Richard Hessler, independent consultant to the WG016 from the U.S. Additionally, the author the WG members are sincerely grateful to the NATO international propulsion community (facilities and their representatives) for their contributions included in this report. Over 50 contributors participated from over 35 companies, universities and agencies. These contributions included information on test hardware, analysis and scaling methods, and support for multiple analysis round robins of simulated and real motor data. A complete list is provided in Appendix A.

2.0   BURNING RATE FUNDAMENTALS

2.1   Burning Rate Physics and Features

Knowing burning rates of solid propellants, whether steady or unsteady, under a variety of operating conditions is of critical importance both for applications (due to their sensible influence on performances and cost of propulsive devices) and fundamental reasons (understanding of combustion processes). Furthermore, since no available theory/model is capable of predicting burning rates with accuracies within 1% and including the effects of rate modifiers, they must be measured experimentally. However, while experiments measuring steady burning rates are reasonably robust, those measuring unsteady values are fragile and still a matter of research. Since a variety of experimental hardware and procedures are in use today, even for the common steady-state operations, the need arises to understand and perhaps standardize the different approaches developed among the NATO countries.

2.1.1   Burning Rate Physics[6]

2.1.1.1 Background

Energetic materials in general are capable of a dual reacting regime:
- Supersonic regime: a combustion wave preceded by a strong shock wave brings about a detonation wave, propagating at a speed on the order of several km/s and limited by the total thermochemical energy content of the reacting material;
- Subsonic regime: a combustion wave brings about a deflagration wave, propagating at a speed on the order of cm/s and limited by heat and/or mass diffusion.

For a more detailed background, which lies outside the scope of this writing, the interested reader may wish to consult.[7,8,9,10] Here it is enough to remark that deflagration is the common operating mode for the vast majority of engineering applications. Thus, only subsonic combustion waves (or deflagration waves) are considered in this report.

Whether steady or unsteady, deflagration waves in energetic solid materials in general consist of an initial condensed phase and a final phase, and in most cases essentially gaseous reaction products. The interface between the condensed phase and gas phase is called the *burning surface*. The propagation rate of this interface is called *burning rate*; physically, this can also be seen as the regression rate of the condensed phase.

For many studies it is convenient to define, more precisely, a *linear* burning rate (or deflagration rate) as the web thickness burned per unit time in the direction perpendicular to the burning surface.[9]

2.1.1.2 Internal Ballistics

Design and operation of solid rocket motors strongly depend on the combustion features of the propellant charge (burning rate, burning surface, and grain geometry) and their evolution in time. *Internal ballistics* is the applied science devoted to these problems.

4

Burning Rate

In general, burning rates depend on:

- Nature of energetic material (basic ingredients and their mixture ratio);
- Details of chemical composition (catalysts, modifiers, additives, etc. usually present in small or fractional percentages);
- Physical effects (particle size distribution, presence of wires or staples, etc.);
- Details of manufacturing process and other miscellaneous factors (see Sections 2.2 and 3.0);
- Operating conditions (pressure, initial temperature, natural and/or external radiation, heat losses, gas flow parallel to the burning surface, acceleration, etc.);
- Mode of operation (steady vs. unsteady).

This report is primarily concerned with the measurement of steady burn rates, implying a steady set of operating conditions and equilibrium combustion.

For propulsive applications, the influences of pressure (typically, in a range from 1-30 MPa) and initial temperature (typically, in a range from 219-344 K for air-launched missile motors) on burning rate are of paramount importance. Natural radiation is important for heavily metallized compositions (15-20% metal addition), while external radiation still is a matter of laboratory experiments; heat losses are important only under special circumstances. High velocity gas flowing parallel to the burning surface can seriously increase the local burning rate (causing the so-called *erosive burning* phenomenon), due to increased heat transfer from the adjacent turbulent boundary layer, especially in the aft-end portion of the motor cavity. Motor acceleration larger than 10 g_0, whether longitudinal or lateral or due to spinning motion, directed into the burning surface and within an angle of 60 to 90 degrees with respect to it, perceivably increases burning rates. Other peculiar ballistic effects, due to details of manufacturing process, may be important for motor operations but are sensibly dependent on the actual configuration. Detailed comments are discussed in later sections of this report, with further reading in References.[9,11,12]

Notwithstanding impressive progress, combustion theory is not yet capable of predicting steady or unsteady rates with sufficient accuracy for routine use in motor predictions. Thus, propulsion designers and engineers require experimental measurements.

Burning Surface

The burning surface of solid energetic materials regresses in a direction essentially perpendicular to itself. In other words, solid propellants are considered to burn by parallel layers and the grain "tends to retain its original configuration until the web has burned through" (Robert's law, 1839); for details.[13,7] Notice that this law, originally proposed for homogeneous compositions, can be extended to the modern heterogeneous compositions if the propellant heterogeneity is limited to a "sufficiently small scale." [7] The actual burning surface and its evolution in time depend on the initial grain geometry and overall combustion processes.

Grain Geometry

The initial grain geometry of a solid propellant strictly depends on the propulsive mission. See Figure 1 [9] for a variety of shapes commonly employed. The following nomenclature is currently used:[9]

- Grain configuration: the designed shape of the initial burning surfaces of a grain in a motor.
- End-burning grain: the propellant grain is a solid cylinder ideally burning, like a cigarette, only in the axial direction.
- Cylindrical grain: a propellant grain in which the internal cross section is constant along the axis regardless of perforation shape.
- Perforation: the central cavity port or flow passage of a propellant grain.
- Inhibitor: a layer or coating of slow- or non-burning material covering parts of the grain's propellant surface to prevent burning.
- Restricted surface: a grain surface restricted from burning by the bonding of an inhibitor layer.
- Sliver: unburned propellant remaining (or lost because ejected through the nozzle) at the time of web burnout.
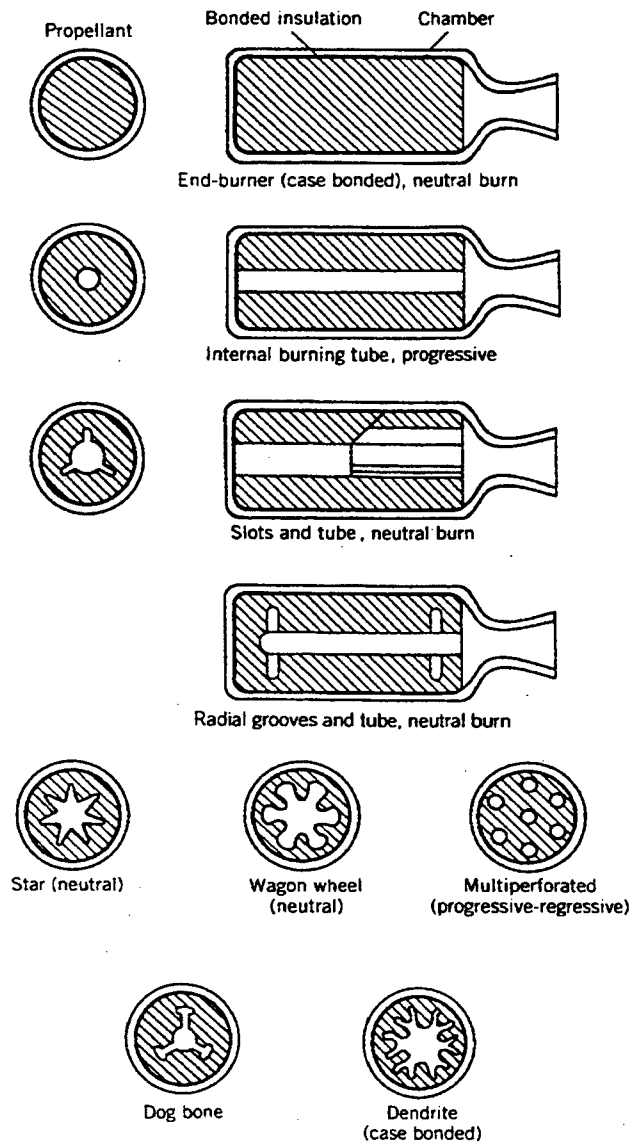
Figure 1. Simplified Diagrams of Several Grain Configurations.[9]

Motor Pressure

Let us assume uniform pressure and burning rate throughout the combustion chamber of a solid propellant rocket motor filled with a perfect gas burned mixture. All properties are considered constant. Transient mass conservation[14] requires

$$m_g = m_d + \frac{d(\rho_c V_c)}{dt} \tag{1}$$

where the mass production of gas due to combustion is

$$m_g = \rho_p A_b r_b$$

the mass flow rate exiting the nozzle is

$$m_d = \frac{p_c A_t}{C_D} = p_c A_t c^*$$

and the mass accumulation rate in the combustion chamber is

$$\frac{d(\rho_c V_c)}{dt} = \rho_c \frac{dV_c}{dt} + V_c \frac{d\rho_c}{dt} = \rho_c A_b r_b + V_c \frac{1}{\Gamma^2 c^{*2}} \frac{dp_c}{dt}$$

where c^*

$$c^* = \frac{1}{\Gamma}\sqrt{\frac{\Re}{M} T_c}$$

is the characteristic velocity.

By substitution in the mass conservation equation, one finds the transient equation of the internal ballistics

$$\frac{dp_c}{dt} = \frac{\Gamma^2 c^{*2}}{V_c}(\rho_p - \rho_c) A_b r_b - \frac{\Gamma^2 c^*}{V_c} A_t p_c \qquad (2)$$

Under steady operations, one obtains the equilibrium pressure of the rocket motor combustion chamber

$$\overline{p_c} = \left(\frac{A_b}{A_t} a_b \rho_p c^*\right)^{\frac{1}{1-n}} \qquad (3)$$

where the steady burning rate has been taken as $\overline{r_b} = a_b \overline{p_c}^n$ and $\rho_p \gg \rho_c$.

2.1.2 Burning Rate Features

Under any circumstances, ideal one-dimensional steady-state combustion waves, if not impossible, are at least very rare. It is important to realize that, besides the main factors summarized in Section 2.1.1, a variety of details conspire against the establishment of an ideal combustion wave. Even for simple strand burners these factors can include size of the sample, lateral surface inhibitor, ignition, and nature and flow rate of the ambient gas, radiative environment, and other factors. Under actual motor operating conditions, further effects worsen the situation even for the simple end-burner configuration. These additional factors include grain processing details, aging, mechanical stresses, contacts with walls, interfaces with inhibitors, migration of various propellant ingredients, rate of polymerization, and propellant state of cure for composite propellants.[12] The high strain grain surface near the bond line of large end-burning grains, for example, encourages the burning surface to become conical from its initially planar shape, as shown in Figure 2.[9] In larger end-burning grains (above approximately 0.5 m diameter) the burning surface does not remain perpendicular to the axis, but gradually increases and assumes a conical shape. The burning rate at the bond line is larger than in the center. The lines in the grain indicate successive burning surface contours. Thus in most cases, including small motors for ballistic evaluation, one-dimensional steady-state combustion wave is only an ideal picture. The factors influencing non-ideal burning are reviewed in more detail in later sections relative to the issue of burning rate scaling. Only the general classes of non-ideal burning are reviewed in this section.
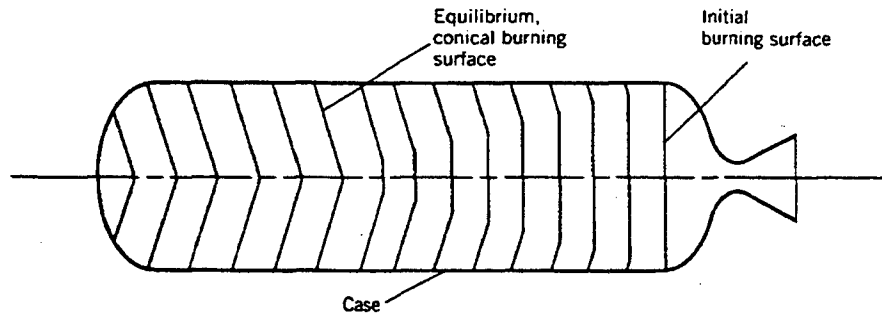
**Figure 2.   Burning Surface Does Not Remain Perpendicular to the Axis
in Larger End-Burning Grains.[9]**

2.1.2.1 Quasi-Steady Burning

For heterogeneous compositions, the combustion wave is by definition the result of local 3-D and unsteady effects depending on the initial loading fractions and particle size distributions of solid ingredients. On a microscale, unsteady effects are due to the arrival of different ingredients at the burning surface and changes of local thermophysical properties of each ingredient. Even for homogeneous compositions (double-base and triple-base solid propellants), different chemical reactions of the ingredients produce unsteady effects due to changes of chemical reaction rates and possible accumulation of carbonaceous residues on scattered sites of the burning surface. In general, the ideal uniform burning surface is rare to achieve due to foam, bubbles, hot spots, material dispersion, etc. occurring for a variety of reasons.[15]   Thus, steady-state combustion processes have to be seen more properly as *quasi-steady* in time, and measurements of linear burning rates must be taken over distances much *larger* than the corresponding thermal wave thickness (as well as the distance required to establish).

2.1.2.2 Mean Steady Burning / Neutral

In general, steady burning rates have to be seen as a mean value occurring over an appropriate time span. In particular, ignition and extinction transients have always to be excluded from the measurement procedure; but in general this is systematically done only in strand burners and ultrasound burners or other specialized rigs. Under these circumstances, a reacting propellant often shows a mean burning rate that is constant in time. With reference to a motor, the combustion process is said to be *neutral* if chamber pressure or thrust behavior are maintained constant in time; but for neutral burn rate, pressure only is required to keep constant in time. Note that (slowly varying) excursions within a typical but arbitrary fraction of 15% of the average value are accepted.[9]   Under actual operating conditions, however, peculiar motor effects may affect burning rates yielding unwanted consequences (see later sections).   For example, hump effects for cast composite propellants manifest an excess burning rate of 3-7% at about halfway through the web.[11]   Thus, neutral burning is a very convenient configuration but not easy to obtain. Most small motors for ballistic evaluation are meant to be neutral.

2.1.2.3 Transient Burning / Non-Neutral

Under transient conditions, burning rate may differ greatly from the equilibrium or steady rate. The degree of the effect depends on instantaneous operating conditions and their time rates of change, past history, and propellant type (primarily through thermophysical properties). In most applications, pressure cannot be held precisely constant. In motors, transient burning commonly contributes to a pressure peak at the beginning of operation, and may also cause extinction of remaining slivers during the depressurization at the end of operation. Through the middle portion of operation, the pressure may also vary with time

because of the grain configuration, nozzle size changes or manufacturing variables, such as the hump effect above. In general, a reacting propellant features a burning rate variable in time.

With reference to a motor, the combustion process is said to be non-neutral. In particular, *progressive* or *regressive* processes are defined if chamber pressure (or thrust) is overall increasing or decreasing in time (causing excursions wider than 15% of the average value[9]). The following definitions illustrated in Figure 3. [9], although arbitrary, are commonly accepted:

- Neutral burning: motor burning time during which thrust or chamber pressure remain approximately constant, typically within a corridor of ± 15%;
- Progressive burning: motor burning time during which thrust or chamber pressure increase (beyond the ± 15% corridor);
- Regressive burning: motor burning time during which thrust, chamber pressure, and burning surface area decrease (beyond the ± 15% corridor).
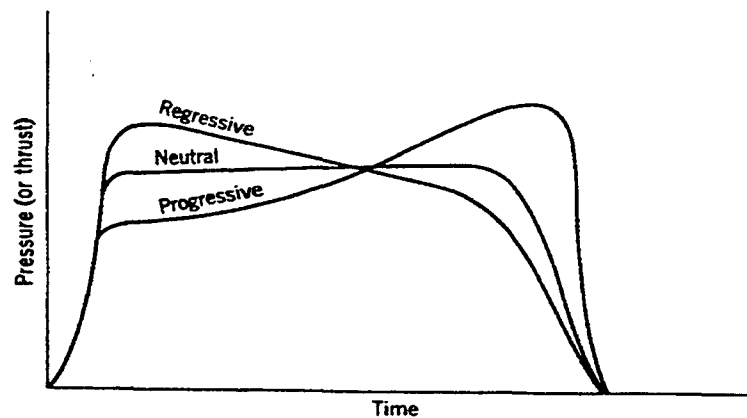
Figure 3. Classification of Grains According to Pressure-Time Characteristics[9]

Even the simplest burners experience dynamic burning effects, at least during the ignition transient, caused by the abrupt hot gas production. For well-designed burners, the associated rapid pressure change is a minor feature. But even if the pressure transient is avoided, the thermal transient still needs to be dealt with. In strand burners, this is accomplished by allowing the strand to burn some distance after ignition before starting the measurement period; likewise, the measurement period is stopped some distance from the strand end to avoid extinction transient. Also in the so-called non-intrusive burners (ultrasound, microwave, laser recoil, and x-ray) in which "instantaneous" (or very short-term averaged) burning rate measurements are obtained, both the starting and ending transients can be avoided. However, in motors the transients are essentially unavoidable, and are necessarily included in the data analysis because the only length known is the total thickness. In principle under no circumstances, including neutral burning, measurements should be taken during transient operations (ignition and extinction). But should diagnostic techniques capable of direct measurements of burning rates (e.g., ultrasound) be available, high-frequency measurements during transient operations can provide a corresponding time-resolved burning rate history.

2.2 Burning Rate Laws

2.2.1. Empirical Burning Rate Laws

Under steady conditions and for a given initial temperature, the Vieille or de Saint Robert law[16,9] is empirically used to describe the burning rate dependence on pressure

$$\bar{r}_b = a_b \bar{p}^n \tag{4}$$

where the two parameters (a_b and n) are constants experimentally defined over some limited measurement range. Figure 4 compares various burning rate pressure relationships.

Propellants showing a region of markedly reduced or zero pressure exponent are known as "plateau" propellants (for example double base propellants with small amounts of lead compounds). Propellants showing small negative values of n over short pressure ranges are called "mesa" propellants. Often it is possible to represent burning rate as a series of straight segments, with different a_b and n for various pressure ranges. To establish a_b and n for one range of pressure and initial temperature, it is industrial practice to use 7 runs (3 at the nominal pressure, 2 at the higher and 2 at lower pressure) at normal initial temperature and 5 runs each at expected temperature extremes.
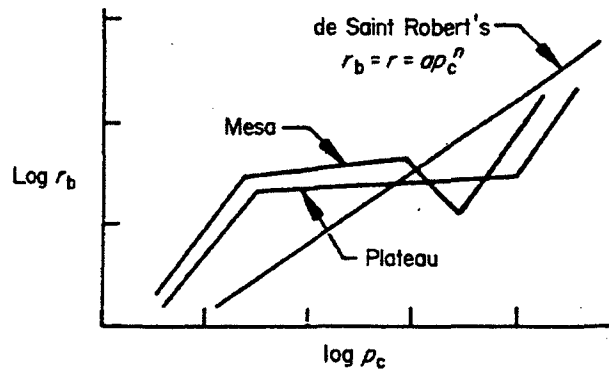
Figure 4. Various Burning Rate versus Pressure Relationships[14]

For years, the industry standard technique to acquire these data has been based on the so-called Crawford bomb.[17] The particular form with $n = 1$

$$\bar{r}_b = a_b \bar{p} \tag{5}$$

has been used in the past to represent steady burning rates of simple single base (nitrocellulose) gun propellants with some accuracy.[10] An alternative form borrowed from artillery and called Muraour law[16]

$$\bar{r}_b = b_b + a_b \bar{p} \tag{6}$$

describes[10] the behavior of many double base propellants for pressures above 200 atm as well or better than Eq. (4) and also provides[7] good estimates of the *constants* b_b and a_b.[7] Basically it yields results similar to Eq. (4) for the pressure interval of interest in rocket propulsion. Another alternative form[16]

$$\bar{r}_b = b_b + a_b \bar{p}^n \tag{7}$$

gives accurate results for many double base propellants over a wide pressure range, but it differs little from both Eq. (4) and Eq. (6) and is anyway inadequate for most rocket propellants.[10] The classical Granular Diffusion Flame (GDF) theory, developed by Summerfield and coworkers [18, 19, 20] can be applied to AP-based composite propellants burning at moderate pressures (0.2-0.8 MPa[7]) leading to the standard expression

$$\frac{\overline{p}}{\overline{r}_b} = a + b \cdot \overline{p}^{-2/3}$$

(8)

where the constants a and b respectively measure the importance of chemical kinetics and mass diffusion in the gas phase.[21,22] For lack of better knowledge, the use of Eq. (4) is recommended.

As an alternative for some particular compositions, the *"normal"* ballistic law (first proposed by Zeldovich[23,24] in 1942 and much used in the Russian literature[25, 26] can be implemented. This burning rate law, of exponential form, under steady conditions is usually written as

$$\overline{m}_{Ze}(\overline{T}_s) = M_s \exp(-\frac{E_{Ze}}{\overline{\Re T}_s})$$

(9)

where $\overline{m}_{Ze} = \rho_c \overline{r}_{b,Ze}$ is the steady surface mass burning rate and the pre-exponential factor M_s is the (asymptotic) maximum mass burning rate. The relationship of Eq. (9) was experimentally shown to hold as an "universal" law for particular compositions, over a wide range of pressure and initial temperature, by taking proper values of the relevant constants: for all known[26] double-base propellants (DBP) and nitrocellulose (NC) the activation temperature $E_{Ze}/\Re$ =5000 K and the pre-exponential factor M_s=1.8 10^3 g/cm^{2}s.[26] In this report, for convenience, the steady burning rate of Eq. (9) is called the *normal or Zeldovich burning rate* law.

2.2.2   Pressure and Temperature Sensitivity

If $\overline{r}_b$ is the steady linear burning rate, the commonly accepted definition (see Figure 4) for the steady burning rate pressure sensitivity is

$$n \equiv \left(\frac{\partial \ln \overline{r}_b}{\partial \ln \overline{p}}\right)_{T_0} = \frac{\overline{p}}{\overline{r}}\left(\frac{\partial \overline{r}_b}{\partial \overline{p}}\right)_{T_0}$$

(10)

while for the steady burning rate temperature sensitivity[9]

$$\sigma_p \equiv \left(\frac{\partial \ln \overline{r}_b}{\partial T_0}\right)_{\overline{p}} = \frac{1}{\overline{r}_b}\left(\frac{\partial \overline{r}_b}{\partial T_0}\right)_{\overline{p}}$$

(11)

Practically, over the appropriate *pressure and initial temperature* intervals, the familiar empirical steady relationships[9] are used

$$\overline{r}_{b,Vi} = a_b(T_{ref}) \cdot \overline{p} \cdot \exp[\sigma_p(T_0 - T_{ref})]$$

(12)

being

$$a_b(T_0) = a_b(T_{ref}) \cdot \exp[\sigma_p(T_0 - T_{ref})]$$

(13)

where T_{ref} is the reference ambient temperature, T_0 is the actual initial or ambient temperature, n and σ_p are constants over some limited operating range. In this report, for convenience, the steady burning rate of Eq. (12), obtained from experiments, is called the generalized power burning rate law also referred to as *Vieille (or Saint Robert) burning rate* law. The steady burning rate laws of Eq. (12) and Eq. (4) are convenient widely used over the appropriate range of operating conditions. Notice that Eq. (12) implies the

11

simplifying assumption that $n=n(p)$ while $a_b=a_b(T_0)$, as often observed due to the limited range of industrial burn rate testing. But this is not necessarily true in general. However, if the assumption is kept, then

$$\sigma_p \equiv \left(\frac{\partial \ln \bar{r}_b}{\partial T_0}\right)_{\bar{p}} = \frac{1}{a_b}\left(\frac{\partial a_b}{\partial T_0}\right)_{\bar{p}} \tag{14}$$

For motor operation, the commonly accepted definition for temperature sensitivity is

$$\pi_K \equiv \left(\frac{\partial \ln \bar{p}}{\partial T_0}\right)_K = \frac{1}{\bar{p}}\left(\frac{\partial \bar{p}}{\partial T_0}\right)_K \tag{15}$$

from which over some limited operating range

$$\bar{p}(T_0) = \bar{p}(T_{ref}) \cdot exp[\pi_K(T_0 - T_{ref})] \tag{16}$$

Moreover, combination of Eq. (12) and Eq. (16) yields

$$\pi_K = \frac{\sigma_p}{1-n} \tag{17}$$

valid if the relevant parameters are constant and small, i.e. $\sigma_p(T_0-T_{ref})<<1$ and $\pi_K(T_0-T_{ref})<<1$, as often observed. As matter of fact, typical values fall in the range $\sigma_p \approx 0.001$ to 0.01 K^{-1} and $\pi_K \approx 0.0005$ to 0.01 K^{-1}; double-base propellants usually feature larger values than composite propellants and ammonium nitrate based compositions are more sensitive than ammonium perchlorate ones. Specific values are reported in References.[7, 9, 12, 8,22, 27, 28, 29]

2.2.3. Analytical Burning Rate Models

Two different viewpoints have been taken to develop analytical models of steady burning rate.[7] Propellant chemists try to understand ballistic properties from a detailed knowledge of chemical kinetics mechanisms, while neglecting other less important physical processes. This approach has proved useful mainly for homogeneous compositions. Aerothermochemists have emphasized the importance of fluid mechanics and heat transfer while idealizing the role of chemistry to a few basic steps. These two different but complementary approaches are explained by examining the complexity of the underlying phenomena.

Still today the basic picture of DB burning (Figure 5) is that originally proposed by Rice[30] and Parr.[31] The burning process can be seen as one-dimensional, but several zones can be distinguished where chemistry plays a dominant role. In the gas-phase a fizz-zone (strong thermal gradient), dark-zone (vanishing thermal gradient, flame temperature around 1500 K, intermediate products), and luminous zone (strong thermal gradient, final flame temperature, final products) are identified. In the condensed-phase a rate controlled concentrated surface decomposition is assumed [30] or, more likely, a distributed foam zone involving exothermic processes and partial gasification of the solid propellant.[58] For increasing pressure, the overall flame thickness decreases. However, for pressures below 0.15 MPa the luminous zone cannot take place for kinetic reasons and the final temperature is that of the dark-zone.
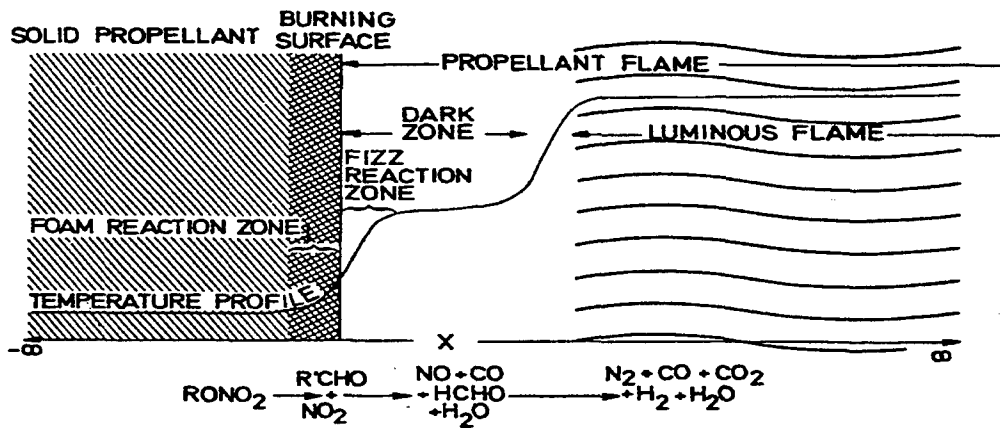
Figure 5. Basic One-Dimensional View of Double Base Propellant Burning [30,31]

Several models were proposed for heterogeneous compositions as well, but rarely based on first principles due to the intrinsically 3D and unsteady nature of the associated burning processes. The GDF two-stage flame model by Summerfield and coworkers [18, 19, 20] (Figure 6) and the BDP [32] multiple flame model (Figure 7) are prominent examples. In the GDF model the burning surface includes dissociative sublimation of NH_4ClO_4 into NH_3+HClO_4 over the oxidizer surface and endothermic zero-order pyrolysis of the solid fuel. A double flame structure is then portrayed in the gas-phase: a primary premixed monopropellant flame (between NH_3 and $HClO_4$ provided by the oxidizer dissociation) followed by a final diffusion flame between gaseous fuel pockets and the oxidizing atmosphere of the premixed flame products. The premixed flame is seen as very thin as compared to the diffusion flame; for pressures below approximately 0.1 MPa the gaseous premixed flame collapses to the burning surface. Thus, the resulting flame structure is seen as one-stage for most operating conditions (from 0.1 to 10 MPa). In the BDP model, the premixed monopropellant flame (between NH_3 and $HClO_4$) over the oxidizer surface takes place simultaneously to a primary diffusion flame confined at the edges of the oxidizer crystal. The main or final diffusion flame subsequently follows both flames between fuel and oxidizer intermediate products.
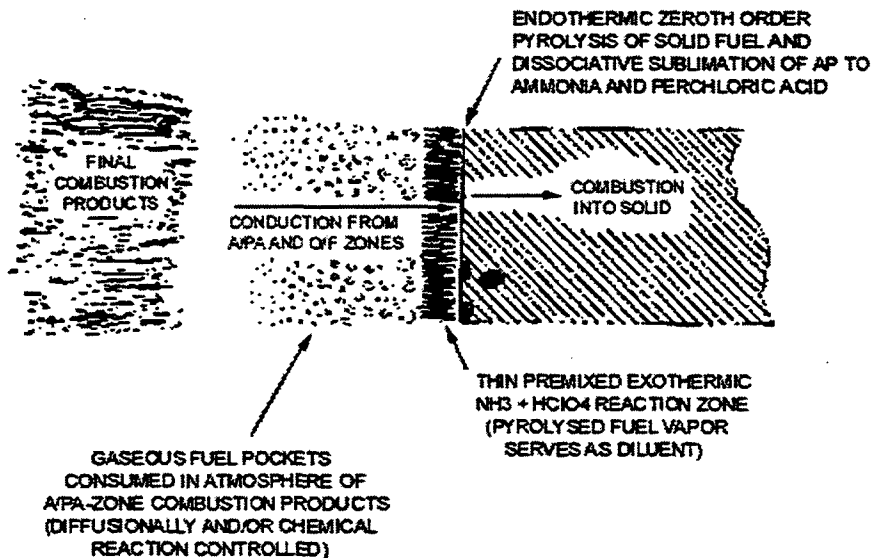
Figure 6. Schematic of Granular Diffusion Flame (GDF) Two-Stage Flame Structure for AP-based Composite Solid Propellants [18, 19, 20]

13

FINAL DIFFUSION FLAME

O₂ PLUS OTHER PRODUCTS

MONOPROPELLANT FLAME

FUEL PRODUCTS

AP DECOMPOSITION PRODUCTS

PRIMARY FLAME

PRIMARY FLAME

OXIDIZER

BINDER

BINDER
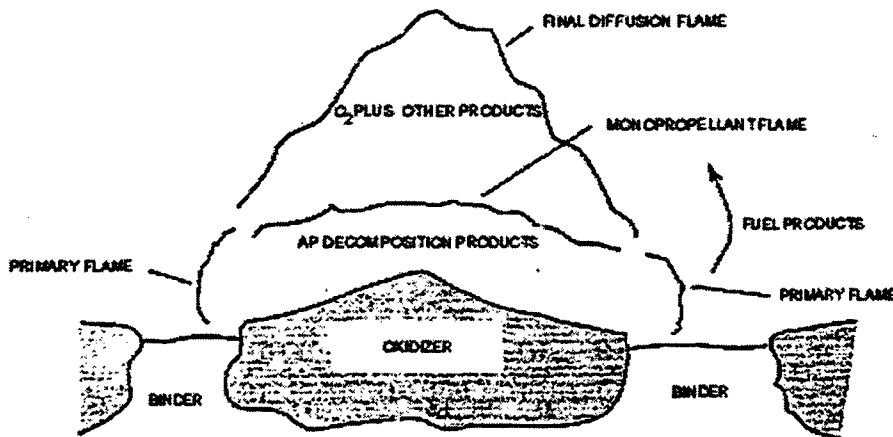
Figure 7. Schematic of Beckstead-Derr-Price (BDP) Multiple Flame Structure of AP-based Propellants[32]

2.3 Combustion Stability

Propellant and/or combustor stability problems may be encountered during any experimental burn rate testing. Both are anomalies to be avoided.

2.3.1 Intrinsic Stability of Propellants

This matter concerns the capability of a reacting solid propellant to recover its initial value of burning rate when perturbed. It is also known as *intrinsic stability* because it is strictly dependent on the nature of the burning solid propellant and operating conditions (typically, but not exclusively, pressure and initial temperature). Following the pioneering work by Zeldovich[23] in 1942, two main approaches, known as Zeldovich-Novozhilov (ZN) method and Flame Modeling (FM) method, have emerged to study intrinsic stability of solid propellants. Both share the basic assumptions of Quasi-Steady gas phase, Homogeneous condensed phase, and One-Dimensional propellant strand (QSHOD framework). Within this framework and for pressure perturbations only, linear stability analyses were first presented by Denison and Baum [33] in 1961 for premixed flames and Novozhilov [34, 25, 35] in 1965 by the ZN method. Both works, in the linear approximation of the problem, relaxed the assumption of constant surface temperature until then used. The linear stability boundary so deduced is the *same*; this boundary was shown later to hold true even under nonlinear conditions.[36] Just on the stability boundary a reacting solid propellant is expected to reveal self-sustained oscillations of the burning rate. The combustion behavior beyond this stability boundary still is a matter of speculation, but likely self-sustained oscillatory burning are observed until no steady solution whatsoever is allowed.[37]

2.3.2 Burning Stability of Motors

Catastrophic, high frequency combustion instability became relatively uncommon with the advent of aluminized propellants in the late 1950's. As a result, related research and development dwindled. However, compelling need for reduced visibility or opacity of rocket exhaust has dictated elimination of significant concentrations of aluminum from many tactical rocket propellants. The instability problem has reemerged at great cost to many motor development programs.

Burning stability concerns the capability of the combustor to recover its initial configuration when perturbed. There are many ways of classifying instabilities, but usually the frequency of the oscillation clearly reveals their source. The instability of concern to the one interested in measuring the burning rate of a propellant and motor configuration arises from coupling of the rate-determining combustion processes with acoustic oscillation modes of the combustion chamber. A rocket motor with a simple center-

perforated grain of reasonably high length-to-diameter ratio acts acoustically as a closed cylinder. The simple acoustic modes of such a cylinder are illustrated in Figure 8. [38]
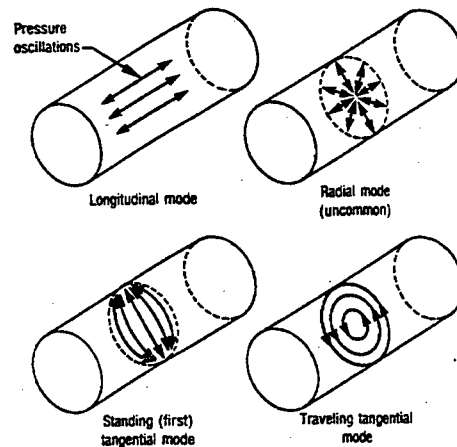
Figure 8. Acoustic Oscillation Modes in a Rigid, Closed Cylindrical Cavity[38]

Burning instabilities manifest as high frequency oscillations of the relevant motor variables (burning rate, pressure, temperature, etc.) superimposed on the corresponding average values, accompanied by corresponding vibrations of the motor case. Pressure histories of heavywall test motors containing an unstable, reduced smoke propellant (i.e., non-aluminized HTPB/AP) often reveal pressure excursions far more than sufficient to rupture a flight weight motor case. Note that in actual industrial practice combustion pressure excursions are not considered serious if below some limiting value (5%[9] or 2.5%[39]). These fluctuations are always undesirable; even though catastrophic failures are not necessarily observed, failure of the mission often still can occur. In general, vibrations are set up and transmitted to the whole propulsive system and vehicle, including payloads. Performances are modified due to shifting of the average chamber pressure, burning time is modified, and mechanical and/or thermal failures may occur. Typically, bulk mode instability occurs in the low frequency range (up to 150 Hz), axial mode instability for combustor cavity lengths between 0.3 and 5 m occurs in a larger frequency range (100 to 2,000 Hz), transverse mode instability for combustor diameter between 0.01 and 1 m occurs in an even larger frequency range (500 to 50,000 Hz).[40]

Bulk mode instability throughout the combustor is associated with low values of $L*$, typical of early burning in space motors where high mass fraction and low combustion pressure (below 20 atm) are usually met. It is a nonsteady mode of operation of rocket motors, involving growing low frequency oscillations possibly leading to a succession of quenching and reignition (also known as *chuffing* mode) without ever reaching a steady-state operation regime. This peculiar mode of operation is not common, it may last for the entire mission or naturally disappear in time due to growing values of $L*$.[41]

The high frequency range, whether axial or transversal, is much more common and usually associated with combustion details. "When oscillatory behavior occurs ... the oscillations would be more correctly attributed to instability of the entire *combustor.* The phenomenon results from a very complex interaction of the combustion, the combustor flowfield, and the combustor cavity walls." [41] Burning instabilities take place when perturbations excite any of the many acoustic oscillation modes of the chamber cavity. This problem is strongly dependent on the details of the fluid dynamics (interaction of oscillations with the mean flow, vorticity, viscosity, flow turning, multiphase flow, etc.) and 3D geometry of the combustion chamber (acoustics) as well as their interactions with the burning solid propellant. The balance of the various contributions (amplifying or damping) is currently assessed by means of a linear analysis; but some nonlinear aspects are also discussed in literature.[42] Although much progress has been made, this problem is far from being understood in its generality. Further comments can be found in References[40, 41, 21, 11]; some practical stability problems are also discussed in References.[21, 43]

15

2.4 Burning Rate Measurement Methods

2.4.1 Test Devices

Early descriptions of burning rate measurement methods were given in a previous AGARD publication by Young [44] and several classical textbooks [7,10,16,45]; more recent descriptions are reported elsewhere.[9,12,21] In general the burning rates obtained by different techniques are not the same; even using identical specimens and the same technique at different facilities, the measured burning rates are different due to a variety of details not fully controllable or controlled. A host of methods, ranging from reduced scale rocket motors to the simple strand burner, is today implemented to measure steady burning rates. In general, small scale motors are preferred to evaluate the burning rate of actual rocket motors (ballistic evaluation), while strand burners are used for quick assessment tests or quality control of large propellant production; other methods are mainly used for special purposes (interrupted burning, high pressure combustion, etc.).

The experimental results from the various methods used today are in general accurate to within ± 2-3% both for small motors and strand burners[12], but accuracy less than of 1% is sought for actual rocket motor design.[15] In most cases, strand burners reveal burning rates below the values of small motors, which in turn fall below full-scale motors. Nitramines seem to be a notable exception by scaling somewhat higher than full-scale motors.[46] Therefore, it is not only important to understand and standardize the technical procedures implemented by different users, but also to estimate the scale factor with respect to the full size engine if the burning rate value under the actual motor operating conditions is desired. In general, motor burning rate increases with the motor size[12]; other possible differences between data collected in motors and strands (changes in slopes or plateaus) are discussed in later sections.

2.4.1.1 Subscale Motors

While the development of gun propellants relies on precise control of the manufacturing procedure and chemical compositions, this is impossible[45] for rocket propellants due to the much more complex chemical composition and dependence on parameters difficult to control (particle size, minor additions of catalytic ingredients, etc.). Thus, the most satisfactory method to evaluate steady burning rates is to fire a certain number of rockets loaded with the actual propellant under test. For practical reasons, reduced cost, and improved safety, different rocket motors of reduced size (typically, 2 to 6 inches - or about 5 to 15 cm - diameter) were specifically developed for ballistic evaluation purposes at many facilities. These reduced scale rocket motors are usually made with heavy case and fitted with nozzles of different sizes to provide a number of convenient operating pressures (see Eq. 18).

Typically, small ballistic evaluation motors are radial burners providing a neutral pressure trace in time (within ± 10%), a sharp tail-off, port area / throat area ratio $A_p/A_t > 6$ and grain length / diameter ratio ≤ 2 to minimize erosive burning, short burning duration (2-10 s) to minimize heat losses and nozzle erosion, small grain web thickness to minimize thermal shrinkage, conical nozzle geometry with $15° \pm 0.5°$ half angle of divergence and no flow separation. The motor nozzle size, A_t, is estimated[12] from the burning rate r_b established from initial strand burner rate measurements based on the mass conservation equation

$$A_t = \frac{A_b r_b \rho_p}{C_D p_c} \tag{18}$$

In some cases, non-neutral pressure traces in time are used to reduce the number of tests, but the determination of the pressure exponent n is less accurate. In the industrial practice, over a pressure range for which a and n remain constant (see Eq. 4), a minimum of seven motors at the nominal operating initial temperature and five at the expected initial temperature extremes are fired.[27]

Tests with small motors provide better correlation with full-scale motor burning rates, but are considerably more time- and money-consuming than tests in strand burners. Tests in small motors are normally performed only after the neighborhood of the final propellant formulation is reached, in order to obtain a more accurate full-scale motor rate prediction and determine the temperature sensitivity of the motor combustion pressure π_K.

Many specific configurations of subscale motors are used in different countries. The term micromotors or the acronyms BEM for ballistic evaluation motors, BTM for batch test motors, BCM for batch check motors, SSTM for subscale test motors and others are randomly found in the literature to identify this specific but loosely defined class of motors. In this report, only the broad expression "subscale motors" is used. Although several suitable motor designs may be implemented, the most common configuration is a neutral burning grain providing a relatively constant combustion pressure p_c. Detailed recommendations on current burning rate measurement test techniques and subscale test hardware for accurate prediction of internal ballistics of a full-scale solid propellant motor are reported in JHU/CPIA CPTR 74.[5] Trends in observed differences in calculated burning rate for the different analysis methods were also evaluated with a goal of making recommendations on preferred analysis methods. These results, including surveys of analysis methods and results of the round robins are reviewed in the following sections of this report and References [1,25]. Further modifications, or complementary tools, of this basic setup are briefly described below.

2.4.1.2 Vented Vessels

In the simplest version, vented vessels are actual rocket motors abruptly extinguished by sudden release of pressure by blowing off the nozzle or by water injection. More sophisticated designs were also developed in which sticks, or slabs, of propellant are burnt and are quenched with water after about half the sample has been consumed. The pressure of operation is controlled by a much larger tubular charge of some faster burning standard propellant. By measurement of the burning time and the dimensions of the propellant sample before and after firing, the rate of burning can be determined directly.[44] This method to obtain burning rates, which is laborious, is no longer practiced. But the technique of vented vessels is used still today for other purposes, such as interrupted burning to examine the conditions of the propellant charge during combustion.[10]

2.4.1.3 Closed Vessels

Several closed vessel configurations are currently available to obtain the burning rate of the propellant from experimental pressure records in time. One option is to burn a small propellant sample in a large closed vessel filled with inert gas, producing a small pressure increase. The burning time is obtained as the time span between the onset and decay of the pressure rise. Another option is to increase the mass of the propellant sample up to a loading density of 0.3 g/cm^3, producing a very large pressure increase and pressurization rate from which the burning rate is deduced. This is not a direct measurement and the overall approach is a laborious process requiring a number of assumptions, but the method is used still today for very high pressure combustion (gun propellants).[7, 10, 15, 47]

An alternative technique to assess performances of gun propellants in particular is to measure the so-called heat of explosion in some type of calorimeter. This is a sensitive and quick method, derived from chemistry, capable of detecting any important changes or gross error in chemical composition. But it is useful in rocket propulsion only if, for the given propellant, the rate of burning is directly related to the heat of explosion,[44] which is not commonly the case.

2.4.1.4 Strand Burners

For about 50 years, the industry standard apparatus for routine measurements of linear burning rates has been the so-called Crawford bomb proposed in 1947.[17] This method, very quick, simple, and economic, is particularly suitable for exploring new propellant compositions or performing quality control of established compositions. Strands of propellant having circular or square cross section, 3 to 6 mm in diameter or side, are employed. The overall strand length usually ranges anywhere from some 10 mm to about 150 mm. These are supported in a suitable holder and inserted into a closed vessel, typically pressurized with nitrogen. The strands are coated with an inhibitor to prevent side burning. In the original configuration, two small holes are drilled, about 5 inches (about 127 mm) apart, along the diameter. Fuse wires are passed through each hole and connected to terminals. The strand is ignited at the top by a hot wire, and the time taken for burning to pass from the first to the second fuse wire is accurately measured. It is usual to take several measurements at each pressure.[13] The burning surface should remain planar and normal to the strand axis.

Over the years, several modifications of this basic setup for solid strands have been proposed. In the most common modification, the whole apparatus can be placed in a thermally controlled environment capable of producing the desired initial temperature range. In another version, called *window strand burner*, the burner is equipped with optical windows allowing optical recording of the burning processes (still photography, movie camera, video camera, etc. both in the visible and infrared ranges).[48] At Thiokol/Huntsville, a bomb holding three strands was used.[46] All configurations are easy and quick to operate, use a minor amount of propellant, and require little instrumentation. Thus, the strand burner method is widely used.

A further modification was developed at Aerojet Solid Propulsion Company (and occasionally used also at other locations), where the additional option of testing liquid strands of the uncured propellant instead of the familiar cured propellant solid strands is implemented. Burn rates of liquid strands are used in propellant manufacturing as controls for acceptance of the uncured propellant before casting into the motor. The liquid strands are obtained by casting the uncured propellant into a proper vessel (6.4 mm diameter paper cup or plastic tube or 6.4 x 6.4 x 139.7 mm rounded solid strip) coated with an inert lacquer; see sketch in Figure 9.[12] The measured burning rate differs with respect to both the solid strands and motor, but values can be correlated, as discussed more fully in later sections. The strand burning rate relationshoip is developed along with other control parameters during propellant development as illustrated in Figure 10. Once the strand burning rate has been established with its tolerance limits, the motor burning rate can be predicted. Challenges and successes in this correlation are reviewed in Section 6.0. A representative comparison of liquid and solid strand data is given in Figure 11. The liquid strand burn rate is of importance once the propellant reaches a production level. The solid strand burn rate is confined mainly to the development stage, where the composition versus burn rate is being established.[12]

An updated description and discussion of various strand burners is given in Reference [21]; further useful comments are reported in References [7, 9, 10, 13, 22].
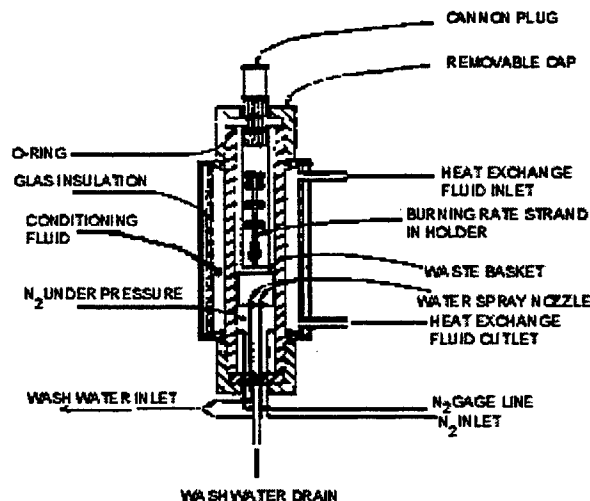
Figure 9. Modern Crawford Bomb (Solid or Liquid Strands)[12]

18

$$r_b = ap^n$$

BURNING RATE

$tg\alpha = n$

PRESSURE
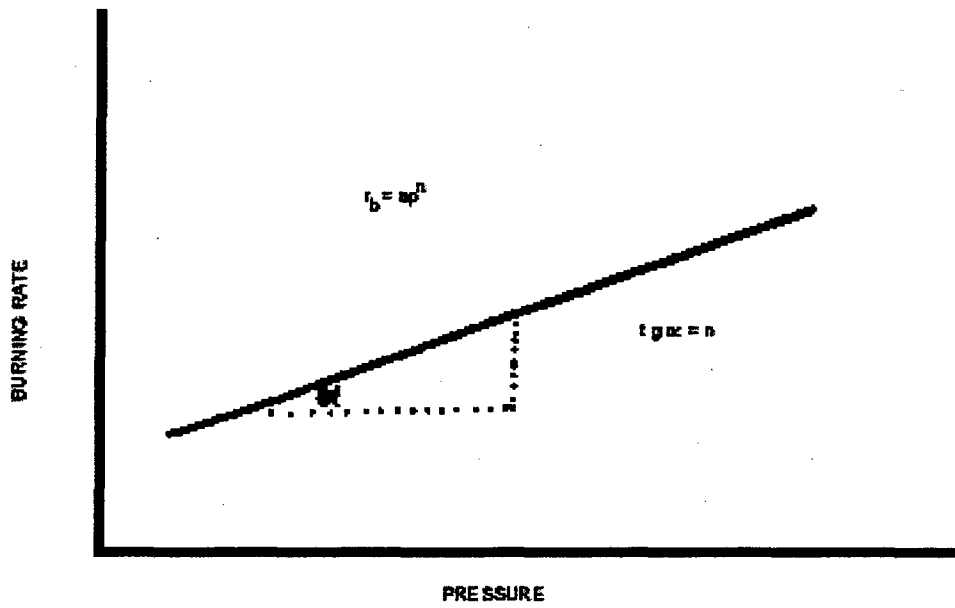
Figure 10. Traditional Power Law Burning Rate Behavior[12]

Pressure, MPa

Burning Rate vs Motor Size
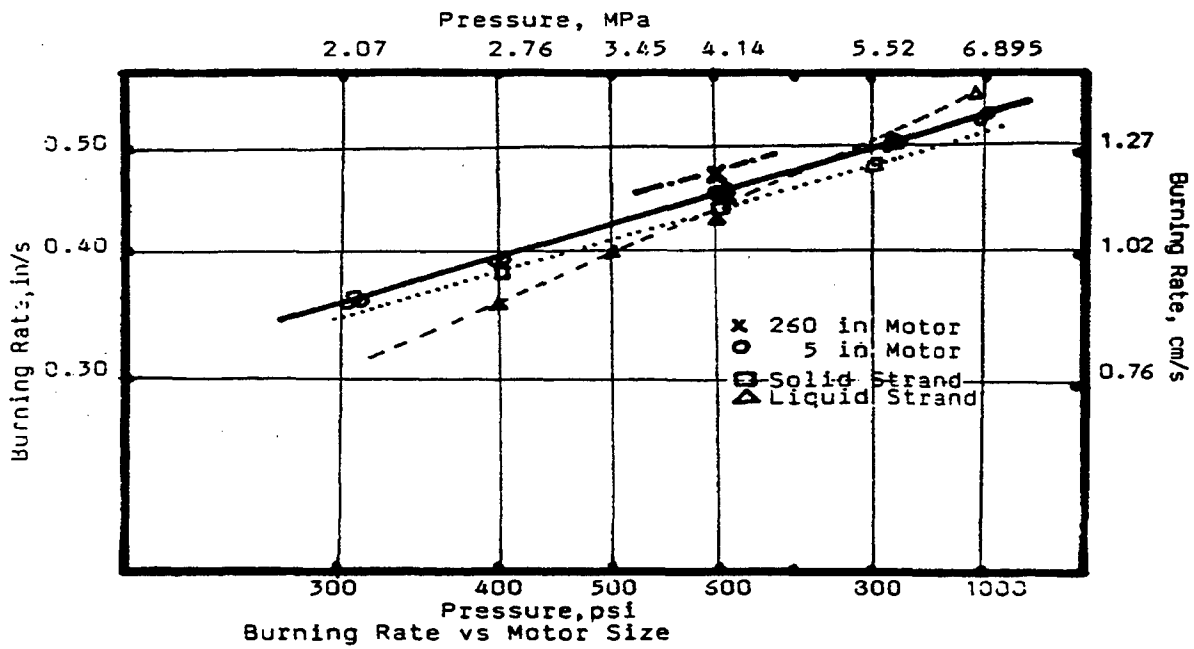
Figure 11. Behavior of Solid and Liquid Strand Burning Rate Relative to Motor Size[12]

2.4.2. Non-Intrusive Methods

Several diagnostic techniques are used to deduce burning rates. The well-known fuse wire technique set up for strand burners[17] allows only discrete measurements and under steady state burning. It is an intrusive method and thus suitable only for operating conditions far from the intrinsic stability boundaries. Other diagnostic techniques, notably non-intrusive and continuous in time, are needed for motors.

Non-intrusive methods were developed with the aim of measuring burning rates while minimizing disturbance of the combustion processes independently of the experimental apparatus. Several techniques are available with a different features and degree of maturity: film or video recording[49], X-rays[50], microwaves[51], ultrasonic[52], acoustic emissions[53], radiation recoil (typically, but not necessarily by a laser source[54]), plasma capacitance.[55] The X-rays technique, while applicable to any burning apparatus, is recommended for full-scale motors. Film or video recording, radiation recoil, and acoustic emissions techniques are more suitable for strand burners. Microwaves and ultrasonic techniques are suitable for both small-scale motors and strand burners. Radiation recoil and acoustic emission techniques do not detect the burning surface position and thus provide an indirect measurement; all other techniques are direct. Several of these techniques (in particular microwaves and ultrasonic) are also apt to measure transient burning rates; in addition, the acoustic emission technique is apt[56] to provide information as to the burning rate nonuniformity (due to localized and intermittent burning rate variations).[1]

2.5   Burning Rate Measurements in Subscale Motors

When testing motors, the burning rate measurement is actually deduced from the observed pressure-time or thrust-time history. Thus, following Hessler [57], it is convenient to recognize from start that appropriate definitions are required for burning rate in motors.

2.5.1   Burning Rate Definitions

Two basic classes of empirical burning rate definitions are in use for motor applications. These two families of fundamentally different burning rate determination each have their advantages and disadvantages. One definition is based on propellant thickness and the burning time and is referred to as the thickness/time (TOT) method, and the second is based on the conservation of mass in the ballistic test motor and is accordingly termed mass conservation or mass balance (MB) method.

The conventional burning rate definition is the fundamental TOT rate, r_{TOT}

$$r_{TOT} = \overline{r}_b = \frac{web\ thickness}{burning\ time} = \frac{w_b}{t_b} \tag{19}$$

requiring the appropriate but elusive value of thickness besides that of the related time. Real world effects such as non-uniform web and non-instantaneous burnout make accurate measurements of burning rate difficult. In attempting to correct for these factors, an alternative definition evolved based on some approximation of the mass conservation equations, rather than the fundamental ratio of Eq. 19 was in use already around 1960.[58]

Mass balance methods evaluate the steady burning rate r_{MB}, indirectly, from the balance between mass flow input from the burning propellant and output through the nozzle throat. Burning is assumed to occur throughout motor operation, implicitly accounting for non-instantaneous burnout.   Mass conservation should include gas storage in the combustion chamber due to density change and/or volume change; accordingly, several versions of this approach exist. The mass balance rate, mass conservation neglecting corrections, features less data scattering than the thickness/time rate, because it partially corrects for non-instantaneous burnout.[58]

Neglecting gas storage in the combustion chamber due to density change and/or volume change, an (average) mass balance rate r_{MB} is written See Figure 12 for notation definitions) as

$$r_{MB} = \frac{W_A - W_G}{t_E - t_B} \frac{\int_B^E p_c \, dt}{\int_A^G p_c \, dt} = \frac{W_{avg}}{t_b} \frac{\int_B^E p_c \, dt}{\int_A^G p_c \, dt} \tag{20}$$

Several variations of Eqn. 20 are used, involving primarily corrections for the neglect of mass storage.
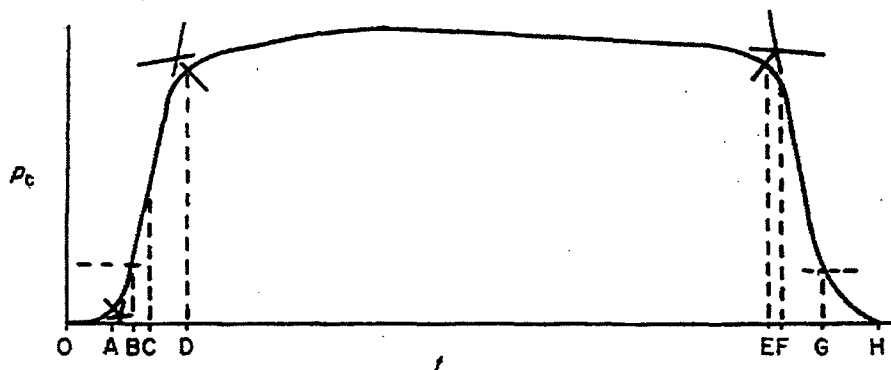
Figure 12. Various Burning Time Definitions[59]

Many r_{TOT} procedures do not explicitly account for non-instantaneous burnout. In fact, r_{TOT} procedures typically define end of burning as the knee of the curve (web burnout), when the experimental pressure trace begins to fall rapidly near the end of motor operation. However, specific choices of time points may make the correction implicitly. Procedures that define end of burning near 50% pressure implicitly assume burning continuation and thus partially avoid non-instantaneous burnout error, but not as well as an r_{MB} definition that actually uses the integral ratio. Due to transient operations, these r_{TOT} procedures tend to behave essentially like r_{MB} procedures. While use of 50% pressure time points for start of burning only has small effect on burning rate, the choice of 50% or more for end of burn during pressure decay can be a source of higher rate bias. A drawback of a 50-50 definition is that the time-averaged pressure differs much more from the rate-averaged pressure because the ending points are much lower down the tailoff curve than for an equilibrium or web-knee definition. More bias in burning rate is introduced, as the rate-averaged pressure is seldom used.

r_{MB} methods yield rates that are systematically low by a mass storage error. In turn, mass storage error also introduces a systematic nonlinearity in measured $r_b(p)$. Procedures essentially behaving like r_{MB} are likewise low by a mass storage error and generate similar nonlinearities. r_{TOT} methods, with instantaneous burnout, avoid the mass storage error yielding negligible nonlinear errors but high bias due to non-instantaneous burnout. Comparisons between MB and TOT analysis methods are more fully discussed in greater detail in the following sections of this report.

2.5.2   Solid Propellant Test Motor Scaling

The scale factor is the ratio of the biased results for two different measurement systems (motors or strand) containing nominally the same propellant.[46] The burning rate measured in small scale bombs is related to the corresponding full scale motor value by means of a constant scale factor and a variable hump factor curve.[56] The hump factor accounts for that part of the motor burning rate that depends on the propellant grain web (i.e. mainly the propellant rheology and motor casting process). The scale factor directly relates the burning rate in the full-scale motor to that measured in the small scale motors. Once a motor is fired, its burning rate is estimated by ballistic analysis. The method essentially involves applying a ballistic

21

model, including proper efficiencies and throat erosion, and in minimizing the difference between the experimental and theoretical pressure curves, by imposing characteristic web times. The scale factor is defined by taking as reference the propellant burning rate on the small scale motor (ratio of the burning rate obtained by analysis on full scale motor and that measured on small scale motors). Note that the above definition of scale factor does not claim an absolute significance, but it is referred to the measurements in a reference small scale motor by a particular set of definitions and procedures.

The scale factor is then applied to the following industrial activities[60]:
- Definition of nominal motor ballistics performance
- Definition of motor performance dispersions
- Definition of the specifications for the propellant ballistic characteristics and acceptance limits on small scale motors, during and at the end of development and qualification, so as to respect the required motor functional ballistic performance
- Prediction of ballistic performance of manufactured motors

Burning rates determined in small scale motors must frequently be scaled 1 to 3% to correlate with burning rates in full-scale motors; 5 to 7% scale-up is required for motors having a diameter one order of magnitude larger than the small scale motor. Larger corrections are often required for full-scale motors with fiberglass cases, where the propellant web thickness changes due to combined propellant grain and case expansion under motor expansion. Another source of error is thermal shrinkage of the propellant grain. Both factors induce a reduction of web thickness and often an increase of burning surface. Failure to acknowledge these factors analytically accentuates the apparent scale-up. It is however accepted that a major contributor to the disagreement between small scale and full-scale motors is inconsistent definition of burn time in small scale motors.[14, 27]

Burning rates from the Crawford bomb are usually accurate to within ± 2 to 3%. Results from small scale motors are within similar tolerances. It has been observed that in most propellants the strand burning rates fall below that of the motors, with nitramines seeming to be a notable exception.[46] The motor burning rate increases with the motor size, perhaps due to the gas flow causing an erosive effect, except nitramines.[46] A typical example is shown in Fig. 11.[12] Another explanation may be due to differences in variation in pressure and pressure exponent in motor and strand. Quite often the strand burning rate versus pressure shows anomalies such as changes in slope or plateaus that may not occur in the motor. The reasons of this behavior are still unknown. It may be the result of the size and shape difference of the test specimen and test method, which in turn may be responsible for different heat losses affecting the combustion processes.[12]

The main objective of small scale motors is to measure burning rate in a motor environment by saving time and money during the actual motor development. These issues are discussed in further detail in JHU/CPIA CPTR 74[5], but in summary the simple 2 in (5. 08 cm) diameter motor is typically the most convenient asset.[39] With respect to the companion 6 in (15.24 cm) diameter motor, the 2 in motor is cheaper to operate, easier to handle, and quicker to setup; thus, it can be fired a greater number of times yielding results with a more sound statistical significance notwithstanding its intrinsic lower precision. The 6 in (15.24 cm) diameter, or even larger small scale motors, are often used for other purposes. In particular, they are used to minimize data scattering by assessing the influence of specific operating parameters (igniter, test setup, data handling, etc.). Another interesting approach is the measurement of burning rate using liquid strands in combination with the other methods. This seems to be the most effective overall strategy, but scale factors among the different steps involved need to be accurately assessed. This can only be done through appropriate experimentation.

It is clear from the preceding discussion that the main characteristics of the burn rate measurement device, along with test and data reduction procedures, should be precision and reliability. The definition of scale factor and its application demand high reproducibility of the measured reference burn rates with data scatter as low as possible. Obviously, allocation batches before propellant manufacturing and for acceptance in the production phase demand the same features. A more thorough treatment of burning rate scaling in solid propellant motors is provided in JHU/CPIA CPTR 73.[4]

3.0   BURNING RATE MEASUREMENT ANALYSIS METHODS

Our understanding of burning rate analysis methods can be improved by examining practices employed by various facilities and countries engaged in the measurement and analysis of burning rate in solid propellant systems. Over 20 facilities from 7 NATO member countries were surveyed for their methods used and their characteristics. Appendix B provides details of the data analysis methods surveyed. This represents a complete survey of all the international facilities involved in burning rate measurement, and is a thorough representation of the fundamental methods used in the solid propulsion community today. The fundamental means of determining burning rate and basic definitions are reviewed first, focusing upon methods encountered in the international survey. Results of the international survey are summarized and findings discussed. Methods developed at different facilities typically yield different measures of the burning rate.   One approach to isolating the data analysis methods from the propellant, motor, and instrumentation variations is to generate and analyze "simulated" motor pressure-time data for an "ideal" propellant in an "ideal" motor with "perfect" instrumentation. Realism may be approached asymptotically by adding known non-ideal propellant, motor, or instrumentation phenomena to the simulated motor data. Alternatively, "real" motor data may be analyzed to expose any effects artificially induced by using simulated data. Both approaches to examining the influences of realism were explored by the WG. The results of multiple analysis round robins, and analysis of real motor data are reviewed and findings discussed. As a minimum, review of the methods and their performance in the assessments can yield the reader suggestions for improving their own methods while understanding others.

3.1   Description of Methods of Burning Rate Analysis

Two families of fundamentally different burning rate determination methods exist. One is based on propellant thickness and the burning time and is referred to as the thickness/time method, and the second is based on the conservation of mass in the ballistic test motor and is accordingly termed mass conservation or mass balance method. These two families may be further divided into the following categories, which are more descriptive of their specific application:

1) Thickness/Time Methods
   a)   Thickness/time Rate (r_{TOT} or R_{TOT})
   b)   Iterated Thickness/Time Rate (r_{TOTn} or R_{TOTn})
   c)   Iterated Two-Point Thickness/Time Rate (r_{HG} or R_{HG})
2) Mass Conservation Methods
   a)   Mass Balance Rate (r_{MB} or R_{MB})
   b)   Iterated Mass Balance Rate (r_{MBn} or R_{MBn})

3.1   Thickness/Time (TOT) Rate

3.1.1   Common Thickness/Time Method

Thickness/time (r_{TOT}) methods evaluate the steady burning rate r_{TOT}, directly, based on the fundamental definition

$$r_{TOT} = \frac{web\ thickness}{burning\ time} = \frac{w_E - w_B}{t_E - t_B} = \frac{w_b}{t_b} \qquad (21)$$

requiring the accurate knowledge of the burned web thickness, w_b, and elapsed burning time, t_b, where w_b is specifically the thickness burned during t_b. It is important to realize that r_{TOT} of Equation 21 is a point measurement, where this definition does not include any average over the surface. This requires that w_b and t_b be consistent, both referring to the same point. It might be appropriate to assume the ignition is instantaneous, but it is almost certainly not appropriate to assume that burnout is instantaneous. Consequently, the choice of w_b is dependent upon the choice of burnout time, and may be expected to perform correctly with an average web thickness only if burnout is instantaneous. In actual experiments, w_b and t_b are elusive values. To complement the burning rate, an average combustion pressure value is

needed. Definitions for web burned, burning times and average combustion pressure are discussed in more detail in later sections.

Cylindrically perforated grains are commonly used with the intent to provide a known and uniform web thickness implying also instantaneous burnout. In reality, web thickness is typically reduced from the nominal value due to misalignment, cure, and thermal shrinkage. In case-bonded grains the web thickness is further reduced near the middle by grain distortion caused by the stresses due to cure and thermal shrinkage. Both misalignment and grain distortion cause burnout to be non-instantaneous.

While no standard definitions for the beginning, t_B, and ending, t_E, of burning time exist throughout the industry, similarities were encountered during the WG016 survey summarized later in Sections 3.4 and 4.0. Based on experience, every facility typically implements its own set of time point definitions. Most definitions are either based on some fixed percentage of some characteristic pressure (a maximum or average pressure), or on some attempt to define the "web burnout" or "knee" at the end of the level portion of motor operation. Although some plausible rationale can be advanced, these definitions are essentially arbitrary.

3.1.2   Iterated Thickness/Time Method

The thickness/time burning rate (r_{TOT}) procedure is the simplest and most fundamental burning rate definition and analysis procedure and is summarized in Appendix B-23. The iterated thickness/time burning rate (r_{TOTn}) procedure, summarized in Appendix B-24, differs from the most commonly used thickness/time rate procedure in the use of the rate-averaged pressure p_{nb} (see Section 3.5) as the associated pressure and the iteration to determine exponent n. The iteration typically converges on the fourth iteration. A variation on this method encountered by the WG involves an iterative process to determine the burning time while still using time-averaged pressure.

3.1.3   Hessler-Glick Two-Point Method

Virtually all the burning rate measurements depend on one of the two burning rate definitions, r_{TOT} or r_{MB}, with various time point definitions. Well-established industrial methods can be found for both rate definitions. A continuing controversy exists about which definition is better. While r_{TOT} will be in error when burnout is non-instantaneous (as usually observed), r_{MB} will be in error if mass storage is neglected. HG avoids both errors by a modified r_{TOT} procedure explicitly recognizing non-instantaneous burnout. Only the HG reference method enforces a set of derivative-based time point definitions following a careful analysis of the physics of motor operation. Two r_{TOT} measurements are made using the average web thickness: r_{bi} using the initial burnout time definition t_{Ei}, and r_{bf} using the final burnout time definition t_{Ef}. The two individual measurements, after correction to a common pressure, and iterated with similar motors to determine the proper exponent, will still be in error because W_{avg} is not the web thickness that should be used in either instance. However, the signs of the errors are *opposite* for the two measurements, so averaging the two tends to eliminate the error. The result of the two-point measurement procedure may be stated as a burning rate definition

$$r_{HG}(p_{nbi}) = \frac{1}{2}\left(r_{TOTi} + r_{TOTf}\left(\frac{p_{nbi}}{p_{nbf}} \right)^n \right) \tag{22}$$

Among the r_{TOT} methods, only the Hessler-Glick (HG, Appendix B-21 and B-27) reference method accounts for non-instantaneous burnout caused by bore misalignment and grain distortion effect by considering an initial t_{Ei} and final t_{Ef} burnout times. In methods implicitly or explicitly assuming instantaneous burnout, usually $t_E \cong t_{Ei}$, implying shorter combustion times and higher burning rates.

3.2   Mass Balance (MB) Rate

An alternative approach based on some approximations of the mass conservation equation was developed around 1960 [61,62,63,64] in an attempt to correct for the factors affecting the thickness/time rate. In general, mass balance rate features less data scattering than thickness/time rate, because it corrects for non-instantaneous burnout.

Mass balance methods evaluate the steady burning rate r_{MB}, indirectly, from the balance between mass flow input from the burning propellant grain and mass flow output through the nozzle throat. The latter includes mass accumulated in the combustion chamber due to an increase in pressure and increase in volume (due to propellant consumed). Burning is assumed to occur throughout motor operation, implicitly accounting for non-instantaneous burnout. Transient mass conservation requires[65] in general, where Γ is a function of the gas constant k

$$\frac{dp_c}{dt} = \frac{\Gamma^2 c^{*2}}{V_c}(\rho_p - \rho_c)A_b r_b - \frac{\Gamma^2 c^*}{V_c}\eta_t A_t p_c \qquad (23)$$

For quasi-steady burning

$$A_b r_b \rho_p = \frac{\eta_t A_t p_c}{c^*} + \rho_c A_b r_b = 0 \qquad (24)$$

alternatively, this can be expressed as the instantaneous mass balance to show the various contributions more clearly

$$A_b r_b \rho_p = \frac{\eta_t A_t p_c}{c^*} + \rho_c \frac{dV}{dt} + \frac{d\rho_c}{dt}V \qquad (25)$$

The left-hand side is the mass produced by the burning propellant surface. The first right-hand side term accounts for the mass flow through the nozzle while the second and third terms account for mass storage in the combustion chamber due to volume increase and pressure increase respectively.

For $\rho_p \gg \rho_c$, quasi-steady burning rate is evaluated as

$$r_b = \frac{p_c \eta_t A_t}{c^* \rho_p A_b} \qquad (26)$$

Neglecting gas storage in the combustion chamber due to density change and/or volume change, a (average) mass balance rate r_{MB} may be written as

$$r_{MB} = \frac{w_A - w_G}{t_E - t_B} \frac{\int_B^E p_c dt}{\int_A^G p_c dt} = \frac{w_{avg}}{t_b} \frac{\int_B^E p_c dt}{\int_A^G p_c dt} \qquad (27)$$

Several variations of Equation 27 have been used, primarily corrections for the neglect of mass storage, which causes the main error (bias low) in use of the Mass Balance rate definition. Note that r_{MB} compensates for the inconsistency between w_A-w_G and w_{avg} by letting $t_E = t_{Ei}$.[66, 67]

The burning rate for the mass balance method (r_{MB}) defined in Equation 26 is based on the balance in the mass flows developed during steady state burning. Due to a developing boundary layer in the nozzle, the occurrence of a "borda effect" for the case of a poorly manufactured nozzle, due to thermal expansion of a nozzle throat insert (tungsten or molybdenum) causing a contraction of the nozzle throat, or due metal oxide deposition on the nozzle throat, the actual nozzle throat may be smaller than the geometric value measured before the test. To account for these effects the factor η_t is included. Equation 26 requires

25

accurate knowledge of the average combustion pressure (p_c), the effective nozzle throat area ($A_t \cdot \eta_t$), the propellant density (ρ_p), the burning surface (A_b), and of the characteristic velocity (c^*). The effective nozzle throat area may be determined by measuring the geometrical nozzle throat diameter using an appropriate measurement procedure. The factor η_t may be based on experience, and may be different for each nozzle, propellant and combustion pressure and its choice may be ambiguous. This can produce additional errors. The propellant density may be either measured or calculated from the propellant composition, when a measured value is not available. The burning surface area may be calculated based on accurate measured grain dimensions. The burning surface is constant for the case of an EB grain (coning not considered), but will generally change with time when a CP grain is used. The characteristic velocity is a thermodynamic property, which relates to the efficiency of the combustion and is essentially independent of the process-taking place in the nozzle. The theoretical characteristic velocity is fully determined by the ratio of specific heats, the molar mass of the combustion products and the equilibrium combustion temperature.

Mass balance rate shown in Equation 27, differs from the thickness/time rate of Equation 21 by a correction factor. Mass balance rate has the reputation of being more rigorous, but also incorporates implicit assumptions. For example, it is assumed that negligible mass is stored in the combustion chamber, and also that the propellant is burning all the time that pressure is nonzero. Mass Balance burning rate definitions contain the implicit assumption that the average burning surface during burning time is the same as during total time. Although this assumption is not correct, its effect is to approximately correct for early burnout because of misalignment or distortion, and accounts for the improved reproducibility reported for the mass balance methods as compared to the thickness/time methods[68].

Representative mass balance methods currently in use by facilities surveyed by WG016 include:

1) Common Mass Balance Method
2) Vellacott's Method
3) Brooks' Improved Method
4) Jordan's Combined Mass Balance with Thickness/Time Method

3.2.1   Common Mass Balance Method

The Common Mass Balance method neglects all storage terms. In Equation 28 the mass balance burning rate (for an exact web) equals the mass balance burning rate (for a nominal web) multiplied by a correction based on pressure integrals for web burned during the burning time $t_b = (t_B - t_E)$, and $t_{total} = (t_G - t_A)$. Time definitions are discussed in Section 3.4 (See Figure 14 and Table 3).

$$r_b = \frac{w_b}{t_b} \cdot \left(\frac{\int_{t_b} P\,dt}{\int_{t_{total}} P\,dt} \right) \qquad (28)$$

Development of this equation begins with the fundamental r_{TOT}, thickness/time rate relationship in Equation 21. Using the average pressure defined as[64]

$$\overline{P_c} = \frac{\overline{A_b} \cdot \rho_p \cdot c^* \cdot r}{A_t} \qquad (29)$$

where $\overline{A_b}$ is an average value. When rewriting c^* and ρ_p as

$$c^* = \frac{A_t \cdot \int P\,dt}{W_p} \qquad (30)$$

and

26

$$\rho_p = \frac{W_p}{A_b . w_b} \quad (31)$$

Where Wp is the propellant weight used for the test. When replacing c^* and ρ_p in Equation 29 the burning rate becomes the following

$$r_b' = \frac{w_b \overline{P_c}}{\int\limits_{t1}^{t2} P dt} \quad (32)$$

Brooks' Common Mass Balance Method is also expressed by Equation 33, but with the end of burn t_2 (or t_E) defined by Equation 40 or Equation 9.1 of Appendix B-9. Alternatively integrating over the total action time t and using Equations 41 and 42 (or Equations 9.2 and 9.3 of Appendix B-9) for α_p

$$r_b = \frac{w_b \overline{P_c}}{\alpha_p \int\limits_{t1}^{t} P dt} \quad (33)$$

In essence, Equation 30 and 31 are identical to replacing the time in Equation 21 by the ratio of the pressure integral and the average pressure.

When considering a typical subscale test with a neutral CP grain, Equation 21 gives the most accurate results from tests yielding the least amount of impulse in the tail-off. When assessing the influence of the total tail-off impulse on Equation 21, this will become explicit. When taking for example two aft-tangent points, one at t_e and another at $t_e+\delta$, burning rate obtained with Equation 21 will differ by a fraction $(t_e+\delta)/t_e$. The average pressure determined over two intervals in Equation 33 will differ much less than this fraction (about half). Therefore, the burning rate as given in Equation 33 shows less variation. For the case when there is no tail-off, the two methods yield identical results. Equation 21 becomes decreasingly accurate with increasing impulse in the tail-off.

See Appendix B-25 for a summary of the common mass balance method, and Appendix B-9 for a more thorough discussion of the Brooks' common mass balance method, as well as the Appendixes for many other facilities that use the fundamental mass balance method as summarized in Section 4.0.

3.2.2 Vellacott's Method

It is relatively easy to account for the volume increase (second term right-hand side of Equation 25), as is shown in Equation 22. This term results from the chamber volume freed by the burned propellant.

$$\rho_c . \frac{dV}{dt} = \rho_c . r_b . S_b \quad (34)$$

The MB burn rate including mass storage due to volume increase is:

$$r_b = \frac{\eta_{\cdot} . A_t}{c^* . \rho_p . A_b} . p_c \left(\frac{1}{1 - \dfrac{\rho_c}{\rho_p}} \right) \quad (35)$$

Note that the term between brackets does not relate to the actual volume change, but merely is determined by the ratio of the density of the combustion product, which is determined by the combustion pressure, and the propellant density.

To assess the effect consider a conventional AP/HTPB propellant with a solid loading of 85%. The correction due to the volume increase can be calculated theoretically using a thermodynamic code, e.g. the NASA-Lewis code to determine the density of the combustion products as a function of pressure. The results for a pressure range of 2 - 10 MPa is given in Table 2. The addition of aluminum to the propellant formulation does not substantially affect the correction factor.

Table 2. Evaluating Effect Chamber Volume Increase

Combustion Pressure [MPa]	Density of Combustion Products [kg/m3]	Correction Factor X 10^{-3}
2	2.11	1.28
4	4.19	2.55
6	6.27	3.82
8	8.35	5.09
10	10.42	6.36

When the volume change is assumed to be important, the following result is obtained, which is known as Vellacott's method or "equilibrium burning rate":

$$r_b = \frac{w_b}{t_b} \cdot \left(\frac{\int_{t_b} p\,dt}{\int_{t_{total}} p\,dt} \right) \left(\frac{1}{1 - P_c \big/ \rho_p R_g T_f} \right)$$ (36)

An additional correction term is added to the rate equation neglecting storage terms given in Eqn. 28.

The burn rate correction due to a changing pressure is more difficult to account for because the pressure generally varies during the test. When the pressure increases, the contribution is positive while when the pressure decreases the contribution is negative. The contribution is proportional to the free chamber volume; hence, when the free chamber volume is small and the pressure variation during an experiment is small as well, the third right-hand side term may be neglected. This should be evaluated for each small-scale burner.

3.2.3 Brooks' Improved Method

Brooks' improved mass balance method approximates all storage terms

$$r_b = \frac{w_b}{t_b} \cdot \left(\frac{t_b \int p\,dt}{t_{total} \int p\,dt} \right) \left(1 + \frac{V_b(p_E - p_B)}{w_p R_g T_f} \right) \left(\frac{1}{1 - P_c \big/ \rho_p R_g T_f} \right)$$ (37)

Equation 37 equals the common mass balance rate of Equation 28, but includes an exact web thickness/time correction to the nominal thickness/time (w_b / t_b), a storage correction for density change due to the influences of pressure variation during the test, and a correction for volume change in the chamber due to propellant consumption. See Appendix B-9 for a more thorough discussion of Brooks improved method.

3.2.4 Jordan's Combined Method

Jordan's combined method simultaneously solves for the mass balance and thickness/time burning rates, assuming only one burning rate properly defines the propellant, regardless of the method. The method calculates a thickness/time burning rate curve using the beginning and ending times. This burning rate curve and the pressure integral fractions at a defined time are used to calculate a mass balance surface versus web burned curve (SW). This SW curve and time-defined fractional pressure integrals are iterated until the calculated SW curve matches the real grain geometry. This surface matching technique assures conservation of mass, and is relatively insensitive to ignition spikes and tail-off anomalies. Coefficients of variation from 0.09% to 0.23% were obtained using Jordan's Method on groups of 12 high quality (nominally replicate) motor firings.

Frank Jordan was active in the past in complex solid propellant rocket motor firing analysis methods. The methods developed were implemented as computer codes for various different solid propellant rocket motor manufacturing companies. For example at Atlantic Research Corp., a data reduction procedure called Static Firing Analysis (SFA) was developed, at Talley Defense Systems, the procedure was called Talley Rocket Analysis Code (TRAC), while at Aerojet, a procedure called Aerojet Rocket Motor Analysis Code (ARMAC), was written for the Advanced Solid Rocket Motor (ASRM) project [69, 70, 71].

All these computer codes were essentially based on the same analysis procedure, while in addition, some codes had special capabilities that were unique to the company for which they were written. Jordan's method applies a web sliver correction to mass balance

$$r_b = \frac{w_b + \varepsilon}{t_b}$$

(38)

to yield an instantaneous approximation and mean values of burning rate in an iterative procedure

$$r_b = \int \frac{p \, A_t \, \eta_t}{\rho_p \, A_s \, c^*} d_t$$

(39)

The most expanded and complete version of the code could analyze any type of solid propellant rocket motor firing. While reportedly automated, successful implementation requires review of the data by an experienced analyst. See Appendix B-17 for a more thorough discussion of Jordan's method. See Appendix B-11 for a description of Atlantic Research Corp.'s analysis method.

3.2.5 Iterated Mass Balance Method

The iterated mass balance burning rate (r_{MBn}) procedure differs from the common mass balance rate procedure (Appendix B-25) in the use of the rate-averaged pressure p_{nb} as the associated pressure and the iteration to determine exponent n. A variation on this method involves an iterative process to determine the burning time while still using time-averaged pressure. Further details are provided in Appendix B-26.

3.3 Grain Web Thickness Definitions

The propellant grain configuration can be end burning (EB), circular centrally perforated (CCP), or may have a more exotic shape (e.g. a star shaped grain). It may be relatively easy to measure the web for an EB configuration. While for a CP configuration, the web may vary in the grain length and tangential directions, making an accurate measurement very complicated in practice. In all cases, the web measurement procedure should be well defined. The method used for the production of the propellant samples largely affects the geometrical accuracy of the sample dimensions.

3.3.1 Web Thickness Determination - End-Burning Grains

Before the experiment to measure the burning rate of a particular propellant can be carried out, the propellant web has to be determined. A measured web thickness is preferred over a thickness taken from a drawing. Measuring the propellant web at three places at 120 degrees interval and arithmetically averaging the values may do this. In a practical situation the propellant will be cast into a plastic (e.g. nylon) cylinder, and propellant discs are milled from this cylinder on a lathe. This yields relatively flat discs. The nylon functions as an inhibitor. For most conventional composite rocket propellants good bonding between the nylon and the propellant may be obtained, however, for propellants that may yield poor bonding, the propellant may start burning between the inhibitor and the propellant. When this occurs, the experimental results will deviate (may be observed from the pressure vs. time trace). The deviation will be larger for tests tuned to higher pressures. When the effect is small it may not be observed but will influence the results to some extend.

Another unexpected increase in pressure may be due to a non-uniform regression of the grain surface, resulting in a burning rate enhancement along the inhibitor called "coning" [72,73]. Explanations as to why this occurs are:
1. Strain on the propellant;
2. Migration of curing agent or other propellant ingredients (from within the propellant and/or from the inhibitor into the propellant) that may increase the burning rate;
3. A different propellant composition near the inhibitor (e.g. a local concentration of fine particles),
4. Deviation from the 1D heat transfer situation due to a better heat conduction along the inhibitor.

All these effects will change the burning rate locally and the overall pressure vs. time trace of the test; and through this the measured burning rate.

3.3.2 Web thickness Determination - Centrally Perforated Grains

A typical web shape for a CP grain is given in Figure 13.
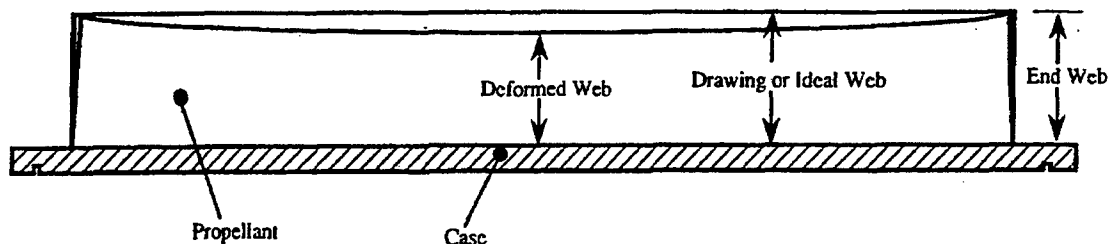
Figure 13. Typical Web Shape of CP Grain

Inaccurate results will be obtained when mandrel or drawing dimensions are used to determine the web thickness[70] as the changes that the propellant web undergoes between casting and curing are completely ignored. Shrinkage due to the curing process, thermal deformations (e.g. propellant shrinkage during cooldown) and deformations due to motor pressurization all occur and result in web changes that can result in burning rate errors of up to 5 %.[74]

In the end, the number available to use for burning rate calculation is usually either:
1. Drawing dimensions,
2. Drawing dimensions corrected for theoretical shrinkage, or deformation
3. A measured "average".

Note that each choice yields some kind of average thickness. The difference between the choices on the results can be considerable. Improved accuracy can be obtained by measuring grain bore and case inside diameters. Diameter measurements 1 – 2 web thickness into the grain bore will essentially eliminate most of the web bias caused by taking measurements at the grain ends (compare Figure 13), but the

thinnest point is usually near the center. Moreover, mandrel roundness, straightness and alignment imperfections can result in up to 10 % web bias over drawing dimensions and result in inaccuracies for the burning rate of up to 3 %. When a grain is cast into phenolic sleeves or into a steel case with relatively thick liners on the inside surface, the grain outside diameter will be rather difficult to determine and simultaneously the web thickness, again enhancing inaccuracy. Methods for compensating for shrinkage, hardware variation, grain distortion and misalignment are offered by Hessler and Glick.[68]

3.3.3   Web Thickness Determination - Other Grains

For all grains shapes the propellant burning situation is considered as one-dimensional (burning velocity vector pointing perpendicular inwards). This assumption is most realistic for the end-burning grains, it is less realistic for the centrally perforated (CP) grains, while it is even less realistic for the star shaped propellant grains. The more exotic grain shapes are not considered here in order not to further complicate the discussion. Also important for an accurate determination of the web are deviations from the desired grain shape due to the propellant grain production process. CP grains generally have some taper due to the production process (mandrel taper). Taper normally is not applied to the mandrels of small grains.

3.4   Burning Time Definitions

3.4.1   Beginning and End Burning Times

The motor action time follows from the pressure versus time trace, which starts at the beginning of motor operation, and ends at the end of motor operation (see Figure 14). The burning time is determined from this trace as the period from the moment that all propellant is considered burning till the moment the web is considered consumed. For burning rate determination, the burning time is the appropriate time period to use. The two periods define four moments in time on the pressure vs. time trace. These time points are often referred to by the use of different number or letter subscripts. Two such examples are presented in Table 3.
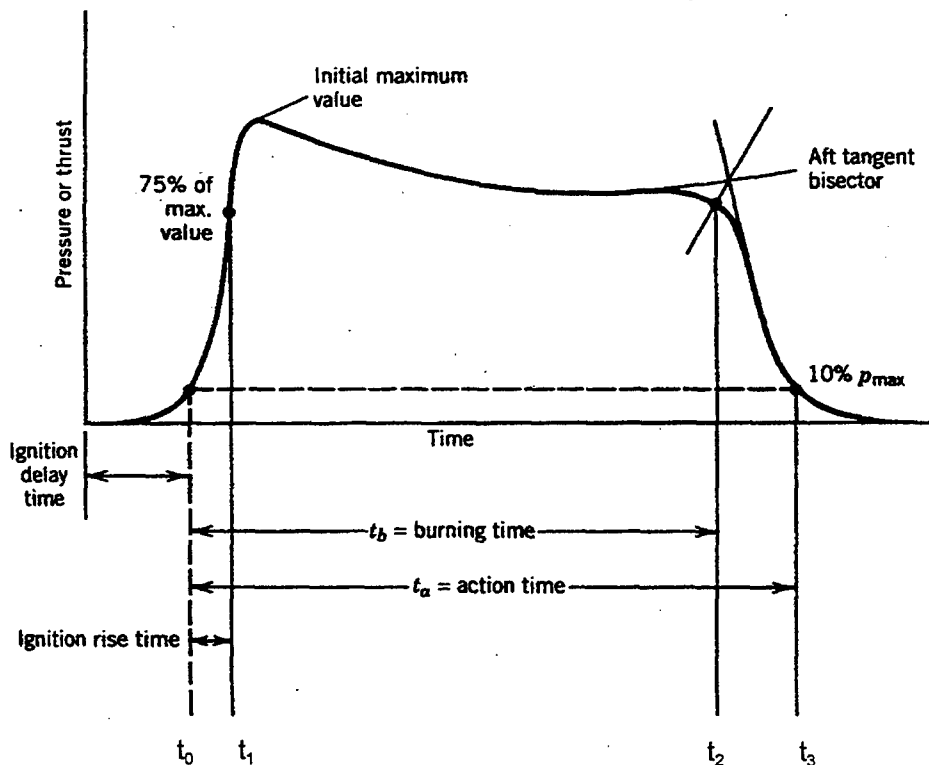
Figure 14. Definitions of the Burning Times

Table 3. Burning Time Definitions

Time point	Variant 1	Variant 2
Beginning of motor operation	t_0	t_A
Beginning of burning	t_1	t_B
Ending of burning	t_2	t_E
Ending of motor operation	t_3	t_G

When Miller and Barrington[62] conducted their review in the late 1960's a number of methods existed for determining the beginning and ending burn times for solid propellant systems. These definitions, listed below in Table 4 for convenience, are illustrated in greater detail in Figure B-23 of Appendix B-22. Miller & Barrington indicated that no one definition seemed to have proved superior in all applications up to the late-1960s.

Table 4. Burning Time Definitions Summarized in Miller & Barrington's 1969 Review

Surface Ignition Time Definitions (Identified on the Pressure Rise of Figure B-23)

1. First pressure raise (point O)
2. The inverse tangent bisector (point A),
3. A fixed pressure or a fixed percentage of the average or maximum pressure (point B),
4. The initial inflection (point C),
5. The forward tangent bisector (point D).

Web Burnout Time Definitions (Identified on the Pressure Decay of Figure B-23)

1. The aft tangent bisector (point E),
2. The point to maximum rate of change of curvature during tailoff (point F),
3. A fixed pressure or fixed percentage of the average or maximum pressure (point G),
4. Point when pressure returns to zero (Point H).

In the US there exist a few basic references[75,76,77], which for years have provided a basic set of reference burning time definitions. These references and their respective definitions are summarized in Table 5. Recent trends identified by the WG016 will be compared with these earlier findings in Section 4.2

Table 5. Historical Sources of Characteristic Time Definitions in US

Time	Definition	References
t_B	**Grain Burning Begins** $0.05\,P_a$ $0.10\,P_a$ 100 psia	 CPIA Pub 174[77] Mil Std 292C[75] Mil Std 292C, CPIA Pub 80[76]
t_E	**Web Burnout Time** Tangent Bisector $0.95 \displaystyle\int_{tB}^{tF} p\,dt$	 CPIA Pub 80, CPIA Pub 174 CPIA Pub 174
t_F	**Action Time Terminus** $0.05\,P_a$ $0.10\,P_{max}$ 100 psia	 CPIA Pub 174 Mil Std 292C, CPIA Pub 80 CPIA Pub 80

The following methods for defining burn time determination are discussed below, viz.:

1) Constant P or %P
2) Tangent-Bisector
3) Brimhall
4) Brooks'
5) Hessler-Glick

These well established methods (and variants) have been used to reduce different sets of pressure-time data within the context of evaluations using simulated motor (discussed in Section 5.0), and real motor (discussed in Section 6.0) behavior.

3.4.2 Constant P or %P

Burning time, $t_b = (t_2 - t_1)$ (Figure 14), may follow from the pressure-time trace by taking the time values at a certain pressure level or a constant percent of some characteristic measured pressure, such as P_{max}. Typical %P_{max} values used by facilities surveyed include 10%, 50%, 60% and 75%, with 10 % of the maximum pressure being used most often. While it is standard in many facilities, experience has shown that 10% may be too soon to start burn time in some test cases. The P_{max} occurring during the test is generally the pressure due to the ignition transient when the combined action of the igniter and the burning propellant yield higher than normal burning pressures. The igniter size will have a considerable effect on P_{max}, however, since the ignition transient is generally fast the effect on the action time may be substantial due to the tail-off. Constant P or %P definitions are often considered ad hoc, and will yield results biased to different degrees. However, burning times based on such definitions do give reproducible results when the definitions are in the steepest portions of the pressure rise or decay.

When a CP propellant grain is used, the maximum pressure may occur somewhere during the experiment, the point which is determined by the L/D ratio of the particular grain. There are many variations to this relatively simple burning time definition, i.e. a different pressure level may be chosen. It is clear that different choices yield different results for the burn rate, particularly due to the tail-off transient. Different results are also obtained for the burn rate vs. pressure relation. For example, if the locations of t_1 and t_2 move respectively to the left and the right, an apparent increase for the burning time results yielding a lower burn rate and a corresponding slightly lower average combustion pressure. This causes the burn rate vs. pressure relation to shift downwards, while possibly affecting the burning rate exponent (e.g. Vieille's relation, Equation 4) as well. Hence, effects occurring during the tail-off transient strongly affect the measurement, as illustrated further below by variations in the grain manufacture process. An advantage of this simple definition is its ease of implementation in software as part of a data reduction procedure.

Unfortunately, the burning time does not begin at the start of web burning since a large portion of the ignition pressure rise is due to ignition material burning. Also the end of the action time does not coincide with the end of web consumption as the tail-off pressure trace includes contributions from stored combustion chamber gases, from burning insulation and liner material and residual propellant sliver as a results of mandrel misalignment or non-ideal grain geometry.

Motors can experience an effect, called "hump" or BARF (Burn Anomaly Rate Factor) effect in motor pressure-time behavior. This effect can create varying challenges for the burning rate analysis methods. This effect is the result of radial variations in burning rate caused by the rheology of the grain manufacturing process, e.g. casting the grain and subsequently plunging the mandrel. The radial variations of burning rate across the propellant web can influence burning rate bias by 4.5%.[70] The "hump" effect will affect the pressure trace, and in particular the value of P_{max}, and hence, affecting any burning time definition relying on P_{max}. Casting with the mandrel in place can essentially eliminate the hump effect, as illustrated in Figure 15, which shows typical pressure-time traces for two manufacturing methods. The influence of grain manufacturing on the scaling of burning rate is discussed more fully in JHU/CPIA CPTR 73.[4]
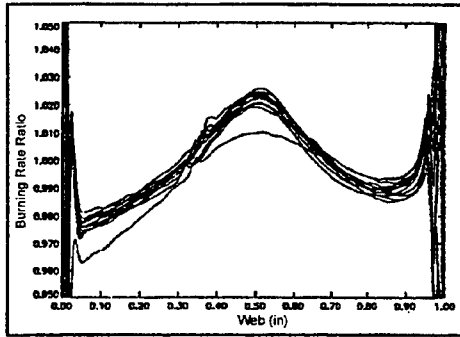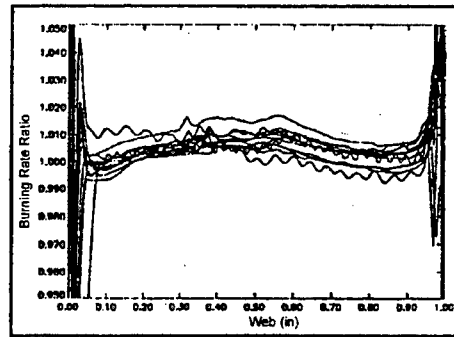
5C3-9 Plunge Cast   5C3-9 Cast with Mandrel in Place

Figure 15. "Hump" Curves for 5-Inch CP Grain with 3-inch Bore, 9 inch Length

3.4.3 Tangent Bisector Method

Defining burning time using the Tangent Bisector method (Figure 16) begins with the identification of the start of burning (typically t_1 is taken at the first 10% P_{max} point). The end of burning is determined in an effort to minimize the effect of the tailoff integral. This is important since the tailoff integral is commonly four to ten time larger than the ignition integral. However, the method neglects tailoff burning, which is the part of the web that continues burning after the anticipated end of burn. While viewed as arbitrary, it is also a historically "consistent" method of evaluating the end of burn.
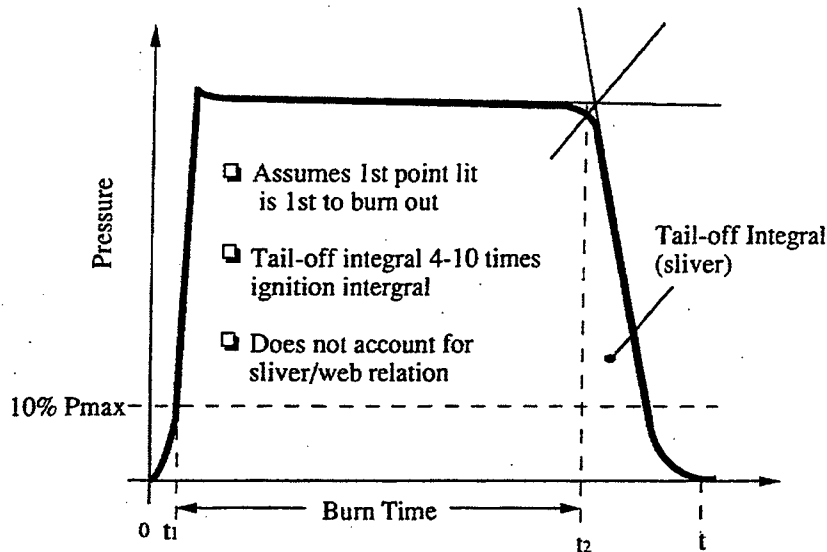
Figure 16. Definitions of Tangent-Bisector Method

Actually, two definable points exist in the burnout process, initial and final burnout. This process begins in the vicinity of the knee of the pressure trace. The Tangent Bisector method really determines the initial burnout point, as do most end of burn time definitions. The method originated in the 1940s when recorders were slow and the knee of the pressure trace looked sharp. As faster recorders came into use and interest in rate accuracy increased, it became obvious the knee was not am sharp corner. As a result, several variants of the bisector method came into being including, bisector of the angle, bisector of the area between trace and tangents, and normal to the trace from the tangents intersection. The Tangent Bisector method usually defines a point in time that represents an arbitrary web burn out point and not the actual burn out point. In particular, non-neutral pressure histories are difficult to reduce due to the varying judgment of the analyst, and can cause up to a 1/2% bias in burning rate variations for the same motor.

34

Different motors might indicate up to a 3% bias in rate because of different grain web shape The Tangent Bisector method may be more difficult to implement in software as part of a data reduction procedure than the constant pressure (or constant %P) definitions. However, the maximum intercept approximation of web bisector is relatively easy to program.

3.4.4 Brimhall Method

Defining burning time using the Brimhall Method again begins with the identification of the start of burning (typically t_1 is taken at the first 10% P_{max} point). The end of burning is determined by identifying an inflection point on the tail-off curve when the second derivative of the pressure, $d^2P_c/dt^2 = 0$ or dP/dt is a positive maximum during tail-off. Typically, this point occurs after the time determined by the Tangent Bisector method. This definition of burning time excludes consideration of the tailoff integral. Tailoff burning with this definition causes problems similar to those experienced using the Tangent Bisector method. Brimhall is an ad hoc definition, with more variation than Tangent Bisector if much variation in web thickness exists. For a given fixed motor manufacturing process with tight grain port alignment, it is more repeatable than the Tangent Bisector. The Brimhall method may be easily implemented in software as part of a data reduction procedure for data that is not noisy. The method fails when pressure histories have multiple inflections or spikes in the tailoff transient. Using a definition involving dP/dt = minimum may avoid this failure.

3.4.5 Brooks' Method

Defining burning time using the Brooks' Method (Figure 17) again begins with the identification of the start of burning (typically t_1 is taken at the first 10% P_{max} point). The end of burning is determined from the pressure integral as defined in Equation 40 below. The end of burning point (t_2) is a correction of the time point determined by the Tangent Bisector method (t_b). This point is corrected using the total pressure integral and a correction term α_p. This definition of burning time does not consider the entire tailoff integral. Tailoff burning with this definition causes problems less than those experienced using either the constant pressure or the Tangent Bisector methods.

$$t_2 = \frac{\int_0^t Pc\ dt}{\int_{t_1}^{t_b} Pc\ dt} * (t_b - t_1) * \alpha_p$$

- Assumes 1st point lit is 1st to burn out
- Tail-off integral 4-10 times ignition intergral
- Does not account for sliver/web relation

Tail-off Integral (sliver)

Pressure

10% Pmax

Burn Time

0 t1   tb t2   t
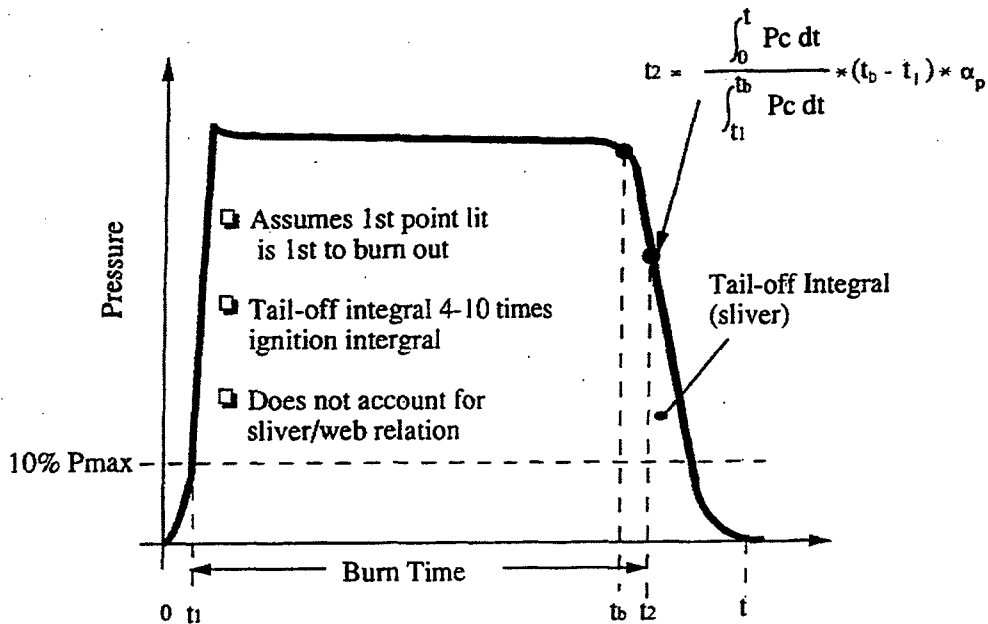
Figure 17. Definitions of the Brooks Method

While the Improved Brooks Method accounts for stored chamber gases and some of the tailoff pressure integral, the Common Brooks Method does not account for the stored gases. Both methods are based on the ratio of the total pressure integral to average pressure over the Tangent Bisector time. Both methods improve burn time calculations as the sensitivity to inaccuracy of the aft-tangent location is reduced.[70]

$$t_2 = \frac{\int_0^{t} p_c \, dt}{\int_{t_1}^{t_b} p_c \, dt} \cdot (t_b - t_1) \cdot \alpha_p \qquad (40)$$

The normal tail-off in a motor varies with pressure at burn out. Therefore, α_p is available and is essentially a linear function of pressure [78], and is defined by

$$\alpha_p = m \cdot P_w + b \qquad (41)$$

Where, P_w is the pressure at web burn out, b is an empirical constant based on data. The slope m is a theoretical value based on the empty chamber volume (V), the molecular mass of the gas (M), the gas constant (R), the flame temperature (T_c) and the total propellant weight (W_p)

$$m = -\frac{M}{R \, T_c \, W_p} \qquad (42)$$

Typical values are $m = 4.83 \cdot 10^{-2}$ Pa^{-1} and $b = 0.97$. The Brooks t_2 of Equation 40 approximates the Hessler-Glick time of $t_{Eavg} = (t_{Ei} + t_{Ei})/2$ discussed in the next section. The Brooks' method is more fully described in Appendix B-9.

3.4.6 Hessler-Glick Method

For determination of the burning rate, the web thickness based on the design dimension, τ_{dsg}, is used[79]. The reason is that τ_{dsg} is accurately defined, even if it is biased slightly.

As to the burning time, the following definitions are suggested:

$$t_{bi} = t_{Ei} - t_B \qquad (43)$$

$$t_{bf} = t_{Ef} - t_B \qquad (44)$$

where the relevant time points are defined as:

- Beginning of Burning t_B : The midpoint of the time interval immediately preceding the first perceptible rise in dp/dt on the last sustained pressure rise to equilibrium motor operation.

- Initial Burnout t_{Ei} : The midpoint of the time interval immediately preceding the negative step to negative value of d^{2}p/dt^2 during the blow down period after the end of equilibrium motor operation.

- Final Burnout t_{Ef} : The midpoint of the time interval immediately preceding the positive step to positive value of d^{2}p/dt^2 at or following the end of equilibrium motor operation.

The burning rate can than be defined using the two burnout times and the design web thickness, as

$$r_{bi} = \tau_{dsg} / (t_{Ei} - t_B) \qquad (45)$$

$$r_{bf} = \tau_{dsg} / (t_{Ef} - t_B) \qquad (46)$$

The reference rates for initial and final burnout represent two independent estimates of rate. They are averaged together to yield the HG burning rate

$$r_{HG} = \frac{r_{bi} + r_{bf}}{2} \qquad (47)$$

The Hessler-Glick method is more fully described in Appendixes B-21 and B-27.

3.5 Average Pressure Definitions

The pressure usually associated with a measured burning rate is the *time-averaged pressure*

$$p_b = \frac{\int_{t_B}^{t_E} p \, dt}{t_E - t_B} \tag{48}$$

However, any measured point $[r_{meas}, p(r_{meas})]$ must simultaneously satisfy also the Vieille[80] burning rate equation $r = ap^n$, which requires use of *rate-averaged pressure*[81, 82, 83]

$$p(r_{meas}) \equiv p_{nb} = \left(\frac{\int_{t_B}^{t_E} p^n \, dt}{t_E - t_B} \right)^{\frac{1}{n}} \tag{49}$$

The rate-averaged pressure p_{nb} is the pressure that should be associated with measured rates. For exponent n less than unity, rate-averaged pressure is less than time-averaged pressure. Consequently, use of time-averaged pressure p_b results in rates corrected to reference pressure that are low. Both the rate correction to reference pressure, Equation 50

$$r_{b-ref} = r_b \left(\frac{p_{ref}}{p_b} \right)^n \tag{50}$$

and the rate-averaged pressure Eqn. 49 require a value of exponent n. This is usually accomplished by performing a least-squares fit of the data to the Vieille rate equation, using the form

$$\ln r_{meas} = \ln a + n \ln p(r_{meas}) \tag{51}$$

For methods using time-averaged pressure, the least-squares fit (Equation 51) is performed one time. For methods using rate-averaged pressure, it is necessary to solve Equations 49 and 51 simultaneously by iteration, if multiple motors with the same rate equation are available. An iteration beginning with the time-averaged pressure as the starting point (which corresponds to an initial guess of $n = 1$) typically converges in three to five steps.

The average pressure for each burnout time for the HG burning rate method is the rate-averaged pressure, viz.:

$$p_{nbi} = p(r_{bi}) = [(\int_{tbi} p^n dt) / t_{bi}]^{1/n} \tag{52}$$

$$p_{nbf} = p(r_{bf}) = [(\int_{tbf} p^n dt) / t_{bf}]^{1/n} \tag{53}$$

Actually, to carry out the above analysis, an estimate of the pressure exponent is required to determine both rate-averaged pressure and for carrying out the correction to the reference pressure. The value for the pressure exponent may be obtained from historical data, or from a rapidly converging iterative procedure when at least two motors are available at the same initial temperature but different pressure.

3.6   Comparison of Analysis Methods

Many r_{TOT} methods do not explicitly account for non-instantaneous burnout. In fact, r_{TOT} methods typically define end of burning as the knee of the curve (web burnout), when the experimental pressure trace begins to fall rapidly near the end of motor operation. However, specific choices of time points may make the correction implicitly. Methods that define end of burning near 50% pressure implicitly assume burning continuation and thus partially avoid non-instantaneous burnout error, but not as well as an r_{MB} definition that actually uses the integral ratio. Due to transient operations, these r_{TOT} methods tend to behave essentially like r_{MB} methods. While use of 50% pressure time points for start of burning only has small effect on burning rate, the choice of 50% or more for end of burn during pressure decay can be a source of higher rate bias. A drawback of a 50-50 definition is that the time-averaged pressure differs much more from the rate-averaged pressure because the ending points are much lower down the tailoff curve than for an equilibrium or web-knee definition. More bias in burning rate is introduced, as the rate-averaged pressure is seldom used.

r_{MB} methods yield rates that are systematically low by a mass storage error. In turn, mass storage error also introduces a systematic nonlinearity in measured $r_b(p)$. Methods essentially behaving like r_{MB} are likewise low by a mass storage error and generate similar nonlinearities. HG fully avoids the mass storage error, so it will be linear and systematically yield higher rates than r_{MB} methods. r_{TOT} methods with instantaneous burnout also avoid the mass storage error yielding negligible nonlinear errors but high bias due to non-instantaneous burnout.

4.0   INTERNATIONAL SURVEY OF ANALYSIS METHODS AND DEFINITIONS

The burning rate analysis methods and definitions used by the international solid propellant rocket industry are summarized and discussed in this section. Over 20 facilities from 7 NATO member countries were surveyed to identify the methods and definitions used and their characteristics. This represents a complete survey of all the international facilities involved in burning rate measurement, and is a thorough representation of the fundamental methods used in the solid propulsion community today. Two conceptually different families of methods for burning rate determination exist, as indicated in Section 3.0. Each family incorporates a number of different definitions and methods to determine the burning rate of a solid propellant from a small-scale rocket motor firing. These analysis methods were examined using multiple round robins involving simulated motor data (Section 5.0) and real motor data (Section 6.0). Comparison of the methods and their relative accuracy are discussed. Small motor data quality, including uncertainty and error analysis, is reviewed in Section 7.0.

Subscale rocket motors and batch check motors are used in a number of countries to measure the burning rate of experimental propellants and commercially produced propellants. These motors differ in construction and means of operation. The reader is referred to JHU/CPIA CPTR 74[5] for an account of the different types used by the various facilities and countries.

4.1   Review of Historical Surveys

Our understanding of analysis methods can be improved by first examining the trends in practices employed within the solid propulsion industry. The examination of three historical surveys can contribute to this insight, one conducted by Miller and Barrington[62] in the late 1960s, a second conducted by Brooks and Hermsen[84] in the late 1970s, and the last by Fry[85] in the mid 1990's.

When Miller and Barrington conducted their review in the late 1960's the fundamental thickness/time burning rate (r_{TOT}) procedure for calculating solid propellant burning rates was the widely held practice. While web w_b was readily measured, establishment of t_b involved the identification of surface ignition time and web burnout time on the pressure-time trace, as summarized previously in Table 4. and shown in Appendix B-22, Figure B-19. Miller and Barrington reviewed several definitions for t_b, but indicated no one method seemed to have proven superior in all applications. Miller and Barrington indicated in their review that, based upon data provided by Brooks, using pressure integrals for determining the burning time may minimize motor-to-motor variation (e.g. due to sliver or nozzle erosion effects on tail-off). This was of course the rationale for the original development of the mass balance burning rate (r_{MB}) methods for

38

calculating solid propellant burning rates. Fry indicated trends in the U.S. suggest the fundamental TOT methods are being replaced by MB methods or TOT methods incorporating an improved method for accounting for non-ideal tailoff in the burning time determination.

Brooks and Hermsen[84] reported on a survey of U.S. facilities conducted in 1979 for the purpose of establishing standardized analysis methods. Fifteen of the 23 U.S. facilities contacted responded indicating both fundamental thickness/time burning rate (r_{TOT}) and mass balance burning rate (r_{MB}) methods were in use for calculating solid propellant burning rates. All respondents except one indicated they used the aft tangent bisector as at least one method, and most used it as their principal method to define end of burn. A constant $\%P_{max}$ was the next most common method, followed by other methods such as maximum dP/dt in the tailoff. Web was measured by some and considered constant by some. Results showed more reliance was being made on the use of pressure integrals for determining the burning time. The principle here was the calculated value of average pressure is more insensitive to the judgment of the analyst and the tailoff. Two means of defining burning time based on average pressure were in use

1. Normalized burning time

$$t^{\cdot} = \int_{total} \frac{Pdt}{\overline{P}_b}$$

(54)

$$r^{\cdot} = \frac{w_b}{t^{\cdot}}$$

(55)

This approach produces better results for good pressure-time traces, or when $\int Pdt = 0$ in the tailoff.

2. Nominal fraction of burning time

$$t_c = \alpha_p \int_{total} \frac{Pdt}{\overline{P}_b}$$

(56)

$$r_c = \frac{w_b}{t_c}$$

(57)

This approach can accommodate cases where $\int Pdt \neq 0$ in the tailoff. It also produces results identical to the first method for good pressure-time traces.

4.2 Current NATO WG016 Survey

Our understanding of analysis methods is further improved by examining the current practices employed by the over 20 facilities from 7 NATO member countries surveyed by the WG016. An overview of data analysis methods is given in Table 6. This table summarizes the source of the method by country and facility, the fundamental type and the location in Appendix B of a detailed description of the method.

A detailed examination of Appendix B provides insight into the methods and key definitions used by those surveyed, and are summarized in Table 7. This table summarizes the source of the definitions by country and facility, the fundamental method type, and definitions for start burn time, end burn time and method used to determine it, how web or mass was defined and the averaging method used for the pressure integrals. Table 8 summarizes the frequency of use of the methods and definitions given in Table 6. The data show the European facilities universally employ the fundamental thickness/time method, while the thickness/time and mass balance methods are used almost equally in the U.S./Canada. Internationally, the survey indicates a preference toward the thickness/time method. This is deceiving, as almost half of the European countries survey also use an end of burn time definition based upon the pressure integral in the tailoff, thus mitigating inaccuracies that can typically accompany thickness/time methods for non-ideal pressure-time tailoff behavior. Some facilities use multiple methods for different type of motors or as prescribed by the customer. The vast majority of facilities surveyed define start of burn time by either a

constant P or a constant %P, as shown in Table 8. Two reference methods from the U.S., Hessler & Glick and the various others surveyed by Miller & Barrington use slightly more rigorous definitions such as those involving dP/dt or forward tangent bisector in the pressure rise. Some facilities use more than one definition. On the other hand, a wider variety of definitions are in practice for defining the end of burn time. Sixteen of the 25 facilities surveyed use a more rigorous definition for the end of burn time, involving the pressure integral, a simple Brimhall d^2P/dt^2 (NAWCWD), or a more complex use of d^2P/dt^2 (Hessler-Glick). As such, these facilities are seeking to account of inaccuracies typically associated with non-ideal pressure-time tailoff behavior. Another 8 of the 25 facilities surveyed use an end of burn time defined by a standard tangent bisector procedure or tangent bisector corrected by a constant close to 1. The remaining 3 facilities simply use a constant %P to determine the end of burn time. A majority of the facilities, therefore, have determined greater rigor should be exercised in determining the end of burn time. Generally all facilities use a constant web value, either measured or taken from a drawing. Finally, the vast majority of the facilities use time-averaged, rather than rate-averaged pressure. The advent of faster more capable computers should make rate-averaged pressure a more attractive means of reducing rate bias up to an additional ½%.

Table 6. Summary of Data Analysis Methods (Refer to Appendix B)

COUNTRY	FACILITY	METHOD TYPE[1]	APPENDIX B
CANADA	DREV	R_{TOT}	B-1
FRANCE	SNPE / ONERA	R_{TOTn}	B-2
GERMANY	BAYERN-CHEMIE	R_{TOT}	B-3
ITALY	FIAT AVIO	R_{TOTn}	B-4
NETHERLANDS	TNO-PML	R_{TOT}	B-5
UNITED KINGDOM	RORM	R_{TOT}	B-6
UNITED STATES	AEROJET	R_{TOT}, R_{MB}	B-7
	AFRL / PLE	R_{TOT}	B-8
	ALLIANT TECH SYSTEMS	R_{MB}	B-9
	AMCOM	R_{MB}	B-10
	ATLANTIC RESEARCH CORP	R_{MB}, R_{MBn}	B-11
	BF GOODRICH / UNIV PROP	R_{TOT}	B-12
	GD / ORDNANCE & TACT SYS	R_{TOT}	B-13
	NAWCWD CHINA LAKE	R_{TOT}, R_{MB}	B-14
	NSWC	R_{MB}	B-15
	P&W / CSD	R_{MB}	B-16
	SNAP / JORDAN	R_{MBn}	B-17
	STONE ENGINEERING	R_{MBn}	B-18
	TALLEY DEFENSE SYS	R_{TOT}	B-19
	THIOKOL PROPULSION	R_{TOT}, R_{MB}	B-20
REFERENCE	HESSLER/GLICK (HG)	R_{HG}	B-21
	MILLER & BARRINGTON	R_{TOT}, R_{MB}	B-22
	FUNDAMENTAL METHODS		
	1) Thickness/Time Rate (R_{TOT})		B-23
	2) Iterated Thickness/Time Rate (R_{TOTn})		B-24
	3) Mass Balance Rate (R_{MB})		B-25
	4) Iterated Mass Balance Rate (R_{MBn})		B-26
	5) Iterated Two-Point Thickness/Time Rate (R_{HG})		B-27

---

[1] Methods Defined in Reference Category, Fundamental Methods

Table 7. Summary of Burning Rate Analysis Methods and Definitions

COUNTRY	FACILITY	ANALYSIS METHOD	Start Burn — Time	Time	End Burn — Method	Time	Web / Mass	Pressure
CANADA	DREV	r_{TOT}	0.7 MPa	0.98 P_{mf}[2]	T-B[3] Corrected by a constant		Constant web	Time-averaged
FRANCE	ONERA	r_{TOTn}	50% P_e[4]	50% P_e	Pressure integral over burn time		Effective, calc.	Time-averaged
	SNPE	r_{TOTn}	50% P_e	50% P_e	Pressure integral over burn time		Effective, calc.	Time-averaged
GERMANY	BAYERN-CHEMIE	r_{TOT}	50% P_a[5]	50% P_a	Constant % of P_a		Constant web	Time-averaged
ITALY	FIAT AVIO	r_{TOTn}	50% P_e	50% P_e	Pressure integral over burn time		Effective, calc.	Time-averaged
NETHERLANDS	TNO-PML M1	r_{TOT}	10% P_{max}	10% P_{max}	Constant % of P_{max}		Constant web	Time-averaged
	M2	r_{TOT}	2.5 MPa	Mod T-B	Modified T-B		Constant web	Time-averaged
UNITED KINGDOM	RORM	r_{TOT}	10% P_{max}	T-B	T-B		Constant web	Time-averaged
UNITED STATES	AEROJET	r_{TOT}	10% P_{max}	T-B	T-B		Constant web	Time-averaged
	AFRL / PLE	r_{TOT}	60% P_{max}	60% P_{max}	Constant % of P_{max}		Constant web	Time-averaged
	ALLIANT TECH SYS M1	r_{MB}	10% P_{max}	Mod T-B	T-B Corrected by PI w/o storage corrections		Constant mass	Time-averaged
	M2	r_{MB}	10% P_{max}	Mod T-B	T-B Corrected by PI w storage corrections		Constant mass	Time-averaged
	AMCOM	r_{MB}	10% P_{max}	Mod PI[6]	Pressure integral over burn time		Constant mass	Time-averaged
	ARC M1	r_{MB}	10% P_{max}	Mod PI	Pressure integral over burn time		Constant mass	Time-averaged
	M2	r_{MBn}	10% P_{max}	Mod PI	Pressure integral over burn time		Constant mass	Time-averaged
	BF GOODRICH / UP	r_{TOT}	10% P_{max}	T-B	T-B		Constant web	Time-averaged
	NAWCWD M1	r_{TOT}	60% P_{max}	Brimhall	Brimhall, d^2P/dt^2 = maximum in tailoff		Constant web	Time-averaged
	M2	r_{MB}	60% P_{max}	Mod PI	Pressure integral over burn time		Constant mass	Time-averaged
	NSWC	r_{MB}	10% P_{max}	Mod PI	Pressure integral over burn time		Constant mass	Time- & Rate-averaged
	P&W / CSD M1 & M2	r_{MB}	10% & 75% P_{max}	PI < constant	Pressure integral < Constant in tailoff		Constant mass	Time-averaged
	SNAP / JORDAN	r_{MBn}	10% P_{max}	Mod PI	Pressure integral over burn time		Constant mass	Time-averaged
	STONE ENGIN	r_{MBn}	10% P_{max}	Mod PI	Pressure integral over burn time		Constant mass	Time-averaged
	TALLEY DEFENSE	r_{TOT}	10% P_{max}	T-B	T-B		Constant mass	Time-averaged
	THIOKOL PROP M1	r_{TOT}	10% & 50% P_{max}	T-B	T-B		Constant web	Time-averaged
	M2	r_{MB}	10% & 50% P_{max}	T-B	T-B		Constant mass	Time-averaged
REFERENCE	HESSLER / GLICK	r_{HG}	Fwd $+dP/dt$	Aft d^2P/dt^2	Inflection in d^2P/dt^2 in tailoff		Constant web	Rate-averaged
	MILLER & BARRINGTON	r_{TOT}, r_{MB}	Various	Various	Various (See Appendix B-22)		Various	Time-averaged

---

2   P_{mf}, Pressure at burnout
3   T-B, Tangent-Bisector
4   P_e, Average effective pressure over burning time
5   P_a, Average chamber pressure over action time
6   Initial estimate of end of burn time modified by Pressure Integral

Table 8. Summary of Frequency of Use of Analysis Methods and Burn Time Definitions

ANALYSIS METHOD		
Geographic Region	Thickness/Time (r_{TOT})	Mass Balance (r_{MB})
European	7	0
U.S. / Canada	8	10
Total	15	10

BURNING START TIME DEFINITION							
Geographic Region	Constant %P				Constant P	Other	
	10%	50%	60%	75%		dP/dt	Various
European	2	4	-	-	2	-	-
U.S. / Canada	13	2	3	1	-	1	1
Total	15	6	3	1	2	1	1
Total	27					2	

BURNING END TIME DEFINITION								
Geographic Region	Constant %P	T-B	T-B Corrected by		Pressure Integral (PI)	Other		
			Constant	PI		Brimhall	d^2P/dt^2	Various
European	2	2	1	-	3	-	-	-
U.S. / Canada	1	5	-	2	8	1	1	1
Total	3	7	1	2	11	1	1	1
Total	11				16			

43

5.0   ASSESSMENT OF METHODS USING SIMULATED MOTOR DATA

During the working period of RTO/AVT WG016 assessments were made of the various thickness/time and mass balance analysis methods taken from the international survey. The objectives of these assessments were to:
- Clarify distinctions of small motor analysis methods
- Identify sources of the differences

The assessment approach involved using both simulated and real motor data as described earlier in Section 1.3. Table 9 summarizes the scope of these assessments and the degree of involvement by the volunteer participants. The assessment using simulated motor data involved carrying out four Round Robin evaluations as described and discussed in this section. The assessment using real motor data is discussed in Section 6.0. The Round Robin analyses were carried out with the objective of comparing the results of the various analysis methods as they are commonly used in Canada, France, Germany, Italy, The Netherlands, UK and the U.S. and the various organizations in these countries. Each Round Robin was essentially carried out as a blind experiment, where individual participants were given minimal knowledge of the motor geometry and no information on the propellant-burning rate behavior. Simulation programs were used, or if not available developed, to generate the Round Robin pressure versus time data. It was argued that an accurate knowledge of the input burning rate data was useful for comparison with the results obtained from the data reduction.

The discussion of each Round Robin evaluations is organized beginning with a description of its design, followed by a presentation of the analysis results, and closing with conclusions. Design details of each Round Robin are provided in Appendix C. Typical results are discussed relative to reference burning rates r_7 and r_{10} (burning rates at respectively 7 and 10 MPa (50 and 70 psi)), the burning rate coefficient a and exponent n of the power law relation, the reduced burning rate data (used to obtain power law relation) and their relation to the input reference values used to generate the Round Robin data.

The design and execution of the Round Robin #1 and #2 simulations were found to embody properties that placed limitations on the conclusions that could eventually be drawn from the results. These issues are reviewed individually with the discussion of each Round Robin. As a result two final Round Robins #3 and #3X were designed and executed to overcome these shortcomings.

Table 9. Burning Rate Analysis Round Robin Summary

COUNTRY	FACILITY[7]	ANALYSIS METHOD[8]	ROUND ROBINS PARTICIPATION[9]			
			RR #1	RR #2	RR #3 Groups1,2	RR #3x Groups 3-10
CANADA	DREV	r_{TOT}			✔	
FRANCE	ONERA	r_{TOTn}	✔	✔		
	SNPE	r_{TOTn}	✔	✔	✔	
GERMANY	BAYERN-CHEMIE	r_{TOT}	✔	✔	✔	
ITALY	FIAT AVIO M1 & M2	r_{TOTn}	Experimental P-t motor data only			
	POLIMI[10]					
	BAYERN-CHEMIE	r_{TOT}			✔	✔
	HESSLER/GLICK	r_{TOTn}			✔	✔
	BAYERN-CHEMIE	r_{TOT}	Experimental P-t motor data			
	SNPE	r_{TOTn}	Experimental P-t motor data			
	POLIMI Mass Balance	r_{MB}	Experimental P-t motor data			
	FIAT AVIO M1 & M2	r_{TOTn}	Experimental P-t motor data			
	HESSLER/GLICK	r_{TOTn}	Experimental P-t motor data			
NETHERLANDS	TNO-PML M1	r_{TOT}	✔	✔	✔	
	M2	r_{TOT}	✔	✔	✔	
	M2[11]	r_{TOT}				✔
	TNO-PML M1[12]	r_{TOT}	Experimental P-t motor data			
	BC	r_{TOT}	Experimental P-t motor data			
	HESSLER/GLICK	r_{TOTn}	Experimental P-t motor data			
UNITED KINGDOM	RORM	r_{TOT}		✔	✔	
UNITED STATES	AEROJET	r_{TOT}	✔			
	ALLIANT TECH SYS M1	r_{MB}	✔		✔	
	AMCOM	r_{MB}			✔	
	ARC M1	r_{MB}			✔	
	BF GOODRICH / UP	r_{TOT}			✔	
	NAWCWD M2	r_{MB}		✔	✔	
	NSWC	r_{MB}	✔	✔	✔	
	P&W / CSD	r_{MB}		✔	✔	
	SNAP / JORDAN	r_{MBn}	✔	✔	✔	
	STONE ENGIN	r_{MBn}			✔	
	TALLEY DEFENSE	r_{TOT}	✔			
	THIOKOL PROP	r_{TOT}	✔		✔	
REFERENCE	HESSLER / GLICK	r_{HG}, r_{TOTn}	✔	✔	✔	✔

[7] WG016 member facilities ONERA, SNPE, BAYERN-CHEMIE, POLIMI, TNO-DML, and RORM
[8] Analysis methods described in Appendix B, and Round Robin Designs described in Appendix C
[9] Participation on volunteer basis, ✔ completed Round Robin
[10] Politecnico di Milano, Dipartimento di Energetica graduate students analyzed RR#3, RR#3X and Real motor data
[11] TNO-PML graduate students analyzed RR#3X data using TNO M2 method
[12] TNO-PML graduate students analyzed Real Motor data using selected methods

5.1 International Round Robin #1 Results

Round Robin (RR) #1 is based on GasGen Version 2.0 ('93). GasGen is a spreadsheet program based on a relatively straightforward simulation logic developed by WG016 member Dr. Robert Frederick at UAH, U.S. Propellant burning rate and other propellant data, and propellant geometry data form the input. Details of RR#1 design and input data are summarized in Appendix C-1. A simple endburning grain as shown in Figure C-1 of Appendix C was simulated. RR#1 consists of four pressure-time traces for the cases listed in Table 10.

Table 10. RR #1 Small Motor Ballistic Simulations Examined

Group	Cases	Perturbation
1	1	Neutral - Baseline
	2	Progressive
	3	Regressive
	4	Progressive with noise added

Pressure-time behavior for these cases is given in Figure 18.
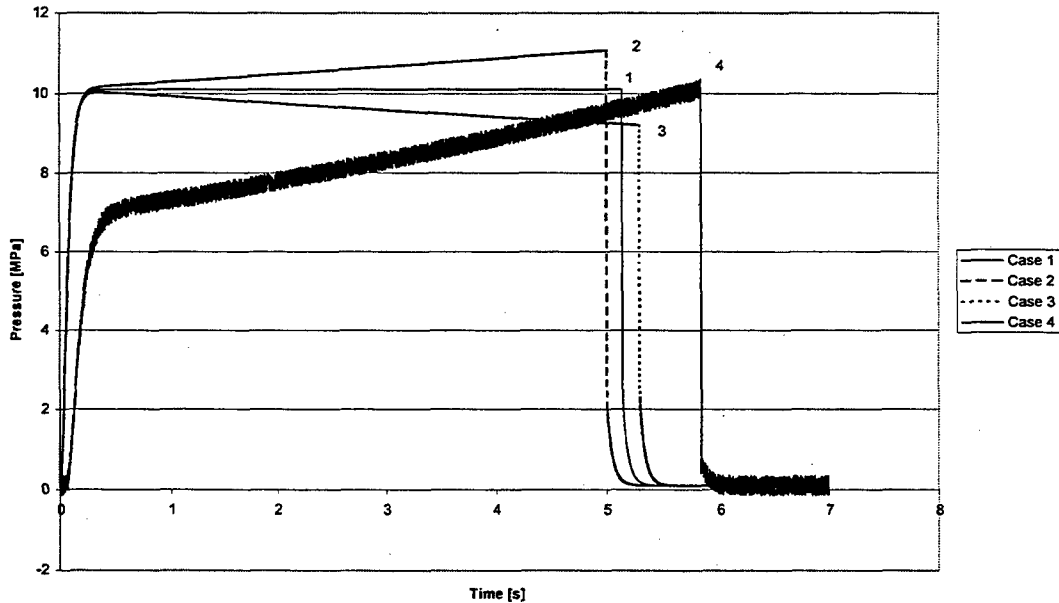
Figure 18. Pressure versus Time Traces for the Round Robin #1 Cases

The first three cases have similar pressurization rates while the fourth case has slower pressurization. Moreover, the noise added to case 4 had peak-to-peak amplitude of about 5%. Routine measurements of different batch check motors revealed a typical noise level ranging from 0.1 through 0.4% of the motor pressure, which is an order less. When due attention is given to the experimental setup through instrument shielding and grounding provisions, a level of 0.05% (two orders less) of motor pressure is achievable [86].

5.1.1 Round Robin #1 Analysis

The RR #1 data was supplied to a number of U.S., French, German, UK and Netherlands companies/organizations. Each participant was asked to analyze the data using their preferred method(s) and determine the average burning rate and average pressure. Analysis results for RR #1 data were received from the following eleven volunteer participants as shown in Table 9, including SNPE, ONERA, Bayern Chemie (BC), TNO-PML, Aerojet, Alliant Tech Systems, (formerly Hercules), Hessler-Glick (HG), F. Jordan/ SNAP, NSWC, Talley Defense Systems, and Thiokol. The methods used to analyze the data

and determine the (average) propellant burning rates were mainly thickness/time (TOT) methods, with a Alliant Tech, Jordan and NSWC using mass balance (MB) methods as summarized in Table 9. A typical set of results using the HG method for all cases is summarized in Table 11.[86] Table 12 compares the correlations of the data as obtained using the commonly employed power law relation for the RR #1 participants. The differences in results are clearly shown in Figure 19 where the burning rate at 7 MPa (r_7) and 10 MPa (r_{10}) relative to the reference (or input) rate are plotted for each organization.

Table 11. Typical Burning Rate Analysis Results NATO RTO/AVT WG016 RR #1[86]

HG Method	RR#1 Cases			
	1	**2**	**3**	**4**
Burn Time, s	5.142	5.002	5.290	5.783
Burning Rate, mm/s	19.6255	20.1748	19.0764	17.4502
Iterated Exponent	0.58661			
Average Pressure, MPa	9.91154	10.3656	9.4599	8.1172
Reference Rate at 10 MPa	19.7195			
Reference Rate, mm/s	19.7146	19.7389	19.6951	19.7295
Deviation	-0.025%	+0.098%	-0.124%	+0.051%

Table 12. RR #1 – Power Law Relations Obtained from Correlating the Received Data

Country / Company	Coefficient		Exponent		Burning Rate			
	a	$\dfrac{a}{a_{ref}} - 1$	**n**	$\dfrac{n}{n_{ref}} - 1$	r_7	$\dfrac{r_7}{r_{7,ref}} - 1$	r_{10}	$\dfrac{r_{10}}{r_{10,ref}} - 1$
		%		%	mm/s	%	mm/s	%
Reference	4.8808	0.000	0.600	0.000	15.690	0.000	19.430	0.000
France - SNPE	5.1512	5.540	0.583	-2.767	16.030	2.167	19.740	1.595
- ONERA	4.9593	1.608	0.600	0.000	15.940	1.593	19.740	1.595
Germany - BC	5.2178	6.905	0.578	-3.650	16.070	2.422	19.750	1.647
Netherlands - TNOM1	5.2181	6.911	0.576	-4.083	15.990	1.912	19.630	1.029
- TNOM2	5.1693	5.911	0.582	-3.017	16.040	2.231	19.740	1.595
US - Aerojet	5.5298	13.297	0.559	-6.883	16.400	4.525	20.020	3.037
- Alliant Tech	5.0549	3.567	0.592	-1.417	15.980	1.848	19.730	1.544
- Hessler	5.1106	4.708	0.587	-2.233	16.000	1.976	19.720	1.493
- Jordan/SNAP	4.1378	-15.223	0.680	13.333	15.540	-0.956	19.810	1.956
- NSWC	5.3063	8.718	0.569	-5.150	16.060	2.358	19.670	1.235
- Talley DS	4.6736	-4.245	0.624	3.950	15.730	0.255	19.650	1.132

Figure 19 and Table 12 indicate the burning rate is generally over-predicted by 2-4.5%, with the majority of the participants showing a 1-2% deviation.

The power law exponent, shown in Figure 20, is typically under-predicted by 1-5%, with a couple outliers. While the power law coefficient, shown in Figure 21, is typically over predicted b 1-7%. The differences between the 7 MPa and the 10 MPa relative results are due to these observed differences in the power law exponent and coefficient.
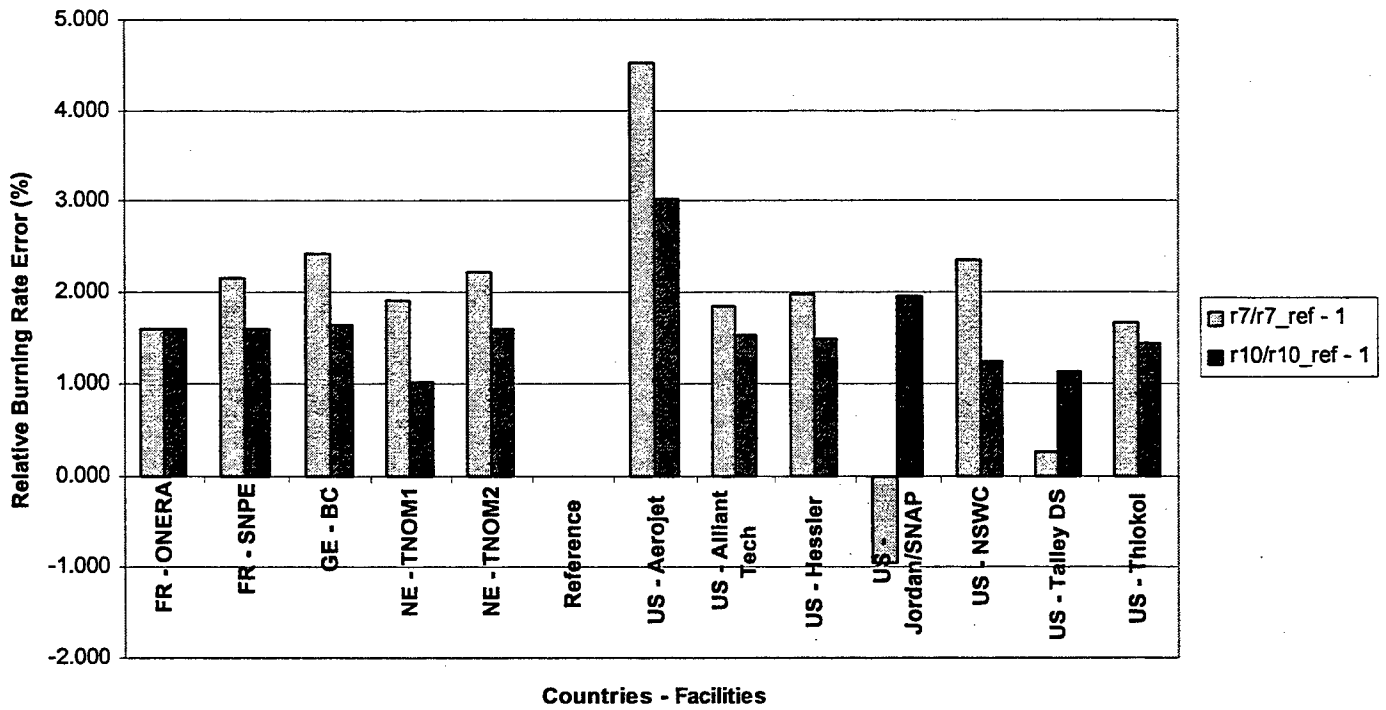
Figure 19. RR#1 - Relative Burning Rate Error (%) at 7 MPa and 10 MPa Reference Pressures
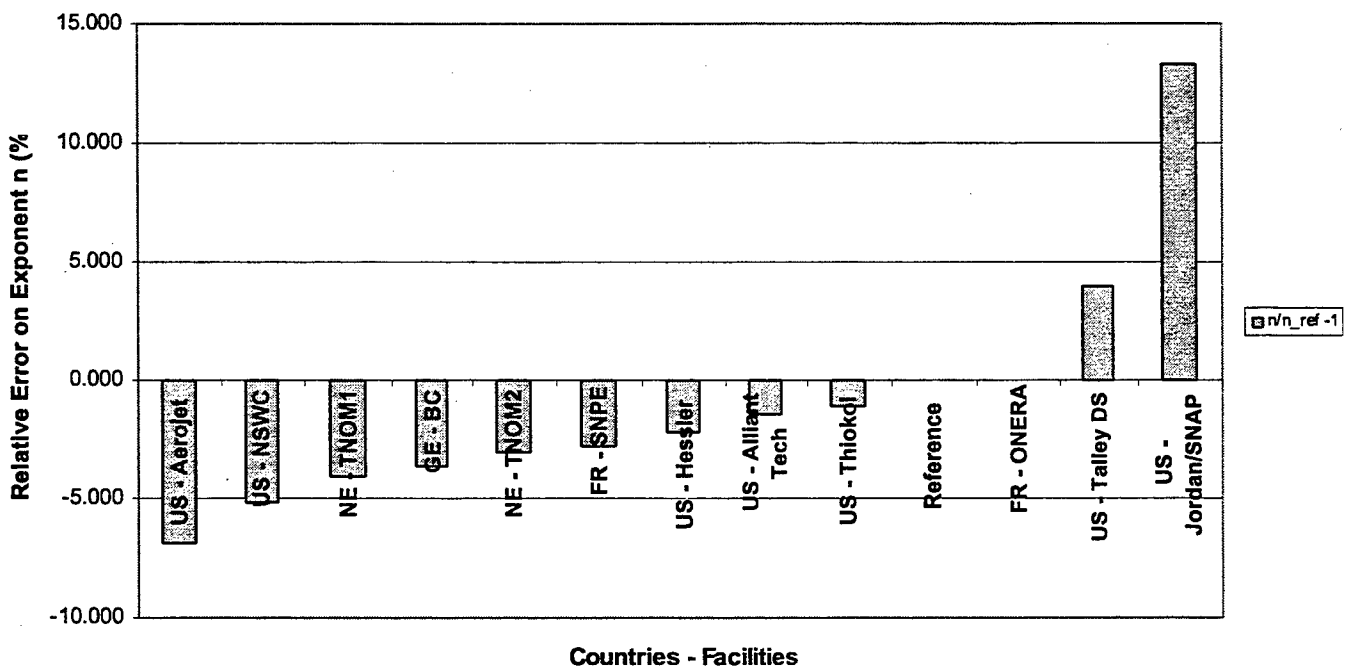
Figure 20. RR#1 – Relative Exponent Error (%) at 7 MPa and 10 MPa Reference Pressures
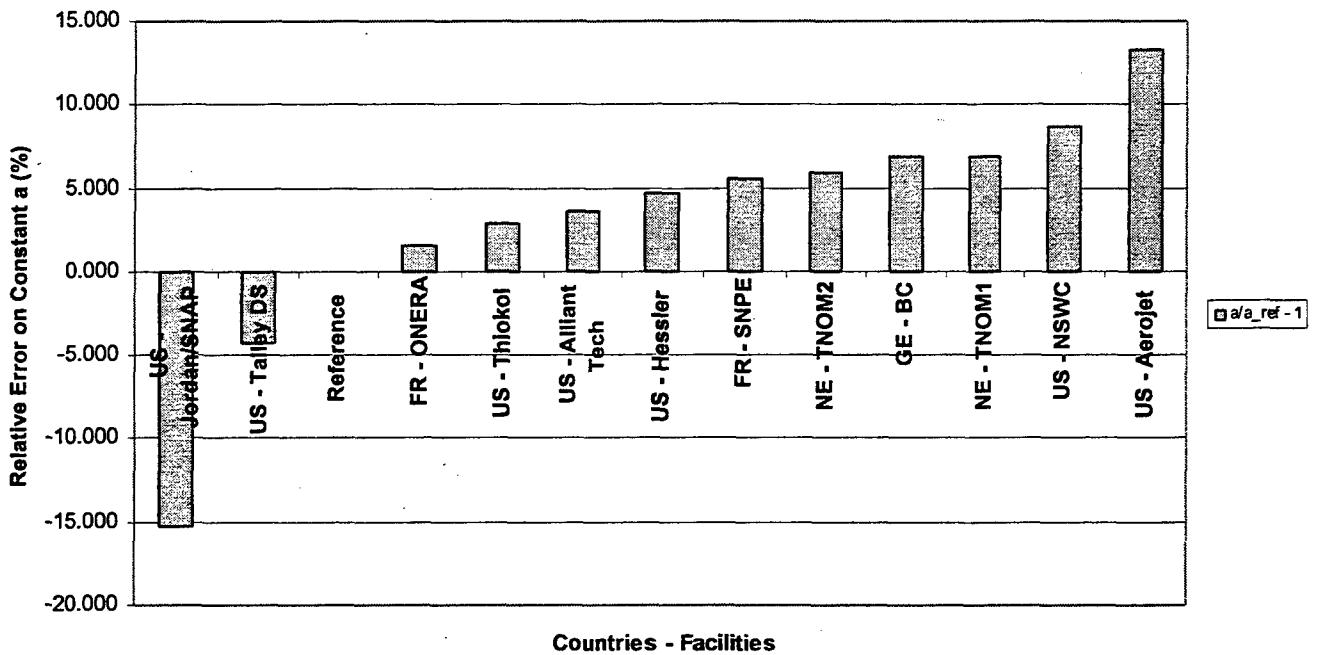
Figure 21. RR#1 - Relative Coefficient Error (%) at 7 MPa and 10 MPa Reference Pressures

All burning rate data from the 4 cases are plotted in Figure 22 on a linear pressure scale, instead of the more common log-log scale to enhance the visibility of differences among the results. Figure 23 shows an expanded section of Figure 22.
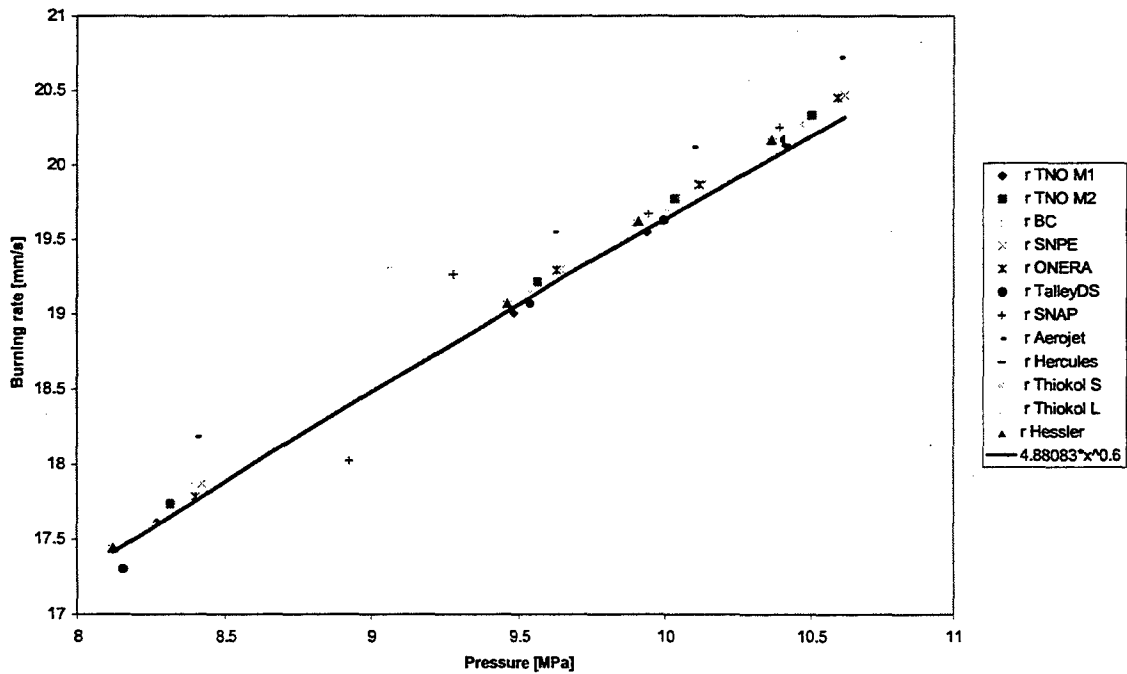
**Figure 22. RR #1 - Burning Rate versus Pressure Behavior for all
4 Cases Compared with Reference**
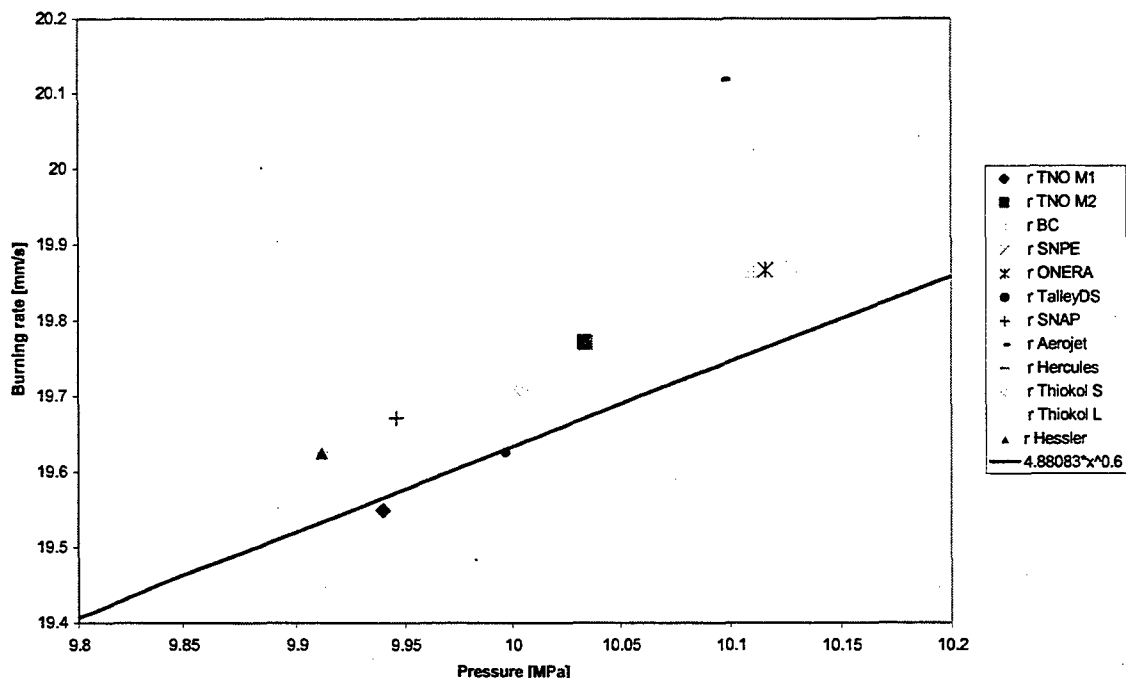
**Figure 23. RR #1 - Burning Rate versus Pressure Behavior for Case 1
Compared with Reference (Expanded Scale)**

The 4 cases are grouped from left to right in Figure 22 corresponding to the average pressures shown in Table 11, viz.: case 4, case 3, case 1 and case 2. Most of the data is grouped together for each case showing small deviations to the reference (line visible in the figure). Each case shows a typical distribution of the result as obtained from the different organizations. The overall trend is in line with the reference data, although the deviation differs from case to case. In general the absolute value of the difference steadily increases from the neutral, to the progressive, to the regressive burning cases. Deviations in the calculated average pressure data are also observed in the range of ±0.2 MPa. Small differences in results between Bayern Chemie, SNPE and ONERA are due to similarities in their analysis methods. The small deviations observed are due to slight differences in the implementation method employed.

5.1.2 Round Robin #1 Conclusions

The design and execution of the round robin simulations were found to embody properties that place limitations on the conclusions that may eventually be drawn from the overall RR#1 results:

1) First, the data covered a limited pressure range (8.1 – 10.4 MPa). Due to this, conclusions on deviations among the burning rate relations in power law form may be of limited value (Table 12) as effects of errors may be exaggerated.

2) By design, burnout in the round robin simulations is instantaneous. This steep decay is normally not observed in real motors and is an artifact of the spreadsheet programming used to generate the data. In reality, the blow-down phase (part of tail-off) exhibits an exponential decaying pressure towards ambient pressure. This exponential decay is modified by heat losses and by the transition from sonic to subsonic flow. This artificially steep decay causes several definitions for end of burning to yield precisely the same answer. Consequently, conclusions on the relative merits of the end of burning definitions are unwarranted.

3) In execution, an error was introduced in pressure during blowdown after burnout. This causes errors in the pressure integrals, upon which various Mass Balance definitions of burning rate rely. This error will also carry into the time calculations used by any method relying on the

50

determination of a total pressure integral. Consequently, conclusions on the relative merits of Thickness/Time and Mass Balance burning rate definitions are unwarranted.

4) By design, one of the simulations included 0.5 MPa of simulated instrumentation noise. This unrealistic noise level (12 to 50 times more than recent data, 100 times larger than good instrumentation) undoubtedly produces artificial burning rate errors in this particular simulation. This particular simulation is pivotal in pressure exponent calculations because of its relative isolation in rate-pressure space, and error due to the noise will unduly influence the calculated exponent. Consequently, conclusions on the relative merits of time-averaged and rate-averaged pressures in burning rate correlations may be compromised for Case 4.

5) Presentation of the raw simulation data results in a minor (0.01%) ambiguity in web thickness burned.

Table 13. RR #1 - Variation of Exponent and Reference Rate with Mean Pressure   Definition and Burn Time Definition[86]

Analysis using Time-Averaged Pressure

Burn Time Definition	Exponent	Ref Rate at 10 MPa
P'min > Web	0.60098	19.67022
0% > Web	0.61608	19.66935
10% > Web	0.59337	19.70866
50% > Web	0.55207	19.82397

Analysis using Rate-Averaged Pressure

Burn Time Definition	Exponent	Ref Rate at 10 MPa
P'min > Web	0.58661	19.71948
0% > Web	0.58951	19.71893
10% > Web	0.58337	19.73279
50% > Web	0.54536	19.83056

Despite these limitations however, some conclusions may be drawn regarding beginning of burning rate definitions for thickness/time methods, and time-averaged versus rate-averaged pressure definitions. Both reference rate and exponent are significantly affected by the definitions used to detect the beginning of burn time as illustrated in Figure 24, which represents data provided in Table 13. The quasi-rigorous definition using the first derivative minimum yields approximately the lowest rate and highest exponent (labeled Theory). The definitions based on fractions (0%, 10%, and 50%) of P_{max} are ad hoc definitions resulting in modified values. The average pressure used in the referencing calculation also affects reference rate and exponent appreciably. Reference rate values based on the theoretically defined time-averaged pressures (circles) are higher than those based on rate-averaged pressure (Xs), while the pressure exponents are lower for time-averaged than for rate-averaged pressures.
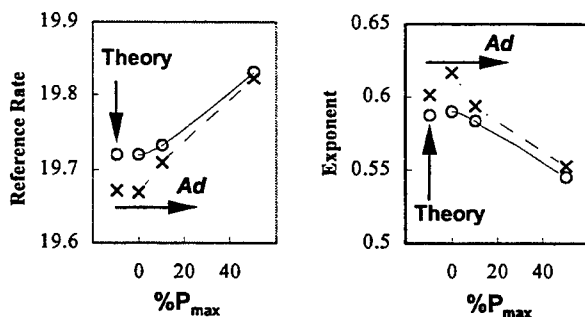
Figure 24. Measured Reference Rate at 10 MPa and Exponent versus Pressure Level at Beginning of Burning Definition[86]

Table C-1 of Appendix C presents the reduced data from the RR #1 simulations using several different start burn time definitions. Data tabulated for each simulation includes burn time, burning rate, and time-averaged and rate-averaged pressures. The data supports the sensitivity of burning rate and average pressures to the beginning of burn time definitions discussed above. Following the identification of these findings and shortcomings, a second Round Robin was designed, distributed and the results are discussed in next section.

5.2 International Round Robin #2 Results

Round Robin #2 is based on using the Solid Performance Program (SPP) Version 7.0 to simulate simple 2x4-inch motor ballistics. The method of approach used by the SPP is to predict solid rocket motor performance by calculating deviations from ideal performance using a series of independent efficiency models. The SPP analysis consists of two parts: nozzle performance and motor performance. The motor performance module, which was used to generate the RR #2 data, contains different design modules (for axisymmetric 2D and 3D grains) and uses an internal ballistics module. Details of the RR#2 design and input data are summarized in Appendix C-2. A simple 2x4-inch motor configuration as shown in Figure C-2 was simulated. RR #2 consists of twelve different simulated pressures-time traces for the cases representing the successive addition of different motor perturbations shown in Table 14.

Table 14. RR #2 Small Motor Ballistic Simulations Examined

Group	Cases	Perturbation
1	1, 2	Baseline
2	3, 4	Baseline with increased L*
3	5, 6	Baseline with added igniter effect
4	7, 8	Baseline with added igniter effect and erosive burning
5	9, 10	Baseline with added igniter effect, erosive burning and nozzle erosion
6	11, 12	Baseline with added igniter effect, erosive burning, nozzle erosion and bore offset

Each pair of cases represents identical motors except for different nozzle sizes used to produce high or low pressure. The same pair of nozzle sizes was used for successive pairs of simulation cases. The input pressure versus time traces are combined and compared in Figure 25. By the nature of the design of the cases, RR #2 actually attempts to answer two kinds of questions:

- The original issue, what is the error associated with a given analysis method?
- What effect does perturbations of motor parameters have?
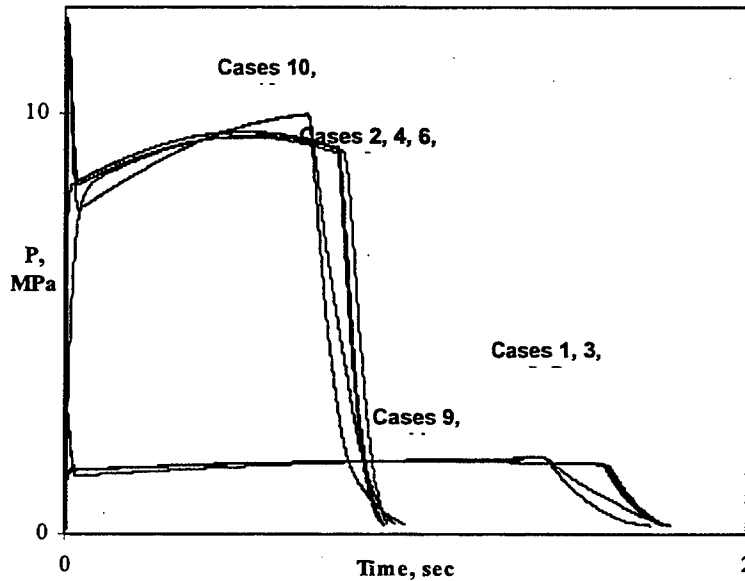
Figure 25. Pressure-Time Behavior for Round Robin #2 Test Cases

5.2.1 Round Robin #2 Analysis

The RR #2 data was supplied to a number of U.S., French, German, UK and Netherlands companies/organizations. Each participant was again asked to analyze the data using their preferred method(s) and determine the average burning rate and average pressure. RR #2 responses were received from the following ten volunteer participants as shown in Table 9, including ONERA, SNPE, Bayern Chemie, TNO-PML, Royal Ordnance, NAWCWD, NSWC, P&W/CSD, SNAP/Jordan and R. Hessler (HG). The methods used to reduce the data and determine the propellant burning rates were thickness/time (TOT) for the European participants, and R. Hessler and mass balance (MB) for the remaining U.S. participants as summarized in Table 9.

Typical RR #2 results are first described using the TNO-PML analysis Method #2 (described in Appendix B-5) to allow as easy comparison of the data cases. Following this, selected results are compared using the preferred analysis methods of the participants. Some results are not shown due to difficulties with the RR #2 design as discussed later.

Summary of Typical Analysis Results for the RR #2 Cases

The results of the TNO-PML analysis are presented in Table 15 The burning rate versus average pressure results for all the cases are plotted in Figure 26 on a log-log scale, while Figures 27 and 28 show respectively the low pressure and the high pressure results enlarged on a linear scale.

Table 15. RR #2 - Typical Burning Rate Analysis Results NATO RTO/AVT WG016[13]

Case Description	Case Number	P_{max} [MPa]	Start $t_{2.5}$[13] [s]	End t_{T-B}[14] [s]	Total t_b[15] [s]	r_{aver} [mm/s]	P_{aver} [MPa]
Baseline	1	1.729	0.05	1.591	1.586	8.008	1.671
	2	9.577	0.05	0.807	0.802	15.835	9.228
Large L*	3	1.729	0.05	1.595	1.590	7.987	1.669
	4	9.481	0.05	0.823	0.817	15.545	9.003
Ignition	5	1.735	0.05	1.585	1.580	8.038	1.688
	6	9.563	0.06	0.803	0.798	15.915	9.298
Erosive Burning	7	1.733	0.05	1.586	1.581	8.033	1.685
	8	9.453	0.05	0.807	0.802	15.835	9.191
Nozzle Erosion	9	1.8103	0.05	1.410	1.405	9.039	1.657
	10	9.998	0.05	0.712	0.707	17.963	9.132
Off-Axis Bore	11	1.8118	0.05	1.420	1.415	8.975	1.659
	12	10.005	0.05	0.722	0.717	17.713	9.150
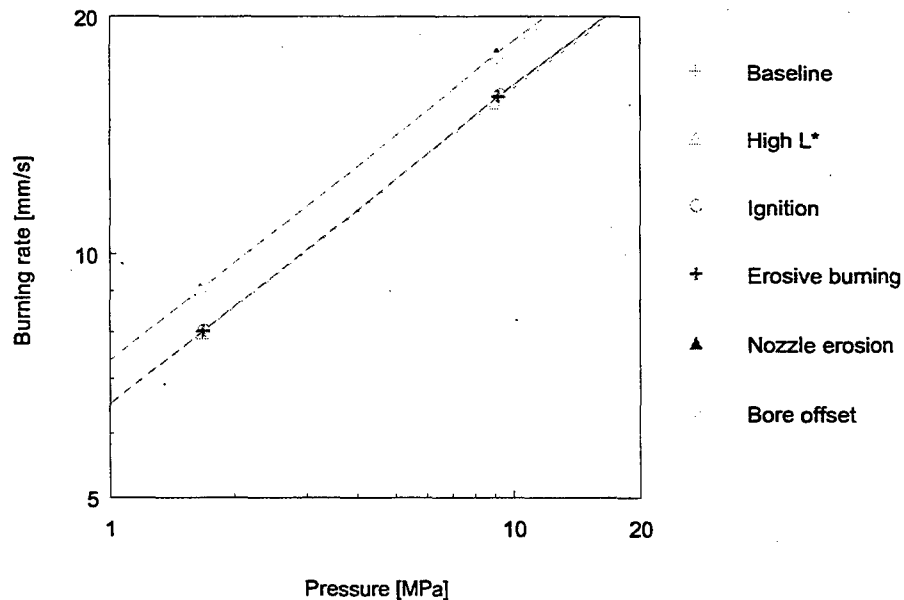
Figure 26. RR #2 - TNO-PML Round Robin Results (All Cases)

---

[13] TNO-PML Method #2 used to analyze data. High-pressure (odd numbered) traces were taken at a 10%P_{max} value. As ignition transients are very fast and the low-pressure (even numbered) traces do not achieve pressure levels over 2.5 MPa, the $t_{2.5}$ point cannot be determined so the 10 % value seems to be an appropriate choice.

[14] Tangent-Bisector Method used.

[15] Total $t_b = t_{T-B} - t_{2.5}$
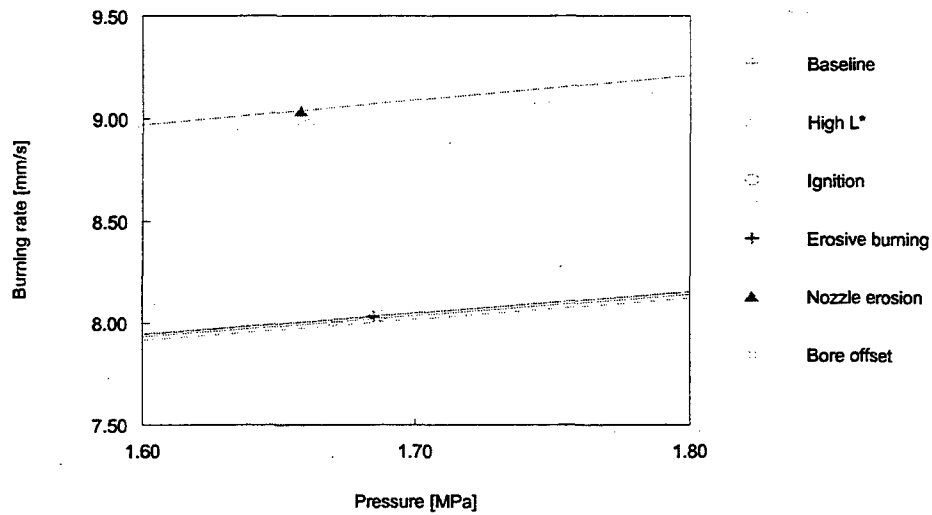
Figure 27. RR #2 - TNO-PML Round Robin Results (Low Pressure)
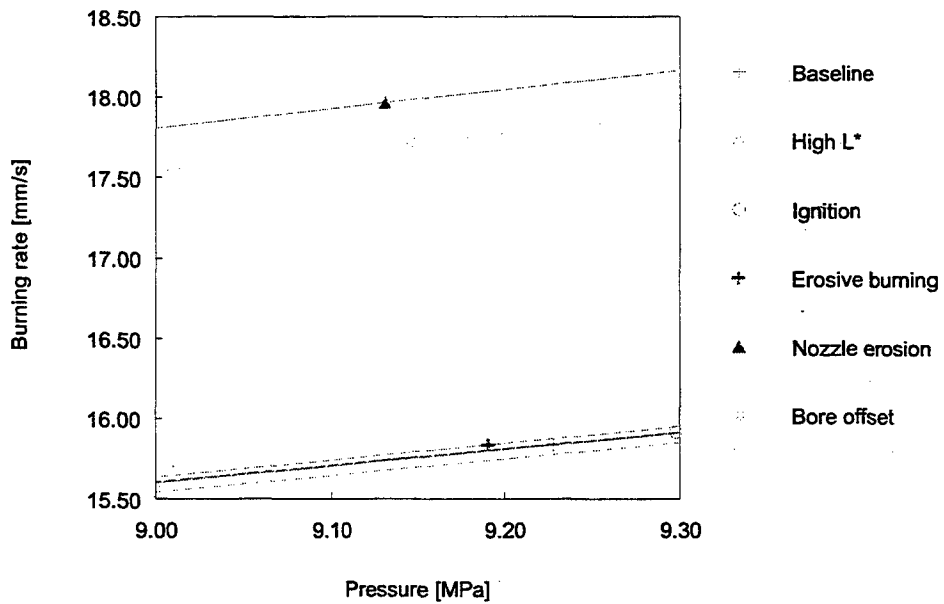
Figure 28. RR #2 - TNO-PML Round Robin Results (High Pressure)

The TNO analysis produced consistent results for the motor perturbations examined. The SPP simulation indicated nozzle erosion and off-axis bore strongly influences the results, reducing the burning time considerably and increasing the burning rate as shown in Figure 26. A high L* value, an ignition peak and

55

erosive burning influence the results only slightly; although the average combustion pressure is higher due to the ignition peak and lower for the high L* value and the erosive burning test. While only two tests are available for each "perturbation", all resulting curves in Figure 27 have a slope that is very close to the input reference slope. The burning rate coefficients do deviate, as discussed below.

Comparison of Selected RR #2 Results

The burning rate r_7 (at 7 MPa) results, and power law burning rate exponent and coefficient, and r_7 relative to the baseline cases $r_{7,Cases\ 1-2}$ and the reference $r_{7,ref}$ for 7 different RR #2 participants are presented respectively in Tables 16 through 19. Relative burning rates, and power law exponents and coefficients are charted in Figures 29 through 31. The participant's bar charts appear in the order shown in the legend.

Table 16. RR #2 – Burning Rate r₇ Determined by Several Participants

Case Description	Case Numbers	Reference Burning Rate, r₇							
		Ref. [mm/s]	TNO [mm/s]	BC [mm/s]	RO [mm/s]	SNPE [mm/s]	ONERA [mm/s]	NAWC [mm/s]	CSD [mm/s]
Baseline	1-2	12.773	14.182	13.525	14.365	13.482	13.517	12.800	12.762
Large L*	3-4	12.773	14.074	13.370	14.194	13.400	13.407	12.770	12.612
Ignition	5-6	12.773	14.206	13.565	14.402	13.515	13.562	12.852	12.822
Erosive Burning	7-8	12.773	14.201	13.536	14.394	13.483	13.562	12.824	12.815
Nozzle Erosion	9-10	12.773	16.141	14.549	16.934	14.611	14.676	12.692	12.757
Off-Axis Bore	11-12	12.773	15.921	13.980	16.948	14.055	14.100	12.766	12.713

Table 17. RR #2 – Power Law Exponent (n) Determined by Several Participants

Case Description	Case Numbers	Power Law Exponent, n							
		Ref.	TNO	BC	RO	SNPE	ONERA	NAWC	CSD
Baseline	1-2	0.4	0.399	0.397	0.387	0.393	0.395	0.384	0.396
Large L*	3-4	0.4	0.395	0.391	0.383	0.392	0.391	0.383	0.389
Ignition	5-6	0.4	0.400	0.398	0.388	0.394	0.396	0.386	0.397
Erosive Burning	7-8	0.4	0.400	0.397	0.387	0.393	0.396	0.384	0.397
Nozzle Erosion	9-10	0.4	0.402	0.392	0.387	0.393	0.395	0.347	0.395
Off-Axis Bore	11-12	0.4	0.398	0.395	0.389	0.394	0.396	0.374	0.396

Table 18. RR #2 – Power Law Coefficient (a) Determined by Several Participants

Case Description	Case Numbers	Power Law Coefficient, a							
		Ref.	TNO	BC	RO	SNPE	ONERA	NAWC	CSD
Baseline	1-2	5.865	6.525	6.250	6.745	6.270	6.270	6.060	5.908
Large L*	3-4	5.865	6.525	6.254	6.729	6.251	6.251	6.062	5.916
Ignition	5-6	5.865	6.519	6.258	6.743	6.280	6.280	6.069	5.918
Erosive Burning	7-8	5.865	6.520	6.252	6.745	6.275	6.275	6.075	5.917
Nozzle Erosion	9-10	5.865	7.377	6.789	7.580	6.803	6.803	6.463	5.914
Off-Axis Bore	11-12	5.865	7.337	6.481	7.568	6.528	6.528	6.172	5.878

Table 19. RR #2 – Relative Burning Rates at 7 MPa
(Relative to Baseline $r_{7Cases\,1-2}$ and to Reference $r_{7,ref}$)

Case Description	Case Numbers	Relative Burning Rate, $r_7/\,r_{7ref}$						
		TNO	BC	RO	SNPE	ONERA	NAWC	CSD
Method Used →		r_{TOT}	r_{TOT}	r_{TOT}	r_{TOTn}	r_{TOTn}	r_{MB}	r_{MB}
Relative to Baseline $r_{7Cases\,1-2}$								
Baseline	1-2	1	1	1	1	1	1	1
Higher L*	3-4	0.992	0.989	0.988	0.994	0.992	0.998	0.988
Ignition	5-6	1.002	1.003	1.003	1.002	1.003	1.004	1.005
Erosion	7-8	1.001	1.001	1.002	1.000	1.003	1.002	1.004
Nozzle Eros.	9-10	1.138	1.076	1.179	1.084	1.086	0.991	0.999
Off-Axis Bore	11-12	1.123	1.034	1.180	1.042	1.043	0.997	0.996
Relative to Reference $r_{7,ref}$								
Baseline	1-2	1.110	1.059	1.125	1.056	1.058	1.002	0.997
Higher L*	3-4	1.102	1.047	1.111	1.049	1.050	1.000	0.987
Ignition	5-6	1.112	1.062	1.128	1.058	1.062	1.006	1.004
Erosion	7-8	1.112	1.060	1.127	1.056	1.062	1.004	1.003
Nozzle Eros.	9-10	1.264	1.139	1.326	1.144	1.149	0.994	0.999
Off-Axis Bore	11-12	1.246	1.095	1.327	1.100	1.104	0.999	0.995
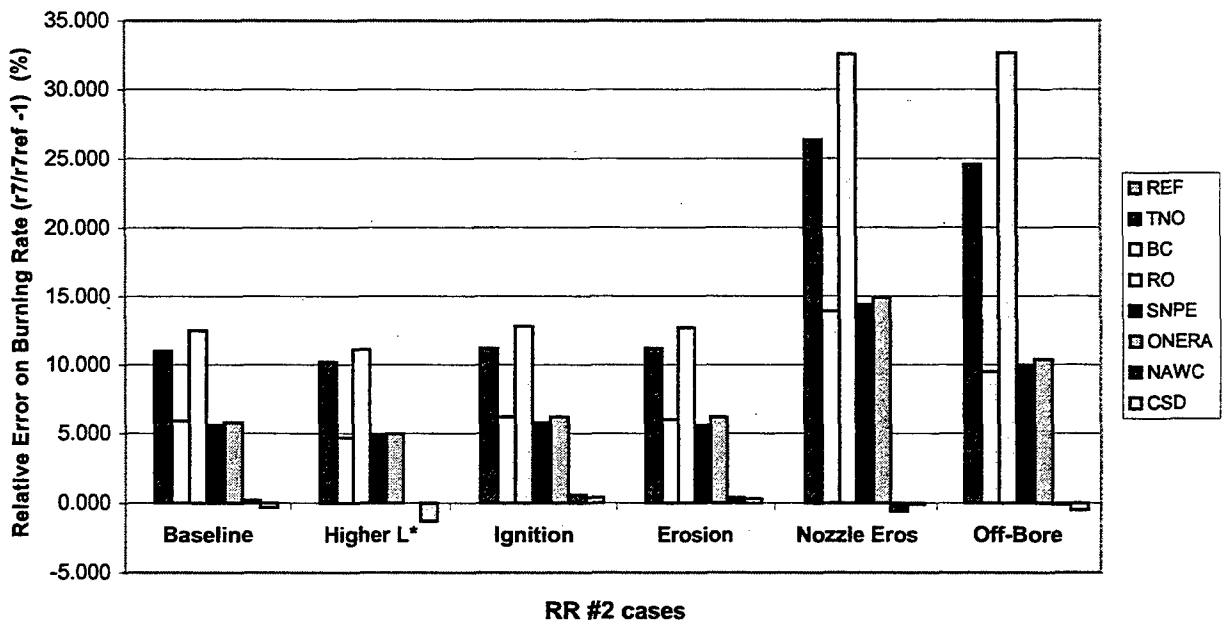
Figure 29. RR #2 – Comparison of Burning Rate Error (%) at 7 MPa
Relative to the Reference Rate $r_{7,ref}$ without Web Correction (Data from Table 19)
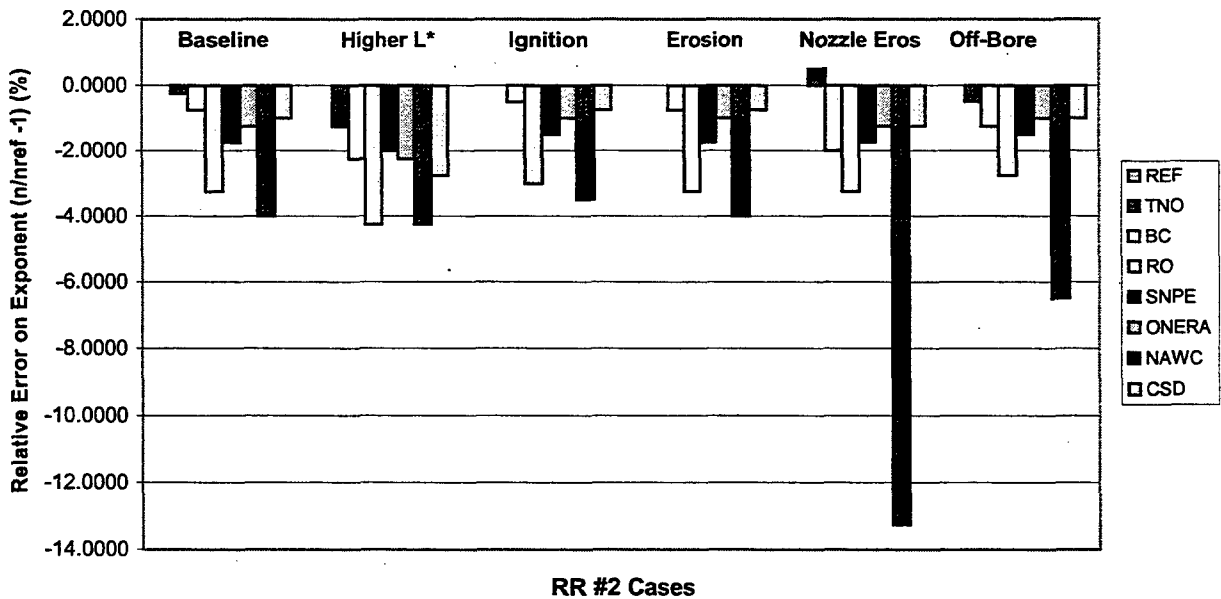
Figure 30. RR #2 – Comparison of Power Law Exponent Error (%)
Relative to Reference (Data from Table 17)
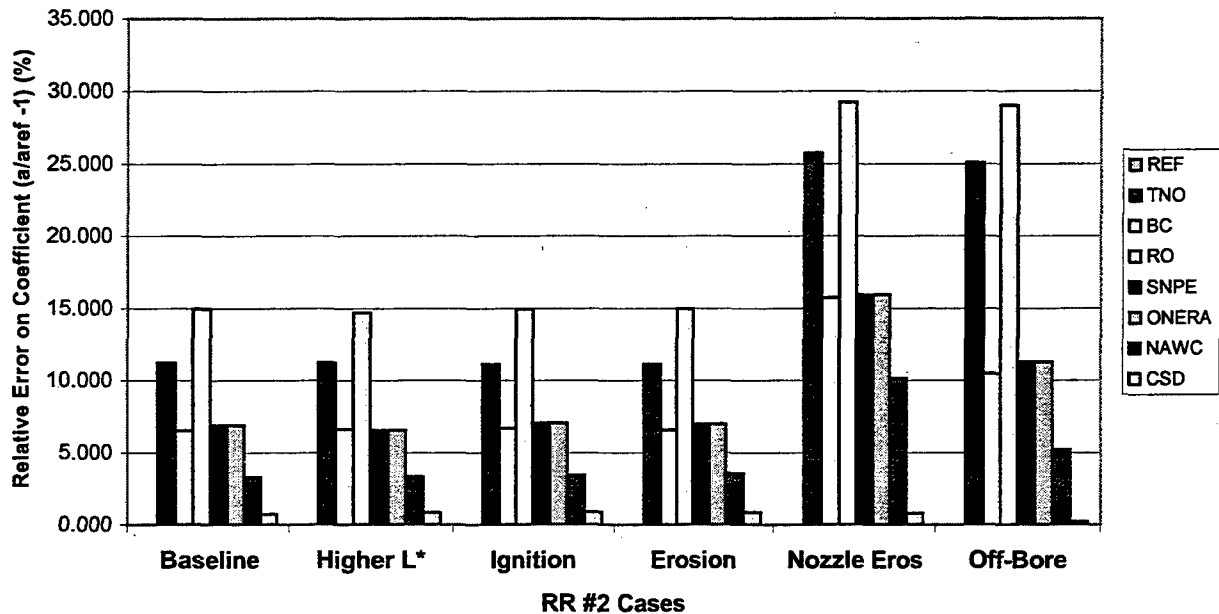
**Figure 31. RR #2 - Comparison of Power Law Coefficient Error (%)
Relative to Reference (Data from Table 18)**

Less than 1% deviation in burning rate is seen (Table 19) for the TOT methods relative to the baseline for the cases of high L* data (3-4), the influence of ignition (5-6) and erosive burning (7-8). A deviation in burning rate relative to the baseline for the TOT methods of up to 18%, however, is seen for the nozzle erosion (9-10) and off-axis bore (11-12) cases. The deviation for the TOT methods with respect to the reference is even larger. The deviation in burning rate relative to either the baseline or the reference for the MB methods remained at less than 1% for all the cases examined.

The results obtained at Bayern Chemie (r_{TOT}), SNPE (r_{TOTn}) and ONERA (r_{TOTn}) are very similar, in particular for the $r_{7Cases\ 1-2}$ and $r_{7,ref}$ and the burning rate exponent and coefficient. The burning rates and burning rate coefficients were over-predicted, while the exponents were under-predicted within approximately 4%. When comparing the results to the SPP input data, NAWCWD (r_{MB}) and CSD (r_{MB}) results predict the burning rate at 7 MPa correctly (less than 0.25%), but are less correct on burning rate exponent and coefficient.

5.2.2   Round Robin #2 Conclusions

The stated objectives of the round robin were to clarify distinctions among several existing burning rate measurement analysis methods and to determine the causes of differences between them. The RR #2 dataset contains several flaws, some of which are sufficient to severely obstruct attainment of the stated objectives. The following flaws in the RR #2 dataset are summarized here, with a more complete discussion provided in Appendix C-2:

- *An instantaneous initial pressure rise time* - Instantaneous initial pressure rise prevents discrimination among definitions for beginning of burning. Moreover, due to a 'peculiarity' of the SPP code, the onset and end of burning occurred at pressures higher than zero pressure (30 psi

59

equivalent to 0.2 MPa). The timepoint definitions lower than about 30 psi cannot be properly applied (e.g. 10% P_{max}).

- *The extended tailoff required the truncation of the total pressure integral* - Mass balance methods and time point definitions based on pressure integral cannot be properly executed.

- *Uncertainty in the web thickness burned* - Comparison of the furnished web thickness with the furnished surface-web tables makes it immediately clear that the furnished web thickness is the thickness at final burnout. However, the simulations appear to have ended before final burnout was reached. Burning effectively ended at the end of the time history, so full web thickness was not burned.

- *Influence of reference pressure used due to other flaws* -- Results for the different cases show varying degrees of bias as a result of the various perturbations and because of choice of associated pressure. Clarifying this point with the round robin results is possible, and would be a positive result in future such round robin analyses. The correction to reference pressure is well founded and generally accepted. The error for the round robin cases will be dominated by the choice of associated pressure because of the extended tailoff of all cases, and will largely be resolved by the associated pressure determination.

Despite these flaws some conclusions may be drawn from the RR #2 results in terms of influences of the analysis methods and effects of perturbations of motor parameters. While flaws in the simulated dataset hamper definitive discrimination among timepoint definitions and among burning rate definitions, some general trends are suggested.

Influences of Analysis Methods

The design of Round Robin #2 was a trade-off of a manageable number of cases to analyze versus applying changes to allow discrimination of each effect. The SPP output files were further processed to obtain data simulating a test with a 1 kHz sample rate. For each case (higher L*, ignition transient, etc.) the input to the RR#2 consisted of two tests, one each at low and high pressure. The various changes were applied cumulatively making a proper distinction of the effect of each variation on the burning rate more difficult. The pressures-time curves were not full curves. They started and ended at 0.2 MPa. This prevented some data reduction methods from being properly applied. Also the fact that only two data points were available to derive a power law burning rate relation is a disadvantage. Moreover, erosive burning was not very pronounced since a typical 2x4-inch motor is normally not affected by erosive burning; it is actually designed not to be.

The RR#2 results did not recover the reference-burning rate that was input to the SPP simulation. However, all analysis methods yielded an average deviation of 0.5% relative to the baseline for the cases of high L* data (3-4), the influence of ignition (5-6) and erosive burning (7-8). A deviation in burning rate for the TOT methods of 4 - 18% relative to the baseline, however, is seen for the nozzle erosion (9-10) and off-axis bore (11-12) cases. The deviation for the TOT methods with respect to the reference is even larger. The deviation in burning rate relative to either the baseline or the reference for the MB methods remained at less than 1% for all the cases examined. All methods over-predicted burning rate and burning rate coefficient, while under-predicting burning rate exponents. The MB methods seem to provide better agreement when compared with either the baseline or the reference burning rate, exponents or coefficients. These results are biased toward the MB methods due to an error in the web used in the analysis.

When evaluating the web burned during each test, it was observed that unburned web remained in all tests. More web remained at the low-pressure tests than at the high-pressure tests. Corrections were made to the web for one of the data reduction methods (TNO method) and the data were reduced for the actual web burned. The results are considerably better with less than 0.2 % deviation relative to the baseline for all cases except for the L* case which was about 0.8%. These results illustrate that proper knowledge of the actual web burned is important for TOT methods for determining the burning rate and power law relation correctly. It also illustrates the inherent robustness of the MB methods to accommodate such errors.

Based on the above, it may be concluded that greater care should have been exercised in RR #2 in the use of the SPP code to simulate 2x4-inch motor pressure-time behavior. The WG 016 decided it was prudent to conduct a third and final Round Robin, RR#3. A well-validated model was used for RR #3 that was developed by R.O. Hessler, U.S. independent consultant supporting the WG 016.

Effects of Perturbation of Motor Parameters

By the nature of its design RR #2 seeks to answer a second question of what effects do perturbations of motor parameters have? The following comparative discussion examines the cases more closely. While the trends appear consistent, due to the flaws in the dataset, caution should be exercised in making too much of the detailed results reported here.

Cases 1& 2: Cases 3 & 4: Effect L* Value

The cases 3 & 4 show slightly lower values for the burning rate at 7 MPa as compared to baseline cases 1 & 2, hence, it may be concluded that the effect of a larger chamber volume although not very pronounced for this particular case yields lower burning rate data. The effect is mainly visible through power law burning rate exponent (n), while the coefficient is marginally affected.

Cases 1&2: Cases 5 & 6: Effect Igniter Functioning

An ignition pulse has a limited effect on the reduced burning rate data although it is clearly visible from the pressure-time plot (Figure 23). The burning rate exponent is slightly increased while the coefficient and the burning rate at 7 MPa are relatively unaffected.

Cases 7 & 8: Cases 5 & 6 With Erosive Burning Added

The effect of the erosive burning does not give a pronounced effect on the results. The burning rate at 7 MPa and the coefficients are about the same while the exponent either increases or decreases depending on the data reduction method. It should, however, be noted that a 2x4-inch rocket motor is designed to be relatively unaffected by erosive burning effects, and the SPP code simply simulated what is designed to occur in test.

Cases 9 & 10: Cases 7 & 8 With Eroding Nozzle Added

All methods yield higher r_7 burning rate results (except the NAWC and CSD mass balance methods). The burning rate exponent is either higher or lower depending on the method employed, while the burning rate coefficient is generally higher. This shows that nozzle erosion has considerable affect on the results, the extent of which depends on the extent of the nozzle erosion. Some methods are more affected, others less.

Cases 11 & 12: Cases 9 & 10 With Bore Offset

The off-axis bore counteracts the deviation due to the eroding nozzle. In the burning rate at 7 MPa, a slight reduction is visible, while the exponent again either increases or decreases depending on the particular analysis method.

5.3   International Round Robin #3 Results

Round Robin #3 is based on a computer program, created by R.O. Hessler and R. Glick in support of the WG 016, to generate simulated motor data for research into burning rate measurement methods.[79] Details of the RR #3 design and input data are summarized in Appendix C-3. Once again, a simple 2x4-inch motor configuration as shown in Appendix C Figures C-5 and C-6 was simulated. RR #3 consists of ten different pressure-time traces for 5 baseline and 5 off-axis bore cases as listed in Table 20. Each group contains five motors, equally spaced in log pressure. RR #3 responses were received in early-1999 from the following 18 volunteer participants, including DREV, SNPE, ONERA, Bayern Chemie, POLIMI (using

HG), TNO-PML (two methods), Royal Ordnance, Alliant Tech Systems, AMCOM, ARC, BF Goodrich, Hessler, Jordan/SNAP, NAWCWD, P&W/CSD, Stone Engineering, and Thiokol. Nine of the participants, Canada, the European facilities, Thiokol, and R. Hessler used TOT methods to reduce the data and determine the propellant burning rates, while the remaining participants from the U.S. used MB methods. Lessons learned on RR #3 and #3X are summarized following a description of the results for each Round Robin.

Table 20. RR #3 Small Motor Ballistic Simulations Examined

Group	Cases	Perturbation
1	1-5	Baseline
2	6-10	Bore offset

Ten pressure-time histories were simulated for a generic 2x4-inch motor and are comprised of two groups. Each group contains five motors, equally spaced in log pressure (3.5, 5, 7, 10, and 14 MPa). The only difference between the motors within a group is the nozzle size. The only difference between the two groups is the degree of eccentricity or offset of the cylindrical bore. For motors having the same nozzle size in the two groups, the data is identical until the burnout process begins. After initial burnout, the tailoff is appreciably different. Burn out and tailoff are ideal in cases 1 through 5 (Figure 32). Burnout and tailoff are prolonged due to offset of the core mandrel for cases 6 through 10 (Figures 33 and 34).
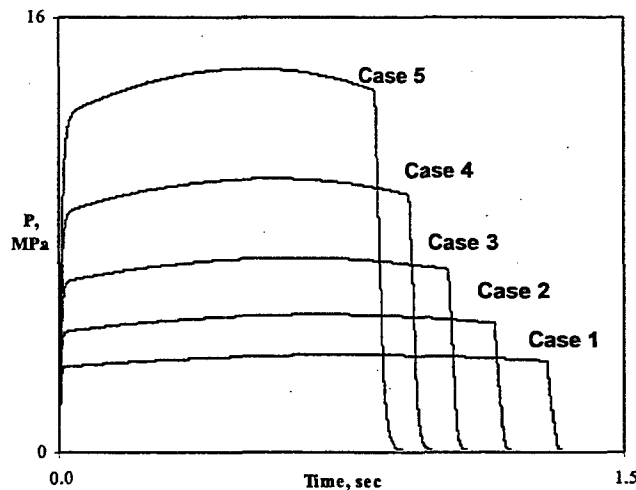
Figure 32. RR #3 - Pressure-Time Behavior for Round Robin #3,
Group 1 with Concentric Grain Bore Cases
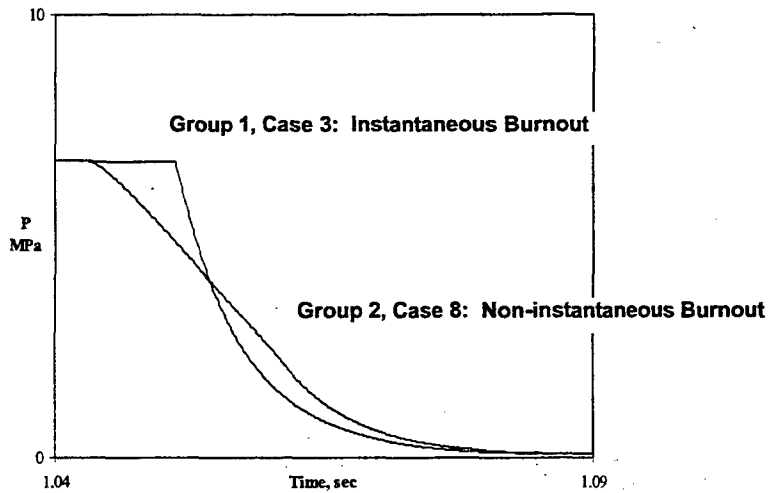
**Figure 33. RR #3 - Pressure-Time Behavior for Round Robin #3,
Group 2 with Grain Bore Offset Cases**
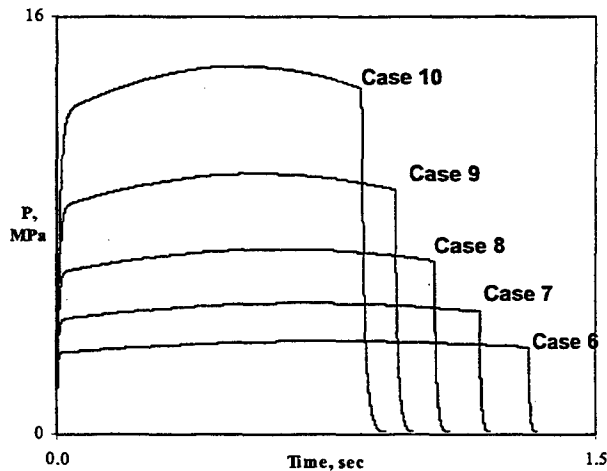
**Figure 34. Comparison of Burnout and Tailoff Processes for RR #3
Group 1 Baseline and Group 2 with Grain Bore Offset**

Data reduced from real motors of this design indicates non-instantaneous burnout corresponding to 0.3 to 0.9% of web thickness due to bore offset. An intermediate bore offset was used in the simulations. The offset value is zero for Group 1, and is the same for all motors in Group 2. The actual value for the offset viz. 0.096279 mm on a web of 12.7 mm was not furnished to the participants.

Burning rate data reduced from the simulated motor data can be used to examine two specific questions considered critical to understanding of burning rate measurements:

- What is the bias (scale factor) and precision (non-reproducibility) of a given analysis procedure when applied to an ideal motor with perfect instrumentation?
- What is the effect of non-instantaneous burnout upon that analysis procedure?

5.3.1 Round Robin #3 Analysis

The RR #3 data was supplied to a number of U.S., French, German, UK, Netherlands and Canadian companies/organizations. Each participant was again asked to analyze the data using their preferred method(s) and determine the average burning rate and average pressure. RR #3 responses were received in early-1999 from the following 18 volunteer participants, including DREV, SNPE, ONERA, Bayern Chemie, POLIMI (using HG), TNO-PML (two methods), Royal Ordnance, Alliant Tech Systems, AMCOM, ARC, BF Goodrich, Hessler, Jordan/SNAP, NAWCWD, P&W/CSD, Stone Engineering, and Thiokol. Nine of the participants, Canada, the European facilities, Thiokol, and R. Hessler used TOT methods to reduce the data and determine the propellant burning rates, while the remaining participants from the U.S. used MB methods as summarized in Table 9.

Power law relations for the burning rate were determined from the reduced data. The baseline and off-axis bore results are respectively presented in Tables 21 and 22. Relative burning rate at 7 and 10 MPa taken from Tables 21 and 22 for the baseline and bore offset cases are plotted in Figures 35 and 36. Relative error in burning rate taken from Tables 21 and 22 for the baseline and bore offset cases are plotted in Figures 37 and 38. Results for the participants are shown in order with under-predicted to over-predicted errors from left to right. The 16 of 18 participants predicted the baseline reference within ± 0.5%, while 11 of 18 predicted the off-axis bore reference within ± 0.5%. The greatest relative errors are observed using TOT methods with simple definitions for burning time, i.e. 10%P, or Tangent-Bisector.

Table 21. RR #3 – Group 1 Combined Baseline Results and Relative Errors

Country/ Company	Coefficient		Exponent		Burning Rate			
	a	$\dfrac{a}{a_{ref}}-1$ [%]	n	$\dfrac{n}{n_{ref}}-1$ [%]	r_7 [mm/s]	$\dfrac{r_7}{r_{7,ref}}-1$ [%]	r_{10} [mm/s]	$\dfrac{r_{10}}{r_{10,ref}}-1$ [%]
Reference	6.594	0.00	0.316	0.00	12.189	0.00	13.642	0.00
Canada - DREV	6.642	0.73	0.308	-2.53	12.100	-0.73	13.506	-1.00
France - SNPE	6.606	0.18	0.313	-0.95	12.153	-0.29	13.590	-0.38
- ONERA	6.609	0.23	0.313	-0.95	12.149	-0.30	13.584	-0.40
Germany - BC	6.588	-0.09	0.316	0.00	12.190	0.00	13.645	0.00
Italy - POLIMI	6.595	0.12	0.316	-0.10	12.190	0.01	13.643	0.01
Netherlands-TNOM1	6.672	1.18	0.303	-4.12	12.028	-1.32	13.400	-1.77
-TNOM2	6.619	0.35	0.314	-0.63	12.203	0.11	13.652	0.07
UK - RO	6.593	-0.02	0.316	0.00	12.201	0.10	13.659	0.12
US - Alliant Tech	6.587	-0.10	0.319	0.95	12.232	0.35	13.707	0.48
- AMCOM	6.581	-0.20	0.317	0.32	12.194	0.04	13.654	0.09
- ARC	6.581	-0.19	0.317	0.19	12.186	-0.02	13.643	0.01
- BF Gdrich / UP	6.715	1.84	0.309	-2.22	12.252	0.52	13.679	0.27
- Hessler	6.595	0.02	0.316	0.00	12.190	0.01	13.642	0.00
- Jordan / SNAP	6.593	-0.02	0.316	0.00	12.193	0.03	13.648	0.04
- NAWCWD	6.602	0.12	0.313	-0.95	12.142	-0.39	13.577	-0.48
- P&W / CSD	6.697	1.55	0.310	-1.9	12.232	0.35	13.660	0.13
- Stone Engin	6.614	0.30	0.315	-0.32	12.209	0.16	13.660	0.14
- Thiokol	6.599	0.08	0.315	-0.32	12.176	-0.11	13.623	-0.14

Table 22. RR #3 – Group 2 Combined Off-Axis Bore Results and Relative Errors

Country / Company	Coefficient		Exponent		Burning Rate			
	a	$\dfrac{a}{a_{ref}}-1$ [%]	n	$\dfrac{n}{n_{ref}}-1$ [%]	r_7 [mm/s]	$\dfrac{r_7}{r_{7,ref}}-1$ [%]	r_{10} [mm/s]	$\dfrac{r_{10}}{r_{10,ref}}-1$ [%]
Reference	6.594	0.00	0.316	0.00	12.189	0.00	13.642	0.00
Canada - DREV	6.642	0.73	0.308	-2.53	12.097	-0.75	13.502	-1.03
France - SNPE	6.611	2.60	0.313	-0.95	12.149	-0.33	13.583	-0.43
- ONERA	6.616	0.11	0.312	-0.32	12.143	-0.09	13.573	-0.12
Germany - BC	6.590	-0.06	0.316	0.00	12.179	-0.08	13.630	-0.09
Italy - POLIMI	6.595	0.02	0.316	-0.095	12.190	0.010	13.643	0.01
Netherlands- TNOM1	6.672	0.50	0.305	-3.48	12.001	-1.54	13.381	-1.91
- TNOM2	6.670	1.15	0.314	-0.63	12.297	0.89	13.756	0.84
UK - RO	6.645	0.77	0.316	0.00	12.285	0.79	13.750	0.79
US - Alliant Tech	6.571	-0.35	0.312	-1.26	12.234	0.37	13.710	0.50
- ARC	6.581	-0.19	0.317	0.41	12.203	0.11	13.665	0.17
- BF Gdrich / UP	6.403	-2.89	0.333	5.38	12.241	0.43	13.785	1.05
- Hessler	6.595	0.02	0.316	0.00	12.190	0.01	13.643	0.01
- Jordan / SNAP	6.606	0.18	0.316	0.00	12.218	0.23	13.675	0.24
- NAWCWD	6.581	-0.20	0.315	-0.32	12.146	-0.35	13.590	-0.38
- P&W / CSD	6.701	1.62	0.309	-2.22	12.231	0.34	13.657	0.11
- Thiokol	6.599	0.08	0.315	-0.32	12.181	-0.07	13.629	-0.09
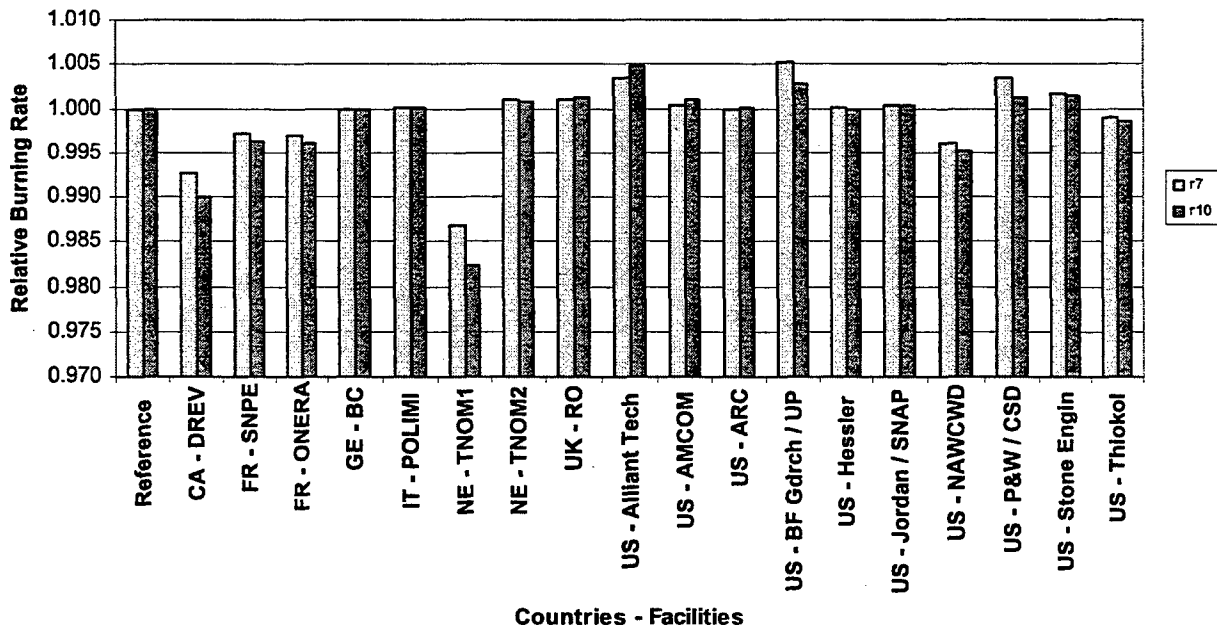
Figure 35. RR #3 – Group 1 Baseline Relative Burning Rate
at Reference Pressures 7 and 10 MPa
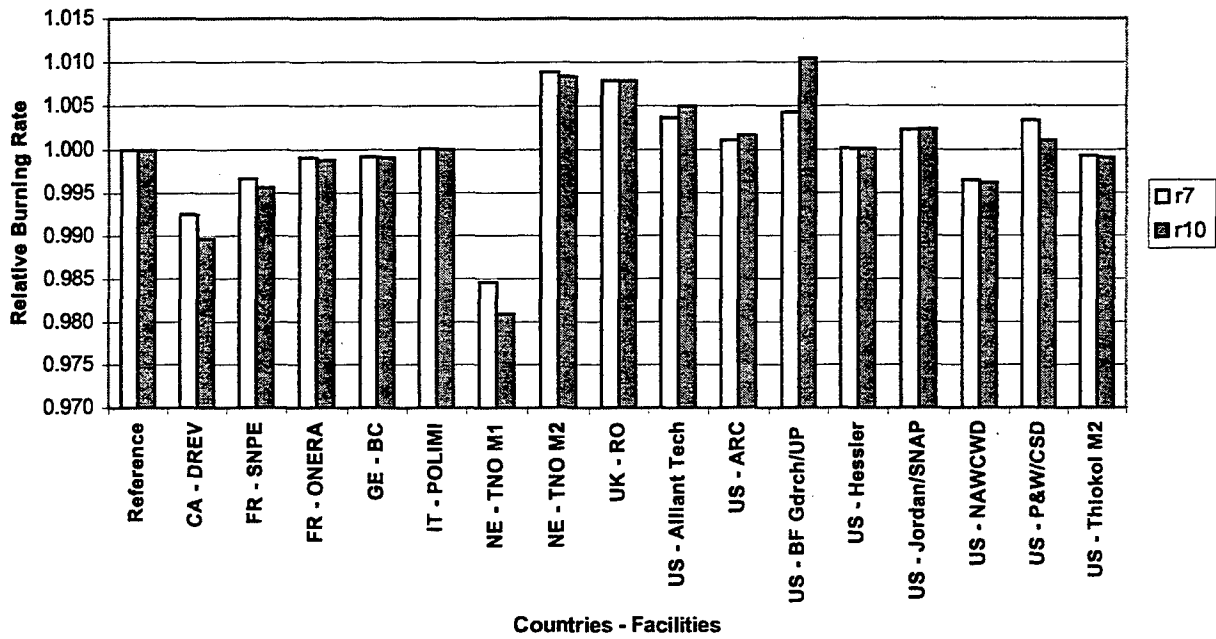
Figure 36. RR #3 – Group 2 Off-Axis Relative Burning Rate at Reference Pressures 7 and 10 MPa
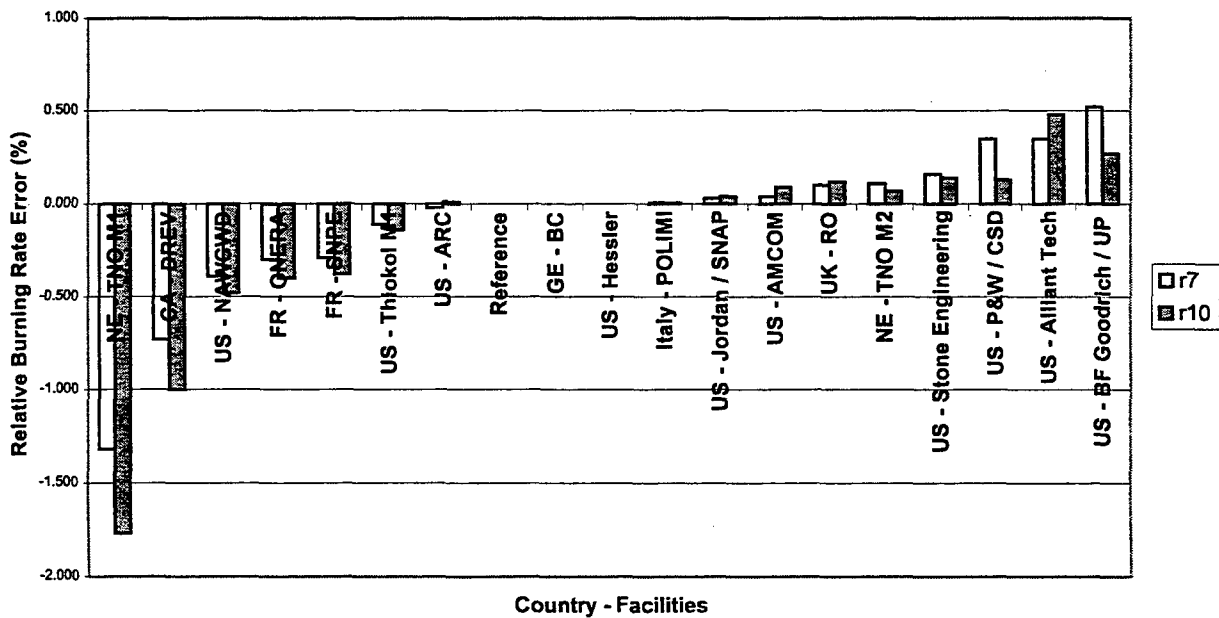
Figure 37. RR #3 – Group 1 Baseline Burning Rate Relative Error (%)
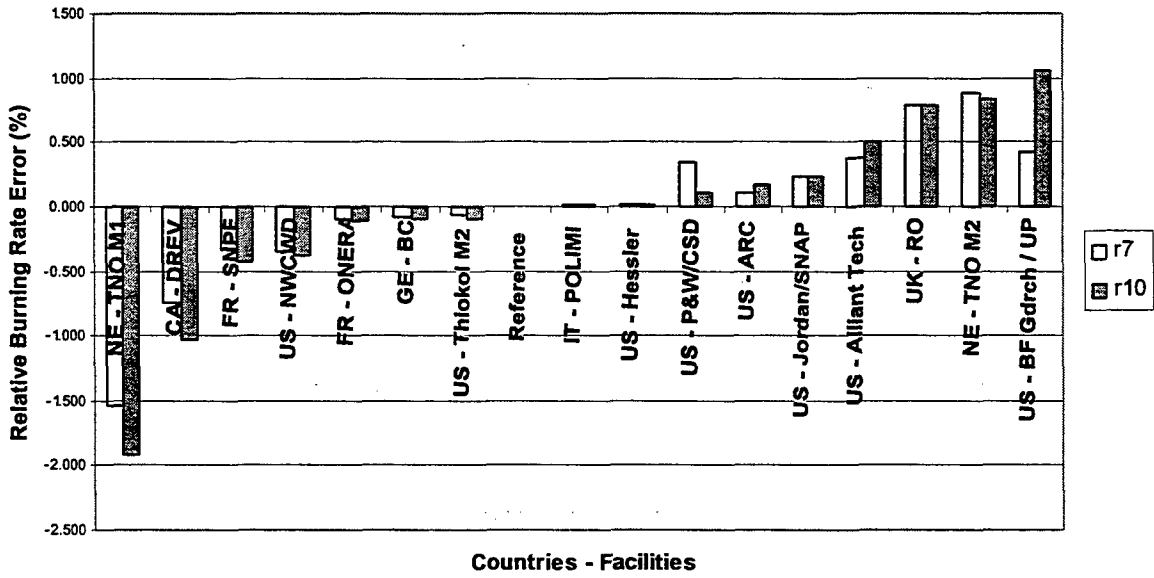
Figure 38. RR #3 – Group 2 Off-Axis Bore Burning Rate Relative Error (%)

The participant's ability to reproduce the reference power law coefficient and exponent are shown in Figures 39 through 42 for the Group 1 Baseline and Group 2 Off-axis bore cases, respectively.
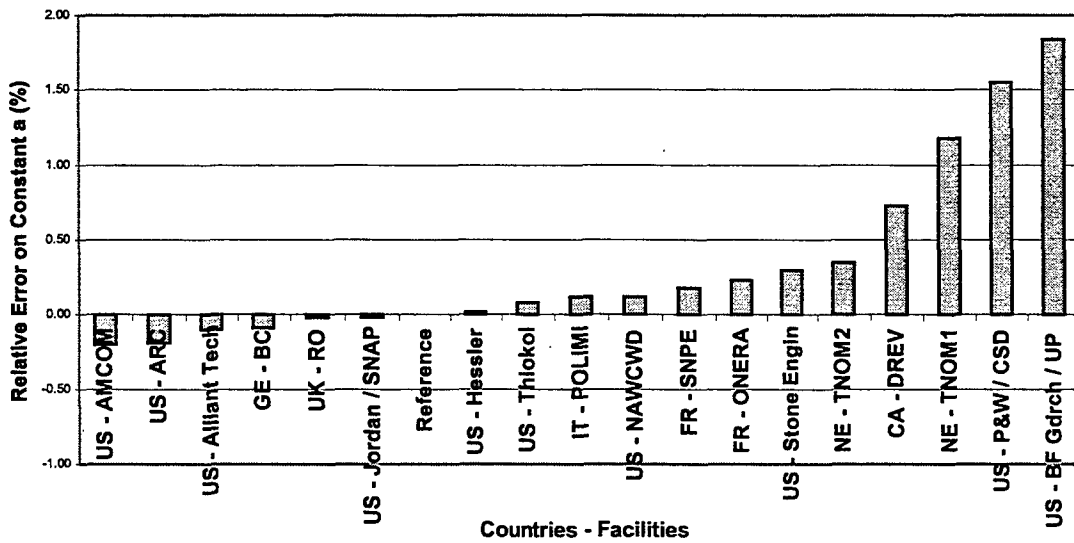
Figure 39. RR #3 – Group 1 Baseline Constant (a) Relative Error (%)
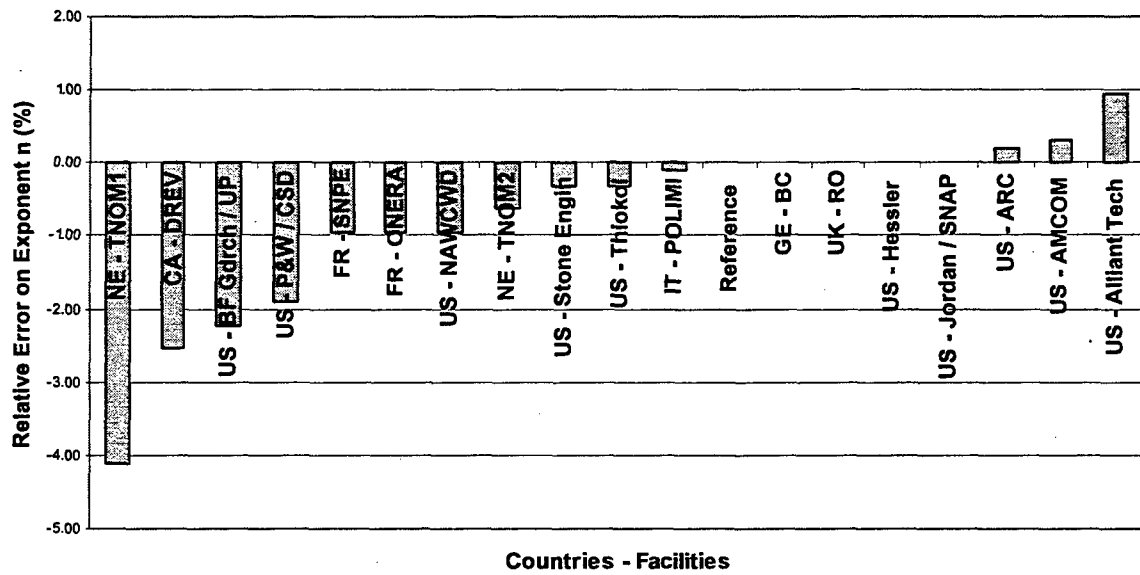
Figure 40. RR #3 – Group 1 Baseline Exponent (n) Relative Error (%)
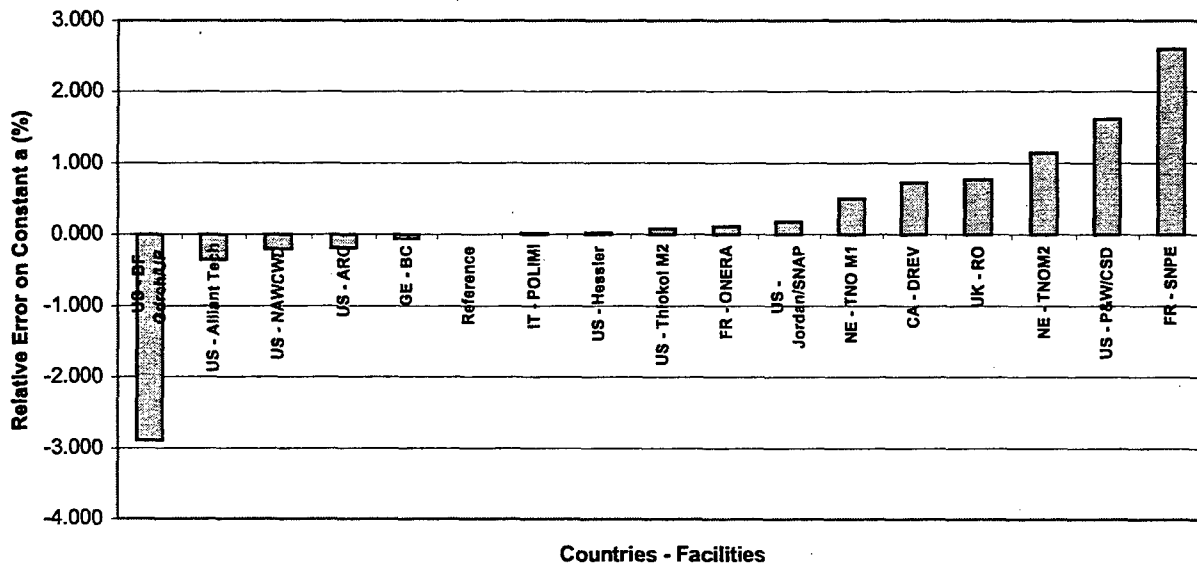
Figure 41. RR #3 – Group 2 Off-Axis Constant (a) Relative Error (%)
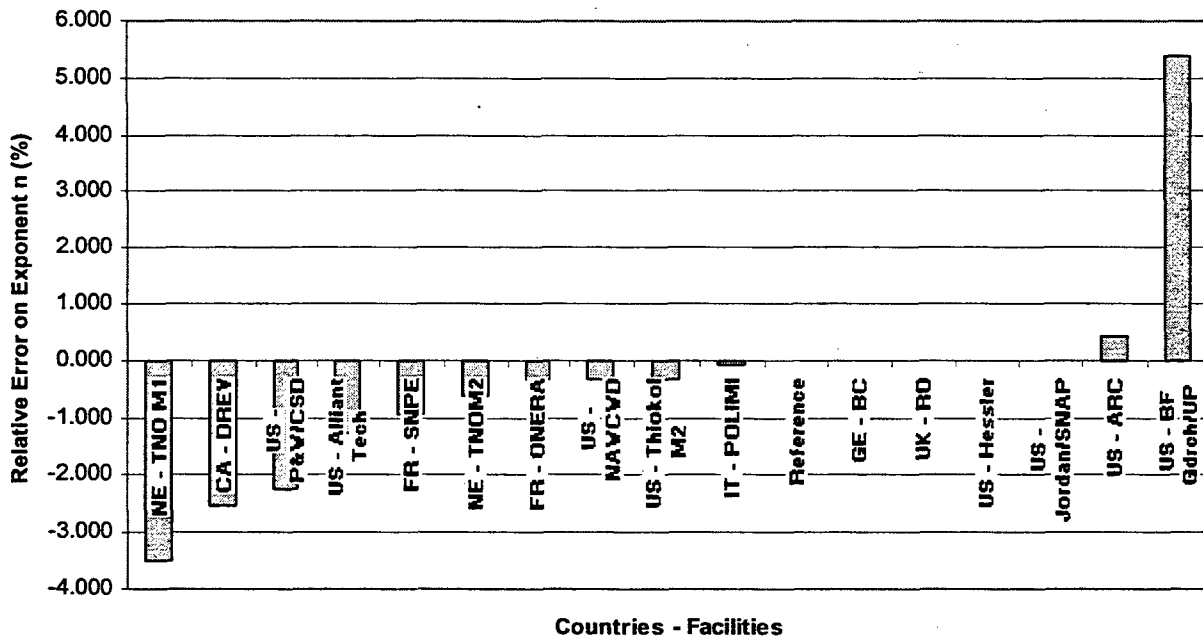
Figure 42. RR #3 – Group 2 Off-Axis Exponent (n) Relative Error (%)

The RR #3 Group 1 baseline data indicates ARC, BC, HG, POLIMI (Using HG), and Jordan/SNAP methods recovered the reference burning rate within an average of 0.04%, AMCOM and TNO M2 within 0.1%, Stone and Thiokol within 0.15%, P&W/CSD within 0.25%, Alliant Tech, BF Goodrich, NAWC, ONERA, and SNPE within 0.5%, while DREV and TNO M1 were within 1.5%. The smallest relative errors are observed using methods that more effectively account for non-ideal tailoff, which is more easily seen with the Group 2 off-axis bore cases. The greatest relative errors are observed using TOT methods with simple definitions for burning time, i.e. 10%P, or Tangent-Bisector.

The RR #3 Group 2 off-axis data indicates only HG and POLIMI (Using HG) methods recovered the reference burning rate within an average of 0.01%, THIOKOL and BC within 0.1%, ARC and ONERA within 0.15%, Jordan/SNPE and P&W/CSD within 0.25%, Alliant Tech, NAWC, and SNPE within 0.5%, while BF Goodrich, DREV, RO and TNO M2 were within 1% and TNO M1 was within 1.75%. The smallest relative errors are more readily observed in Group 2 for methods that more effectively account for non-ideal tailoff. The greatest relative errors are again observed using TOT methods with simple definitions for burning time. While only the HG method consistently recovered the reference burning rate for both groups, many other methods produced highly respectable results.

The derived power law coefficient and exponents shown in Figures 39 through 42 indicate that 9 of the 18 participants recovered the baseline exponent within 0.5%, while 10 of 18 recovered the off-axis bore exponent within 0.5%. The 15 of the 18 participants recovered the baseline coefficient within 0.5%, while 11 of 18 recovered the off-axis bore coefficient within 0.5%. The general trend was to under-predict the exponent and over-predict the coefficient.

5.3.2 RR #3 Error Analysis[79]

The two groups of simulated motors were reduced by five methods:

1) Thickness/Time Methods
   a) Thickness/time Rate (r_{TOT} or R_{TOT})
   b) Iterated Thickness/Time Rate (r_{TOTn} or R_{TOTn})
   c) Iterated Two-Point Thickness/Time Rate (r_{HG} or R_{HG})
2) Mass Conservation Methods
   a) Mass Balance Rate (r_{MB} or R_{MB})
   b) Iterated Mass Balance Rate (r_{MBn} or R_{MBn})

Each of the methods used the timepoint definitions given previously, as appropriate for the specific procedure. The timepoint values, details of the procedural steps are given in the Appendixes B-23 through B-27. The data for RR #3 Group 1 is presented in log-log format in Figure 43, and appears to be very close to the input rate. However, the resolution of log-log plots is typically inadequate to discern small differences in the data, in this case, a range of about 2% in the data. To improve resolution, the reduced data was normalized by the input rate at the associated pressures, and then converted to an error percentage:

$$\%Error = 100\left(\frac{r_{meas}(p_{meas})}{r_{input}(p_{meas})} - 1\right)$$ (58)

The percent errors of two Thickness/Time burning rate measurement methods applied to the simulated motors are plotted in Figure 44 versus pressure for Group 1 (without bore offset). The most commonly used procedure, r_{TOT} (solid lines), uses Time-Averaged pressure as the associated pressure and produces a slightly negative error. The second procedure, r_{TOTn} (dashed lines), uses the theoretically indicated
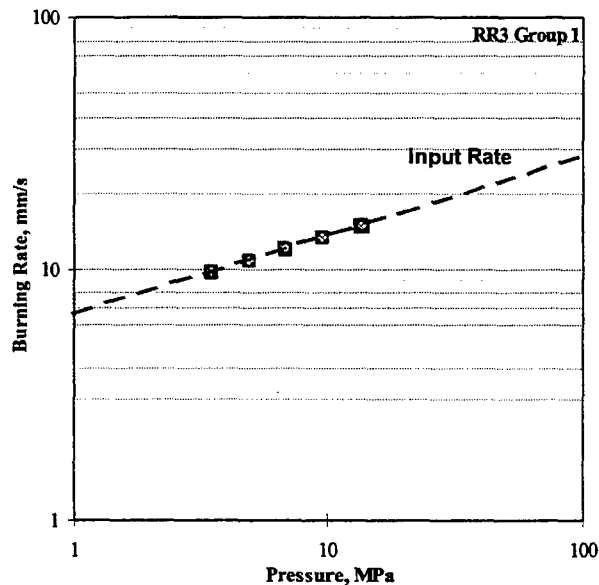
**Figure 43. Rate versus Pressure for
RR#3, Group 1**

71
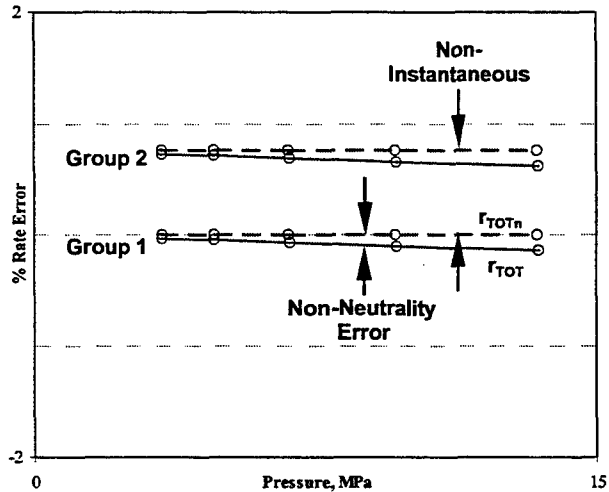
**Figure 44. Errors in Thickness/Time Rate Methods
for RR #3**

Rate-Averaged pressure and an iterative group analysis to determine the required pressure exponent and shows virtually no error, but a slight bias. Comparison of the two methods on Group 1 indicates that r_{TOT} is systematically biased low 0.01%/MPa, while r_{TOTn} is exact to within about 0.5 time resolution units for this particular motor design. Although the Non-Neutrality Error is small for the simulated motors, it may be expected to be order 0.05%/MPa for real motors because of heat loss effects during pressurization. For motors with generally non-neutral (progressive or regressive) pressure-time histories, the Non-Neutrality Error will be significantly larger.

Comparison of Group 1 and 2 indicates that bore offset causes Thickness/Time methods to be systematically biased high by a Non-Instantaneous Burnout Error. This error occurs in r_{TOT} methods because the thickness actually burned at initial burnout is less than the average web thickness usually used for calculations. Comparison of the two groups indicates that bore offset causes Thickness/Time methods to be systematically biased high by the percent offset (about 0.76% in Group 2).
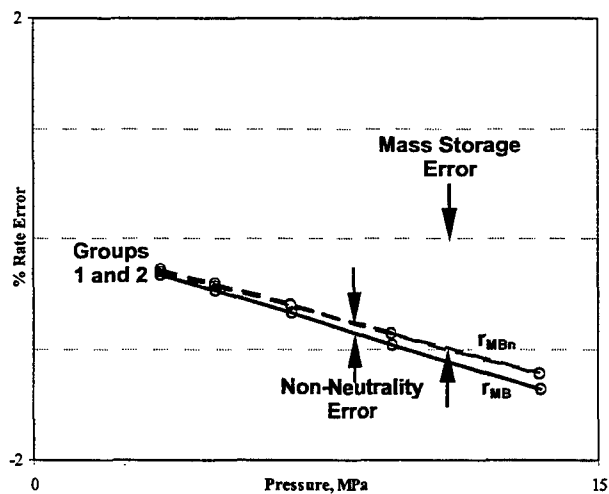
**Figure 45. Errors in Mass Balance Rate Methods
for RR #3**

Mass Balance method results are plotted in Fig. 45. The Mass Balance burning rate definition very effectively compensates for non-instantaneous burnout, and the two simulation groups are consequently superimposed in the plot. In the most commonly used Mass Balance rate method,: r_{MB} (solid lines), mass storage is neglected and Time-Averaged pressure is used as the associated pressure. The modified method, r_{MBn} (dashed lines), uses the Rate-Averaged pressure and iterative exponent analysis, but still neglects mass storage. Results for the two groups, by either method, are the same within about 0.5 time resolution units, indicating that Mass Balance methods effectively eliminate the Non-Instantaneous Burnout Error that affects Thickness/Time rates. Comparison of the two Mass Balance methods indicates that r_{MB} is biased low by about the same Non-Neutrality Error as was found from the Thickness/Time methods r_{TOT}, or 0.01%/MPa. Both Mass Balance methods are systematically biased low by a Mass Storage Error of about 0.09%/MPa.

The Mass Storage Errors that occur in mass balance rates r_{MB} (solid) and r_{MBn} (dashed) are approximately proportional to pressure as shown in Figure 46. The residual error in the modified procedure r_{MBn} is about 0.09%/MPa for this particular motor design. This Mass Storage Error also depends upon chamber volume, so it will vary with motor design. The Mass Storage Error is approximately proportional to pressure, which then causes the measured $\ln r$-$\ln p$ relationship to be nonlinear. This effect is shown in Figure 46 as a systematic convex-upward curvature in the deviations from the fitted line. The Non-Neutrality Error, being also proportional to pressure, has a similar effect. In this specific design, the Non-Neutrality Error is appreciably smaller than the mass Storage Error, and consequently has smaller nonlinearity effect. However, the relative sizes of the two errors should be expected to vary appreciably between motor designs and rate equations.
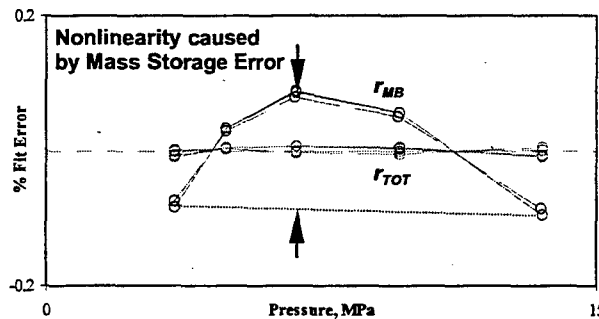
Figure 46. Deviations From Fitted Rate-Pressure Line for RR #3

Figure 47 presents the percent rate error from the iterated two-point thickness/time r_{HG} method. The Non-Instantaneous Burnout Error and the Non-Neutrality Error characteristic of thickness/time methods have effectively been eliminated by use of this method. Data from the r_{HG} method, plotted at greatly magnified scale, indicates that both the bias and the precision of the r_{HG} method are less than the nominal time resolution of 0.01%.

73
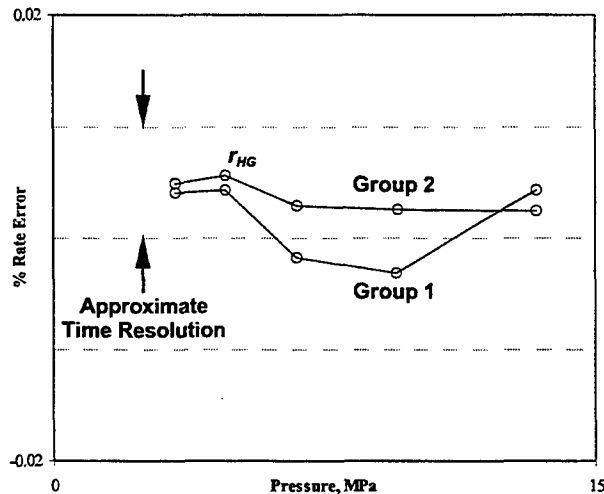
Figure 47. Errors in Iterative Two-Point Thickness/Time Rate for RR #3

5.3.3 Round Robin #3 Conclusions

Round Robin #3 was carried out with an ideal baseline simulation of a 2x4-inch laboratory scale motor. The baseline consisted of a set of five pressures vs. time relations. Another set of five pressures vs. time relations were added that represented an off-axis bore situation that is commonly experienced in real motor firings

Only the HG method recovered the baseline and off-axis reference rates within 0.01%, the approximate time resolution. Ten of 18 participants predicted the baseline reference within ± 0.25%, while 8 of 18 predicted the off-axis bore reference within ± 0.5%. Sixteen of 18 participants predicted the baseline reference within ± 0.5%, while 11 of 18 predicted the off-axis bore reference within ± 0.5%. The deviations increased for the off-axis bore case. The smallest relative errors are observed using methods that more effectively account for non-ideal tailoff, which is more easily seen with the Group 2 off-axis bore cases. This includes iterated MB, MB, iterated TOT, and TOT using a burn time definition that accounts for non-ideal tailoff as discussed in Section 4.2. The greatest relative errors are observed using TOT methods with simple definitions for burning time, i.e. 10%P, or Tangent-Bisector.

While only the HG method consistently recovered the reference burning rate for both groups, many other methods produced highly respectable results.

The derived power law coefficient and exponents indicate that 9 of the 18 participants recovered the baseline exponent within 0.5%, while 10 of 18 recovered the off-axis bore exponent within 0.5%. The 15 of the 18 participants recovered the baseline coefficient within 0.5%, while 11 of 18 recovered the off-axis bore coefficient within 0.5%. The general trend was to under-predict the exponent and over-predict the coefficient.

The Hessler-Glick method proved superior to all other methods when comparing all baseline and off-axis bore results. To explore this superiority further, RR #3 was extended with cases that simulating the effects of: non-neutral trace shapes, different constant and random bore offset, different and random L*, and different rate equation. These effects are explored in RR #3X discussed in the next section.

Lessons learned from RR #3 and RR#3X are both summarized in Section 5.5 following a review of RR #3X results.

74

5.4   International Round Robin #3X Results

Round Robin #3X is also based on the computer program, created by R.O. Hessler and R. Glick in support of the WG 016, to simulate a 2x4-inch motor configuration motor for research into burning rate measurement methods.[87] Details of the RR #3X design and input data are summarized in Appendix C-4. RR #3X consists of 40 additional cases, arranged in eight groups of simulated rocket motors beyond those examined in RR #3. These additional groups are mainly perturbations of the original RR #3 Group 2, which had constant bore offset. These groups are designed to examine the effects of non-neutrality, L^*, further bore offset perturbations, and of higher rate, pressure, and exponent. Data typically unknown, such as the burning rate equation, bore offset, and randomized parameters were withheld from the participants. RR #3X responses were received in late-1999 from POLIMI, who analyzed the cases using TOT methods from Bayern Chemie (BC) and Hessler-Glick (HG).

Details of the RR #3X design and input data are summarized in Appendix C-4. Again, a simple 2x4-inch motor configuration as shown in Figures C-5 and C-6 was simulated. RR #3X consists of 40 additional cases, arranged in groups of five, labeled Groups 3 through 10. These additional groups are mainly perturbations of the original RR #3 Group 2, which had constant bore offset. The exception is Group 9, which is a perturbation from Group 5. The primary perturbations are summarized in Table 23 below. Representative pressure-time plots are shown in Figures 48 through 51. A more complete description of the groups is provided in the next section.

Table 23.   RR #3X Small Motor Ballistic Simulations Examined

Group	Cases	Perturbation
3	11-15	Non-neutral trace shape (Progressive)
4	16-20	Non-neutral trace shape (Regressive)
5	21-25	Different constant bore offset
6	26-30	Random bore offset
7	31-35	Different constant L^*
8	36-40	Random L^*
9	41-45	Higher rate equation and bore offset
10	46-50	Additional random bore offset

The forty pressure-time histories were simulated for a generic 2x4-inch motor and are comprised of eight groups. Each group contains five motors, equally spaced in log pressure (3.5, 5, 7, 10, and 14 MPa).

75
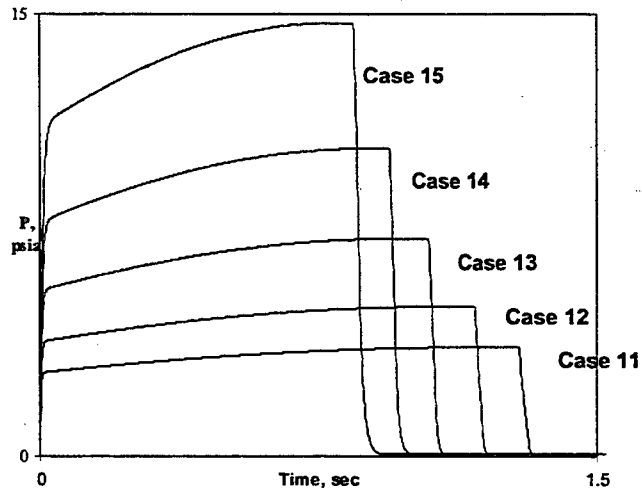
Figure 48. RR #3X Group 3 with Progressive Pressure Trace Shape
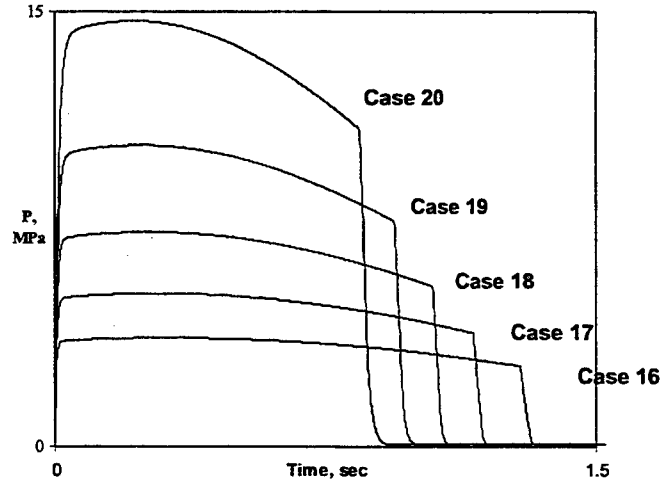
Figure 49. RR #3X Group 4 with Regressive Pressure Trace Shape
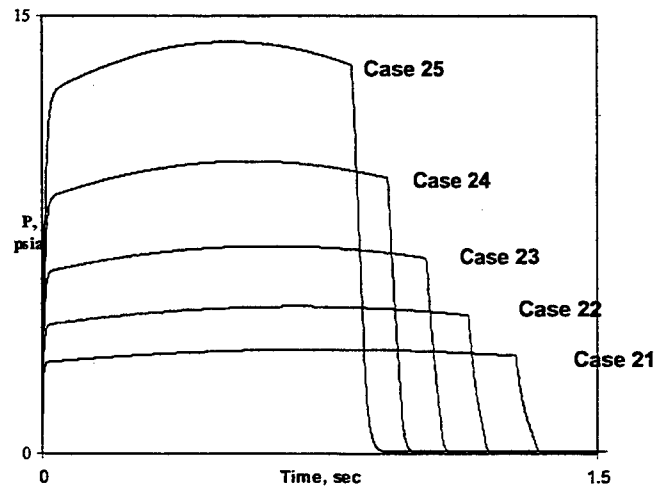
Figure 50. RR #3X Group 5 with Offset. Groups 6-8 and 10 Similar, but with Variations of Ignition Pressurization Rates and Tailoff.

76
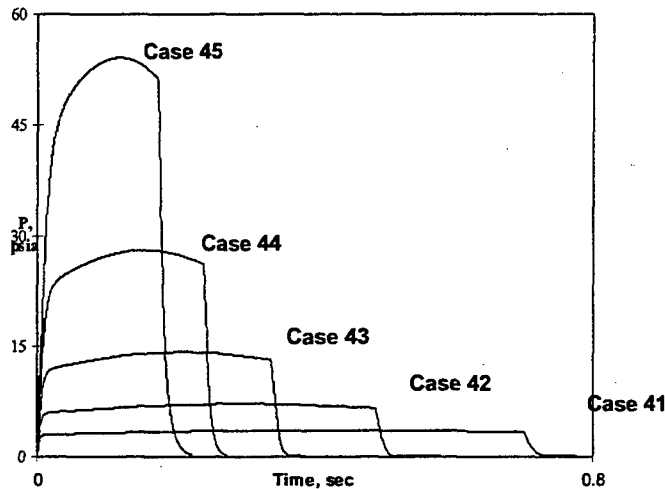
Figure 51. RR 3X Group 9 with Higher Rate Equation and Bore Offset

5.4.1 Round Robin #3X Analysis

To examine the effects of additional variables, the limited number of RR3 tests was extended with numerical experiments simulating further effects: non-neutral trace shapes, different constant and random bore offset, different and random L*, different rate equations, different liners, and different nozzle materials to simulate nozzle clogging and erosion. Thus, RR3X tests were generated proposing many additional groups. A short description of the ten groups follows.

GROUP 1 is the baseline case and it has a concentric bore. The motor case centerline is coincident with the bore centerline and bore offset is zero. Combustion is neutral, the propellant length L=95.25 mm and L_{free}=31.928 mm. Nominal pressures are 3.5, 5, 7, 10 and 14 MPa respectively for cases 1, 2, 3, 4 and 5 obtained with the corresponding nozzle diameters of 10.5435, 9.3650, 8.3160, 7.3863, and 6.5608 mm.

GROUP 2 has a bore offset but the value was not furnished to the RR3 participants. Data reduced from real motors of this design indicates non-instantaneous burnout corresponding to 0.3% to 0.9% of web thickness due to bore offset. The offset value was subsequently furnished as 0.096279 mm on a web of 12.7 mm (0.7581%). Combustion is neutral, L=95.25 mm and L_{free}=31.928 mm. Nominal pressures are 3.5, 5, 7, 10 and 14 MPa respectively for cases 6, 7, 8, 9 and 10.

GROUP 3 has a progressive combustion obtained with a grain length L=120.65 mm, that is different from the other groups but still L_{free}=31.928 mm. The constant bore offset value is the same of group 2. Nominal pressures are 3.5, 5, 7, 10 and 14 MPa respectively for cases 11, 12, 13, 14 and 15.

GROUP 4 has a regressive combustion obtained with a grain length L= 69.85 mm, that is different from the other groups but still L_{free}=31.928 mm. The constant bore offset value used is the same of group 2. Nominal pressures are 3.5, 5, 7, 10 and 14 MPa respectively for cases 16, 17, 18, 19 and 20.

GROUP 5 has a different constant bore offset than the one used for the group 2 to simulate a different non-instantaneous burnout. The value was not furnished. Combustion is neutral, the propellant length L is 95.25 mm and L_{free} is 31.928 mm. The nominal pressures are 3.5, 5, 7, 10 and 14 MPa respectively for the cases 21, 22, 23, 24 and 25 obtained with the respective nozzle diameters of 10.5435, 9.3650, 8.3160, 7.3863, and 6.5608 mm.

GROUP 6 has a random bore offset to approximate tail-off variations in real motors. Combustion is neutral, L=95.25 mm and L_{free}=31.928 mm. Nominal pressures are 3.5, 5, 7, 10 and 14 MPa respectively for cases 26, 27, 28, 29 and 30.

77

GROUP 7 has a different constant L_{free}=158.75 mm. This group has an unrealistically large L_{free} necessary to match slower ignition rise rates observed in real motors with comparable rates, believed caused by heat losses (not included in the simulation). Combustion is neutral, L=95.25 mm. Nominal pressures are 3.5, 5, 7, 10 and 14 MPa respectively for cases 31, 32, 33, 34 and 35.

GROUP 8 has a random free length L_{free} used to approximate variations of thread engagement for motors with pipe threads. Combustion is neutral and the propellant length L is 95.25 mm. The nominal pressures are 3.5, 5, 7, 10 and 14 MPa respectively for the cases 36, 37, 38, 39 and 40 obtained with the respective nozzle diameters of 10.5435, 9.3650, 8.3160, 7.3863, and 6.5608 mm.

GROUP 9 has a different rate equation and a different constant bore offset. Combustion is neutral, the propellant length L is 95.25 mm and L_{free} is 31.928 mm. The nominal pressures are 3.5, 7, 14, 28 and 56 MPa respectively for the cases 41, 42, 43, 44 and 45 obtained with the respective nozzle diameters of 10.5435, 9.3650, 8.3160, 7.3863, and 6.5608 mm. The nozzle diameters are the same of the other groups.

GROUP 10 has an additional random bore offset to approximate, as in the group 6, tail-off variations in real motor. Combustion is neutral, the propellant length L is 95.25 mm and L_{free} is 31.928 mm. The nominal pressures are 3.5, 5, 7, 10 and 14 MPa respectively for the cases 46, 47, 48, 49 and 50 obtained with the respective nozzle diameters of 10.5435, 9.3650, 8.3160, 7.3863, and 6.5608 mm.

The reference burning rates shown in Table 24 were the same for all the Groups except Group 9, and were derived from the power law coefficient a = 6.59441 and exponent n = 0.3157. These values for Group 9 are a = 9.326132, and n = 0.53140.

Table 24. RR #3 Reference Burning Rate Values

p_c, MPa	Groups 1-8,10	Group 9
	r_b, mm/s	r_b, mm/s
3.5	9.79351	18.1476
5	10.9608	21.9348
7	12.1892	26.2293
10	13.6419	31.7031
14	15.1708	37.9100

Table 25. Percent Relative Error ($1-r_b/r_{b,ref}$) of Burning Rates for BC and HG Methods

Group	Perturbation	Relative Error BC (%)	Relative Error HG (%)
1 (Fig. 2a)	Baseline, neutral trace shape	+0.075 to +0.350	+0.004 to +0.007
2 (Fig. 2b)	Baseline, neutral trace, bore offset	+0.040 to +0.480	- 0.007 to - 0.006
3 (Fig. 2c)	Non-neutral trace shape (progressive)	+0.182 to +0.612	- 0.010 to - 0.006
4 (Fig. 2d)	Non-neutral trace shape (regressive)	+0.095 to +0.335	- 0.006 to - 0.006
5 (Fig.	Different constant bore offset	- 0.254 to +0.527	- 0.163 to +0.031
6 (Fig. 2e)	Random bore offset	- 0.254 to +0.527	- 0.163 to +0.031
7 (Fig. 2f)	Different constant L*	+0.088 to +0.559	- 0.020 to - 0.007
8 (Fig.	Random L*	- 0.049 to +0.473	- 0.035 to +0.002
9 (Fig.	Different rate equation with bore offset	- 0.599 to +0.647	- 0.404 to +0.369
10 (Fig	Different random bore offset	- 0.152 to +0.524	- 0.073 to +0.002

Only results obtained[89,90,91] implementing HG and BC methods are here shown; details over a wide range of cases are reported in[90]; more advanced analyses are discussed elsewhere.[68] Over the investigated pressure range 3.5 to 14 MPa, the relative errors ($1-r_b/r_{b,ref}$) of the burning rates calculated by HG (—) and BC (----), with respect to the reference values, are summarized[79] in Table 25.
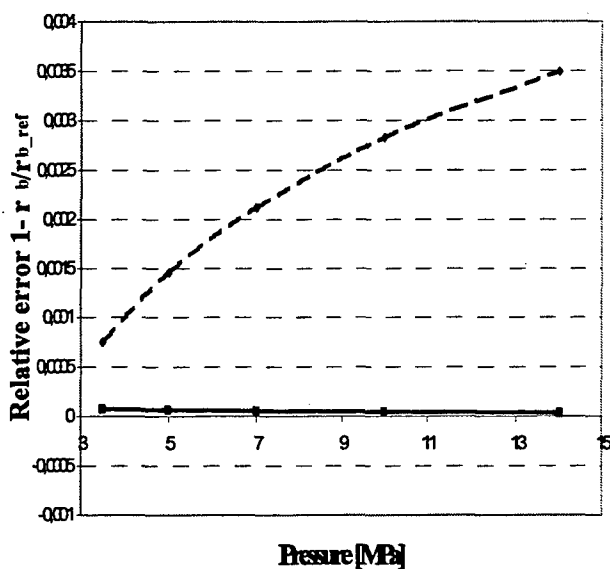
Figure 52. Group 1 Baseline Progressive Burn Relative Error
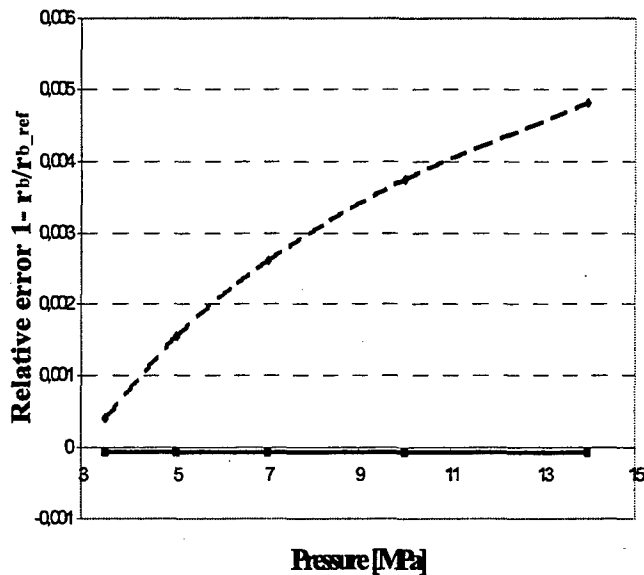
Figure 53. Group 2 Baseline Regressive Burn Relative Error
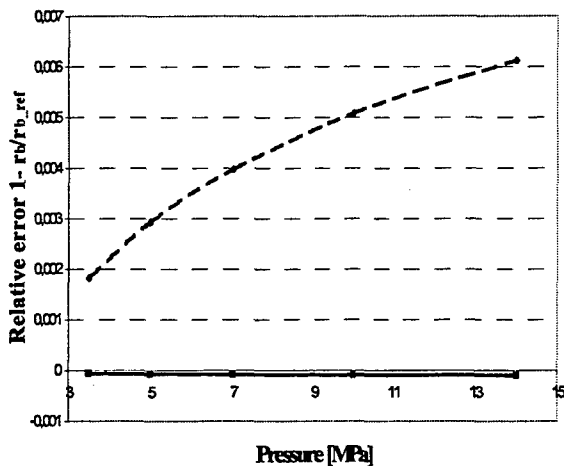
Figure 54. Group 3 Baseline Progressive Burn Relative Error
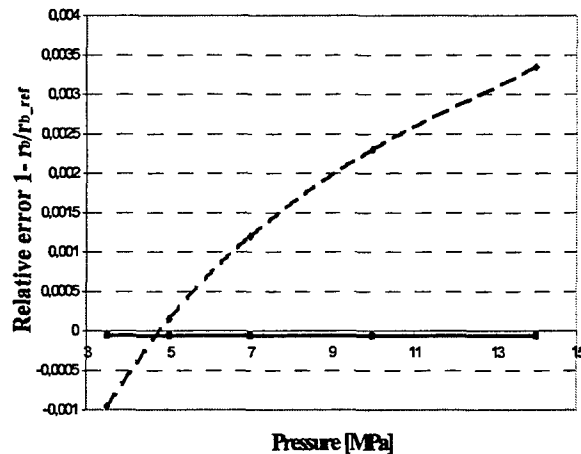
Figure 55. Group 4 Baseline Regressive Burn Relative Error
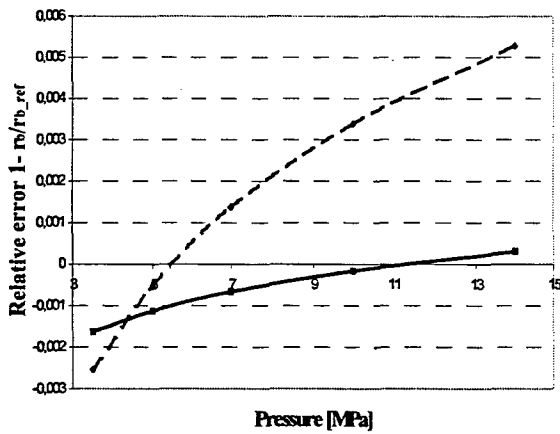
Figure 56. Group 5 Baseline Progressive Burn Relative Error
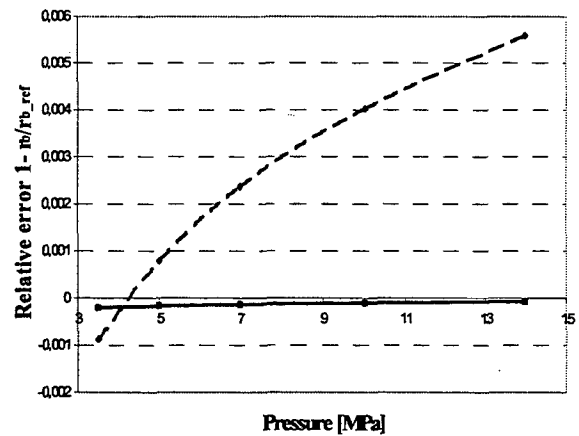
Figure 57. Group 6 Baseline Regressive Burn Relative Error
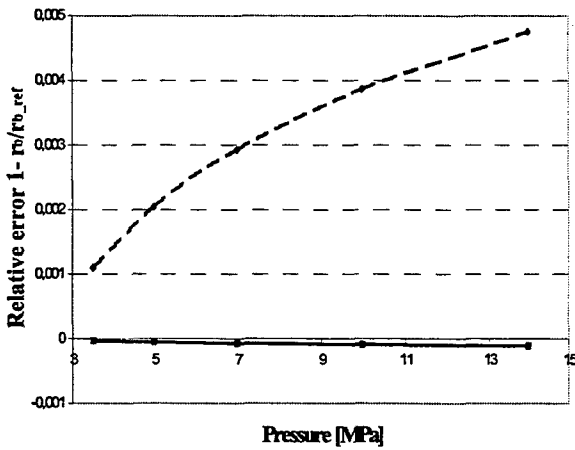
Figure 58. Group 7 Baseline Progressive Burn Relative Error
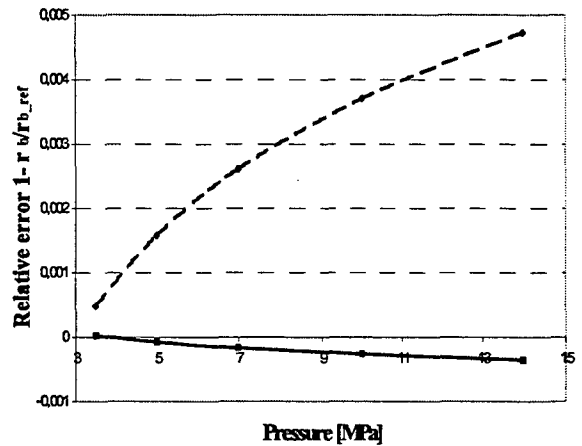
Figure 59. Group 8 Baseline Regressive Burn Relative Error
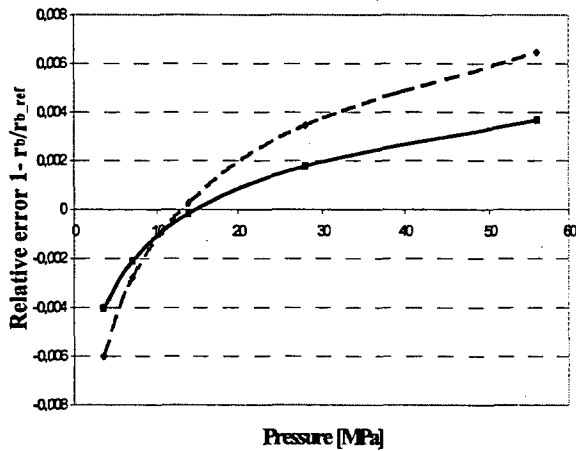
Figure 60. Group 9 Baseline Progressive Burn Relative Error
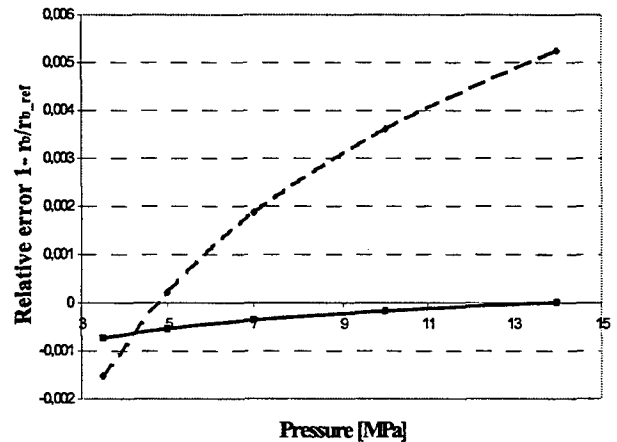
Figure 61. Group 10 Baseline Regressive Burn Relative Error

80
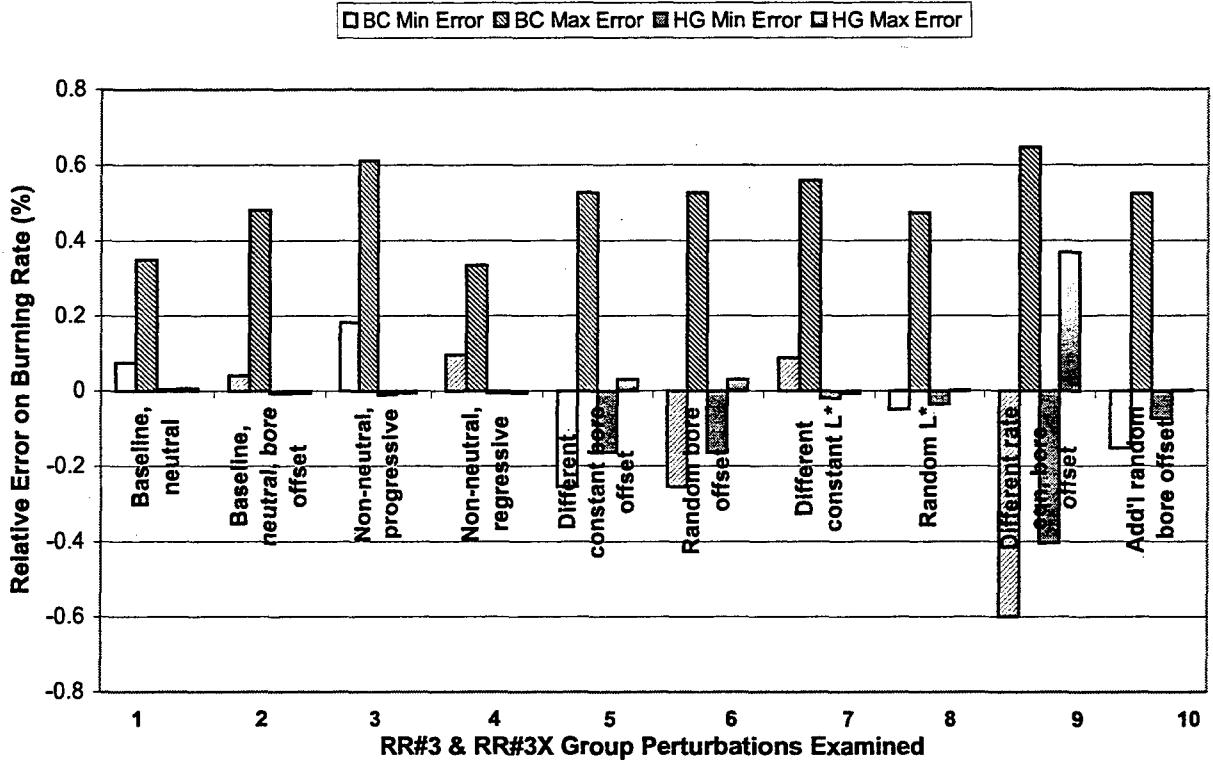
Figure 62. Relative Burning Rate Error for All RR #3 and RR #3X Perturbations
Using BC and HG Analysis Methods

5.4.2 Round Robin #3X Conclusions

RR3 tests have pointed out the quality of applied data reduction methods for a change of selected parameters that influence combustion (bore offset; L^*; non-neutral trace shape; rate equation). The BC method, taken as representative of the industrial TOT methods, is sensitive to all parameters but is less sensitive to a change of L^* and to non-neutral combustion. HG method, only slightly influenced by a change of bore offset and insensitive to other parameters, systematically yields lower errors (see Figures 52 through 61). In treating simulated pressure traces, as confirmed by further analyses[6], HG method proved superior thanks to a careful handling of combustion processes, but each trace requires a specific operator's analysis.

5.5 Lessons Learned From Round Robin Simulated Motor Data

Burning rate measurements in real motors rely almost entirely on one of two burning rate definitions, either r_{TOT} or r_{MB}. In either case, the measurements are almost always based on a nominal or average web thickness, and are associated with the time-averaged pressure p_b. These two historical methods were used to determine motor burning rates in simulated motor data used for RR. Two modified methods, r_{TOTn} and r_{MBn}, were also applied to the RR3 dataset. The modifications consisted of associating the measured rates with the rate-averaged pressure p_{nb} and using an iterative solution to determine the pressure exponent n. Data were also reduced by the two-point HG procedure.

RR3 tests have pointed out the quality of applied data reduction methods for a change of several parameters (bore offset, characteristic length, non-neutral trace shape, rate equation, etc.) influencing combustion. Results from different methods were compared with the rate equation used for the simulations and with each other to identify the following systematic errors inherent in the various methods [6]:

- **Non-Neutrality Error:** Present whenever time-averaged pressure is used as the associated pressure (r_{TOT} and r_{MB}). Caused by non-constant pressure during burning. Corrected by use of rate-averaged pressure as the associated pressure (r_{TOTn}, r_{MBn}, and r_{HG}).

- **Non-Instantaneous Burnout Error:** Present in principle in TOT methods (r_{TOT} and r_{TOTn}). Caused by web thickness variations within individual motors. Avoided by use of MB methods (r_{MB} and r_{MBn}). Corrected by the iterated two-point TOT procedure (r_{HG}).

- **Mass Storage Error:** Present in MB rate methods (r_{MB} and r_{MBn}). Caused by neglect of mass storage in MB rate definition. Avoided in principle by TOT methods (r_{TOT} and r_{TOTn}). Fully avoided by the iterated two-point TOT procedure (r_{HG}). Correctable by accounting for transient operations, but some unknown residual error will remain due to invoked assumptions.

The Non-Neutrality error and Mass Storage error, being roughly proportional to pressure, cause a nonlinearity in the measured log rate versus log pressure relationship. This nonlinearity causes the measured pressure exponent n to appear slightly pressure dependent.

The r_{HG} procedure avoided all three of the errors above, obtaining data accurate to the basic time resolution of the simulations. Thus, in treating simulated pressure traces, HG proved superior to other methods thanks to a careful set of time points definitions, but requires visual inspection of each pressure trace.

The error levels in the reduced data were appreciably smaller than the suspected bias in real motors, evidenced by observation that burning rate in small motors is commonly of order 5% less than in larger scale end-item motors. However, these were *simulations*, and the simulations did *not* include several phenomena that occur in real motors. In particular, the simulation program assumed instant, effortless ignition in an adiabatic chamber, with burning immediately occurring at the equilibrium burning rate for the bulk propellant. In real propellants and motors, heat losses and the transients associated with the development of equilibrium burning extend the pressurization phase of the motor by a factor of two to five. The slower pressurization rate will cause the Non-Neutrality error to be increased by about the same factor. Similar transient phenomena will extend the tail off process, causing the apparent Mass Storage error to be similarly inflated. Observation that both errors cause rates to be underestimated suggests they

may be large contributors to observed rate scale factors. Further lessons learned from analysis of real motor data are summarized in Section 6.3 concluding a review of those results in following section.

6.0   ASSESSMENT OF METHODS USING REAL MOTOR DATA

RTO/AVT WG016 assessments of the various thickness/time (TOT) and mass balance (MB) analysis methods continued with the use of real motor data. The objectives of these assessments were the same as with the simulated motor data, which were to:

- Clarify distinctions of small motor analysis methods
- Identify sources of the differences

This assessment approach of using both simulated and real motor data is summarized in Section 1.3. Table 9 summarizes the scope of the assessments using real motor data and the degree of involvement by the volunteer participants. Several data reduction methods based on the thickness/time (TOT) definition, used by European companies and the reference Hessler-Glick (HG) technique, were applied; for comparison, a simple mass balance method was also examined. FIAT AVIO – Comprensorio BPD, located near Rome, Italy, provided the results of their analysis of their real motor tests using their M1 and M2 methods. Both are TOT methods; with M1 using simple start and stop burn time definitions, and M2 being identical to the SNPE method. Dr. DeLuca, POLIMI and Dr. Gadiot, TNO-PML graciously accepted the responsibility of guiding their respective graduate students in the analysis of the real motor data using various methods. POLIMI used the methods of POLIMI MB, SNPE, FIAT AVIO BPD M1 & M2, BAYERN-CHEMIE (BC), and HG, while TNO-PML used the methods of TNO M1, BC, and HG. Details of all analysis methods are provided in Appendix B.

Real subscale rocket motor data originating from FIAT AVIO and TNO became available to RTO/AVT WG016 for the purpose of evaluating data analysis methods. The real combustion experiments show pressure traces perturbed by noise. The noise is caused by the combustion process, the flow field and instrumentation; and may complicate the data reduction. Filtering (smoothing) the data before applying a data analysis method can (partially) eliminate noise. Moreover, the real pressure traces had a lower sampling rate than the Round Robin data, which means a lower intrinsic accuracy.

6.1 FIAT AVIO BPD Motor Data[88]

6.1.1   Ariane Booster Experimental Motor Pressure-Time Data

Pressure traces obtained in the subscale test motors implemented for Ariane solid propellant boosters are examined in this section. Since the actual burning rates are unknown, results are compared based only on the statistical quality of the deduced ballistic data. Moreover, ease of application and capability of automatic handling are of interest especially for industrial propellant production facilities. Within this framework, specific features and general trends of the analysis methods examined are discussed.

Data reduction methods were contrasted[88] to analyze the Baria (6300g) and 2-inch (350g) experimental pressure traces used to evaluate the ballistic parameters respectively for Ariane-5 and Ariane-4 solid propellant boosters. See JHU/CPIA CPTR 74[5] for a complete description of test hardware details. Fiat Avio – Comprensorio BPD, located at Colleferro, near Rome, Italy, conducted all tests in early-2000. Four series of 9 mixes were made for Ariane-5 and, for each mix; burning tests at 3 different pressure levels were conducted for a total of 108 Baria motor tests. Likewise, a series of 4 mixes were made for Ariane-4 and, for each mix, 6 burning tests (2 at each of the 3 tested pressures) were conducted for a total of 24 2-inch motor tests. For a matter of space, mainly the four series of Ariane-5 mixes are discussed. Comparative analyses were conducted in a series of M.Sc. Theses[89,90,91,92,93] completed at Politecnico di Milano (POLIMI).

For each mix of each series, a group of 3 experimental pressure traces was obtained from Baria testing. Normalized pressure plots were then constructed for each series of 9 mixes. Examples of average shapes for the normalized plots at the 3 burning pressures are shown in Figure 63, and indicate

appreciable but repeated differences between the test pressures. Typical test pressures ranged from 0 – 80 MPa, while typical motor burning times ranged from 0 – 5 seconds. The traces almost overlay from about 50% to 70% of burn. This is probably the only region of truly normal behavior. Motors that are plunge cast typically have trace shapes with the S-shaped decrease and increase beginning about 50% burn. It is believed the S-shape is caused by particle stratification in boundary layers during casting, causing the propellant formulation to vary locally within the thickness of the propellant grain.
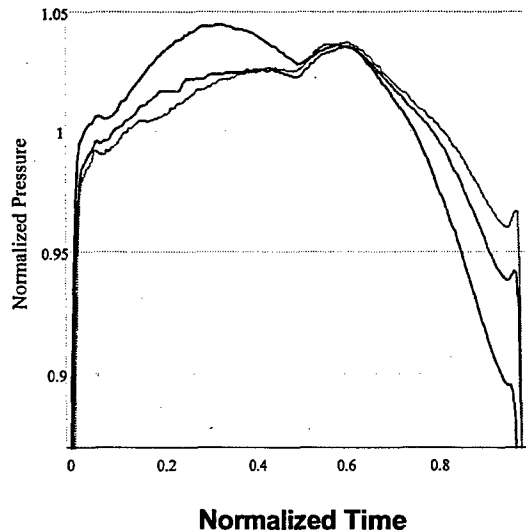
Normalized Time

Figure 63. Average Normalized Pressure-Time Behavior of Baria Motor Tests[88]

From 70% onward, the normalized pressures steadily diverge until they span about 6% at initial burnout. This is interpreted as corresponding to an onset of nozzle erosion around 70%, with the erosion rate increasing with pressure. Nozzle erosion does not affect the burning rate except through the standard effect of pressure in the equilibrium burning rate equation, which is compensated by use of rate-averaged pressure as the pressure associated with the measured burning rate.

The shape of the region from about 10% to 50% of burn varies appreciably with pressure, and probably indicates the action of several processes. The most pronounced effect is the generally increased convexity with increased pressure, believed due to either heat losses or transient combustion response. During transient burning, measured burning rates are in error. Transient burning is not compensated by use of rate-averaged pressure. Transient burning and other peculiar effects can be analyzed in detail by inspecting individual normalized pressure plots.

6.1.2 Filtering of Pressure-Time Traces for the Hessler-Glick Analysis Method[94]

The Hessler-Glick analysis method is unique in that it resorts to derivative-based time point definitions, which was shown to be rigorous for the RR3 simulated data. The standard definitions for beginning of burning t_B, initial burnout t_{Ei} and final burnout t_{Ef} for ideal pressure traces (no noise corruption) were defined earlier in Section 3.4.6.

This is how motors are expected to behave if the whole experimental procedure works perfectly: in ideal motors, pressure profile is not corrupted by noise allowing the HG method to operate fine notwithstanding the use of time derivatives. But due to non-idealities, in real motors the above characteristic features of pressure traces are only trends to be identified: noise confuses the pressure signal and a filtering process is usually needed to extract the wanted information from the recorded signal. However, any filtering process has the potential of not only removing the noise, but also distorting the signal, thereby introducing an error, see Figures 64 through 66. Furthermore, use of derivative definitions requires careful interpretation of events during the burnout process. In Figures 65 and 66, for instance, initial burnout t_{Ei}

occurs at the first decrease of p'/p, followed by probable at least partial extinction (not clearly identifiable because of low amplitude resolution), then reignition and a second extinction at the middle of the figure. Thus, application of HG method to real motors requires good resolution, low noise, and proper handling. A constant, centered, sliding, m wide filter (m being an odd number of points averaged together) was used to average a block of data. That filter can be written as

$$p_m(i) = average \left\langle p\left(i - \frac{m-1}{2}\right) : p\left(i + \frac{m-1}{2}\right)\right\rangle \tag{59}$$

while the first and second derivatives can be defined, using centered finite differences, as

$$p'_M(i) = \frac{1}{2h}\left[p_m(i+1) - p_m(i-1)\right] \tag{60}$$

$$p''_M(i) = \frac{1}{h^2}\left[p_m(i-1) - 2p_m(i) + p_m(i+1)\right] \tag{61}$$

where $M = m + 2$ is the combined filtered-derivative filter width to account for the additional width of the derivative function, and h is the time resolution. The result is numerically very close to, possibly identical with, the results from a Savitzky-Golay[95] filter of order 2 and width M.

Filtering reduces noise, but also distorts the shape of signal transients. As detection of burnout times is specifically searching for steps in p", it is advisable to check the filter effects by comparing the filtered with the raw data. In Figure 64, for instance, p_{19} and p_{39} traces distort the signal well outside the range of the original noisy data p_1 in the region of t_{Ei}.
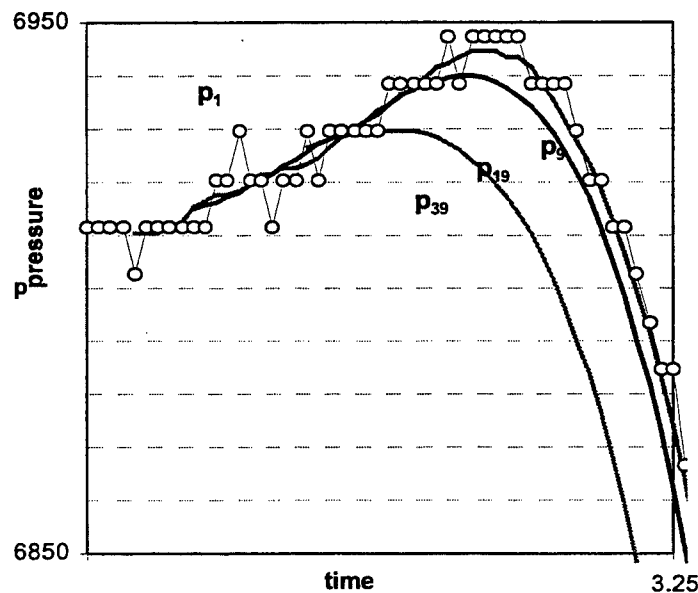
Figure 64. Comparison of Filtered with Raw P-t Data (p_1: black points with line, p_9, p_{19}, p_{39})[94]

85
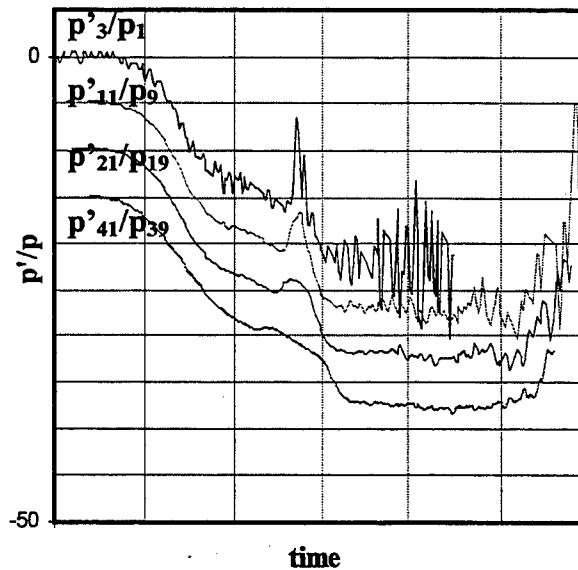
Figure 65. Normalized First Derivatives (p'_3/p_1, p'_{11}/p_9, p'_{21}/p_{19}, p'_{41}/p_{39})[94]

Analysis of p" for the tail-off region of real motors shows that noise may completely obscure the approximate true behavior. It is therefore necessary to use alternative definitions based on p' or p'/p. Inspection of derivative behavior in simulated data indicates that the end of burnout t_{Ef} can also be satisfactorily defined by a negative peak in p'/p. This has the advantage that the resolution of p' is only magnified by $1/(2h)$, so there is generally less noise.

The uncertainty in initial burnout t_{Ei} is also large: again, noise problems preclude any confident use of p" definitions. The best alternative definition for t_{Ei} in motors with large noise problems would be a first perceptible decline of p' type definition. Motors typically feature a "Friedman Curl", so p' will be slightly positive for a short while before the main pressure decay. After filtering, to obtain p_m with m minimal to reduce the noise during the curl to less than some arbitrary percentage of the value of p' minimum, p'_M was calculated and t_{Ei} detected from a p' plot as the first time point which clearly lies below the p' trend (just below its noise level) during the curl. This would consistently locate t_{Ei} very slightly before the peak of the curl, which is where p" is expected to step downward.

Figure 65 shows the normalized first derivative for four filter widths, with the baselines displaced downward for separation by exactly one gridline for successive filter widths. The unfiltered plot, at top, was terminated early to eliminate the large noise level. Note that the normalization causes resolution and noise to be pressure dependent, implying for the general noise level to increase in time as pressure declines.

Figure 66 shows first derivative behavior during burnout and tail off. Increasing filter widths appear to move the first perceptible p' decline earlier in time, to move the minimum later in time, and to move the anomalous peak earlier in time.

HG procedure averages the results for initial and final burnout, so the uncertainty will be reduced to some unknown bias range of order few %. Although any systematic algorithm that is used to detect the time points will reduce the scatter between like motors, each of those algorithms will result in a different scale factor. In order to reduce the bias or scale factor, it is necessary to reduce those uncertainties; the largest single problem is t_{Ef} uncertainty.
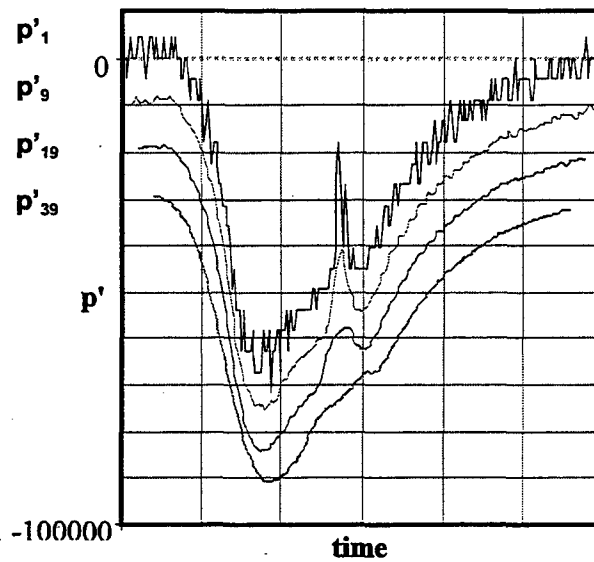
Figure 66. First Derivatives During Burnout[94]

Detection of t_B is difficult too, as shown in Figure 67. As a general rule, motor pressurization is a smooth function; consequently, oscillations should be ignored. The value of t_B should be taken at first rise, using usual p' definition. As both p and p' should be zero before pressure begins to rise, first rise in p is equivalent to first rise in p'. Therefore, t_B = Midpoint Before First Rise in p on last sustained rise is an alternative detection algorithm. Obviously, the rise must be one resolution unit or more above the noise.
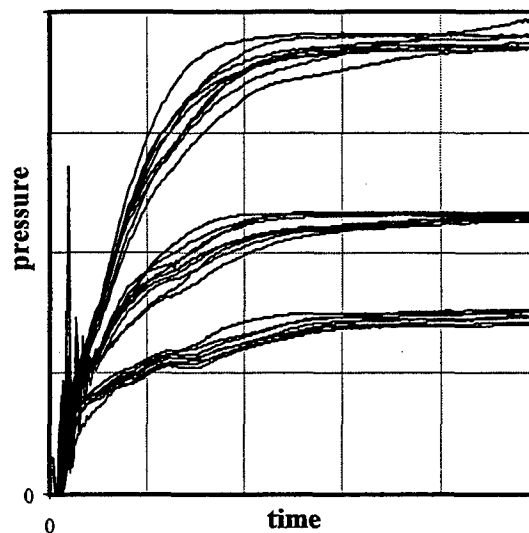
Figure 67. Ignition of Nominally Identical Motors Tested at Three Pressures[94]

Servieri[89] performed initial tests of the above-modified HG method using the experimental pressure traces of Baria B series. A moving filter with $m=9$ was implemented. HG results so obtained were successfully compared with the standard BPD-1 results, as shown in Table 26. Burning rates are reported at the reference value of 4.5 MPa.

87

Table 26. Mean Values of Ballistic Parameters of B Series at Reference Pressure 4.5 MPa for Modified HG and Standard BPD-1 Methods[88]

Group of Motor Tests	Modified HG		BPD-1	
	n	r_b	n	r_b
B-01	0.364	7.249	0.346	7.249
B-02	0.351	7.245	0.339	7.243
B-03	0.356	7.285	0.330	7.282
B-04	0.368	7.265	0.341	7.299

6.1.3   FIAT AVIO BPD Experimental Results and Observed Trends in Analysis Methods

Following this validation, a systematic comparative analysis was conducted[91-93] using the two complete series of experimental pressure traces, A5 and A4, respectively from Ariane-5 (Baria) and Ariane-4 (2-Inch) small-scale test motors. Standard industrial methods were compared to filtered HG (resorting to a variety of digital techniques) and a generic MB method implemented at Politecnico di Milano (POLIMI).

<u>Ariane 5 (A5) / Baria Results</u>

All results are reported at the reference pressure of 4.5 MPa (45 bar) in Table 27 (overall values), Table 28 (mean values), and Table 29 (coefficients of variation). The overall ballistic parameters in Table 27 were obtained by just *one* least-squares fit, to the power law rate equation, of *all* available data groups: the total set of 36 groups (Table 27). The correlation factor shows that results are essentially independent on the implemented data reduction method both for the total set of 36 groups. Results[88] also indicate the same is true for each mix subset of 9 groups. However, subsets indicated series variability in that correlation factor was relatively high for some Baria Series and relatively low for others.

Table 27. Overall Values of Ballistic Parameters and Correlation Factor of All Baria Data Groups at Reference Pressure 4.5 MPa[88]

Method	Type	n	A	r_b	R^2
BC	r_{TOT}	0.3850	4.1686	7.4387	0.9963
BPD-1	r_{TOT}	0.3856	4.1669	7.4423	0.9963
BPD-2	r_{TOTn}	0.3839	4.1662	7.4223	0.9963
POLIMI	r_{MB}	0.3794	4.1785	7.3939	0.9962
SNPE	r_{TOTn}	0.3839	4.1668	7.4233	0.9963
HG	r_{TOTn}	0.3815	4.2187	7.4756	0.9958

The mean ballistic parameters in Table 28. were obtained by simply *averaging* the available power law rate least–squares *fits* (not shown for a matter of space) for all 36 groups. The corresponding coefficients of variation CV of ballistic parameters in Table 29 were obtained as percent ratio of the standard deviation over mean values (as listed in Table 28). These CV are an index of mix variability: averaged values associated with all 36 data groups computed as the quadratic mean among all series are reported in Table 29 (an index of both mix and motor variability).

**Table 28. Mean Values of Ballistic Parameters of All Baria Data Groups
At Reference Pressure 4.5 MPa (standard deviation for 36 groups of fire tests)[88]**

Method	n	a	r_b
BC	0.3843 ± 0.0056	4.1733 ± 0.0347	7.4391 ± 0.0521
BPD-1	0.3849 ± 0.0056	4.1716 ± 0.0350	7.4427 ± 0.0519
BPD-2	0.3832 ± 0.0055	4.1709 ± 0.0342	7.4228 ± 0.0519
POLIMI	0.3787 ± 0.0056	4.1832 ± 0.0339	7.3943 ± 0.0518
SNPE	0.3832 ± 0.0055	4.1715 ± 0.0347	7.4237 ± 0.0520
HG	0.3804 ± 0.0061	4.2193 ± 0.0373	7.4760 ± 0.0517

Industrial TOT methods (BC, BPD-1, BPD-2, SNPE) do not explicitly account for non-instantaneous burnout. However, specific choices of time points may make a partial correction implicitly. Methods that define end of burning near 50% pressure implicitly assume burning continuation and thus partly avoid non-instantaneous burnout error. These TOT methods tend to behave similar to MB methods. MB methods yield rates that are systematically low by a mass storage error. HG fully avoids the mass storage error, so it will systematically yield higher rates than MB methods. TOT methods with instantaneous burnout also avoid the mass storage error but yield high bias due to non-instantaneous burnout.

Examination of motor data for each series of 9 mixes (mix variability) indicates that the industrial methods nominally assuming instantaneous burnout (BC, BPD-1, BPD-2, SNPE) produce mean values that are quite similar, as expected from the general similarity of these methods. Within this group, BPD-2 and SNPE (which differ only in details) produce about the same mean values, while BC produces reasonable results with little effort. Relative to the industrial methods, the generic MB procedure POLIMI produces lower rates and lower exponents; HG produces higher rates and lower exponents. HG and POLIMI methods in general also yield relatively more confined values of standard deviation for the ballistic parameters *n* and *a*. Most of these observed differences appear to be explainable in terms of known physical effects.

Time-averaged pressure is greater than rate-averaged pressure, so any procedure using time-averaged pressure yield a rate equation that is consistently biased low due to the Non-Neutrality error. As HG is the only procedure using rate-averaged pressure as the associated pressure, HG rates are expected to be higher than the others, as observed.

In general, for a fixed average degree of non-instantaneous burnout due to either grain distortion or misalignment, the Non-Neutrality error for a propellant will increase at lower pressures, because the burnout process extends for a greater fraction of the tail-off process.[96] As a consequence, methods that use time-averaged pressure as the associated pressure should be expected to yield rate equations with exponents biased high, while HG exponents are expected lower.

POLIMI detects t_E at the knee of the curve, for which the Non-Neutrality error will be less than for the first group, which all define t_E much later, when pressure has declined to around 50%. Consequently, POLIMI exponent should be expected to generally agree with HG exponent as observed, because although POLIMI does not correct for Non-Neutrality error, the error is not large.

Because POLIMI is a generic MB method, it should be expected to be biased low by a mass storage error, and thus be lower than HG. However, the expectable mass storage error is not sufficient to account for the observed difference. The remaining difference between POLIMI rate and HG rate is unexplained, but is believed related to the effects of non-equilibrium burning and extinction during the burnout process. A similar difference was observed in a comparison of TOT, MB, and HG methods with a different motor.[87]

Table 29. Averaged Mix Variability of all Baria Series At Reference Pressure 4.5 MPa[88]

Method	CV% n	CV% a	CV% r_b
BC	1.4186	0.8452	0.5481
BPD-1	1.4369	0.8481	0.5469
BPD-2	1.3757	0.8259	0.5473
POLIMI	1.3600	0.8112	0.5468
SNPE	1.3955	0.8396	0.5485
HG	1.4463	0.8779	0.5573

Ariane-4 (A4) / 2-Inch

Mean ballistic parameters were also obtained for Ariane-4 series of experimental pressure-time traces by simply *averaging* the available power law rate least-squares fits for each series of fire tests, see Table 30 (2-Inch). The associated coefficients of variation CV (percent ratio of standard deviation/mean value) are reported in Table 31 (2-Inch).

Table 30. Mean Values of Ballistic Parameters of A4 Series at Reference Pressure 4.5 MPa (standard deviation for 4 groups of motor tests)

Method	n	a	r_b
BC	0.3587 ± 0.0068	3.6634 ± 0.0366	6.2829 ± 0.0242
BPD-1	0.3595 ± 0.0067	3.6615 ± 0.0352	6.2873 ± 0.0244
BPD-2	0.3582 ± 0.0071	3.6573 ± 0.0395	6.2683 ± 0.0242
POLIMI	0.3563 ± 0.0067	3.6499 ± 0.0368	6.2376 ± 0.0234
SNPE	0.3582 ± 0.0069	3.6572 ± 0.0380	6.2681 ± 0.0241
HG	Nav	NAv	NAv

Table 31. Mix Variability of A4 Series at Reference Pressure 4.5 MPa

Method	CV% n	CV% a	CV% r_b
BC	1.9098	1.0004	0.3852
BPD-1	1.8666	0.9608	0.3874
BPD-2	1.9925	1.0811	0.3868
POLIMI	1.8726	1.0072	0.3748
SNPE	1.9240	1.0388	0.3844
HG	NAv	NAv	NAv

For severe operating conditions (see the Baria series 016 and 2-inch motor tests)[94], differences between the results from the limited methods examined are no longer clearly distinguished but BPD-1 (simple start/stop burn time definitions) appears more suitable; otherwise, in terms of mix variability, BPD-2 (SNPE-like) performs better than BPD-1. It is fair to say MB methods did not receive a thorough comparison in this study.

6.1.4 Statistical Observations and Non-Equilibrium Burning

As shown in Table 29, analysis methods yielding large coefficients of variation for the ballistic parameters n and a yield at the same time a low coefficient of variation for r_b; and vice versa. Burning rate is usually the preferred quantity of interest. The statistical correlation analysis of the ballistic parameters n and a is explored further in Figure 68 by examining the dependence of burning rate residuals $r_i = log(r_{bi}) - log(r_b)$ on the estimated values (although for a limited number of tests). This nonlinear, V-shaped behavior (deviations of individual motors from fitted rate line) was systematically observed for Baria experimental tests and is reflective of the differences in normalized trace shapes early in burn, as noted in Figure 63.
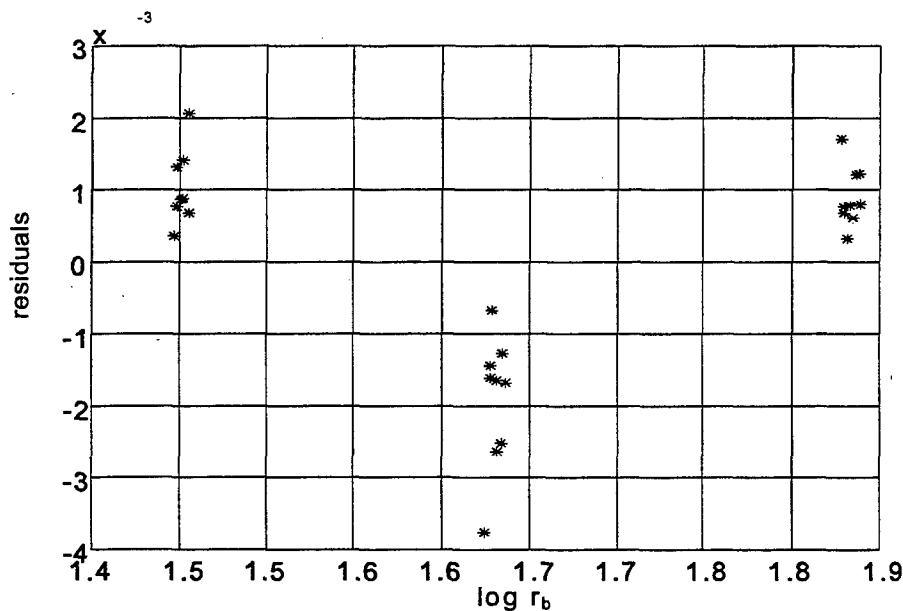
Figure 68. Burning Rate Residuals Dependence on Estimated Values of Burning Rate

Similar patterns of deviations were also commonly observed by Hessler on other motors and propellants at Thiokol, whenever motors were tested at multiple pressures to estimate exponent. The presence of a pattern of deviations/residuals indicates some systematic error (bias). Either the equilibrium rate does not follow a power law as assumed, or there is some systematic difference in how motors with the same propellant operate at different pressures (such as a different extent of non-equilibrium or transient burning). It is suspected both are true, but in the present case it is primarily a difference in non-equilibrium burning, due to systematic differences in the normalized trace shapes at different pressures.

It is suspected the differences in non-equilibrium burning that cause differences of trace shape in Baria motors are related to very small (order 0.001%) pressure oscillations. High frequency data indicates these oscillations are forced acoustic oscillations (they show peaks at the predicted acoustic modes throughout burn), not "combustion instability" (because the oscillations do not tend to "grow exponentially"). Passive linear stability measurement (PLSM) analysis (under development on the

91

AFOSR/EOARD program[97]) indicates that the causative process is generally proportional to burning surface area, which indicates it is probably due to "combustion noise". Combustion noise is proposed to occur because the propellant is not really homogeneous because it is composed of a mixture of discrete AP particles with binder in the spaces between. Because the AP and binder do not have the same burning rates, burning proceeds as a series of small AP "bursts" (rapid burning), followed by a lull as binder is pyrolyzed to expose the next AP, so the burning does not proceed smoothly in a microscopic sense. The aggregate effect of the bursts is the combustion noise.

The PLSM analyses also indicate that the causative process (forcing function) is elevated for the first 20-25% of burn, and for the last 5-10% of burn. It is suspected this indicates non-equilibrium burning related to formulation gradients at the mandrel and at the case and to the development and relaxation of burning surface texture at the ends of motor operation.

Although the instability community is only concerned with DC shifts of mean pressure due to "instability" (any large pressure oscillations, whether stable or not), mathematics of a power law rate relationship requires that there must also be a tiny shift corresponding to tiny oscillations. However, because the "tiny" oscillations occur at all frequencies corresponding to AP sizes and the effect is cumulative, the overall shift isn't really very tiny (may be 1%-2% in Baria motors). While analysis is continuing, it is believed this accounts for much of the variation of trace shapes in the first half of burn of Baria motors, and is a principal contributor to the V-shape of residuals/deviations from fitted rate curve.

Steady pressure oscillations are a form of "non-equilibrium" motor operation, and generally tend to repeat from motor to motor at the same pressure. Consequently, pressure oscillations would tend to make all motors of a particular design at a given pressure exhibit about the same bias due to non-equilibrium operation. This suggests that pressure oscillations due to combustion noise bias both rate and exponent. Further, as the statistics of the combustion noise would be expected to vary with burning surface area (and therefore motor size), and because the acoustic modes of different motor designs are different (and therefore pressure oscillations would be different), it seems likely that the rate bias due to oscillations caused by combustion noise could contribute materially to scale factor.

6.2   TNO-PML Motor Data

6.2.1   TNO-PML Experimental Motor Pressure-Time Data [90,98]

TNO supplied five pressure traces that were generated with a subscale L* burner (see JHU/CPIA CPTR 74[5] for details). The burner has a combustion chamber diameter of 100 mm, a free chamber of 314 cm^3 and employed end-burning propellant disks. The total propellant weight consumed during each experiment was about 125 g. The propellant disks were ignited with two electrical squibs. The pressure traces are presented in Figures 69 through 73 respectively.

Trace 3
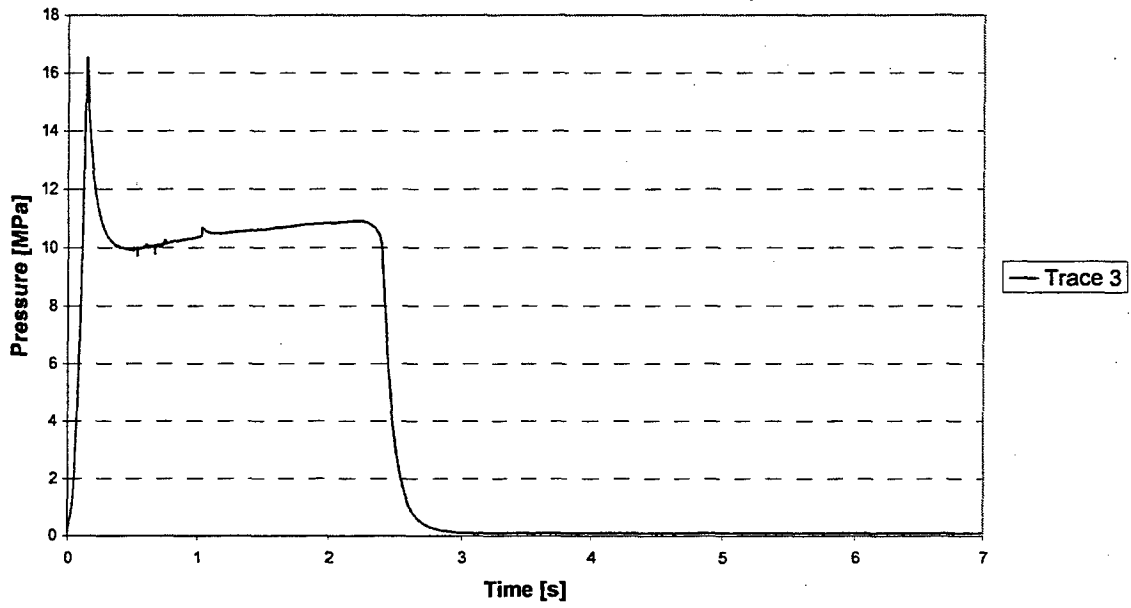
Figure 69. Pressure-Time Behavior for TNO-3 Motor Firing

Trace 4
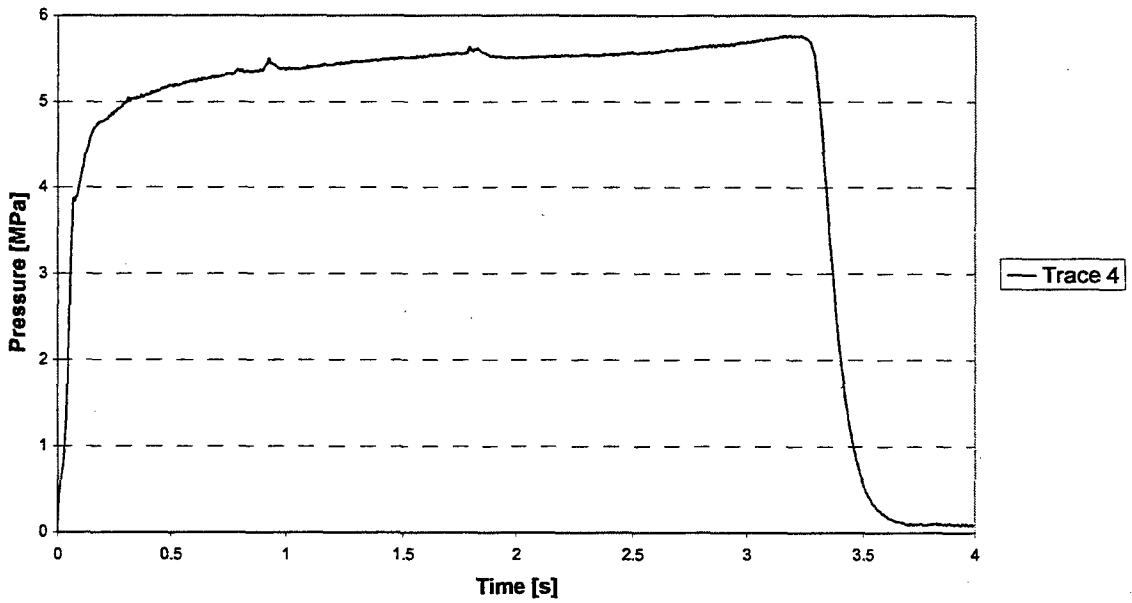
Figure 70. Pressure-Time Behavior for TNO-4 Motor Firing

Trace 5
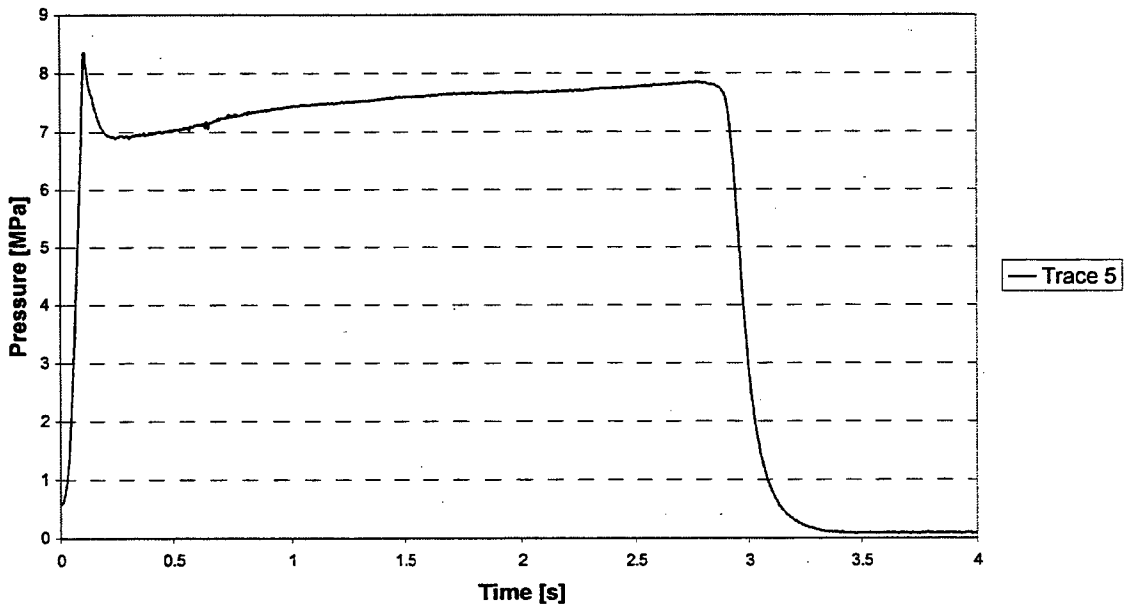
Figure 71. Pressure-Time Behavior for TNO-5 Motor Firing

Trace 6
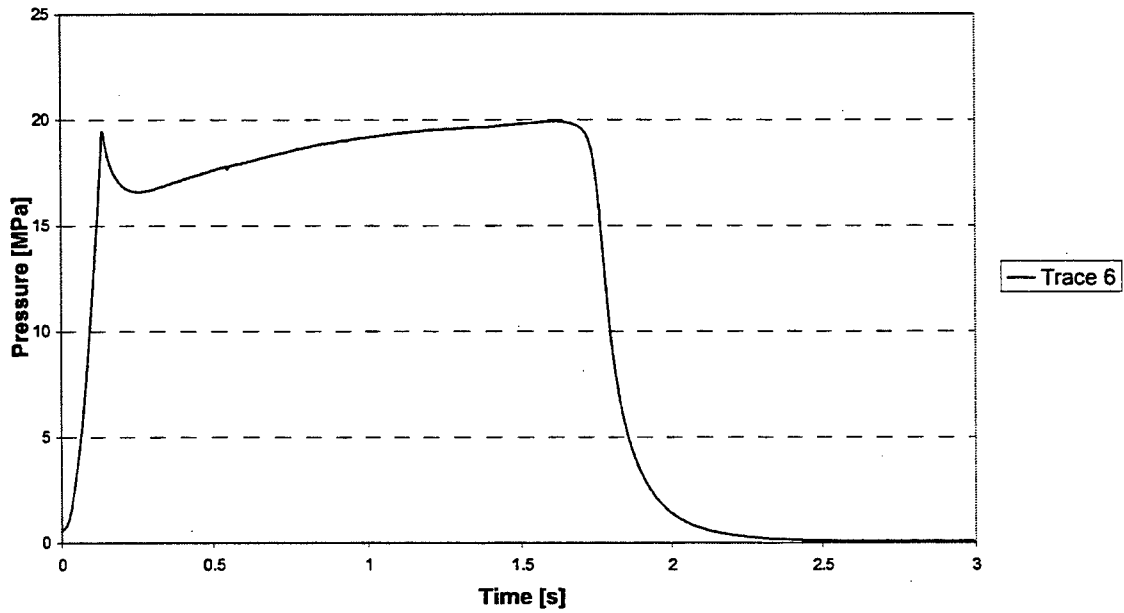
Figure 72. Pressure-Time Behavior for TNO-6 Motor Firing

94
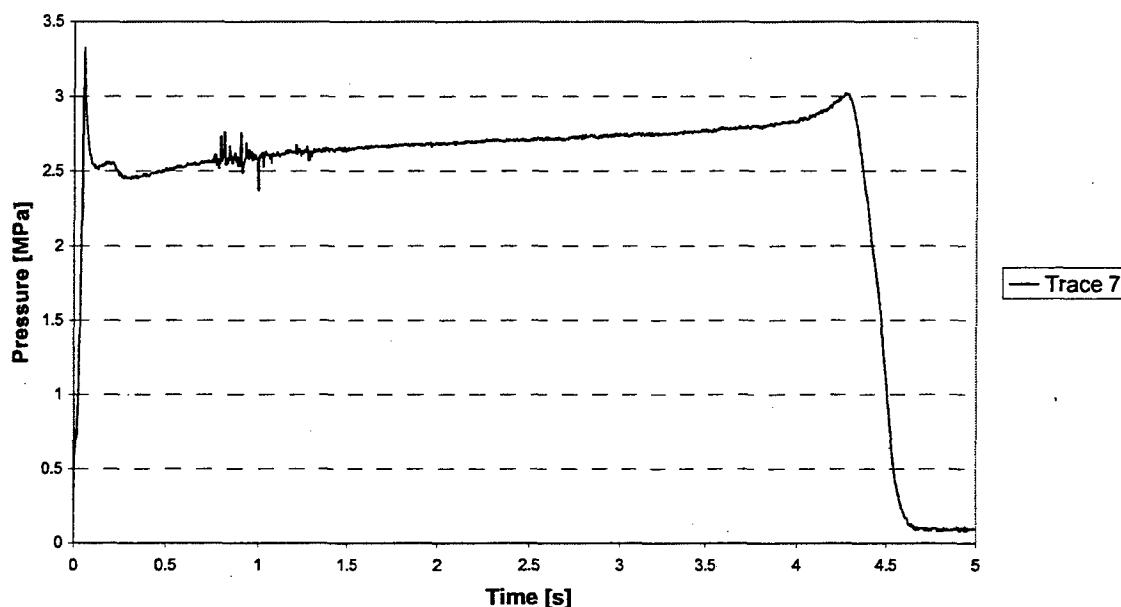
Trace 7

Figure 73. Pressure-Time Behavior for TNO-7 Motor Firing

6.2.2 Filtering of Pressure-Time Traces for Hessler-Glick Analysis Method[90]

The main purpose of the filtering is to eliminate noises from the signal without losing important information. The derivatives of the signal are sensitive to the variations of value and in a particular way the second derivative. After a filtering operation on a pressure trace the analyzer must be able to recognize the steps in the first derivative during the ignition transient and in the second derivative during the extinction transient in order to calculate the parameters of the Hessler-Glick (HG) method according with the definitions. Moreover the signal must be accurate with a high sample rate for not losing important information during the filtering procedure.

A solution for all these problems may be the sampling of the signal (in this case pressure data) at a frequency lower than the original data. But this is a bad way of filtering because if the original data are disturbed are and not very accurate we may cut off important points especially during the transients. There are many other more sophisticated solutions for the problem such as applying a digital filter, for example a Filt-Filt procedure (zero-phase forward and reverse digital filtering) defined in Matlab (the software program). This solution was good for some traces analyzed but not for all of them, in fact it was not always possible to evaluate the time points t_B, t_{Ei} and t_{Ef} defined in the HG method because substantial noise was still present.

The solution adopted in this work is to sample the original signal executing an average on eleven points. The sampled point is the average of five data points before it, itself and five data points after. This method yielded good results. Figures 74 and 75 show an example of the differences between the second derivative of the original pressure trace and the second derivative of the filtered pressure trace during the tail-off transient.

95
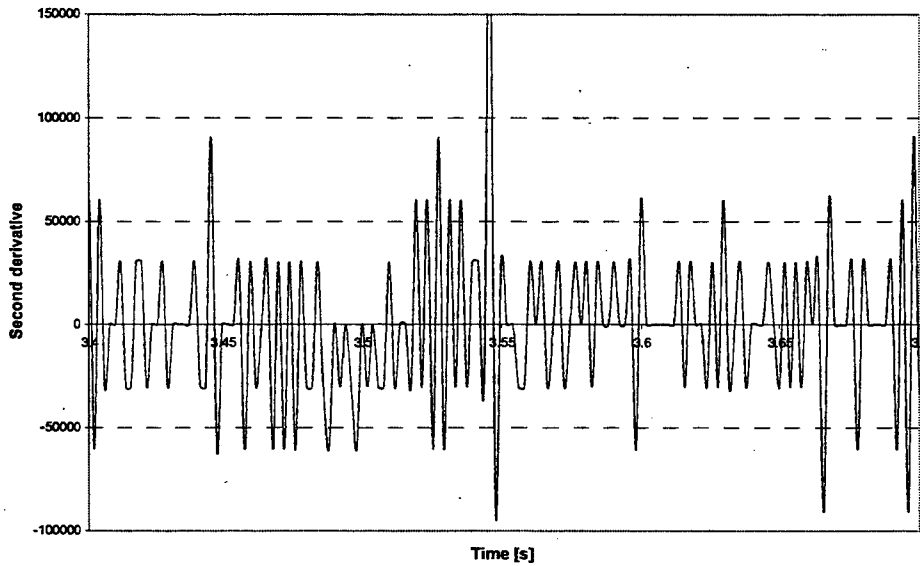
Figure 74. Second Derivative of a Typical Pressure-Time Tail-off Transient
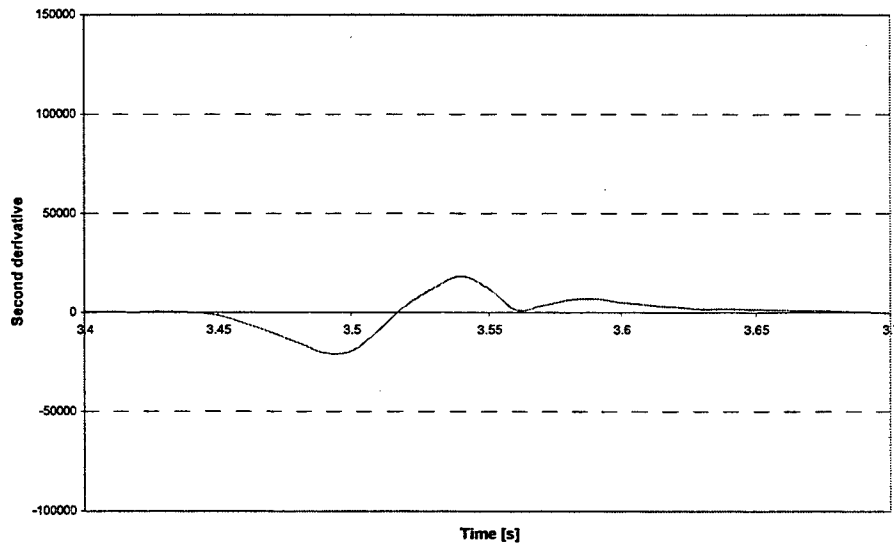
Figure 75. Second Derivative of a Filtered Pressure-Time Tail-off Transient

Adopting this filtering method we sample the signal at $1/5^{th}$ of the original frequency. A problem to avoid during sampling is the aliasing. This phenomenon could occur if the maximum frequency of the signal is higher than two times the sampling frequency. In this case we lose information. But it was not the case in this analysis.

The first step of the application of the HG method is to evaluate the time points. The time t_B is the midpoint of the time interval immediately preceding the first perceptible rise in dp/dt on the last sustained pressure rise to equilibrium motor operation. In the calculation of the first derivative it was not necessary a filtering operation because was possible to recognize a clear rise in the curve.

Second step is to evaluate the time points t_{Ei} and t_{Ef} that are respectively the midpoint of the time interval immediately preceding a negative step to negative value of d^2p/dt^2 and immediately preceding a positive step to positive value of d^2p/dt^2 at or following the blowdown period after the end of equilibrium motor operation. For this evaluation a filtering procedure was necessary. The integral of the pressure was calculated using the original pressure data with the trapezoidal rule.

The iterative procedure starts with an exponent n=1, which means to consider the time-averaged pressure, and typically converges in three to five iteration depending on the noise level present in the trace. Caution should be exercised that the signal is not over filtered. This strongly penalizes the HG method. If the peaks of the oscillations in the derivative occur at discrete levels, it indicates the noise is caused by acquisition amplitude resolution, and will probably result in poor amplitude resolution. Good timepoint resolution requires good time and amplitude resolution.

6.2.3 TNO-PML Experimental Results and Observed Trends in Analysis Methods

The methods used to analyze the different pressure-time traces for the subscale experiments included TNO Method 2, Bayern Chemie and HG. Average pressure and average burning rate results are presented in Table 32 along with percent deviation from the TNO method shown for the BC and HG.

Table 32. Average Pressure and Burning Rate Analysis Using TNO, BC and HG Methods[98]

Test Number	TNO			BC			HG		
	$P_{c,aver.}$	$r_{b,aver.}$	$\frac{r_b}{r_{b,TNO}}-1$ (%)	$P_{c,aver.}$	$r_{b,aver.}$	$\frac{r_b}{r_{b,TNO}}-1$ (%)	$P_{c,aver.}$	$r_{b,aver.}$	$\frac{r_b}{r_{b,TNO}}-1$ (%)
3	10.5503	10.7046	0.00	10.5025	10.4553	-2.33	10.0809	10.5168	-1.75
4	5.4115	7.7481	0.00	5.3742	7.5102	-3.07	5.2838	7.6503	-1.26
5	7.4666	8.7582	0.00	7.4284	8.539	-2.50	7.2597	8.6278	-1.49
6	18.1818	14.8608	0.00	18.1911	14.3495	-3.44	17.0978	14.6487	-1.43
7	2.6886	5.8774	0.00	2.6676	5.6144	-4.47	2.6618	5.7268	-2.56

TNO data were analyzed to obtain a power law correlation. A comparison of the derived power law correlations and the burning rate at 7 MPa (r_{b7}) are presented in Table 33. The accuracy achieved is represented by the value of R^2. The closer the value is to unity, the better the correlation.

Table 33. Overall Values of Ballistic Parameters and Correlation Factor of TNO Tests at Reference Pressure 7 MPa for TNO, BC, and Modified HG Methods[98]

Method	n	a	r_{b7}	R^2
TNO	0.4821	3.4999	8.9429	0.9847
BC	0.4870	3.3643	8.6788	0.9899
HG	0.5003	3.3750	8.9346	0.9854

Results indicate TNO, BC and HG methods provide statistically similar correlation results. TNO and HG provide burning rates within an average of 1.7%, while the BC method provides consistently lower burning rate values, averaging 4% below TNO. Unfortunately no actual burning rate requirement was available hence an absolute judgment and comparison on accuracy was not made. Further statistical analysis was not performed on these data results.

6.3 Lessons Learned from Real Motor Data Analysis

Data reduction of small-scale test motors can be accomplished in two different ways, each including many different versions. In experimental tests the actual burning rates are unknown, and errors are introduced by a variety of sources. These include the method implemented to define r_b, specific experimental set-up, and experimental test methods. Therefore, the quality of the examined methods can only be assessed based on statistical indices.

With good quality data and based on mix-to-mix variation, the POLIMI generic MB procedure (inspired by the U.S. NSWC MB method, Appendix B-15) and the HG two-point TOT procedure resulted in smaller data scatter than the tested industrial methods. TOT methods (BC, BPD-1, SNPE) routinely used by European industry produce quite similar values; SNPE and BPD-2 (a variant of BPD-1) offer slightly smaller data scatter and provide almost identical performance; BPD-1 (simple start/stop burn time definitions) is superior in dealing with Ariane-4 small-scale test motors; and, BC produces reasonable results with little effort. The manual HG and simple POLIMI methods often showed better performances overall.

The industrial methods nominally assuming instantaneous burnout (BC, BPD-1, BPD-2, SNPE) produce mean values that are quite similar, as expected from the general similarity of these methods. Within this group, BPD-2 and SNPE (which differ only in minor details) produce about the same mean values, while BC produces reasonable results with little effort. Relative to the industrial methods, the generic MB procedure used by POLIMI produces lower rates and lower exponents; HG produces higher rates and lower exponents. HG and POLIMI methods in general also yield relatively more confined values of standard deviation for the ballistic parameters n and a. Most of these observed differences appear to be explainable in terms of known physical effects.

Time-averaged pressure is greater than rate-averaged pressure (consistent with RR #1 results), so any procedure using time-averaged pressure yields a rate equation that is consistently biased low due to the Non-Neutrality Error. As HG is the only procedure using rate-averaged pressure as the associated pressure, HG rates are expected to be higher than the others. In general, for a fixed average degree of non-instantaneous burnout due to either grain distortion or misalignment, the Non-Neutrality Error for a propellant will increase at lower pressures, because the burnout process extends for a greater fraction of the tail-off process. As a consequence, methods that use time-averaged pressure should be expected to yield rate equations with exponents biased high, while HG exponents are expected lower. Results verified these expectations.

In treating simulated pressure traces, HG method did best; but while other methods are automated, HG requires some insight and the operator's analysis for each trace. In simulated motors, the HG procedure is not affected by non-idealities of burning process (such as nozzle erosion, non-instantaneous burnout, mandrel eccentricity or bore offset, etc.) and proved to be a reliable method in terms of reproducibility and accuracy of burning rate results. This could not be stated with the same confidence in real operating motors where noise, imperfect instrumentation setup, and different environmental conditions are to be handled. In real test motors, non-idealities in principle favor the class of MB over TOT methods and somewhat compromise the accuracy demonstrated by HG in ideal cases.

As to future work, efforts are being made at POLIMI and Fiat Avio BPD to develop an automatic HG procedure to be implemented on standard desktop computers for the benefit of industrial manufacturers. At the same time, refinements in progress of the HG and POLIMI methods promise to further improve the good performances already shown. In both cases, a relevant benefit could also be gained by further refining the experimental setup and/or test conduction in order to reduce motor variability. More sophisticated statistical analyses of the raw and deduced data are already in progress.

7.0   SMALL MOTOR DATA QUALITY

Many of the significant influences on burning rate are briefly reviewed here relevant to testing and data analysis. The influences of these effects on motor scaling are reviewed in JHU/CPIA CPTR 73[4].

7.1   General

Measurement of a mean burning rate, in any device, depends upon several general, typically implicit, assumptions, including at least the following [99]:
- Propellant is homogeneous, with isotropic properties,
- Specimen has uniform bulk formulation and properties,
- Specimen has known dimensions,
- Specimen is at constant temperature,
- Equilibrium 1D burning prevails throughout,
- Test environment remains constant during entire test, and
- Instrumentation is accurate and noiseless.

Burning rate measurement accuracy and precision depends, directly or indirectly, upon the degree of adherence to these general assumptions in any given experiment. Statistics and physics dictate that all of these assumptions will be violated all of the time, to a greater or lesser degree, even with some degree of deliberate control. The key to better rate measurements probably lies in accepting that assumptions *will* be violated, and in devising ways to measure and correct for the effects of the violations when possible and appropriate. In the process, some measure of the violation will be obtained that will probably be useful either as an estimate of the effect of that type violation in a different motor, or as a statistic of the experiment, or both.

In the design of an experiment, the researcher concentrates on the assumptions that he personally considers most important, and devises various means to minimize their violation. Motors, hence, have the most realistic environment; strands have better resolution on web thickness, more constant pressure, and more freedom from end effects; liquid strands give quick burning rate assessment during propellant batch production; larger specimens are more homogeneous; smaller specimens are more economical; etc.. More direct methods, such as ultrasound, microwave, X-ray extinction, and laser recoil, yield instantaneous measurements, so the test environment assumption may be relaxed somewhat. Each experimental device has its strong and weak points.

The assumption violations that appear to dominate in causing burning rate measurement errors in rocket motors are [99]:
- Real motor propellant dimensions are different from the drawing specifications; even when manufactured according to the drawing, dimensions are allowed to vary within a certain range,
- When tested, real motors have starting and ending transients,
- Real motors employ an igniter, have a burning liner and employ a nozzle; effects of these motor parts on ballistic propellant performance are commonly neglected,
- Real propellants have formulation variations and gradients,
- Data reduction definitions are generally not fully consistent with physics.

The mean effect of these combined violations is to bias the measured burning rate of a particular sample of a given propellant tested in a given device at a given facility, and reduced by a particular data reduction method. The reproducibility of measured burn rate in a series of nominally replicate tests reflects the combined effect of all violations.

7.2   Propellant Effects

Burning rate is considered a bulk propellant property, dependent upon chemical composition (e.g. oxidizers type(s) and size distributions, binder type and content, binder curing, binder additives, catalysts, burning rate modifiers, and their particular fractions). In manufacturing a batch of propellant, considerable care is normally taken to assure the proper weight fractions of the several ingredients and the even

distribution over the propellant mixture, however due to various reasons some small variation always persist. [99]

Variations In Propellant Formulation

For composite propellants, those propellants that contain ingredients consisting of discrete particles of different sizes (actually size distributions) that survive the manufacturing (mixing) process, there is likely some small characteristic size necessary to contain a representative population of these particulates in order to approximate the bulk formulation. For smaller specimens, some of the ingredient particles will be left out (e.g. larger oxidizer crystals), and the formulation and properties of the specimen will deviate from those of the bulk. Estimates indicate that this critical volume may be as large as 1 cm^3.

Formulation Gradients

There are formulation gradients at all boundary surfaces (i.e., free and case bonded) of a propellant specimen, for several reasons:
- The physical impossibility of the center of a particle lying closer than its radius from a solid boundary,
- Due to surface tension and sedimentation (tends to level free cast surfaces),
- Machined or cut boundaries tend to have tool marks, skip over smaller particles in a flexible matrix, and rip out larger particles instead of slicing through.

In each case, the surface is probably binder-rich, with likely a higher concentration of fines immediately below the surface. Burning rate gradients would be expected to diminish exponentially with depth below surface, characteristic depths about half the largest particle size.

Cure Shrinkage Variations

Solid propellant is usually manufactured as a liquid or slurry, cast into a motor or bulk sample, after which it is cured. During the curing process which starts at the end of the mixing process when the curing catalyst has been added, continues during the casting process and is completed in a stove at elevated temperature, the composite propellant shrinks.

It is to be expected that the degree of curing at casting time contribute to ballistic differences experienced between mixes. It may also contribute to differences between samples within a single mix when the number of samples is large, and the samples are cast consecutively.

Motors are typically overcast; partly to allow for cure shrinkage, and partly to be sure of adequate material to be able to machine towards the final configuration. As cure progresses, some of the overcast propellant flows back into the motor to replace propellant volume lost because of shrinkage. It is to be expected that motors will have slightly less apparent cure shrinkage than bulk propellant because of the back filling.

Non-Steady Combustion

Combustion of solid propellants is generally non-steady, mainly for to two reasons:
- Combustion noise due to heterogeneity's in the propellant or in the combustion processes (possibly intrinsically),
- Dynamic response to external stimuli.

On a macroscopic scale, solid propellants are observed to burn in a direction normal to the burning surface, such that planar surfaces remain planar and regress at a constant rate for a given pressure and initial temperature. On a macroscopic scale, solid propellants burn as a homogeneous material. Such observations have led to the fundamental definition of burning rate as thickness burned per unit of time.

On a microscopic scale, however, composite propellants are not homogeneous, but consist of particulate materials in a matrix of binder. Composite propellant burn rates are observed to be sensitive to the distribution of particle sizes, and combustion models indicate that burning rates of individual sizes vary by

an order of magnitude. This large difference in local burning rate is accommodated by a development of a microscopic surface texture. It is hypothesized that the flat macro-surface regresses as a stochastic assembly of surface texture cells, such that the mass flux and burn rate vary both spatially and temporally.

These non-steady mass flux phenomena are believed to be propellant properties that are largely independent of non-steady components of the test environment. These phenomena are referred to as "Combustion Noise", and will cause (typically very small) pressure oscillations in test devices across a very broad frequency range (noise).[100]

Any experiment involving combustion and/or flow is subject to pressure oscillations. In rocket motors, this is generally called "Combustion Instability". Classic theory indicates that the combustion process of solid propellants is the primary driving force.[101] More recent extended theory[102], however, indicates that combustion noise and turbulence or vortices shed at discontinuous variations of the port cross section and transported with the flow will cause small to moderate pressure oscillations in stable motors. Comparisons of data with the extended theory indicate that a significant fraction of "Combustion Instability" problems are probably the results of such forced oscillations in otherwise stable operating motors.

Surface Texture Evolution

At a microscopic level, the propellant surface is not planar, but textured. It takes some finite time for an initially flat cast surface to develop its equilibrium texture. It looks like the distance burned during surface texture equilibration is a great deal larger than the thermal wave thickness, while it also varies with pressure and cross flow.

Ignition Pressure

Most motors have an initial pressure maximum during the initial part of motor operation (ignition). In many motors, this initial overshoot is often followed by a dip before finally approximating equilibrium. While an overshoot is expectable from transient combustion theory, the dip probably is not. *This may indicate a forced L* oscillation, which is also not included in predictions.*

Burnout Point

As the burning surface approaches the burnout point, the thermal diffusivity of material beyond the burnout point must be considered because it will begin to affect the subsurface temperature gradient, and consequently will affect the burning rate. If the propellant grain is bonded to a liner, the liner diffusivity may cause the rate to increase markedly (Friedman Curl). This effect also occurs in double-web samples (NSWC/Indian Head slab burner), motors cast with two layers of different propellants (booster and sustainer) and in grain ports with tangential gradients (e.g. star grains).

On the other hand, propellant bonded directly to a metal case sees near-infinite diffusivity beyond the burnout point, and rate is depressed just before burnout, and propellant burning typically quenches, or extinguishes (Friedman Uncurl).

Size Effect

As sample size is decreased, the propellant formulation of the sample becomes variable. The effect of formulation gradients and end effects on the propellant ballistics increases, and the importance of heat losses may increase. These effects do not average out, and there is a general trend towards a reduced measured burning rate with decreasing sample size.

In general, burn rate motors are also designed for relatively constant-pressure (neutral) operation and low port velocities to avoid erosive burning.

Hump effect

The "hump" or "hump-effect" refers to a little hump that is commonly found in the middle of pressure vs. time traces (mid-run). It is generally accepted that "hump" is related to the casting and curing process

although the exact reason for its occurrence is still unknown. Additional discussion is provided here for completeness on this issue, reviewed earlier in this report and discussed relevant to scaling in JHU/CPIA CPTR 73[4].

The mid-run hump appears as a modest peak superimposed on the mean pressure, perhaps describable as a Gaussian curve, with amplitude 5 - 15 % and a 2σ width of 5 - 10 % of the burning time. However, when one back-calculates rate-surface product versus instantaneous web burned, and divides by predicted surface (basically the way to develop a "hump" correction), the basic "hump" curve is more or less A-shaped, high in the middle, low on the ends, and the two sides may even be fairly straight. This suggests that the "hump" effect (for bottom cast or bayonet cast grains) may consist of sedimentation of larger particles against the walls during casting flow, with the central core flow (in either the bottom upflow or in the bayonet) consequently rich in fine particles. Plunge casting does appear to reduce formulation gradients.

The bulk statistical distribution of particles cannot be maintained at the wall because the wall acts like an infinite particle, and consequently the same statistics cannot apply. Therefore, there is some formulation gradient at the wall (interferes with a possible Friedman curl). There is a similar effect at a free boundary. Precisely at the wall (or free boundary), the formulation is probably binder-rich with a higher content of fine oxidizer particles immediately away from the boundary; and regardless of the casting flow. Passive linear stability measurements (PLSM) indicate increased combustion for 2-5% of burning time before burnout, during the Friedman Curl.[97]

7.3   Testing Effects

Testing of propellants has the objective of obtaining the propellant (ballistic) properties at certain well-defined test conditions (e.g. temperature, accuracy of the data acquisition and data reduction equipment). In real experiments, however, this ideal situation can only be approximated.

Temperature Gradients

While the sample/motor might have been thoroughly temperature conditioned, it takes a finite time to move the motor into the test bay, attach instrumentation, evacuate personnel, and activate the firing sequence. This will typically take 40 s - 5 min. depending on the size of the test motor. When the test motor has sufficient heat capacity (thick walled battleship testing motor) this seems to be no problem. A different situation however is a deeply cooled down flight type motor tested during the high temperatures in the summer.

Temperature Variations

To assess the extent of grain deformation due to thermal deformation (motor temperature variation), an analysis was carried out using the ABACUS Finite Element Model (FEM) with IDEAS pre- and postprocessor to determine the deformation of a typical 2x4-inch propellant grain.

For the analysis the propellant was assumed to be cast and cured in two configurations, one with a thin liner and the other without a liner between the propellant and the steel casing. The steel casing is very stiff as compared to the propellant and thermal shrink will occur mainly with the propellant. Since the propellant is cast and cured at an elevated (e.g. at 60 °C), the propellant was assumed stress and deformation free at this temperature. Also shrink due to curing was not considered for this analysis.
To assess the deformation of the propellant grain, a cool-down from + 60 °C to + 20 °C and to - 54 °C was simulated.

For the analysis a typical (tactical) propellant was employed for which the boundary conditions for the FEM analysis were:

Dimensions:
Length: 9.525 cm
Diameter inner bore casing: 5.08 cm
Width casing: 3 mm
Width liner: 0.8 mm

Material properties:

Casing:	Propellant:
E = 206.8 GPa	E = 10 MPa
ρ = 7.82 kg/m^3	ρ = 1.80 kg/m^3
ν = .29	ν = 0.4999
α = 1.17E-5	α = 1. 10^{-4}

Liner:	For –54 °C test case:
E = 1 MPa	E = 2 MPa
ρ = 1.00 kg/m^3	ρ = 1.00 kg/m^3
ν = 0.4999	ν = 0.4900
α = 1. 10^{-4}	α = 1. 10^{-4}

The calculated deformation of the grain (propellant) surface is plotted in Figure 76. The upper curves in Figure 76 are for - 54 °C while the lower curves are for + 20 °C. The maximum shrink of the propellant occurs at the center of the bore and amounts to about 0.5 mm on a web of 12.7 mm. This is about 4 % (at - 54 °C), which reduces to 1.5 % at ambient conditions. The liner reduces the barrel effect but only slightly. Another important aspect is the stress and strain situation at the grain ends, and in particular near the bondline with the casing. Figure 77 presents a typical example of the strain situation.
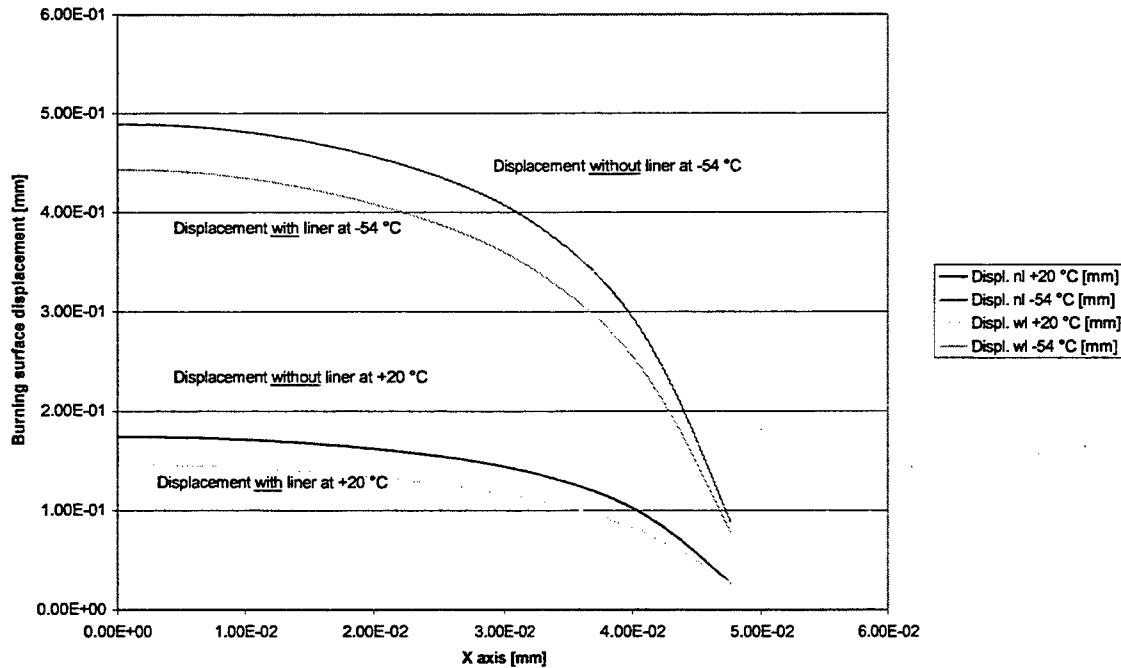
Figure 76. 2x4-inch Grain Deformation at +20 °C and -54 °C

RESULTS: 3-B.C. 0,TIME = 1.0, STRAIN_3
TIMESTEP: 1   TIME: 1.0
STRAIN - MAX PRIN MIN:-2.81E-03 MAX: 1.17E-01
DEFORMATION: 1-B.C. 0,TIME = 1.0, DISPLACEME
TIMESTEP: 1   TIME: 1.0
DISPLACEMENT - MAG MIN: 9.07E-07 MAX: 6.91E-0
FRAME OF REF: PART

VALUE OPTION:ACTUAL
SHELL SURFACE: TOP
1.17E-01
1.05E-01
9.29E-02
8.09E-02
6.90E-02
5.70E-02
4.51E-02
3.31E-02
2.11E-02
9.16E-03
-2.81E-03
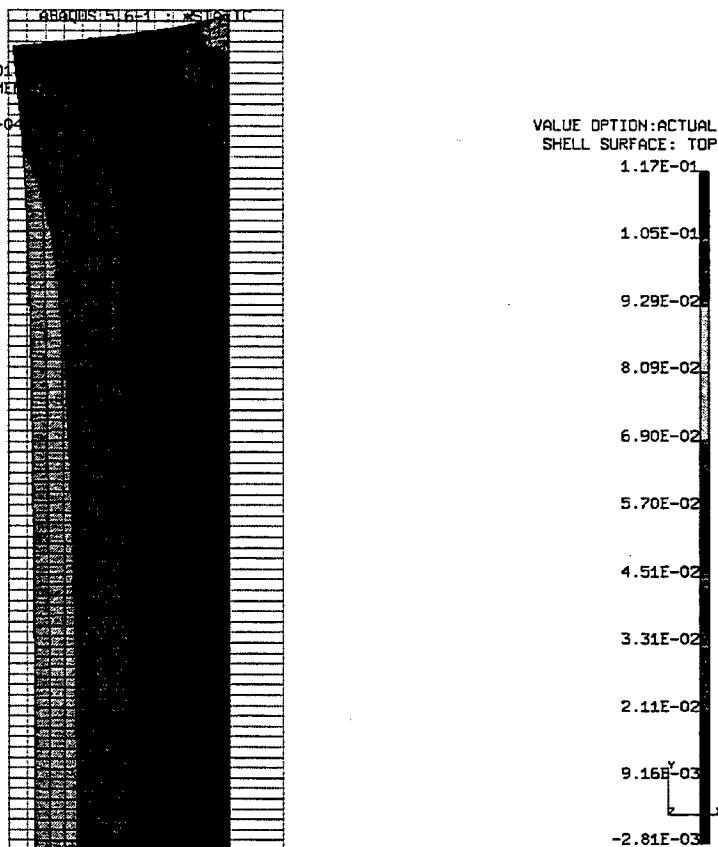
Figure 77. Strain Situation of the 2x4-inch Grain at -54 °C (Deformation x3)

Depending on the properties of the propellant (e.g. propellant formulation, design, production, development, aging study) cracks/debonds may possibly form at these locations. This may result in an anomalous burning behavior and will yield inaccurate burning rate results.

Transducer Frequency Response

Poor zero return almost certainly indicates either poor grounding, or the use of grease-filled transducers and connecting lines. The transducer/line assembly is a Helmholtz resonator. For large damping (high viscosity and/or long line), the damping of the pressure signal becomes critical. For very large damping, the two poles separate along the real axis. The largest real pole gives quick response on ignition and tailoff, but the smaller pole gives a creeping response with very long time constant. This is where most zero return problems come. A solution is to use light oil, e.g. a mineral oil (SAE-05 or SAE-10 for normal temperatures and SAE-30 for low temperatures).

In filling the transducer and lines with chosen fluid, air bubbles may become trapped inside, or may be dissolved in the fluid. This aggravates the problem above. The solution is to vacuum backfill the cells: fill the transducer and line with chosen fluid, attach it to the bottom of a fluid reservoir, and apply vacuum. When fluid bubbling ends, release vacuum, and cell and lines will be filled with air bubble free fluid. This also checks transducer and lines for leaks.

Poor zero return can also be caused by obstructions in the port (can be cleared with a copper wire as part of the setup procedure) or by charred fluid in the end of the line. One may included a T in lines to allow flushing between tests, but then assure proper sealing after flushing.

104

In a 6x12-inch motor containing an unspecified aluminized AP composite propellant, DC pressure was recorded in Figure 78 for burning rate measurements, and AC pressure was recorded for passive measurements of motor stability characteristics.
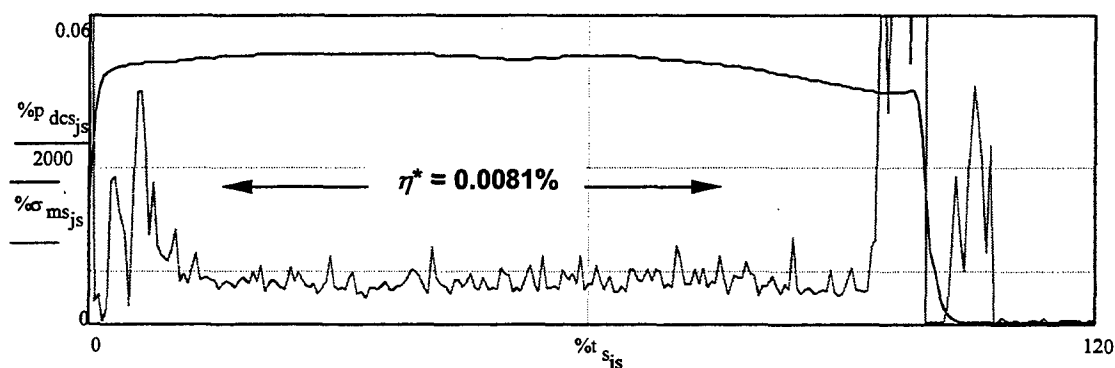
Figure 78. Normalized Motor Pressure and Low-Level Pressure Oscillations.

The data was normalized to mean motor pressure and burning time based on the times at 50% of maximum DC pressure. The data in Figure 78 was smoothed and decimated, using a third order least squares fit of successive ½%t blocks of data, eliminating AC power line frequency harmonics with an "ignore" filter.

The variations of the high frequency pressure about the least squares fit line segments were analyzed to determine the rms noise levels. Average rms instrumentation noise after the end of motor operation for this motor was 0.0021% of mean motor pressure. The rms noise due to motor operation %σ_m, determined by statistically subtracting the average rms instrumentation noise from the rms noise during motor operation, is presented in the lower panel of Figure 78 with the low frequency pressure %p_{dc}.

Characteristic motor noise η^*, the average rms motor noise from 20%t to 80%t, was 0.0081%. Characteristic noise has been proposed as a statistical property measuring the overall susceptibility of a propellant/motor combination to pressure oscillations.

Estimated Combustion Noise[97]

The AC data was examined to determine the presence of low-level pressure oscillations. The FFT waterfall Figure 79 shows oscillations of order 0.001% at the 1600Hz first longitudinal mode and of order 0.0003% at the second longitudinal mode (frequency resolution is 5.56 Hz). Oscillations at these levels are *not* combustion instability, but stable *forced* oscillations caused by combustion and flow noise. Similar low-level oscillations are apparent in all solid rockets when high-resolution data is examined.
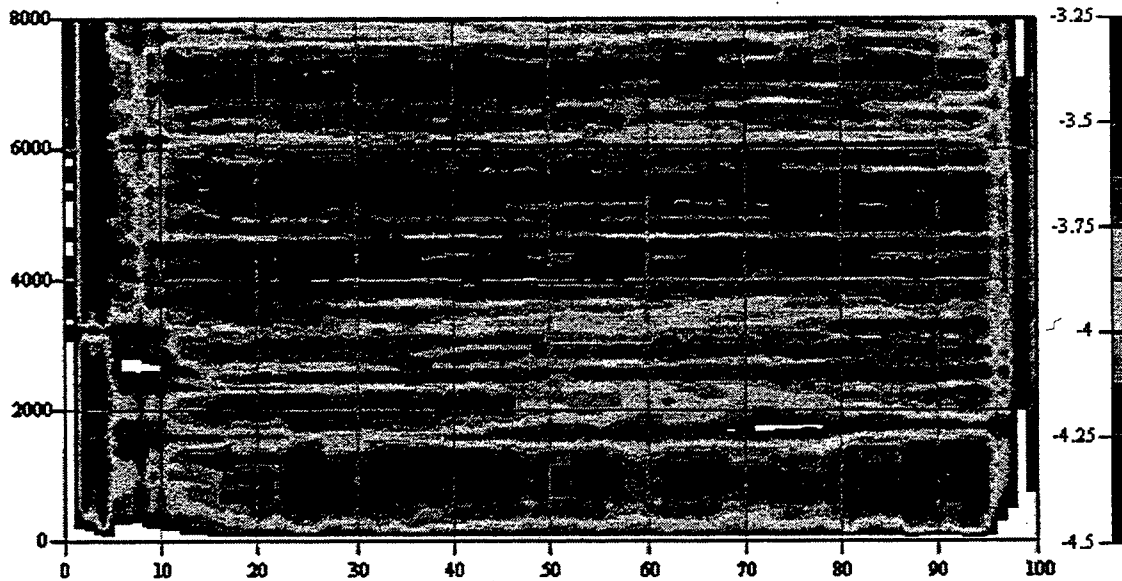
Figure 79. Filtered Waterfall of Log-Magnitude Normalized Pressure (in % of Mean Pressure)

The data were also analyzed with the PLSM (passive linear stability measurement) procedure[103,104] under development, which applies Burg's Method to least-squares fit motor acoustics data to a function with denominator polynomial frequency dependence to estimate the properties of the N acoustic modes within the observable frequency range of a given FFT.

$$B(s) = \frac{b_0}{1 + \sum_{m=1}^{M}\left(b(s)_m s^m\right)} \tag{62}$$

Figure 80 shows a representative FFT at 50% burn with the resulting fitted function B.
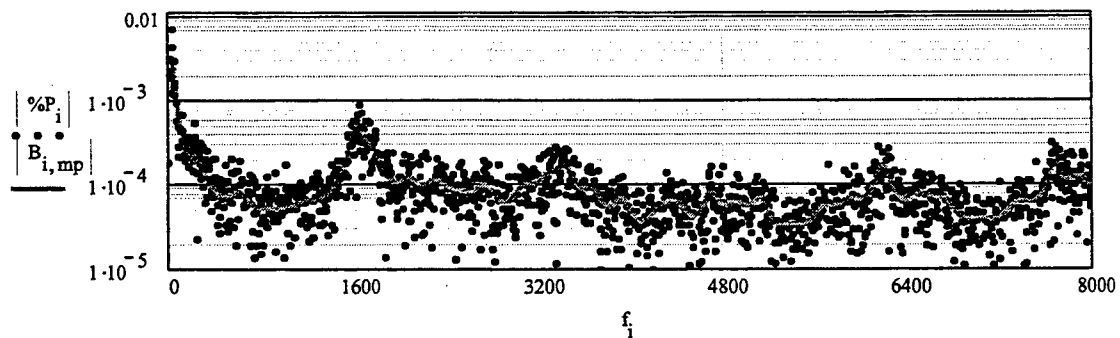
Figure 80. Fitted FFT at 50% Burn, M=70.

The coefficient b_0 is a measure of the forcing function $\%F_0$ due to combined combustion and flow noise in the motor (Figure 80). As the port velocity is very low, $\%F_0$ is presumed to be primarily due to combustion noise.

106

This measurement is very similar to the rms motor noise $\%p_m$ data shown in Figure 81, but with the effects of the acoustic modes and the randomness of the data removed. The forcing function appears to be almost proportional to the burning surface area from about 25% to 95% of burn. The larger forcing function magnitudes before 25% burn likely reflect the combined effects of formulation gradient at the initial cast surface, development of equilibrium burning surface texture, and possibly flow noise (as the port velocity is higher early). The increase of forcing function magnitude at 95% and 96% burn is believed to be due to the formulation gradient at the wall. The slight increase or hump in forcing function magnitude at 58% burn appears to be caused by numerous small pulses. Very large values later than 96% are due to the larger curvature and amplifier overload during the depressurization transient.
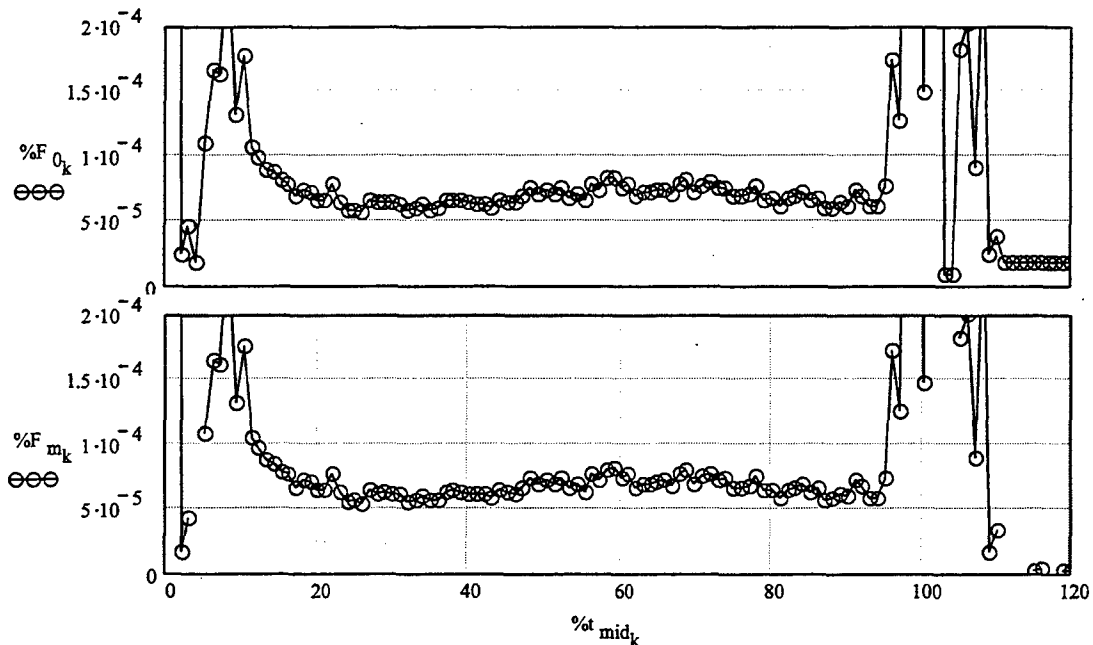
Figure 81. Magnitude of Forcing Function.
(Top as Measured; Bottom Corrected for Post-Firing Noise.)

Small Natural Pulses in Motor[97]

Solid propellant in a rocket motor is usually assumed to be homogeneous, isotropic, and uniform. With this assumption, the variation of mean pressure in a motor is expected to closely follow the shape of the variation of the burning surface area during burn.

However, there is extensive evidence that the burning rates of composite propellant samples are *not* spatially uniform and isotropic, and 10% to 15% spatial and directional variations of burning rates are not at all uncommon in either bulk samples or manufactured motors. In correlations of experimental motor behavior with ballistic predictions and in studies of burning rate and burning rate measurement reproducibility, the effect of these variations of burning rate on motor behavior has come to be known as the "BARF" (<u>b</u>allistic <u>a</u>nomaly <u>r</u>ate <u>f</u>actor) or the "hump" effect. The effect in composite propellants is generally believed to be caused by formulation gradients induced in the propellant volume by the flow during casting, as discussed elsewhere in this report. The s-shaped variation of DC motor pressure from 40% to 70% burn in Figure 78, for instance, is characteristic of motors with cylindrical geometry that have been plunge-cast.

Figure 82 shows example small (0.02% or less of mean pressure) pulses observed in the motor data after detrending and AC noise removal. The pulses do not appear to be instrumentation noise, because the pulse response occurs at the 1L mode frequency, and because earlier motors of the same design with

different transducer type and instrumentation also exhibited pulses. Small pulses such as these would be expected to occur, for instance, if aluminum droplets accumulated on the nozzle entrance surface or oxidizer particles were ejected through the nozzle. However, if the pulses were due to ejection of aluminum droplets, it might be expected that they would be distributed more or less uniformly, or increasing slightly, in time.
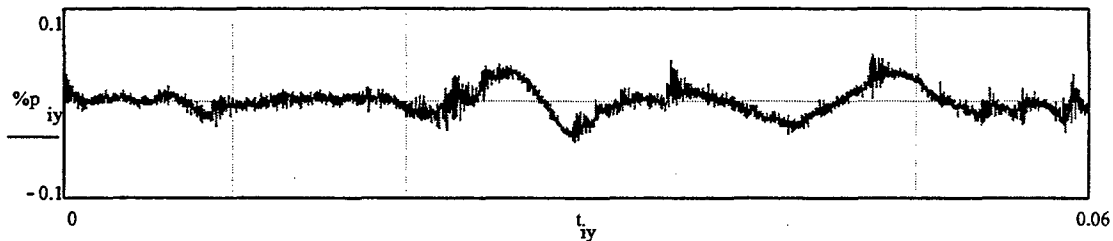
Figure 82. Multiple Small Natural Pulses Occur Throughout Motor Operation,
But Appear to Maximize Near 58% of Burn

Observation that the pulses were more numerous near mid-burn, coincident with the s-shaped excursion of DC pressure associated with plunge casting, suggests that the pulses may be related to the formulation gradients. Similar small natural pulses were observed at the time of the formulation gradient at mid-boost in RS Maverick motors, circa 1975, and incompletely burned oxidizer crystals were recovered downstream from the nozzle. This suggests that the pulses in this motor may be due to ejection of larger oxidizer crystals released from the burning surface when undermined by faster-burning smaller oxidizer, which may be more prevalent in the formulation gradient region.

Acquisition Card Error[97]

In FFT analyses of motor data, the FFT window width should be an exact multiple of the AC period, the AC line frequency should be constant at the stated frequency, and the acquisition sampling rate should be accurate. When these three conditions are met, the AC harmonics appear as increased magnitudes at single frequency points in the FFT, without obvious leakage to adjacent frequencies. In the DC data used for burning rate measurements in Figure 78, however, the higher AC harmonics leaked to neighboring frequencies slightly, and the frequencies of the higher harmonics indicated that the acquisition card sampling frequency was about 0.15% fast. This would cause the measured burning rate for the motor to be low by 0.15%, and may account for some of the mix-to-mix variations of measured burning rates observed between mixes of the same propellant formulation manufactured and tested at different times.

PC-based acquisition cards are widely used in research and industry for burning rate measurements. Specifications on acquisition card operation are extensive and appear to be thorough, which would tend to foster a complaisant reliance on the acquisition cards to perform within specifications. The specifications on leading acquisition cards, for instance, indicate that sampling rates should be accurate to ±0.01% after 15- minute or 20-minute warm up time. However, the present instance of sampling speed error marks the third instance during a one-year research program in which an acquisition card appears to have been operating well outside the specifications. This indicates that a much more aggressive program of acquisition card diagnostics should be implemented by users.

Instrumentation Noise Considerations[97]

The post-firing noise after data conditioning is our best estimate of irreducible instrumentation noise. Pre-firing noise is a less reliable indicator because the electrical circuitry, and therefore the instrumentation noise environment, is subsequently changed by application of the firing voltage to the igniter. Comparison with identically conditioned data at mid-burn indicates that noise magnitudes during motor operation are about 4/1 larger. This increment of noise level is our initial estimate of the forcing function magnitude due to combustion and flow noise. However, it is quite possible that motor operation may also affect the instrumentation noise through three mechanisms:

108

1) First, the motor case is typically grounded, either deliberately to minimize chances of accidental activation of the igniter by electrostatic discharge, or circumstantially by physical attachment of the motor and test stand to a seismic mass embedded in the soil and subsoil of the test site, which also constitutes an electrical connection to the local earth electrical ground potential. Combustion products are typically partially ionized because of the high combustion temperatures, so the discharge of the ionized gases through the nozzle into the atmosphere or impinging on the physical ground surface represents an additional electrical path to the local earth electrical ground that is not present before or after motor operation. The effect of this additional electrical path to ground is probably the cause of the 10/1 increase of the AC noise apparent during motor operation. This effect can be eliminated by deliberately grounding both the instrumentation and the motor *only* to a *good* ground at the test stand. In arid regions with dry subsoil, it may be necessary to drill a well to immerse the ground conductor in the local water table or at least to drill to substantial depth in which to place the ground conductor, refilling the well with hygroscopic materials to assure a *good* electrical ground and eliminate this type noise from recorded data.

2) Second, the flow of ionized gases out the nozzle represents a nontrivial electrical current, generating a magnetic field during motor operation. This magnetic field induces currents in other electrical conductors, such as pressure transducer cables. As the nozzle flow includes a significant random component, the induced current also adds a random component to the signal. This effect can be minimized by use of shielded and twisted-conductor cable, and by use of transducers with low-impedance voltage output instead of transducers with high-impedance charge output. In the present case, although coaxial cabling was used, a high-impedance charge-output transducer was also used, so it is likely that electromagnetic noise pickup did contribute appreciably to the noise during motor operation.

3) Third, the motor exhaust flow generates a moderately severe broadband acoustic field around the motor and test cell. The acoustic pressures applied to the coaxial cable cause vibration and minute distortions of the coaxial cable, which in turn cause variations of the cable capacitance. For high-impedance charge-output transducers, the cable capacitance variations cause significant variations of the charge presented at the charge amplifier input, and consequently correspondingly significant variations of the recorded amplifier output voltage. Although a similar effect occurs with low-impedance voltage-output transducers, the magnitude of the effect is commonly 1% or less of the effect with high-impedance charge-output transducers.

Consideration of these noise mechanisms prompts statement of two recommendations believed fundamental to acquiring good measurements of motor pressure oscillations:

- Instrumentation circuits for each measurement of combustion phenomena should be separately and fully shielded, with the shields for different measurements isolated from each other or from ground except at a single common point, which should be electrically connected to electrical earth ground at the test device.
- Transducers for measurements of dynamic processes associated with rocket motor operation should be of low-impedance voltage-output type.

7.4   Uncertainty and Error Analysis[105]

The treatment of uncertainty in rocket and missile engine testing is based on established statistical methods. Uncertainty is a statistical statement for the degree of agreement to the true value (target value) of measurements. The term "uncertainty" is composed of precision and bias.

Precision of the measurement is the degree of mutual agreement of repeated independent values and describes the random measurement fluctuations of the system about a mean. Statistically, precision is the estimate of the standard deviation of the distribution of an infinite number of measurements under identical conditions.

Bias is the difference between the mean measured value for an infinite number of measurements under identical conditions and the true value. The indeterminate bias has unknown magnitude and usually unknown direction. A tendency to measure a characteristic other than that intended causes bias. Trend statistics can be used to test the randomness (lack of bias) of measurements. To avoid bias, instruments are calibrated against a standard. The hierarchy levels of calibration from the measuring instrument to the National Bureau of Standards are recorded and statistically evaluated. Documented evaluation of the calibration hierarchy of each measurement system used is traceability. When an instrument is used beyond the calibration range, an increase in uncertainty must be calculated.

One of the goals of measurements is the improvement of the model used for prediction. The meaningful correlation of test data with predicted values must be based on statistical concepts since both the measurements and predictions contain uncertainties. The prediction methods can be thought of as an independent measuring procedure using a different set of measured data (reaction rates, etc.). The predicted value is then the mean of a distribution of possible predicted values.

The discussion of uncertainty here is meant to be only a summary of the methods. Further details are provided in Appendix D. A full discussion can be found in references. [106,107]

8.0   ANALYSIS METHOD SUMMARY

8.1   Fundamental Definitions

Two fundamental families of burning rate determination methods exist with the following categories:

1) Thickness/time (TOT) Methods
        a) TOT Rate, r_{TOT}
        b) Iterated TOT Rate, r_{TOTn}
        c) Iterate Two-Point TOT Rate, r_{HG}
2) Mass Balance (MB) Methods
        a) MB Rate, r_{MB}
        b) Iterated MB Rate, r_{MBn}

The iterated procedures normally differ in the use of the rate-averaged instead of the more common time-averaged pressure and an iteration to determine exponent n. Some iterative methods (both TOT and MB) described in this report use time-averaged pressure and iterate only to determine burning time and not exponent. While r_{TOT} is in error when burnout is non-instantaneous (as usually observed), r_{MB} is in error if mass storage is neglected. The HG (Hessler-Glick) r_{TOT} procedure, initially developed for reference purposes in support of WG 016 in the mid-1990s, avoids both errors by explicitly recognizing non-instantaneous burnout.

Representative MB methods currently in use by facilities surveyed by WG016 include:
    1)   Common MB Method
    2)   Vellacott's Method
    3)   Brooks' Improved Method
    4)   Jordan's Combined MB with TOT Method

The common MB neglects all storage terms. Vellacott's method includes a correction for mass storage due to volume increase. The Brooks' improved MB method approximates all storage terms, including correction due to a changing pressure as well as volume. Jordan's combined method simultaneously solves for the MB and TOT burning rates, assuming only one burning rate properly defines the propellant, regardless of the method.

Grain web typically used for burning rate calculation is usually one of the following:
    1)   Drawing dimensions,
    2)   Drawing dimensions corrected for theoretical shrinkage, or deformation
    3)   A measured "average".

While each choice yields an "average" thickness, the difference between the choices on the results can be considerable. Improved accuracy can be obtained by measuring grain bore and case inside diameters. Methods are suggested for improving accuracy.

The motor action time follows from the pressure-time trace, which starts at the beginning of motor operation, and ends at the end of motor operation. The burning time is determined from this trace as the period from the moment that all propellant is considered burning until the moment the web is considered consumed. For burning rate determination, the burning time is the appropriate time period to use. The following burn time definitions were encountered in the WG 016 survey:

1) Constant P or $\%P_{max}$ - 10%, 50%, 60%, and 75%, with 10 % typical
2) Tangent-Bisector
3) Brimhall - $d^2P/dt^2 = 0$ or a maximum negative dP/dt during tail-off
4) Brooks' - Pressure Integral
5) Hessler-Glick - from the first perceptible rise on the *last sustained rise* to *a negative step* of d^2p/dt^2 to negative value (t_{Ei}), and to *a positive step* of d^2p/t^2 to positive value (t_{Ef}).

The pressure usually associated with a measured burning rate is the *time-averaged pressure.* However, any measured point [r_{meas}, $p(r_{meas})$] must also simultaneously satisfy the power law rate equation, which requires use of *rate-averaged pressure.*

8.2   Comparison of Analysis Methods

Many r_{TOT} procedures do not explicitly account for non-instantaneous burnout. Procedures that define end of burning near 50% pressure implicitly assume burning continuation and thus partially avoid non-instantaneous burnout error, but not as well as an r_{MB} definition that actually uses the integral ratio. Due to transient operations, these r_{TOT} procedures tend to behave essentially like r_{MB} procedures. More bias in burning rate is introduced, as the rate-averaged pressure is seldom used.

r_{MB} methods yield rates that are systematically low by a mass storage error. In turn, mass storage error also introduces a systematic nonlinearity in measured $r_b(p)$. Procedures essentially behaving like r_{MB} are likewise low by a mass storage error and generate similar nonlinearities. HG fully avoids the mass storage error, so it will be linear and systematically yield higher rates than r_{MB} procedures. r_{TOT} methods, with instantaneous burnout, also avoid the mass storage error yielding negligible nonlinear errors but high bias due to non-instantaneous burnout.

Three historical surveys exist of burning rate analysis practices employed in solid propulsion industry. One conducted by Miller and Barrington in the late 1960s, a second conducted by Brooks and Hermsen in the late 1970s and the last by Fry in the mid 1990s. Trends suggest the fundamental TOT procedures are being replaced by MB procedures or TOT procedures with burning times evaluated using methods to more effectively account for non-ideal tailoff.

The data analysis methods of 21 facilities from 7 NATO member countries surveyed by the WG016 are summarized by the source of the method by country and facility and the fundamental type. Detailed descriptions of the methods are provided in Appendix B. Review of these data indicates all 7 European facilities use TOT procedures, with approximately half using burning end time definitions that try to account for non-ideal tailoff. Slightly more than half the U.S./Canada facilities use MB procedures, while the majority use burning end time definitions that try to account for non-ideal tailoff. Some facilities possess both TOT and MB capabilities for use in different motor test situations. Over 90% of all facilities surveyed use a simple constant P or %P to define burning start time. Large variability in burning end time definition is seen.

111

8.3 Assessment of Analysis Methods Using Simulated Motor Data

The RTO/AVT WG016 assessed the various TOT and MB analysis methods taken from the international survey for the purposes of (1) Clarifying distinctions of subscale motor analysis methods, and (2) Identifying sources of the differences. The assessment using simulated motor data involved carrying out four Round Robin (RR) evaluations. The design and execution of the RRs are summarized in Appendix C, with detailed results summarized earlier in this chapter.

Lessons from the Simulation Round Robins RR #3 and #3X tests have pointed out the quality of applied data reduction methods for a change of several parameters (bore offset, characteristic length, non-neutral trace shape, rate equation, etc.) influencing combustion. Results from different procedures were compared with the rate equation used for the simulations and with each other to identify the following systematic errors inherent in the various procedures: Non-Neutrality Error, Non-Instantaneous Burnout Error, and, Mass Storage Error. Causes and corrections are summarized.

The r_{HG} procedure avoids all three of the errors above, obtaining data accurate to the basic time resolution of the simulations. Thus, in treating simulated pressure traces, HG proved superior to other methods due to a careful set of time points definitions, but requires visual inspection of each pressure trace. However, these were *simulations*, and the simulations did *not* include several phenomena that occur in real motors, such as the error levels in the reduced data were appreciably smaller than the suspected bias in real motors. Assessments of the methods were therefore conducted using real motor data.

8.4 Assessment of Analysis Methods Using Real Motor Data

Data reduction methods were contrasted to analyze the Baria (6300g) and 2-inch (350g) experimental pressure traces used to evaluate the ballistic parameters respectively for Ariane-5 and Ariane-4 solid propellant boosters. Test hardware details are provided in JHU/CPIA CPTR 74.[5] Fiat Avio BPD conducted all tests in early-2000. Four series of 9 mixes were made for Ariane-5 for a total of 108 Baria motor tests. Likewise, a series of 4 mixes were made for Ariane-4 for a total of 24 2-inch motor tests.

Observed Trends in Analysis Methods

With good quality data and based on mix-to-mix variation, the POLIMI generic MB procedure (inspired by the U.S. NSWC MB method) and the HG two-point TOT procedure resulted in smaller data scatter than the tested industrial procedures. TOT methods (BC, BPD-1, SNPE) routinely used by European industry produce quite similar values; SNPE and BPD-2 (a variant of BPD-1) offer slightly smaller data scatter and provide almost identical performance; BPD-1 is superior in dealing with Ariane-4 small-scale test motors; and, BC produces reasonable results with little effort. The manual HG and simple POLIMI procedures often showed better performances overall.

The industrial methods nominally assuming instantaneous burnout (BC, BPD-1, BPD-2, SNPE) produce mean values that are quite similar, as expected from the general similarity of these procedures. Within this group, BPD-2 and SNPE (which differ only in details) produce about the same mean values, while BC produces reasonable results with little effort. Relative to the industrial methods, the generic MB procedure used by POLIMI produces lower rates and lower exponents; HG produces higher rates and lower exponents. HG and POLIMI procedures in general also yield relatively more confined values of standard deviation for the ballistic parameters n and a. Most of these observed differences appear to be explainable in terms of known physical effects.

Time-averaged pressure is greater than rate-averaged pressure (consistent with RR #1 results), so any procedure using time-averaged pressure yields a rate equation that is consistently biased low due to the Non-Neutrality Error. As HG is the only procedure using rate-averaged pressure as the associated pressure, HG rates are expected to be higher than the others. In general, for a fixed average degree of non-instantaneous burnout due to either grain distortion or misalignment, the Non-Neutrality Error for a propellant will increase at lower pressures, because the burnout process extends for a greater fraction of the tail-off process. As a consequence, procedures that use time-averaged pressure should be expected to yield rate equations with exponents biased high, while HG exponents are expected lower.

In treating simulated pressure traces, HG method did best; but while other methods are automated, HG requires some insight and the operator's analysis for each trace. In simulated motors, the HG procedure is not affected by non-idealities of burning process (such as nozzle erosion, non-instantaneous burnout, mandrel eccentricity or bore offset, etc.) and proved to be a reliable method in terms of reproducibility and accuracy of burning rate results. This could not be stated with the same confidence in real operating motors where noise, imperfect instrumentation setup, and different environmental conditions are to be handled. In real test motors, non-idealities in principle favor the class of MB over TOT methods and somewhat compromise the accuracy demonstrated by HG in ideal cases.

The WG 016 observed that the Hessler-Glick analysis is a promised procedure and merits further developments. An automatic HG procedure for use on standard desktop computers for the benefit of industrial manufacturers is recommended.

9.0   CONCLUSIONS - RECOMMENDATIONS

9.1   General

The NATO RTO AVT WG 016 has identified current practices and areas for improvements in burning rate measurement and analysis methods. Results support the finding that manufacturer burning rate data may not easliy be compared without accounting for industry-wide differences in subscale devices, test methods, and scaling analysis methods. AVT WG 016 surveyed over 25 facilities from 12 countries for the characteristics of test and analysis methods employed. This report represents a complete survey of all major international facilities involved in burning rate measurement and a thorough representation of the fundamental methods used in the solid propulsion community today. Peer review of the results and conclusions was sought outside the WG throughout this effort.

9.2   Burning Rate Fundamentals

Solid propellant burning is not a steady process, but rather an intrinsically unsteady and multidimensional process. The flame structure in solid propellant burning is complex and flame models and empirical burning rate laws are used to seek its understanding. Different measurement techniques are approximate means to define the "real" burning rate. This makes experimental uncertainty and error analysis an important element of this process. Each propellant exhibits an "intrinsic" burning rate, which an ideal experiment, with non-idealities eliminated, seeks to measure.

Knowledge of burning rate of solid propellants, whether steady or unsteady, under a variety of operating conditions, is of critical importance for applications (due to their sensible influence on performances and cost of propulsive devices) and also for fundamental reasons (understanding of combustion processes). Furthermore, since no available theory/model is capable of predicting burning rates with accuracies within 1% while including the effects of rate modifiers, they must be measured experimentally. However, while experiments measuring steady burning rates are reasonably robust, those measuring unsteady values are fragile and still a matter of research. Since a variety of experimental hardware and methods are in use today, even for the common steady-state operations, the need arises to understand and perhaps standardize the different approaches developed among the NATO countries.

The fundamental physics, features, empirical laws and analytical models, stability measurement methods, and scaling of burning rate are reviewed in the report. Analysis results in this study are expressed in terms of the simple power law rate equation, often referred to as the St. Robert's, St. Venant's or Vielle's law, $r = ap^n$. Two fundamental classes of empirical burning rate definitions are in use for motor applications: the thickness/time method and the mass conservation or mass balance method.

9.3   Test Hardware and Measurement Methods

Subscale motors are used to simulate the ballistic flow conditions expected in full-scale motors and to evaluate how the motor conditions influence the "intrinsic burning rate" of the propellant. Furthermore, subscale motors are used because strand burner techniques have historically proven inadequate for predicting full-scale motor burning rate and ballistic behavior on their own.

A wide array of motors, with different design features, exists for measuring burning rate within the 23 facilities in 7 countries surveyed. Complete details of test hardware used by the facilities surveyed are provided in JHU/CPIA CPTR 74.[5] Subscale motor sizes used vary from <250g to over 10,000g. The predominant configuration encountered is the circular, center-perforated grain in the weight classes under 5000g. While the 5x10 cm (2x4 inch) motor is the most widely used tool, this motor is also not standardized with respect to dimensions and propellant mass, which varies between 120g - 450g. The WG recommends standardizing this motor by increasing the web of the propellant grain to nominally 13mm, resulting in a propellant weight of approximately 300-400g. This would cover the majority of propulsion applications and allow greater international cooperation in correlating burning rate data.

The WG created a summary of the use of burning rate measurement hardware in relation to the life cycle of the propellant versus its application. The smaller motor sizes (<200g to 5,000g) are used in the

research/technology, screening and development phases for both tactical and space/strategic propulsion. Large subscale test motors (5,000g to over 10,000g) are mainly used in the screening through performance verification phases for space/strategic applications. WG 016 findings suggest 2000g-5000g motors provide satisfactory scale-up for smaller full-scale motors (D ≤ 76 cm). The largest motors with grain weights from 22kg up to 60 kg permit satisfactory scaling for very large boost motors for space or strategic applications.

Recommended burning rate measurement practices, including test hardware, instrumentation, and data reduction are summarized in JHU/CPIA CPTR 74.[5] Further attention to refining experimental methods in order to reduce motor test data variability is warranted.

9.4   Analysis Methods

The fundamental definitions and variations for burning rate, grain web, burning times, and average pressure used by the facilities and countries surveyed are reviewed in detail. Complete details of analysis methods used by the facilities surveyed are provided in Appendix B to this report. The fundamental behavior of thickness/time and mass balance methods and associated inherent errors are reviewed in detail. The advantages and disadvantages of the two fundamentally different families of burning rate determination merit continuing study. Historical preferences seem to dictate which methods are used. Analytical reasons exist for their application in specific situations. Historical surveys over 30 years of burning rate analysis practices suggest the fundamental thickness/time methods are being replaced by mass balance methods or thickness/time methods with burning times that more effectively account for non-ideal tailoff. The large variability in burning rate definitions makes assessment of the analysis methods difficult. Some consistency in these definitions would promote ease in correlating data internationally.

The round robin approach using simulated motor data has contributed successfully to pointing out the quality of applied data analysis methods and their sensitivity to several parameters influencing burning rate. The parameters examined include non-neutral pressure behavior, bore offset, characteristic length, rate equation, igniter effects, erosive burning, and eroding nozzle. Complete details of the round robin designs are provided in Appendix C to this report. Analysis results using different methods were compared with the reference rate used in the simulations and with each other to identify the following systematic errors inherent in the various procedures: Non-Neutrality Error, Non-Instantaneous Burnout Error, and, Mass Storage Error. Causes and corrections are summarized. Simple thickness/time procedures do not explicitly account for non-instantaneous burnout. Mass balance methods are influenced by a mass storage error. Results illustrated the inherent robustness of the mass balance methods to accommodate either data errors or changes in parameters influencing burning rate. The Hessler-Glick reference method avoided all the errors inherent in currently used thickness/time or mass balance methods, obtaining data accurate to the basic time resolution of the simulations. However, these were *simulations*, and the simulations did *not* include several phenomena that occur in real motors.

Real subscale rocket motor data became available for the purpose of evaluating data analysis methods. The real combustion experiments provided pressure traces perturbed by noise caused by the combustion process, the flow field and instrumentation. Moreover, the real pressure traces had a lower sampling rate than the simulated data, providing a lower intrinsic accuracy. In real test motors, non-idealities in principle, favor the class of mass balance over thickness/time methods and somewhat restrict the accuracy demonstrated by Hessler-Glick in ideal cases. The WG recommends further development of the promising Hessler-Glick analysis method. An automatic HG method for use on standard desktop computers for the benefit of industrial manufacturers is recommended. Elements of the Hessler-Glick method should be applied to mass balance methods.

Significant factors influencing small motor data quality are reviewed relevant to data analysis. These factors include propellant effects, testing effects and uncertainty and error analysis. A more complete review of uncertainty and error analysis is provided in Appendix D to this report.

9.5 Non-Intrusive Measurement Methods

The WG surveyed facilities and countries on non-intrusive measurement techniques emphasizing those currently employed, including ultrasonics, X-ray, microwave, plasma capacitance gages, acoustic emission, and laser recoil. Results identified in this report for the methods in use include the motivation for using the technique; the characteristic strengths and weaknesses; example applications; an assessment of advantages, limitations and future prospects; and, a list of reference documents. Since these non-intrusive techniques are generally research-oriented, past work has been more focused on development rather than industrial application. A critical assessment is made of the non-intrusive methods for measuring steady-state propellant burning rate. This assessment includes operational limitations, temporal and spatial limits, steady-state burning rate uncertainty, cost, maturity, advantages, limitations, and prospects for use for routine ballistic testing.

Ultrasonic instrumentation is recommended for application to routine ballistic evaluation of propellants in research and industrial settings. Plasma Capacitance Gage (PCG) is recommended for further development. The acoustic emission technique is endorsed as a routine method for ballistic characterization of propellant strands, and for further development in applications to full-scale motors for grain evolution monitoring. X-ray diagnostics and the microwave technique are not recommended as routine ballistics tools. Recommendations are provided for improving existing techniques, which can provide for further advancements in burning rate measurements.

The WG 016 supports the view that even though new breakthrough techniques using basic principles could still be developed in the future, further advancements in burning rate measurements will depend largely upon improvements in the existing techniques. One fundamental limitation of all techniques investigated is that they measure properties that are proportional to distance. Since the desired parameter of interest is burning rate, some thinking should be done on a measurement technique that is sensitive or proportional to the surface velocity instead of the surface displacement. This approach bypasses the uncertainties amplified in data when time derivatives are taken of displacement data.

Another future prospect for the recommended devices is the correlation of data from all sizes of tests. In principle, a subscale motor can be tested with ultrasonic instrumentation and PCG's in the laboratory, in production checks, on full-scale tests, and in flight. The PCG technology should receive priority for investment to mature this technique. This technology has great potential. If successful it could provide ballistic information at all points in the research, development, and use of solid rocket motors. The most practical aspect and recommendation of this work must be to encourage NATO nations to adopt ultrasonic instrumentation into their propellant development process.

9.6 Test Motor Scaling

Propellant burning rate is one of the most significant variables influencing the accuracy of solid rocket thrust-time prediction. An analytic methodology is recommended for correlating burning rate through this performance prediction. A thorough means of predicting full-scale experimental results from theoretical analysis should include two correcting factors, a constant scale factor correction and a variable correction resulting mainly from the grain manufacturing process.

The underlying reasons for the differences observed in burning rate between large-scale motors, subscale motors, strands and non-intrusive methods are summarized and reviewed in detail. Some are evident from a consideration of burning rate physics and can be identified independently in the laboratory. Some are derived from a consideration of the engineering design of the motor and its operating environment. The degree of scaling exhibited by a strand burner, subscale or full-scale motor will vary in proportion to the effect exhibited by the influencing parameters. Understanding and accounting for these parameters, in subscale hardware design serves to mitigate the scaling effects. Factors that should be avoided in subscale hardware that typically contribute to modeling complexity and confounding test results are summarized.

Historically, "scale factor" has been a measure of the uncertainty to define the differences in burning rate between a subscale burning rate measurement device or subscale motor and a larger motor. Current

thorough industrial practices seek to identify the sources of the differences in order to reduce uncertainty (or "scale factor" dispersion) in burning rate between scales.

Industry challenges and successes in strand burner-to-motor and subscale-to-full-scale burning rate comparisons are reviewed. Correlations between strands and subscale motors are recommended in order to determine the influence of the controlling factors. The strand burner is a better tool for measuring statistically significant effects of small formulation changes for quality control work, given proper test design and conduct. Solid rocket motor performance predictions are possible by establishing a correlation between full-scale motor performance, subscale test motors, and liquid and solid strand burning rate tests. The confidence and accuracy of these predictions will be maintained if the correlation between motor performance and any of the subscale test methods remains constant.

Selected facilities and countries were surveyed to identify industrial scaling practices. Relatively few facilities and countries develop and field large solid rocket motors. This is reflected in the fact that only a portion of the propulsion community surveyed have established test motor scaling practices. Many countries and facilities use only a constant scale factor correction. Methods of evaluating scale factor may or may not attempt to account for some of the fundamental factors influencing scaling. Various companies in the U.S. and France include the recommended variable motor scale factor correction, but seek different means of accounting for the principle parameters that contribute to differences in real motor internal geometry with scale. An effort to agree on consistent scaling methods would contribute to success in international cooperative programs.

The NATO RTO AVT WG 016 activities have acted as a catalyst for efforts to improve burning rate measurement and analysis methods within the NATO community. The WG recommends, as a minimum, that members of the NATO propulsion community review these findings as a means of advancing their own burning rate measurement and analysis methods.

9.7 Future Developments

Factors crucial to industrial acceptance are cost effectiveness and robustness. Until recently, ballistic test motors were focused on burning rate characterization. However, passive motor stability diagnostics provide concurrent modal frequency and stability margin estimates from low-level pressure oscillations present. Therefore, the cost effectiveness of the ballistic test motor *as a propellant charactizer* can be increased by nothing more than increasing the sensitivity of the pressure measurements.

New measurement techniques will require a re-examination of propellant characterization techniques and hardware, as well as test technique development. For example, ballistic test motors having characteristic frequencies in regimes of interest will be desirable; this will necessitate new geometric configurations. In a similar way, the ability of measurement techniques to enhance the accuracy of sensitivity measurements, the key to empirical formulation development, will instigate the development of instantaneous, multiple, simultaneous rate difference measurements in a variable-pressure environment. Lastly, concurrent measurement of burning rate, sensitivities, and stability-related information offer potentially valuable interactions. The ZN methodology, for example, connects steady and nonsteady behavior. Therefore, with both steady and nonsteady information in hand, other information can be accessed.

Refinement of current techniques, development of innovative techniques and necessary theoretical accessories will provide excitement and improved solid rockets in the future. Detailed solid rocket simulations in progress will assist these potential developments. A fully-coupled ballistic test motor simulation, for example, would demonstrate the effects of cure shrinkage and grain temperature on the web; the effect of ordered particle distributions near the case and bore; combustion efficiency dependence upon heterogeneity, etc.; and, connection between low-level pressure oscillations and physical processes.

10.0   REFERENCES

[1] "Evaluation of Methods for Solid Propellant Burning Rate Measurements," NATO RTO Advisory Report, NATO RTO AVT Working Group 016, Chaired & Edited by R. S. Fry, Johns Hopkins University/CPIA, August 2001.

[2] Brooks, W.T., "Burn Rate Considerations in Solid Rocket Motor Performance Prediction," AIAA Paper 76-601, presented at AIAA/SAE 12th Propulsion Conference, Palo Alto, CA, July 1976.

[3] Fry, R. S., "Solid Rocket Motor Test and Test Techniques, Component Testing & Verification, Solid Propellant Burning Rate," AIAA Solid Rocket Technical Committee Lecture Series, 36th Aerospace Sciences Meeting, January 1998.

[4] Fry, R.S., "Solid Propellant Test Motor Scaling," JHU/CPIA CPTR 73, September 2001.

[5] Fry, R.S., "Solid Propellant Subscale Burning Rate Test Techniques and Hardware for U.S. and Selected NATO Facilities," JHU/CPIA CPTR 74, July 2001.

[6] DeLuca, L.T., "Burning Rate Fundamentals," Chapter 2 of "Evaluation of Methods for Solid Propellant Burning Rate Measurements," NATO RTO Advisory Report, NATO RTO AVT Working Group 016, Chaired & Edited by R. S. Fry, Johns Hopkins University/CPIA, August 2001.

[7] F.A. Williams, M. Barrère, and N.C. Huang. Fundamental Aspects of Solid Propellant Rockets. Technivision Services Slough, UK, 1969. AGARDograph 116.

[8] F.A. Williams. Combustion Theory. The Benjamin/Cummings Publishing Company, Menlo Park, CA, 2nd edition, 1985. pp.

[9] G.P. Sutton, Rocket Propulsion Elements. Wiley, New York, NY, USA, 6th edition, 1992.

[10] R.T. Holzmann, Chemical Rockets, Marcel Dekker, New York, NY, USA 1969.

[11] A. Davenas., Solid Rocket Motor Design, volume 170, AIAA Progress in Astronautics and Aeronautics, "Tactical Missile Propulsion", edited by G.E. Jensen and D.W. Netzer, chapter 4, pages 57-113. AIAA, Reston, VA, USA, 1996.

[12] K. Klager, and G.A. Zimmerman. Steady Burning Rate and Affecting Factors: Experimental Results, volume 143, AIAA Progress in Astronautics and Aeronautics, "Nonsteady Burning and Combustion Stability of Solid Propellants", edited by L.T. DeLuca, E.W. Price, and M. Summerfield, chapter 3, pages 59-109. AIAA, Washington, DC, USA, 1992.

[13] C. Huggett, C.E. Bartley, and M.M. Mills, Solid Propellant Rockets. Number 2 in Princeton Aeronautical Paperbacks. Princeton University, Princeton, NJ, USA, 1960

[14] Y.M. Timnat. Advanced Chemical Rocket Propulsion. Academic Press, London, UK, 1987

[15] V.E. Zarko and K.K. Kuo. Critical Review of Methods for Regression Rate Measurements of Condensed Phase Systems, pages 600-623. Special Topics in Chemical Propulsion, "Non-Intrusive Combustion Diagnostics", edited by K.K. Kuo and T.P. Parr. Begell House, Inc., New York, NY, USA, 1994.

[16] M. Barrère, A. Jaumotte, B. Fraeijs De Veubeke, and J. Vandenkerckhove. Rocket Propulsion. Elsevier Publishing Company, Amsterdam, Netherlands, 1960.

[17] B.L. Jr. Crawford, C. Huggett, and F. Daniels, and R.E. Wilfong. Direct Determination of Burning Rates of Propellant Powders. Analytical Chemistry, 19(9): 630-633, 1947.

[18] M. Summerfield, G.S. Sutherland, M.J. Webb, H.J. Taback, and K.P. Hall, Burining Mechanism of Ammonium Perchorate Propellants, Volume 1 of AIAA Progress in Astronautics and Aeronautics, "Solid

Propellant Rocket Research", edited by M. Summerfield, pages 141-182. Academic Press, New York, NY, USA, 1960.

[19] J.A. Steinz, and M. Summerfield, Low Pressure Burning of Composite Solid Propellants. Volume 88 of Advances in Chemistry Series, chapter 9, pages 244-295. American Chemical Society, Washington, DC, USA, 1969.

[20] J.A. Steinz, P.L. Stang, and M. Summerfield. The Burning Mechanism of Ammonium Perchlorate Based Composite Solid Propellants. Technical Report AMS-830, Princeton University, Princeton, NJ, USA, 1969. PhD Thesis, Aerospace and Mechanical Sciences Department.

[21] A. Davenas et Collaborateurs, Technologie des Propergols Solides. Masson, Paris, France, 1989.

[22] J.W. Cornelisse,H.F.R. Schöyer, and Wakker K.F. Rocket Propulsion and Spaceflight Dynamics. Pitman Publishing Limited, London, UK, 1979.

[23] Ya.B. Zeldovich. On the Combustion Theory of Powder and Explosive. Journal of Experimental and Theoretical Physics, 12:498-510, 1942.

[24] Ya.B. Zeldovich, O.I. Leypunskii, and V.B. Librovich. The Theory of the Unsteady Combustion of Powder. Nauka, Moscow, Russia. 1975.

[25] B.V. Novozhilov. Nonstationary Combustion of Solid Rocket Fuels. Nauka, Moscow, Russia, 1973. Translation AFSC FTD-MT-24-317-74.

[26] A.A. Zenin. Thermophysics of Steady Combustion Waves of Solid Propellants, volume 143, AIAA Progress in Astronautics and Aeronautics, "Non steady Burning And Combustion Stability of Solid Propellants" edited by L. DeLuca, E.W. Price, and M. Summerfield, chapter 6, pages 197-231. AIAA, Washington, DC, USA, ,1992.

[27] W.H. Miller and Barrington. A Review of Contemporary Solid Rocket Motor Performance Prediction Techniques. Journal of Spacecraft and Rockets, 7 (3), 1970.

[28] N. Kubota. Survey of Rocket Propellants and Their Combustion Characteristics, volume 90, of AIAA Progress in Astronautics and Aeronautics, Fundamentals of Solid Propellant Combustion, edited by K.K. Kuo and M. Summerfield, chapter 1, pages 1-52. AIAA, Washington, DC, USA, 1984.

[29] N. Kubota. Temperature Sensitivity of Solid Propellants and Affecting Factors: Experimental Results, volume 143 of AIAA Progress in Astronautics and Aeronautics, Nonsteady Burning and Combustion Stability of Solid Propellants, edited by L. DeLuca, E.W. Price, and M. Summerfield, chapter 4, pages 111-143. AIAA, Washington, DC, USA, 1992.

[30] O.K. Rice and R. Ginell. The Theory of the Burning of Double-Base Rocket Powder. Journal of Physical and Colloid Chemistry, 54 (6): 885-917, 1950.

[31] R.G. Parr and B.L. Jr. Craford. A Physical Theory of burning of Double-Base Rocket Propellants. Journal of Physical and Colloid Chemistry, 54 (6): 929-954, 1950

[32] M.W. Beckstead, R.L. Derr, and C.F. Price. A model of composite solid-propellant combustion based on multiple flames. AIAA Journal, 8(12): 2200-2207, 1970.

[33] M.R. Denison and E. Baum. A Simplified Model of Unstable Burning in Solid Propellants. ARS Journal, 31:1112-1122, 1961.

[34] B.V. Novozhilov. Stability Criterion for Steady-State Burning of Powders. Journal of Applied Mechanics and Technical Physics, 6(4): 157-160, 1965.

[35] B.V. Novozhilov. Theory of Nonsteady Burning and Combustion Stability of Solid Propellants by the ZN Method, volume 143 of AIAA Progress in Astronautics and Aeronautics, 'Nonsteady Burning and Combustion Stability of Solid Propellants' edited by L. DeLuca, E.W. Price, and M. Summerfield, chapter 15, pages 601-641. AIAA, Washington, DC, USA, 1992

[36] L.T. DeLuca, R. DiSilvestro, F. Cozzi. Intrinsic Combustion Instability of Solid Energetic Materials. Journal of Propulsion and Power, 11(4):804-815, 1995. See also Comments, Journal of Propulsion and Power, 13(3):454-456,1997.

[37] L.T. DeLuca, M. Verri, F. Cozzi, A. Jalongo, and G. Colombo. A Survey of Pressure-Driven Burning of Energetic Solid with Arrhenius Surface Pyrolysis. In "Challenges in Propellants and Combustion 100 Years After Nobel" edited K.K. Kuo, pages 493-514. Begell House, New York, USA 1997.

[38] Zucro, M.J. and J.D. Hoffman, "Gas Dynamics," John Wiley & Sons, 1977, Vol II.

[39] A. Annovazzi. Burning Rate Measurement at FIAT AVIO - Comprensorio BPD. Private communication, 13 November 1997.

[40] E.W. Price. Experimental Observations of Combustion Instability, 1984, volume 90 of AIAA Progress in Astronautics and Aeronautics, Fundamentals of Solid Propellant Combustion, edited by K.K. Kuo and M. Summerfield, chapter 13, pages 733-790. AIAA, Washington, DC, USA, 1984.

[41] E.W. Price. L' Instability, 1992, volume 143, AIAA Progress in Astronautics and Aeronautics, , Nonsteady Burning and Combustion Stability of Solid Propellants, edited by L. DeLuca, E.W. Price, and M. Summerfield, chapter 9, pages 325-361. AIAA, Washington, DC, USA, 1992.

[42] F.E.C.Culick, and V. Yang. Prediction of the Stability of Unsteady Motions in Solid-Propellant Rocket Motors, volume 143, AIAA Progress in Astronautics and Aeronautics, "Nonsteady Burning and Combustion Stability of Solid Propellants", edited by L. DeLuca, E.W. Price, and M. Summerfield, chapter 18, pages 719-779. AIAA, Washington, DC, USA, 1992.

[43] H.B. Mathes. Applications of Combustion Stability Technology to Solid Propellant Rocket Motors, volume 143, AIAA Progress in Astronautics and Aeronautics, "Nonsteady Burning and Combustion Stability of Solid Propellants" edited by L. DeLuca, E.W. Price, and M. Summerfield, chapter 19, pages 781-804. AIAA, Washington, DC, USA, 1992.

[44] G.H.S. Young. Methods of Burning Rate Control in Solid Propellants, pages 285-302. AGARD Combustion and Propulsion Panel. Pergamon Press, 1960.

[45] S.F. Sarner. Propellant Chemistry. Reinhold Publishing Corporation, New York, NY, USA, 1966.

[46] R.O.Hessler. Private communication, 15 December 1997.

[47] A.A. Juhasz, and C.F. Price. The Closed Bomb Technique for Burning Rate Measurement at High Pressure, volume 63 of AIAA Progress in Astronautics and Aeronautics, "Experimental Diagnostics in Combustion of Solids", edited by T.L. Boggs and B.T. Zinn, pages 129-151. AIAA, Washington, DC, USA, 1992.

[48] C. Zanotti, A. Volpi, M. Bianchessi, and L.T. DeLuca. Measuring Thermodynamic Proprieties of Burning Propellants, volume 143, AIAA Progress in Astronautics and Aeronautics 'Nonsteady Burning and Combustion Stability of Solid Propellants', edited by DeLuca, L.T., E.W. Price, and M. Summerfield, chapter 5, pages 145-196. AIAA, Washington, DC, USA, 1992.

[49] N. Eisenreich, H.P. Kugler, and F. Sinn. An Optical System for Measuring Burning Rates of Solid Propellants. Propellants, Explosive, Pyrotechnics, 12:781-80, 1987.

[50] J.M. Tauzia and P. Lamarque. Solid Rocket Propellant Behaviour During Static Firing Test Using Real Time X-Ray Radioscopy. In AGARD PEP 90th Symposium on Advanced Non-Intrusive Instrumentation for Propulsion Engines, Paper 35. AGARD, Paris, France, 1998.

[51] L.D. Strand, A.L. Schultz, and G.K. Reedy. Microwave Measurement of Solid Propellant Pressure Coupled Response Function. Journal of Spacecraft and Rockets, 17(6): 483-488, 1980.

[52] P.Kuentzmann, J.C. Demarais, and F. Cauty. Mesure de la Vitesse de Combustion des Propergols Solides par Ultrasons. La Recherche Aérospatiale, (1):55-79, 1979.

[53] L.H. Caveny, A.J. Saber, and M. Summerfield. Propellant Combustion and Burning Rate Uniformity Identified by Ultrasonic Acoustic Emissions. AIAA, Washington, DC, USA, 1976. AIAA Paper 76-696.

[54] C.M. Mihlfeith, A.D. Baer, N.W. Ryan. The Response of Burning Rate Propellant Surface to Thermal Radiation. AIAA Journal, 10(10):1280-1285, 1972.

[55] L.C. Yang, Miner, E.L., and Ramanos, "Application of Plasma Capacitance Gage (PCG) for Real Time Measurements of Solid Rocket Motor Internal Insulation Erosion", AIAA Paper 90-2327, July 1990.

[56] S. Rampichini, D. Ruspa, and L.T. DeLuca. The Acoustic Emission of Underwater Burning Solid Rocket Propellants. In: Special Topics in Chemical Propulsion "Combustion of Energetic Materials", edited by K.K. Kuo and L.T. DeLuca. Begell House, New York, NY, USA, 2001.

[57] R.O.Hessler. An Analysis of Burning Rate Round-Robin Data. Technical Report, JANNAF Combustion Meeting, West Palm Beach, FL, 27-31 October 1997.

[58] R.O. Hessler, and R.L. Glick. Comparison of Burning Rate Calculation Methods. Technical report, JANNAF Combustion Meeting, West Palm Beach, FL, 27-31 October 1997, 1997.

[59] Miller, W.H. and Barrington, D.K., "A Review of Contemporary Solid Rocket Motor Performance Prediction Techniques," Journal of Spacecraft and Rockets, 7 (3): 225-237, 1970.

[60] R. De Amicis. Burning Rate Measurement at FIAT AVIO - Comprensorio BPD. Private communication, 10 October 1997.

[61] Whitney C.K., Owens T.F., Paskind J., and Rubin M.B., Scout Motor Performance and Prediction Study (PAPS), NASA-CR-336, NASA Langley Research Center, December 1965.

[62] Miller, W.H. and Barrington, D.K., "A Review of Contemporary Solid Rocket Motor Performance Prediction Techniques," Journal of Spacecraft and Rockets, 7 (3): 225-237, 1970

[63] Brimhall K., unpublished, circa 1980. (In personal communication with R.L. Glick, about 1995, Brimhall stated that his derivative definition had merely been a suggestion in a workshop. In Brooks, W.T., "Proposed Standardized Method for Correlating Subscale Motor Burn Rates," CPIA Publication 300, Vol. II, May 1979, Brimhall's definition was not included in a summary of US methods; in Brooks, W.T., "Workshop Report: Burn Rate Determination Methodology," CPIA Publication 347, Vol. II, October 1981, pp183-191, Brimhall's method was included, dating the definition as about 1980. Brooks referred to "Curve Inflection (Brimhall)," which is a minimum in dp/dt.)

[64] Brooks W.T., "A Method for More Reproducible Burning Rate Determination", Journal of Spacecraft and Rockets, Vol. 7, No. 12, December 1970.

[65] Timnat Y.M., Advanced Chemical Rocket Propulsion. Academic Press, London, UK, 1987.

[66] Hessler R.O. and Glick R.L., "Comparison of Burning Rate Calculation Methods," JANNAF Combustion Meeting, West Palm Beach, FL, USA, 27-31 October 1997.

[67]   Hessler R.O. and Glick R.L., "Behavior of Pressure Derivatives During Burnout of Simulated Rocket Motors," JANNAF Combustion Meeting, West Palm Beach, FL, USA, 27-31 October 1997.

[68] Hessler, R.O. and Glick, R.L., "Consistent Definitions for Burning Rate Measurement in Solid Rocket Motors", Workshop on "Measurement of Thermophysical and Ballistic Properties of Energetic Materials", Politecnico di Milano, MI, Italy, 22-24 June 1998.

[69] Myers, J.W. and Jordan F.W., "Computerized Static Firing Analysis of Batch Check Motor Firings", Atlantic Research Corp. JANNAF Performance Standardization Subcommittee Meeting, 1982.

[70] Watson T.J., Jordan F.W. and Stóckham L.W., "Accurate Burn Rate Determination for Sub-Scale Test Motors", Aerojet, ASRM Division, luka, MS., AIAA 93-2060, Monterey, Ca 1993.

[71] Jordan F.W., Watson T.J. and Stockham L.W., "Propellant Mass Balance Burn Rate and Pressure Exponent", Aerojet ASRM Division, luka, MS, AIAA 93-2062, Monterey, CA, 1993.

[72] Joley, W.H., Hooper, Hilton, P.R. and Bradfield, W.A., "Studies on Coning in End-burning Rocket Motors", AIAA Paper 85-1179.

[73] Gonthier, B. and Tauzia, J.M., "Burning Rate Enhancement Phenomena in End-burning Solid Propellant Grains", AIAA Paper 85-1435.

[74] Friedlander, M.P., Jordan, F.W. and Hazelette, D.F., "Factors Which Affect the Accuracy of Burn Rate Calculation of Batch Check Motor Firings", AIAA Paper 84-1439, June 1984.

[75] Anon., "Ballistic Nomenclature, Rocket Static Tests, " MIL-STD-292C, 24 February 1961.

[76] Anon., "Solid Propulsion Nomenclature Guide," CPIA Publication 80, May 1965.

[77]   Brown, B., Henderson, C.B., and Coughlin, J.P., "Recommended Procedures for the Measurement of Specific Impulse of Solid Propellants," CPIA Publication 174, August 1968.

[78] Brooks, W.T., "Workshop Report: Burn Rate Determination Technology", CPIA Publication 347, October 1981.

[79] Hessler, R.O. and Glick, R.L., "Error Analysis of Burning Rate Measurement Procedures," Memorandum in support of the NATO RTO/AVT WG016, and presented at a Workshop on "Errors and Noise in Energetic Material Combustion Experiments", Politechnico di Milano, Milan Italy, 15-16 March 1999.

[80]   Sutton G.P., Rocket Propulsion Elements. Wiley, New York, NY, USA, 6th edition, 1992.

[81]   Brock, F.H., "Average Burn Rate, Average Pressure Relationships in Solid Rockets," Journal of Spacecraft and Rockets, Vol. 3, Dec. 1966, pp. 1802-1803.

[82]   Glick R.L., "Reduction of Solid Rocket Data when Pressure -Time History is Non-Neutral," Journal of Spacecraft and Rockets, Vol. 12, No. 6, June 1975, pp. 383-384.

[83] Hessler, R.O. and Glick, R.L., "Error Analysis of Burning Rate Measurement Procedures," Memorandum in support of the NATO RTO/AVT WG016, and presented at a Workshop on "Errors and Noise in Energetic Material Combustion Experiments", Politechnico di Milano, Milan Italy, 15-16 March 1999.

[84] Brooks, W.T. and Hermsen, R.W., "A Proposed Standard for Correlating Subscale Motor Burn Rates," JANNAF Performance Standardization Subcommittee, 12th Meeting, Appendix 10, Jan 1979.

[85] Fry, R.S., "Review of Burning Rate Measurement Methods in the US," briefing to the NATO RTO/AVT WG 016 (formerly AGARD/PEP WG 27), October 1995.

[86] Hessler, R.O., "An Analysis of Burning Rate Round Robin Data", JANNAF Combustion Meeting, West Palm Beach, CPIA Pub 662, Vol I, PP 521-526, October 1997.

[87] Hessler, R.O., and Glick, R.L., "A Ballistic Prediction for Burning rate Motors and Non-Instantaneous Burnout," Memorandum in support of NATO RTO/AVT WG 016, October 1998.

[88] DeLuca, L.T., Morandi, C., Ratti, A., Annovazzi, A., Tosti, E., Hessler, R.O., and Glick, R.L., "Burning Rate Data Reduction of Ariane Boosters Small-Scale Test Motors," 2nd European Conference on Launcher Technology, Solid Space Propulsion, Paper XXX, Rome, Italy, 21-24 Nov 2000. Proceedings under press by CNES, France, Sep 2001.

[89] Servieri M., "Sensibilità Termica e Velocità di Combustione Stazionaria di Propellenti Solidi Compositi," M.Sc. Thesis in Aerospace Engineering, Dipartimento di Energetica, Politecnico di Milano, Milan, Italy, February 1999.

[90] Pace F., "Internal Ballistics of Solid Propellant Small-Scale Motors," M.Sc. Thesis in Aerospace Engineering, Dipartimento di Energetica, Politecnico di Milano, Milan, Italy, and TNO Prins Maurits Laboratory February 2000.

[91] Morandi C., "Applicazione del Metodo HG alla Riduzione Dati Balistici di Motori Reali," M.Sc. Thesis in Aerospace Engineering, Dipartimento di Energetica, Politecnico di Milano, Milan, Italy, Dec 2000.

[92] De Nigris A., "Metodi di Riduzione Dati Balistici da Motori a Razzo in Scala Ridotta," M.Sc. Thesis in Aerospace Engineering, Dipartimento di Energetica, Politecnico di Milano, Milan, Italy, February 2000.

[93] Ratti A., "Metodi di Riduzione Dati Balistici per i Boosters a Propellente Solido di Ariane-4 e di Ariane-5," M.Sc. Thesis in Aerospace Engineering, Dipartimento di Energetica, Politecnico di Milano, Milan, Italy, April 2000.

[94] DeLuca, L.T., DeNigris, A., Morandi, C., Pace, F., Ratti, A., Servieri, M., Annovazzi, A., Tosti, E., Hessler, R.O., and Glick, R.L., "Burning Rate Data Reduction from Small-Scale Test Motors, 5-ISICP Proceedings on Combustion of Energetic Materials," Paper 045-6-OP-CM, Stresa, Italy, 18-22 Jun 00. Proceedings edited by K.K. Kuo and L.T. DeLuca, under press by Begell-House, NY, Aug 2001.

[95] Savitzky G. and Golay M.J.E., Smoothing and Differentiation of Data by Simplified Least Square Procedures, Analytical Chemistry, Vol. 36, pp. 1627-1639, 1964.

[96] Hessler R.O. and Glick R.L., "Consistent Definition for Burning Rate Measurement in Solid Rocket Motors," FGV Fizika Goreniya i Vzryva, Special Issue, Vol. 36, No. 1, Jan-Feb 2000. Presented at the Workshop on "Errors and Noise in Energetic Material Combustion Experiments", Politecnico di Milano, Milan, Italy, 15-16 March 1999.

[97] Hessler, R.O., Glick, R.L., and DeLuca, L.T., "Passive Diagnostics of Dynamic Combustion Phenomena," European Office of Aerospace Research and Development, Air Force Office of Scientific Research, Air Force Research Laboratory, under Contract No. F61775-99-WE082, Quarterly Progress Report, August 2001.

[98] Gadiot, G., Memorandum to R. Fry, NATO RTO AVT WG 016, 28 October 2000.

[99] Hessler, R.O., and Glick, R.L., "Comments on Burning Rate Measurement in Rocket Motors," Memorandum to RTO/AVT WG016, Dec. 1997.

[100] Hessler, R. O., "Studies of Motor Instability Problems," CPIA Pub 308, Vol II, Dec 1979.

[101] Culick, F.E.C., "Acoustic Oscillations in Solid Propellant Rocket Chambers," Astronautica Acta, 12, 2, pp. 113-126, 1966.

124

[102] Deur, J.M. and Hessler, R.O., "Forced Oscillation Theory," AIAA-84-1356, Cincinnati, OH, July 1984.

[103] Hessler, R.O., "Passive Linear Stability Measurements," JANNAF Combustion Meeting, West Palm Beach, FL, October 1997.

[104] Hessler, R.O., Glick, R.L, Bertelé, R., Cedro, D., Fiorentino, G., and DeLuca, L.T., "Frequency Response of a Model Subscale Rocket Motor," Fifth International Symposium on Special Topics in Chemical Propulsion (5-ISICP), Stresa, Italy, June 2000.

[105] Anon., "JANNAF Rocket Engine Performance Test Data Acquisition and Interpretation Manual," CPIA Pub 245, April 1975.

[106] Abernethy, R.B. and Colbert, D.L., "ICRPG Handbook for Estimating the Uncertainty in Measurements Made with Liquid Propellant Rocket Engine Systems," CPIA Pub 180, April 1969.

[107] Abernathy, R.B. and Thompson, J.W., "Handbook – Uncertainty in Gas Turbine Measurements," ADEC-TR-73-5, February 1973.

APPENDIX A

NATO PROPULSION INDUSTRY CONTRIBUTORS

COUNTRY	FACILITY	REPRESENTATIVE(S)
CANADA	DEFENSE RESEARCH ESTABLISHMENT VALCARTIER (DREV)	R.A. Stowe
FRANCE	SNPE	R. Couturier[1], D. Ribereau[1], V. Bodard1
	ONERA	J-P Reynard[1], J-C Traineau[1]
GERMANY	BAYERN-CHEMIE GmbH	R.A.H.Strecker[1], H.L.Besser[1]
	DYNAMIT NOBEL	R. Mackowiak
	WIWEB (formerly BICT)	Nicklas
ITALY	FIAT AVIO / BPD	L. DeLuca[1], R. DeAmicis, A. Annovazzi
	POLITECNICO di MILANO	A. DeNigris, C. Morandi, F. Pace, A. Ratti, M. Servieri
	CNR – TeMPE	U. Carretta
NETHERLANDS	TNO PML	G.Gadiot[1]
NORWAY	NORDIC AMMUNITION COMPANY	St. Haugen
SPAIN	INSTITUTO NACIONAL DE TECNICA AEROSPACIAL (INTA)	M. Mulero
UNITED KINGDOM	ROYAL ORDNANCE	A. Whitehouse[1]
UNITED STATES	AEROJET SACRAMENTO OPERATIONS	M. Eagar, K. Smith, D. Eckley
	AIR FORCE RESEARCH LAB (AFRL) PHILLIPS LABORATORY	C. Merrill
	ALLIANT TECH SYSTEMS	M. Harsh, C. Shanholtz
	AMCOM / STONE ENGINEERING	M. Lyon, S. Mustaikis II
	ATLANTIC RESEARCH CORPORATION	B. Waltz, P. Graham, K. Graham, N. Rotchford
	JOHNS HOPKINS UNIV / CPIA	R. Fry[1](Chairman)
	BF GOODRICH / UNIVERSAL PROPULSION COMPANY	H. McSpadden
	CONSULTANTS	R. Glick, R. Hessler
	GD / ARMAMENT SYSTEMS / PCRL	N. Messina
	GD / ORDNANCE & TACTICAL SYSTEMS	J. McAvinew
	NAVAL AIR WARFARE CTR / WPNS DIV CHINA LAKE, CA	J. Hitner
	NAVAL SURFACE WARFARE CENTER INDIAN HEAD, MD	S. Craven
	PENN STATE UNIV/ DEPT MECH ENGIN	K. Kuo
	PRATT & WHITNEY CHEMICAL SYSTEMS DIVISION	R. Hammond, G. Jensen, M.Emanual, G. Hawkins
	SNAP TECHNOLOGY	F. Jordan, N. Trudell
	THIOKOL PROPULSION	K. Wanlass, J. Furfaro, S. Palopoli, J. Edwards, A. Neunzert
	TALLEY DEFENSE SYSTEMS	F. Davis
	UNIV ALABAMA / HUNTSVILLE	R. Frederick[1]

---

[1] NATO RTO AVT WG 016 Member

A-3

APPENDIX B

Burning Rate Measurement Analysis Methods

INTERNATIONAL SURVEY

APPENDIX B
Burning Rate Measurement Analysis Methods
International Survey

TABLE OF CONTENTS

Appendices B-1 through B-27 provide details of the data analysis methods surveyed. A brief summary of some of the methods was provided in Sections 3 and 4. Table 9 of Section 5 lists those methods applied to the Round Robin exercises.

---

[1] Methods Defined in Reference Category, Fundamental Methods

APPENDIX B-1: CANADA

DEFENSE RESEARCH ESTABLISHMENT VALCARTIER (DREV)

Introduction

The method for analyzing 2 x 4 inch small scale rocket motor tests at the Defence Research Establishment Valcartier (DREV) is described below. DREV uses the fundamental thickness/time burning rate (r_{TOT}) procedure for calculating solid propellant burning rates. A more detailed description is given elsewhere.[2]
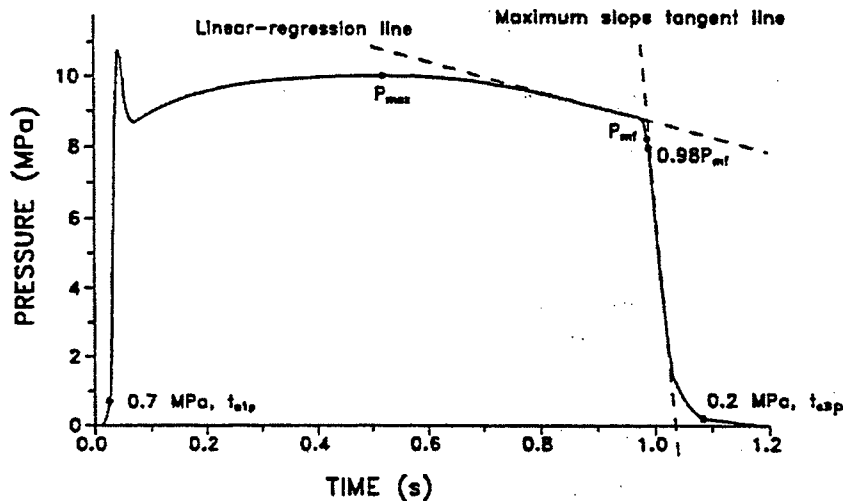
Fig. B-1 Typical 2 x 4 Inch Pressure-Time Profile

Definitions

A_t	Nozzle throat area, defined by Eq. 1.8
b	Related to end of burning time
c^*	Characteristic velocity, defined by Eq. 1.9
d_{ti}	Initial throat diameter
d_{tf}	Final throat diameter
D_i	Initial grain diameter
D_f	Final grain diameter
w	Grain web
L	Grain length
P	Pressure
P_{avg}	Average pressure, defined by Eq. 1.1
P_{max}	Maximum pressure
P_{mf}	Burnout pressure, defined at the intersection of the linear regression line and the maximum slope tangent line
r	Burning rate, defined by Eq. 1.6
r_{avg}	Average burning rate, defined by Eq. 1.7
t_{a1p}	Ignition time, defined as 0.7 MPa as in Fig. B-1
t_{a3f}	End of action time tailoff, defined as 0.2 MPa as in Fig. B-1
t_b	Burning time, defined as the difference between the times at 0.98 P_{mf} and t_{a1p}
t_{max}	Time at maximum pressure
ΔM_p	Propellant mass burned, difference between before and after firing propellant mass

---

[2] Stowe, R., "Strand Burning Rates of Solid Rocket Propellants", Defence Research Establishment Valcartier, Report DREV R-4675/92, June 1992.

φ Propellant mass fraction burned, defined by Eq. 1.2
ρ Propellant density

Description of the Method

The data reduction of a 2 x 4 Inch motor firing at the Defence Research Establishment Valcartier (DREV) in Canada is based upon two pressure-time curves from pressure transducers normally sampled at 1 kHz. The data is processed in a computer program to yield an estimate for the average burning rate at a particular pressure. The two pressure readings are averaged and the resulting pressure-time profile is fitted with several "characteristic" parameters such as burn times, maximum and average pressure, etc. Figure B.1 shows these parameters for a typical 2 x 4 inch rocket motor firing.

The first point chosen are the time t_{a1p} at the point during ignition when the pressure reaches 0.7 MPa, the time t_{a3p} at the point during tailoff when the pressure drops to 0.2 MPa and the time t_{max}, located on the last two thirds of the data (avoiding the ignition peak), where the pressure is a maximum (P_{max}). The program then starts at the bottom of the tailoff and searches backwards along the curve where the slope is less than 0.25 P_{max} / t_{max}. When this point is found, the program finds the maximum slope tangent line to the right (the tailoff) and then calculates a linear-regression line through the latter half of the profile to the left of the point. No point used to calculate this linear-regression line can lie more than a certain amount from it; if any point does, points on the left end of the line are dropped from the calculation until the criteria are satisfied. The intersection of the linear regression line and the maximum slope tangent line is directly above the point on the curve that determines P_{mf}. The time t_{mf} is the difference between the times at P_{mf} and t_{a1p}. The burning time t_b is defined as the difference between the times at 0.98. P_{mf} and t_{a1p}. The average pressure P_{avg} is:

$$P_{avg} = \frac{\int_0^b p.dt}{t_b} \qquad \qquad 1.1$$

After the characterization of the pressure-time profile, the amount of propellant consumed versus time is determined. It is assumed that the mass fraction of propellant burned (φ) can be calculated from the pressure-time profile:

$$\varphi = \frac{\int_0^t A_t.p.dt}{\int_0^{t_{a3p}} A_t.p.dt} \qquad \qquad 1.2$$

The mass of propellant consumed as a function of time can be calculated from the experimental measurements of φ and ΔMp, the difference between the before- and after-firing masses of the motor. The amount the propellant burned for a web thickness (w) can then be found from:

$$\varphi.\Delta M_p = \frac{\pi}{4}(D_f^2 - D_i^2).L.\rho - \frac{\pi}{4}(D_f^2 - (D_i + 2w)^2)(L - 2w).\rho \qquad 1.3$$

where D_i is the initial grain diameter, D_f the final grain diameter and L the grain length. Last equation is differentiated with respect to time, the only function of time being φ and l:

$$\frac{d\varphi}{dt}.\Delta M_p = \frac{\pi.\rho}{2}(D_f^2 - D_i^2 + 2.D_i.L - 8.D_i w + 4.L.w - 12.w^2).\frac{dw}{dt} \qquad 1.4$$

Equation (1.2) can also be differentiated to give:

$$\frac{d\varphi}{dt} = \frac{A_t \cdot p}{\int_0^{a3p} A_t \cdot p \cdot dt} \qquad \text{1.5}$$

Rearranging Eqs. (1.4) and (1.5) and defining the burning rate r as dw/dt gives:

$$r = \frac{dw}{dt} = \frac{A_t \cdot p}{\int_0^{a3p} A_t \cdot p \cdot dt}\left(\frac{2 \cdot \Delta M_p}{\pi \cdot \rho}\right)\frac{1}{\left(D_f^2 - D_i^2 + 2 \cdot D_i \cdot L - 8 \cdot D_i \cdot w + 4 \cdot L \cdot w - 12 \cdot w^2\right)} \qquad \text{1.6}$$

The average burning rate r_{avg} for a 2 x 4 Inch motor is then:

$$r_{avg} = \frac{\int_0^b r \cdot dt}{t_b} = \frac{w_{t_b}}{t_b} \qquad \text{1.7}$$

Nozzle erosion (or growth due to chemical reaction or an accumulation of residue) is also taken into account during the calculations. The throat area A_t is estimated by:

$$A_t = \frac{\pi}{4}\left(d_{t_i} + (d_{t_f} - d_{t_i})\frac{\int_0^t p \cdot dt}{\int_0^{a3p} p \cdot dt}\right)^2 \qquad \text{1.8}$$

c* can be calculated from:

$$c^* = \frac{1}{\Delta M_p}\int_0^{a3p} A_t \cdot p \cdot dt \qquad \text{1.9}$$

Once the average burning rate at each pressure is known, a linear-regression analysis identical to that for strands is performed to yield the burning-rate law.

Comments

At DREV, four motors are usually fired to characterize the propellant, this being a balance between accuracy and effort (cost).

APPENDIX B-2: FRANCE
SNPE / ONERA

Introduction

SNPE and ONERA both use an iterated thickness/time burning rate (r_{TOTn}) procedure for calculating solid propellant burning rates. The SNPE/ONERA methods provide accuracy resembling a mass balance burning rate (r_{MB}) procedure for by virtue of the method used to define end of burn and account for the pressure tailoff. SNPE base their data reduction on absolute pressure, while ONERA commonly uses relative pressure levels.
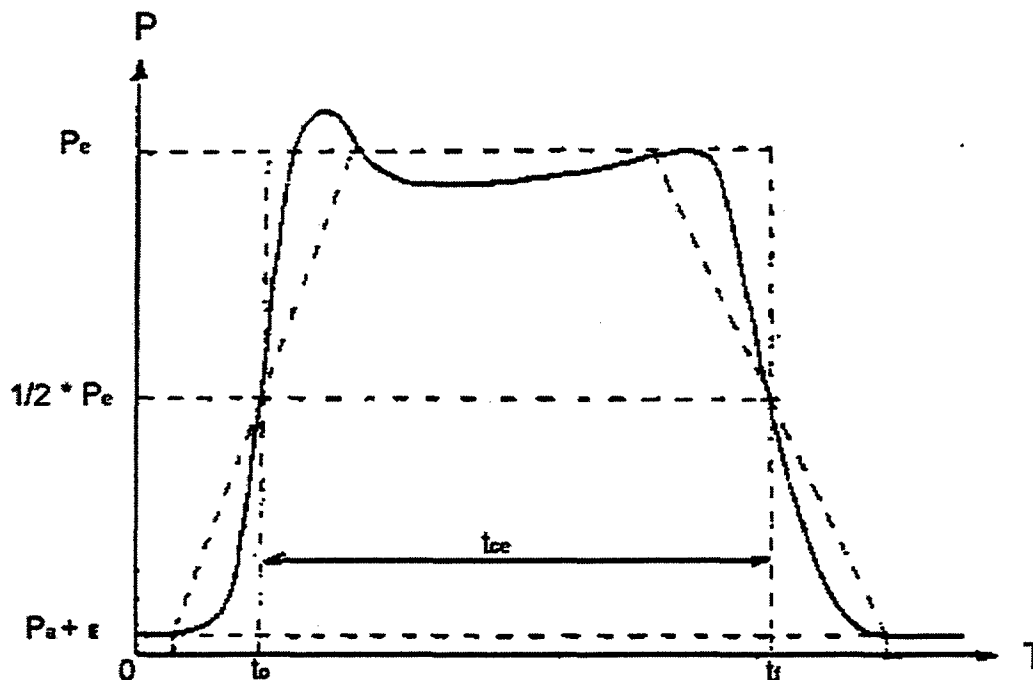
Fig. B-2 French Iterative Method

Definitions

P_a Atmospheric pressure
ε 1% of the range of the pressure sensor (13 - 22 MPa)
t_o First time point when p > Pa + ε on last sustained rise
t_f First time point when p < Pa + ε on final decline
I_{pt} Integral over time interval t_{ce} of combustion pressure
P_e Average effective pressure, defined by iteration below
r_{ave} Average burning rate
Se the effective surface area
$S(e)$ the combustion surface area
t_{ce} Calculated duration of combustion; period during which the combustion pressure is above the average effective pressure. The value is obtained via iteration on P_e starting from I_{pt}.
w_b effective burned grain web

Description of the Method (Note: All pressures are given in absolute values.)

Summary of the iterative method (Step 1 through 5):

1. $P_e (0) = (P_a + \varepsilon) + (I_{pt} - (t_f - t_0).(P_a + \varepsilon))/(t_f - t_0)$

2. $t_{ce} (0) = (I_{pt} - (t_f - t_0).(P_a + \varepsilon))/(P_e - P_a - \varepsilon)$

3. $P_e (1) = (P_a + \varepsilon) + (I_{pt} - (t_f - t_0).(P_a + \varepsilon))/t_{ce}(0)$

4. $P_e (1)$ is compared to $P_e (0)$. When the difference is more than 1 %, step 2 is repeated yielding $t_{ce} (1)$. This process is repeated until $| P_e (n+1) - P_e (n) | < 1$ %.

5. $r_{ave} = w_b/ t_{ce}$

The effectively burned web (w_b) is the web for a CP grain and is for a star grain described by:

$$w_b = \int_0^{ef} S(e).de/ Se \qquad \qquad 2.1$$

Comments

The method is an iterated thickness/time method whose accuracy resembles a mass balance method. When Steps (2) and (5) are combined they give

$$r_{ave} = \frac{w_b \cdot p_e}{I_{pt}} \qquad \qquad 2.2$$

This resembles Equation 9.10 of the common Brooks mass balance method described in APPENDIX B-9. The iteration procedure SNPE/ONERA method is only to define the time points and does not include determination of the pressure exponent.

APPENDIX B-3: GERMANY
BAYERN-CHEMIE GmbH

Introduction

Bayern Chemie in Germany uses a fundamental thickness/time burning rate (r_{TOT}) procedure for calculating solid propellant burning rates.
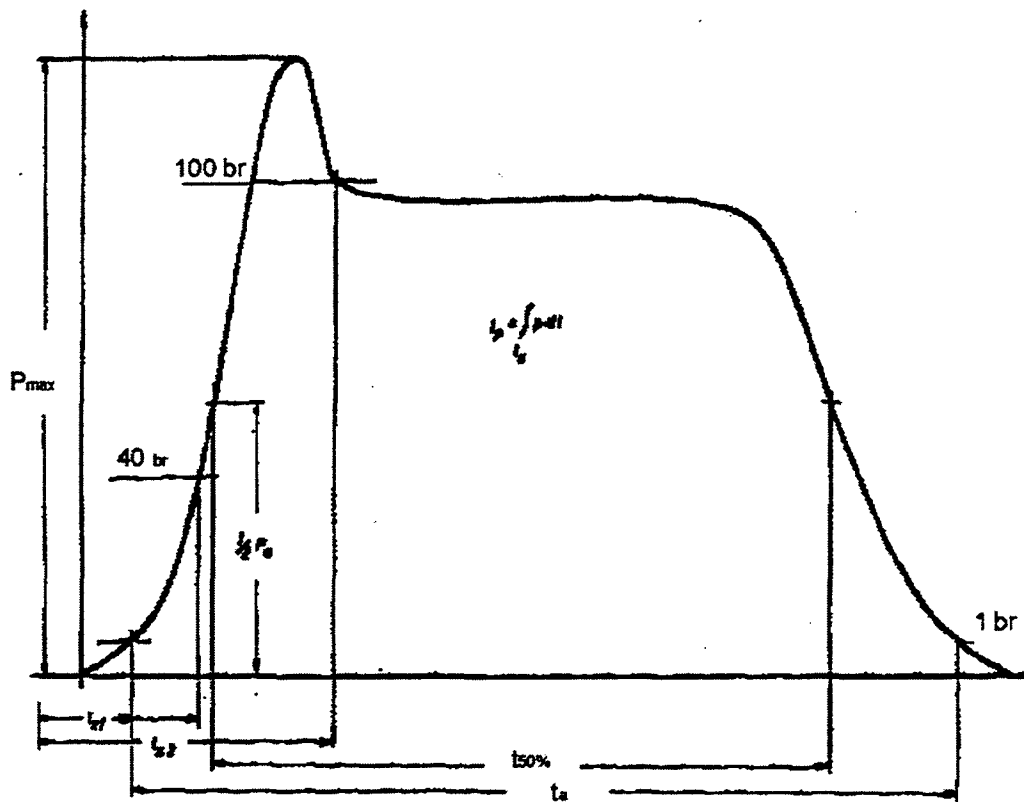
Fig. B-3 Method Employed at Bayern Chemie

Definitions

P_a average chamber pressure for interval t_a
$P_{50\%}$ time-averaged chamber pressure for interval $t_{50\%}$
t_a time between threshold pressure values (e.g. 0.7 MPa)
$t_{50\%}$ time between 50 % of P_a
$r_{50\%}$ average burning rate for interval $t_{50\%}$
w_b web thickness

$$r_{50\%} = \frac{w_b}{t_{50\%}} \qquad 3.1$$

$$p_a = \frac{1}{t_a} \cdot \int_{t_a} p_c \cdot dt \qquad 3.2$$

$$p_{50\%} = \frac{1}{t_{50\%}} \cdot \int_{t_{50\%}} p_c \cdot dt \qquad 3.3$$

Description of the Method

The following steps 1 through 5 summarize the method:

1. Determine t_a based on threshold pressure value; e.g. 0.7 MPa
2. Calculate P_a based on t_a (total integral)
3. Determine $t_{50\%}$ based on 50% P_a value
4. Calculate $r_{50\%}$
5. Calculate $P_{50\%}$

Comments

The Bayern Chemie method is clearly a thickness/time rate definition. However, a 50-50 definition for time points yields nearly the same result as produced by the assumption in mass balance that burning continues until final zero return (and began at first rise). Consequently, this method may be expected to yield almost the same rate as mass balance definitions used. In short, a 50-50 burning time definition compensates to some extent for non-instantaneous burnout, but not as well as a mass balance definition that actually uses the integral ratio.

The drawback to a 50-50 definition is that the time-averaged pressure differs much more from the rate-averaged pressure because the ending points are much lower down the tailoff curve than for an equilibrium or web-knee definition. More bias in burning rate is introduced, as the rate-averaged pressure is seldom used.

Introduction

FIAT AVIO uses two methods, which are both derivatives of an iterated thickness/time burning rate (r_{TOTn}) procedure for calculating solid propellant burning rates. Method 1 is the official method used at FIAT for Ariane 4 and 5 boosters. FIAT also uses a second method (Method 2) virtually identical to that used by SNPE and ONERA as described in APPENDIX B-2. The Italian methods provide accuracy resembling a mass balance burning rate (r_{MB}) procedure for calculating solid propellant burning rates.

Definitions for Method 1
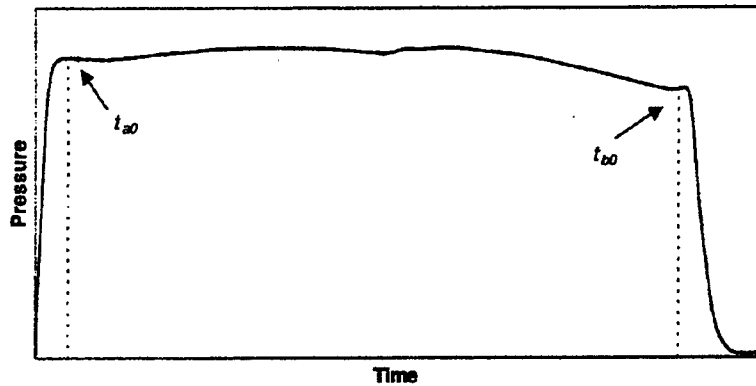
Figure B-4 Definitions FIAT AVIO Method 1

I_p integral over time of combustion pressure, $I_p = \int\limits_{t1}^{t2} P dt$

P_e average effective pressure

t_{a0} initial estimate of start of burning, a time point chosen at the beginning of steady pressure phase

t_{b0} initial estimate of end of burning, a time point chosen at the end of steady pressure phase

t_e effective burning time, determined by iteration described below

P_m average combustion pressure, $P_m = \dfrac{I_p}{\Delta t}$

r_b grain burning rate

w_b nominal grain web

Description of Method 1 (Note: all pressures are given in absolute values.)

Summary of the iterative method (Steps 1 through 8)

1) Estimate of pressure integral, $I_{p1} = \int\limits_{ta0}^{tbo} P dt$

2) Estimate of average combustion pressure, $P_{m1} = \dfrac{I_{p1}}{(t_{b0} - t_{a0})}$

3) Determine new start and stop times, t_{a1} and t_{b1} on pressure rise and decline, corresponding to $P_{m1}/2$

4) Corrected pressure integral, $I_{p2} = \int_{ta1}^{tb1} P\,dt$

5) Corrected average combustion pressure, $P_{m2} = \dfrac{I_{p2}}{(t_{b1} - t_{a1})}$

6) If $|P_{m2} - P_{m1}| < 0.002$ then $P_e = P_{m2}$ and $t_e = \dfrac{I_{p2}}{P_e}$

7) If $|P_{m2} - P_{m1}| > 0.002$ repeat step 3) to 6) with new P_m

8) $r_b = \dfrac{w_b}{t_e}$

Definitions for Method 2
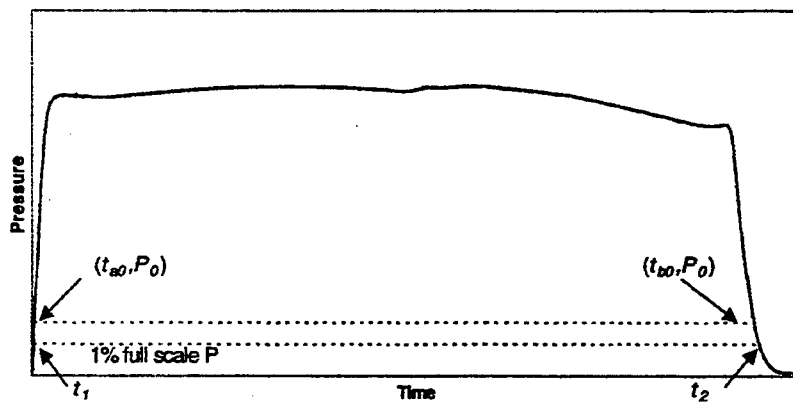
Figure B-5 Definitions FIAT AVIO Method 2

P_a Atmospheric pressure
ε 1% of the full scale range of the pressure transducer (13 - 22 MPa)
t_1 First time point when $P > P_a + \varepsilon$ on last sustained rise, neglecting the ignition peak
t_2 First time point when $P < P_a + \varepsilon$ on final decline
I_p Integral over time interval t_e of combustion pressure
P_e Average effective pressure, defined by iteration below
t_e Calculated duration of combustion. Period during which the combustion pressure is above the average effective pressure. The value is obtained via iteration on P_e starting from I_p
r_b grain burning rate
w_b nominal grain web

Description of Method 2 (Note: all pressures are given in absolute values)

Summary of the iterative method (Steps 1 through 8)

1) $I_p = \int_{t1}^{t2} P\,dt$

2) Considering the point (t_2, P_2), take the first point (t_{b0}, P_0) where P_0 is higher than P_2
   On the pressure rise take the point (t_{a0}, P_0)

3) $I_{p0} = 2P_0(t_{b0} - t_{a0})$

4) If $I_{p0} < I_p$ then take another point (t_{b1}, P_1) on the pressure decline above the point (t_{b0}, P_0) and the corresponding point (t_{a1}, P_1). Repeat step 2 and 3;

5) If at nth-step $I_{pn} = 2P_n(t_{bn} - t_{an}) > I_p$ take I_{pn} and I_{pn-1}

$\Delta t_n = (t_{bn} - t_{an})$
$\Delta t_{n-1} = (t_{bn-1} - t_{an-1})$

6) Calculate the straight line passing through the points $(I_{pn}, \Delta t_n)$, $(\Delta t_{n-1}, I_{pn-1})$. Corresponding to I_p evaluate t_e

$$t_e = \Delta t_{n-1} - \frac{(\Delta t_n - \Delta t_{n-1})}{(I_{pn} - I_{pn-1})} * (I_{pn-1} - I_p)$$

7) $P_e = \dfrac{I_p}{t_e}$

8) $r_b = \dfrac{w_b}{t_e}$

Comments

Politecnico di Milano is examining various additional methods including a basic mass balance after US / NSWC, and an iterated two-point thickness/time after US / Hessler-Glick. FIAT AVIO's Method 2 is virtually identical to that used by SNPE and ONERA, which is described in APPENDIX B-2. The iteration procedure of FIAT AVIO Method 2 method is only to define the time points and does not include determination of the pressure exponent.

APPENDIX B-5: NETHERLANDS
TNO-Prims Maurits Laboratory (PML)

Introduction

TNO-PML has two methods available for data reduction of small scale rocket motor firings. Both TNO-PML methods use the fundamental thickness/time burning rate (r_{TOT}) procedure with different burning time definitions for calculating solid propellant burning rates. Method I is a conventional quite straight-forward method, while method II was developed in the late 1980's.
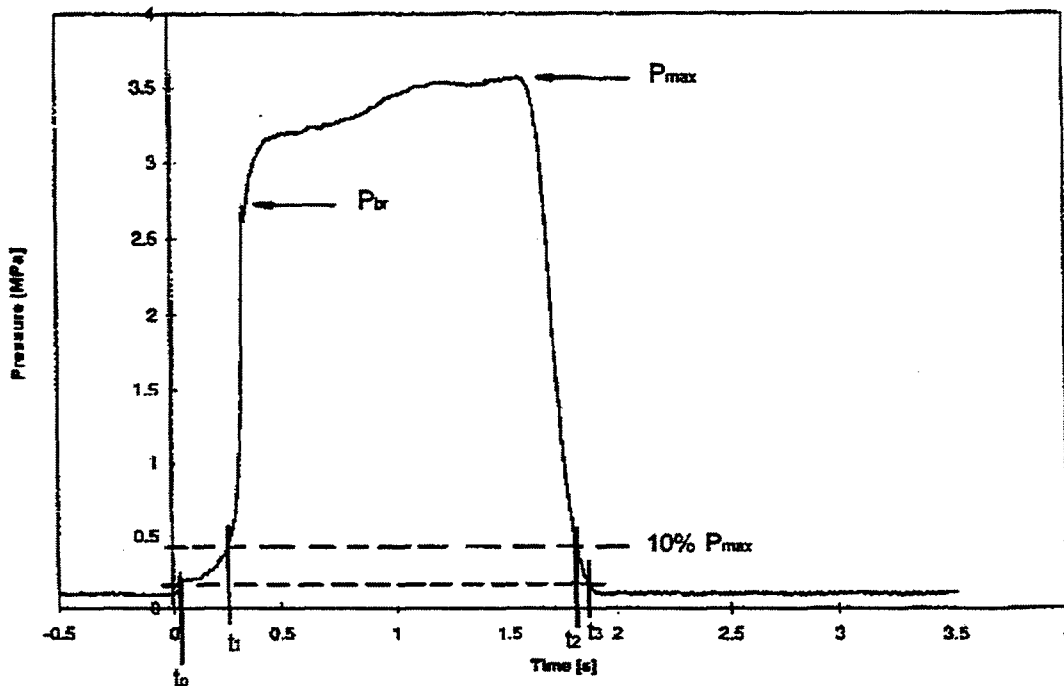
Fig. B-6 Definitions TNO Method I

Definitions Method I

P_{br} the pressure at which the rupture disk opens. The rupture disk is employed to pre-tune the pressure during a test. A thin stainless steel disk is positioned after the nozzle. It ruptures when the chamber pressure reaches a certain value. This value is chosen to correspond to the pressure expected during the test

P_{max} the maximum combustion pressure occurring during a test, excluding P_{br}

t_0 the time point immediately after initiation where the pressure has reached 1% of P_{max}

t_1 the time point immediately after initiation where the pressure has reached 10% of P_{max}

t_2 the time point after P_{max}, where the pressure has reduced to 10% of P_{max}

t_3 the time point at the end of the test where the pressure has decreased to 1% of P_{max}

w_b web thickness

Description of Method I

The average burning rate is defined as

$$r_{aver} = \frac{w_b}{t_2 - t_1}$$

5.1

B-14

P_c is the average combustion pressure, given by

$$P_c = \frac{\int_{t1}^{t2} p.dt}{t_2 - t_1}$$ 5.2

The integration of the digitized data is carried out according to trapezium rule. The average pressure is used in the burning rate vs. pressure plot. A number of measurements (i.e., one propellant, one temperature) are then used to determine the coefficients of Vieille's relation ($r = a P_c^n$). Vieille's relation is determined using least-squares method.
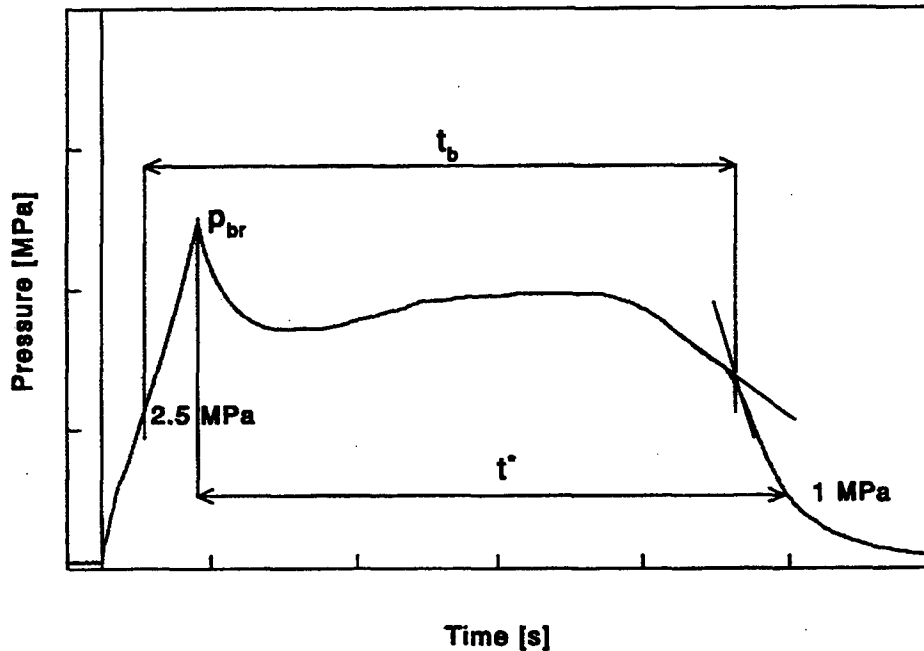
Fig. B-7 Definitions TNO Method II

<u>**Definitions Method II**</u>

P_{br} as in method I

P_c the average combustion pressure determined over t_b

$t_{2.5}$ the time point immediately after ignition where the combustion pressure has reached 2.5 MPa

t_e t_e is the time point at the end of burning as determined by a modified tangent bisector method. The method is different from the tangent bisector method commonly employed and is described in Fig. B-6

t_b ($t_e - t_{2.5}$) is the time period between the moment immediately after ignition where the combustion reaches 2.5 MPa and the end of burning. End of burning is determined by a vertical tangent method (compare Fig. B-7)

w_b web thickness

<u>**Description of Method II**</u>

The average burning rate is defined as

$$r_{aver} = \frac{w_b}{t_b}$$ 5.3

P_c is the average combustion pressure, determined over the period t_b. It follows from

$$P_c = \frac{\int_{t2.5}^{te} Pc.dt}{t_b} \qquad 5.4$$

Comments

Tests are commonly conducted with end-burning propellant disks that yield relatively flat pressure traces. However, in particular when inhibitors used to assure one-dimensional burning are applied by hand (only for cases where the propellant cannot be cast, e.g. when it is machined from a block of propellant or when it is cast), deviations from this expected behavior can occur. The time points and burning time are determined using an in house software package.

Measurement System Details
The basic information on the data acquisition system used is presented in Table B-1. The two pressures are measured in order to verify immediately after each test if the pressure measurements are reliable, e.g. by plotting the two results in one figure.

Table B-1 Some Characteristics of the Data Acquisition System

Pressure sensor	Kistler 701A piezo electric Range: 0 – 25 MPa Linearity: < 0.5 % FSO Natural frequency: □70□kHz
Amplifier	Kistler 5011 Linearity: < 0.05 %
Data acquisition	Keithley A/D converter Conversion frequency (12 bits): 500 Hz

Introduction

The RORM method uses the fundamental thickness/time burning rate (r_{TOT}) procedure for calculating solid propellant burning rates.

Definitions

r_b	Burning rate
$S(x)$	Burning surface at web x
A_t	Throat area
V_0	Initial propellant volume
P	Motor Pressure
P_{max}	Maximum pressure
P_b	Pressure at burnout
t_0	Start of motor burn, typically time at 10% P_{max}
t_b	Burning time, defined by tangent-bisector method
t_a	Action time, typically time at 10% P_b

Description of Method

1) Expected form of pressure curve for Slab and Disc Analysis (Hardware described in APPENDIX A)
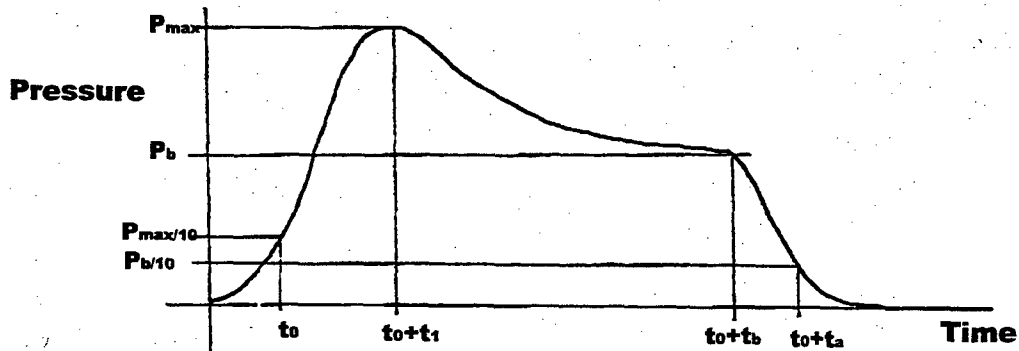
Figure B-8 Expected Form of Pressure Curve for RORM Method

Time (t_0 + t_b) and pressure P_b at burnout are determined manually using intersecting Tangent-Bisector method. Analysis software determines the burning start time (t_0).

2) Throat Area Variation

Initial and final throat diameters are measured and input as data. Throat erosion is assumed linear with time.

3) Calculation of Burning Rate

Integrations are performed for 505 equally spaced time values from (t_0) to (t_0 + t_b)

$$r_b S(x) = \frac{A_t P(t_0 + t)}{\int_{t_0}^{(t_0 + t_b)} A_t P \, d_t} V_0$$

6.1

S(x) is determined from propellant geometry, this may be either a slab or disc, while *P(t₀+t)* is read from recorded data.

Graphs of burn rate against pressure and restriction ratio (burning surface area/throat area) are displayed on log-log paper.

4) C* Determination

$$\overline{A_t} = (A_i + A_f)/2 \qquad\qquad 6.2$$

$$\overline{P} = \frac{1}{t_0} \int_{t_0}^{t_0+t_a} P\, dt \qquad\qquad 6.3$$

$$C^* = (\overline{A_t}\,\overline{P}\, t_a)/M \qquad\qquad 6.4$$

APPENDIX B-7: UNITED STATES
AEROJET

Introduction

Aerojet uses the fundamental thickness/time burning rate (r_{TOT}) procedure for calculating solid propellant burning rates.

Definitions and Description

Ignition Delay: Nominally the time between fire switch signal or igniter pressurization and grain ignition, typically at 100 psi

Burning Time: Time interval used for determination of burn time depends on the customer's requirement. Normally, 10% P_{max} is used to identify the start of burning and the method of tangent-bisector is used to define the end of burning.

Burning Rate: Definition of average burn rate is r_{TOT}, or web thickness / burn time (web is a pre-test measurement, and burn time is calculated as above)

Average Burning Pressure: Definition of average burning pressure is the mathematical average of all pressure data points between start and stop of burn

Burning Rate Relation: Vieille relation is used, $r_b = aP^n$

Comments

1. Additional pressures evaluated on the pressure vs. time trace: igniter chamber pressure, and maximum pressure

2. C* calculations are not routinely calculated by the Burning Rate Laboratory but the integral is taken from the times listed above (used for average pressure). $C^* = \int P dt \, A_t \, g_o / W_p$, where W_p=weight of propellant.

3. Temperature sensitivity, $\pi_k = 100 \ln (P_2/P_1)/(T_2-T_1)$, with units of % / °F.

APPENDIX B-8: UNITED STATES
AIR FORCE RESEARCH LAB (AFRL), PROPULSION DIRECTORATE
EDWARDS AFB, CA

Introduction

The AFRL, Phillips Lab burning rate analysis approach uses the fundamental thickness/time burning rate (r_{TOT}) procedure for calculating solid propellant burning rates. This procedure is applied primarily to the 2-inch x 4-inch small motor test hardware.

Definitions

P_c Average combustion pressure of the motor

P_{max} Maximum measured pressure of the motor

t_1 Start of motor burning time, defined as time when 60% P_{max} is attained on the initial pressure rise

t_2 End of motor burning time, defined as time when 60% P_{max} is attained on the pressure decay

t_b Motor burning time, defined as ($t_2 - t_1$)

w_b Nominal web thickness burned

κ_n Ratio of propellant grain port to nozzle throat cross-section areas

Description of Method

Near the middle of the burn rate data a particular motor firing the highest motor pressure is noted. If peak motor pressure is not near the middle of the burn rate data array, the motor firing is abnormal and should either be thrown out or crudely analyzed to get an approximate burn rate at a roughly determined pressure.

Start of motor burning time, t_1, and end of motor burning time, t_2, are determined as defined above.

Burning time for the 2x4 motor is determined as

$$t_b = (t_2 - t_1) \qquad\qquad 8.1$$

Burning rate for a particular 2 by 4 motor firing is derived as the result of dividing propellant grain web thickness (typically 6.4 mm (0.25 inch)) by the motor action time.

$$r_b = w_b / t_b \qquad\qquad 8.2$$

The average combustion pressure of the motor for this burning rate is given by

$$P_c = \frac{\int_{t1}^{t2} p.dt}{t_2 - t_1} \qquad\qquad 8.3 \quad \centerdot$$

The Vieille's burning rate versus pressure law is used $r_b = a\,P^n$ to report the burning rate data. Similar treatment can provide an equation of the same form relating κ_n and motor pressure from a log-log plot of κ_n versus pressure.

Comments

This method of determining 2 x 4 motor burning rate came by trial and error comparisons over the years with burning rate data from a similarly configured, but larger test motors with 34.1 kg (75 pound) propellant grains. More elaborate data reduction methods for determining 2 x 4 motor data points have been examined, but little improvement was found in burning rate comparisons with the larger 34.1 kg (75 pound) motor firings using the same propellants. Burning rate values at different

pressures, obtained when a range of nozzle sizes are employed, can be plotted by computer routine or manually and burning rate pressure exponent determined from the slope of a log-log burning rate-pressure plot.

Introduction

Alliant Tech Systems uses the common and improved mass balance (r_{MB}) Brooks Methods[3] developed by Ted Brooks during his tenure at Alliant (formerly Hercules) for calculating solid propellant burning rates.

Definitions and Description of Method

$$t2 = \frac{\int_{0}^{t} Pc\ dt}{\int_{t1}^{tb} Pc\ dt} * (t_b - t_1) * \alpha_p$$

- ❏ Assumes 1st point lit is 1st to burn out
- ❏ Tail-off integral 4-10 times ignition intergral
- ❏ Does not account for sliver/web relation

Tail-off Integral (sliver)

10% Pmax

Pressure

Burn Time

0 t1   tb t2   t
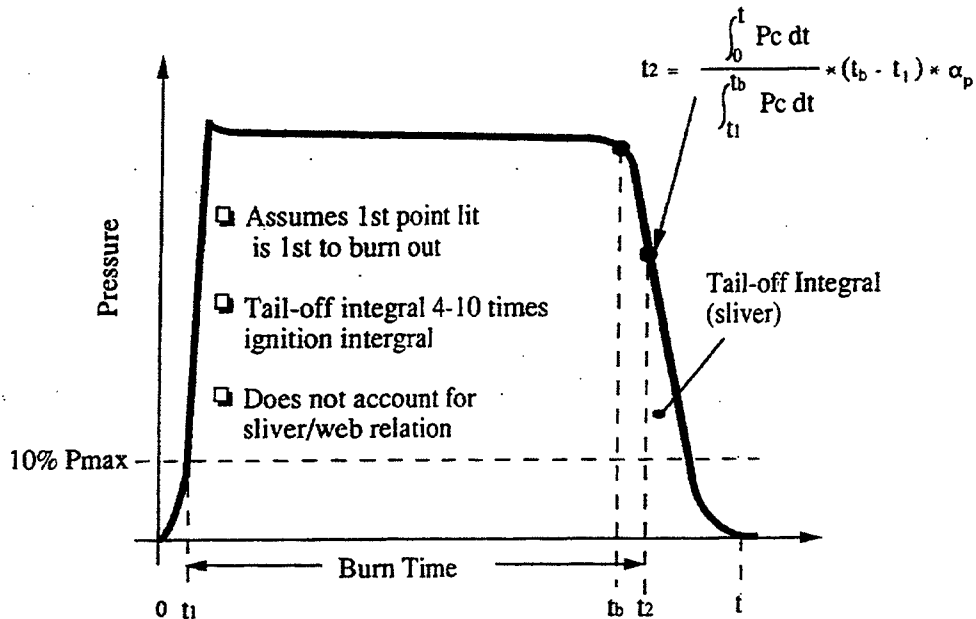
Figure B-9 Definitions of the Brooks Method

Burning Time Determination

For the Brooks' method (Figure B-9), the start of burning (t_1) is taken at the first 10% P_{max} point. The end of burning is determined from the integral presented in Equation 9.2. The uncorrected end of burning is determined in a similar way as the Tangent-Bisector or Brimhall's method and excludes the tail-off integral. The end of burning point (t_2) is a correction of the point determined with the Tangent-Bisector method (t_b). This correction uses the total pressure integral and a correction term α_p. The term α_p is an analytic variable here rather than the motor-to-motor experimental variable used in some methods.

Brooks method accounts for stored chamber gases and the tail-off pressure integral. The method is based on the ratio of the total pressure integral to average pressure over the tangent bisector time. This improves burn time calculations as the sensitivity to inaccuracy of the aft-tangent location is reduced.[3,4]

$$t_2 = \frac{\int_{0}^{t} P_c.dt}{\int_{t1}^{tb} P_c.dt}.(t_b - t_1).\alpha_p \qquad 9.1$$

The normal tail-off in a motor varies with pressure at burn out. Therefore α_p is a variable and is a linear function of pressure [3], and is defined by

$$\alpha_p = m \cdot P_w + b \qquad \qquad 9.2$$

where, P_w is the pressure at web burn out, and b is an empirical constant based on data.

The slope m is a theoretical value based on the empty chamber volume (V_f), the molecular mass of the gas (M) and total propellant weight (W_p), or propellant density ρ_p , the universal gas constant (R), and the flame temperature (T_f)

$$m = -\frac{M}{R.T_f.W_P} = -\frac{1}{R\,T_f\,W_f\,\rho_p} \qquad \qquad 9.3$$

The intercept b is an empirical constant with typical values $0.97 \leq b \leq 1.0$. The method reduces the scatter and standard error normally encountered in a linear regression analysis of burning rate data. Proper selection of a value for b should not alter historical correlations between subscale and full-scale motor data. Typical values are $m = -4.83.10^{-2}$ Pa^{-1} and $b = 0.97$. Typical values observed by Alliant Tech Systems for a 2-inch motor and a given propellant are $0.990 < \alpha_p < 0.995$ over the pressure range 70 MPa (500psi) $< P_w <$ 220 MPa (1500 psi). While, yet another motor and propellant combination can yield $0.955 < \alpha_p < 0.960$ over the same pressure range.

Brooks' Common Mass Balance Method

Brooks' common mass balance method neglects all storage terms.

$$r_b = \frac{w_b}{t_b} \cdot \left(\frac{\int_{tb} P.dt}{\int_{ttotal} P.dt} \right) \qquad \qquad 9.4$$

Development of this equation begins with the fundamental R_{TOT}, web thickness over burning time relationship

$$r_{TOT} = \frac{w_b}{t_b} \qquad \qquad 9.5$$

using the average pressure defined as [4]

$$\overline{P_c} = \frac{\overline{A_b} \cdot \rho_p \cdot c^* \cdot r}{A_t} \qquad \qquad 9.6$$

where $\overline{A_b}$ is an average value. When rewriting c^* and ρ_p as

$$c^* = \frac{A_t \cdot \int P.dt}{W_p} \qquad \qquad 9.7$$

and

[3] Brooks, W.T., "Workshop Report: Burn Rate Determination Technology", CPIA Publication 347, Vol III, October 1981.

[4] Brooks, W.T., "A Method for More Reproducible Burning Rate Determination", J. Spacecraft, Vol. 7, No. 12, Dec. 1970, pp. 1488-1489.

$$\rho_p = \frac{W_p}{A_b \cdot w_b} \qquad 9.8$$

Where Wp is the propellant weight used for the test. When replacing c^* and ρ_p in Equation 9.6 the burning rate becomes the following using Equation 9.1 for t_2

$$r_b{}' = \frac{w_b \cdot \overline{P_c}}{\int_{t1}^{t2} P\,dt} \qquad 9.9$$

or, alternatively integrating over the total action time t and using Equations 9.2 and 9.3 for α_p

$$r_b = \frac{w_b \overline{P_c}}{\alpha_p \int_{t1}^{t} P\,dt} \qquad 9.10$$

In essence, Equation 9.9 and 9.10 are identical to replacing the time in Equation 9.5 by the ratio of the pressure integral and the average pressure.

Brooks' Improved Method

Brooks' improved method approximates all storage terms mentioned in Chapter 4, Section 4.1.2, Equation 4.16 and is given here in Equation 9.11.

$$r_b = \frac{w_b}{t_b} \cdot \left(\frac{\int_{t_b} p.dt}{\int_{t_{total}} p.dt} \right) \left(1 + \frac{V_b(p_E - p_B)}{w_p.R_g.T_f} \right) \cdot \left(\frac{1}{1 - \frac{P_c}{\rho_p.R_g.T_f}} \right) \qquad 9.11$$

Equation 9.11 equals Equation 9.4, but includes an exact web thickness/time correction to the nominal thickness/time (w_b / t_b), a storage correction for density change due to the influences of pressure variation during the test, and a correction for volume change in the chamber due to propellant consumption.

Comments

When considering a typical subscale test with a neutral CP grain, the fundamental r_{TOT} expression in Equation 9.5 gives the most accurate results from tests yielding the least amount of impulse in the tail-off. When assessing the influence of the total tail-off impulse on Equation 9.5, this will become explicit. When taking for example two aft-tangent points, one at (t_e) and another at (t_e + δ), the burning rate obtained with Equation 9.5 will differ by a fraction $(t_e + \delta)/ t_e$. The average pressure determined over two intervals in Equation 9.9 and 9.10 will differ by much less than this fraction (about half). Therefore, the burning rate as given in Equation 9.9 and 9.10 shows less variation than Equation 9.5. For the case when there is no tail-off, the two methods (r_{TOT} and r_{TOT}) yield identical results. Equation 9.5 becomes decreasingly accurate with increasing impulse in the tail-off.

Hessler[5] offers a further discussion to aid in the understanding of the Brook's correction term α_p that appears in Equation 9.1.

---

[5] R.O. Hessler and R.L. Glick, "A Ballistic Prediction for Burning Rate Motors and Non-Instantaneous Burnout," memorandum in support of NATO RTO/AVT WG016, October 1998.
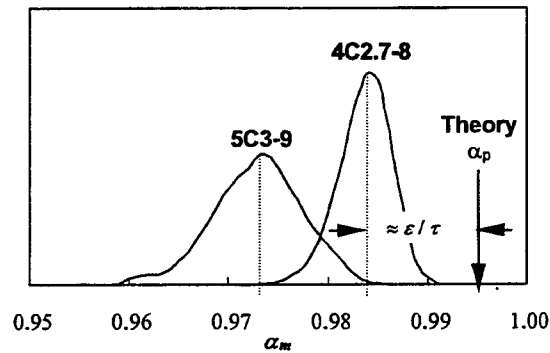
Figure B-10 Frequency Distribution of Integral Ratio.[6]

The ratio α_m formed by the pressure integral during web time divided by the total pressure integral is a rough measure of the degree of barrel-shape and eccentricity.[7] The theoretical value corresponds to the correction factor in Brooks' (Improved) Method, α_p. The difference between mean values for a motor type and its theoretical value corresponds to the web thickness variation caused by grain distortion (barrel-shape), about 1.1% for the 0.64 in. web of the 4C2.7-8 motors, and about 2.2% for the 1.00 in. web of 5C3-9 motors. The widths of the distributions correspond to the combined effects of eccentricity, skew, or ovality, and the effects of non-reproducible timepoint detection, mean shrinkage, or mean temperature. The standard deviations were 0.23% on the 4C2.7-8 motors and 0.43% on the 5C3-9 motors. Web time was detected on the 4C2.7-8s by the maximum intersection definition for initial burnout, and by Jordan's iterative procedure (APPENDIX B-17) on the 5C3-9s.

---

[6] Hessler, R.O., Glick, R.L., Jordan, F.W., and Fry, R.S. "Burning Rate Measurement in Batch Test Motors," JANNAF Combustion Meeting, Monterey, November 1996.

[7] Hessler, R.O. and Glick, R.L., "Comparisons of Burning Rate Calculation Methods," JANNAF Combustion Meeting, West Palm Beach, October 1997.

APPENDIX B-10: UNITED STATES
US ARMY AVIATION & MISSILE COMMAND (AMCOM)

Introduction

The U.S. Army Aviation and Missile Command (AMCOM) uses the mass balance burning rate (r_{MB}) procedure for calculating solid propellant burning rates. This technique requires transient pressure traces from the chamber of the burning motor, geometrical measurements of the motor, mass/density measurements of the propellant, and thermo-equilibrium solutions for the propellant formulation.

Definitions

A_t Throat area

C^* Characteristic exhaust velocity, $C^* = \dfrac{\sqrt{\gamma R T_c}}{\sqrt{(2/\gamma+1)^{(\gamma+1/\gamma-1)}}}$

m Mass flow rate
P Chamber pressure
R Gas constant
ρ_p propellant density
r_b Linear burning rate
S Propellant surface area
T_c *Average* chamber temperature, assumed to be propellant adiabatic flame temperature
V Chamber volume

Description of Method

AMCOM engineers have used the following method for several years to calculate linear burning rates of small propellant samples. Irrespective of the vessel in which the propellant burns, one will have the same mass conservation equation

$$\dot{m}_g = \dot{m}_e + \dot{m}_s \qquad \qquad 10.1$$

where *e* denotes gas exiting through the nozzle, g denotes gas generated, and *s* denotes gas stored in the motor chamber. The ideal gas equation of state describes the stored gas in terms of measurable quantities through the equation,

$$\dot{m}_s = \frac{V\dot{P}}{RT_c} + \frac{P\dot{V}}{RT_c} \qquad \qquad 10.2$$

Note that an implicit assumption of Equation 10.2 is that the chamber temperature is relatively constant with respect to time. From standard rocket performance predictions, the mass flow exiting through the nozzle is

$$\dot{m}_e = \frac{PA_t}{C^*} \qquad \qquad 10.3$$

The mass flow rate being generated is

$$\dot{m}_g = r_b S \rho_p \qquad \qquad 10.4$$

Finally, noting that $\dot{V} = r_b S$, and plugging Equations 10.2, 10.3, and 10.4 into Equation 10.1, the burning rate expression becomes

$$r_b = \frac{\dfrac{PA_t}{C^*} + V\dfrac{\dot{P}}{RT_c}}{S\left(\rho_p - \dfrac{P}{RT_c}\right)} \qquad \qquad 10.5$$

Here C^* and T_c are, by assumption, based on the adiabatic flame temperature of the propellant.

Comments

This method is similar to another described in APPENDIX B-18 from Stone Engineering, also located in Huntsville, Alabama. Both methods rely on mass conservation and the ideal gas equation of state to calculate instantaneous mass generation rates. Moreover, they assume that the gas is calorically and thermally perfect, and that the motor is adiabatic. Either method could incorporate an estimated heat transfer without adding too many complications.

APPENDIX B-11: UNITED STATES
ATLANTIC RESEARCH CORP (ARC)

Introduction

The Atlantic Research Corporation (ARC) uses mass balance burning rate (r_{MB}) and iterated mass balance burning rate (r_{MBn}) procedures for calculating solid propellant burning rates.

Definitions and Description of Method

2x4 Motor Analysis

The burning rate at equilibrium pressure is calculated from the following

$$r_{eq} = \left[P_{eq} \times \left(m_p + m_{ign} \times c^*_{ign} / c^*_p \right) \right] \div \left[\bar{A}_b \times \int Pdt \times \left(\rho - P_{eq} / 12RT \right) \right]$$ 11.1

where

P_{eq}	motor equilibrium pressure defined by the user
m_p	propellant mass
m_{ign}	igniter mass
c^*_{ign}	igniter Cstar
c^*_p	propellant Cstar
A_b	average burning surface
r_{eq}	equilibrium burning rate
$\int Pdt$	pressure time integral
ρ	propellant density
R	propellant gas constant
T	propellant flame temperature

6-Inch Rohm and Haas 10 Pound Motor Analysis

Two methods are used for the 6-Inch Rohm and Haas motor.

The first method uses an *average or bulk rate* calculated from measured data (P vs t, F vs t) according to the following:

$$r_{ref} = w_b \times P^n_{ref} / \int_{fpii}^{fpit} P^n_c dt$$ 11.2

The second method calculates an *instantaneous burning rate* and integrates over the web time. Adjustments are made to correct for offset mandrels, bowed mandrels, etc. until the integrated web and input web are within ~0.25%.

$$r_{bi} = \left(P_{ci} \times A_{ti} \times \eta_t \times g_c \right) / \left(c^*_p \times A_{bi} \times \rho \right)$$ 11.3

$$web = w_{bi} = \int_{fpii}^{fpit} r_{bi} dt$$ 11.4

where

P_{ci}	instantaneous pressure
A_{ti}	instantaneous throat area
η_t	average throat efficiency
A_{bi}	instantaneous burning surface area
w_{bi}	instantaneous web

w_b measured web

Comments

The Atlantic Research Corporation data reduction procedure called Static Firing Analysis (SFA) that calculates *instantaneous burning rate* was developed following procedures and references outlined in APPENDIX B-17 SNAP/JORDAN. Frank Jordan contributed actively to developing this solid propellant rocket motor firing analysis procedure.

APPENDIX B-12: UNITED STATES
BF GOODRICH / UNIVERSAL PROPULSION

Introduction

BF Goodrich / Universal Propulsion uses the fundamental thickness/time burning rate (r_{TOT}) procedure for calculating solid propellant burning rates.

Definitions

t_{burn} Burning time established between $t_{ignition}$ and the point of maximum rate of change of curvature on the pressure-time record, i.e. tangent bisector method was used to determine the end of web burning time as illustrated in Figure B-11.

$t_{ignition}$ Ignition time, typically 10% P_{max}

t_{total} Total burning time from zero until chamber pressure reaches atmospheric conditions

P_{avg} Average pressure of the interval from time zero until t_{burn}

Pressure Integral (t_{burn})   Integral of the pressure-time curve from time zero until t_{burn}

Pressure Integral (t_{total})   Integral of the pressure-time curve from time zero until t_{total}

Figure B-11 Definitions of Tangent-Bisector Method

Description of the Method

The burning rate for RR III, Group 1a (Baseline, concentric bore) was found using the fundamental thickness/time burning rate (r_{TOT}) procedure by dividing the given web distance by t_{burn}.

Introduction

GD / Ordnance & Tactical Systems (formerly Primex Aerospace, formerly Olin Aerospace, formerly Rocket Research) uses the fundamental thickness/time burning rate (r_{TOT}) procedure for calculating solid propellant burning rates.

GD-OTS, Moses Lake Facility, manufactures propellants used for Gas Generators – used for inflating bags, pushing pistons, or filling chambers. The burning rate measurements use thickness/time methods at two different pressures. Normal pressures used are 1000 and 2500psi. Two additional methods employing propellant strands are used, depending on propellant type. In the first method, the burn time is measured from ignition until the flame front reaches a thermocouple at the end of the sample slug. In the second method, the burn time is measured as the flame front passes two thermocouples imbedded in the propellant "strand". Both methods use inhibited samples, so the flame forms a flat front that burns progressively from one end. All tests are conducted at constant pressure. Six samples are taken at each of two pressures, to provide average burn rate and a sense of the variability within a batch. Results are sorted for anomalies using the Dixon method. The resulting slope equations are used for acceptance criteria or to determine web thickness, in the case of production propellant, or for performance prediction in the case of development work.

The propellants are in two families – one uses a binder, the other does not. Binder propellants are tested using strands cut from a larger grain. The non-binder propellants are tested using sample slugs, compacted to net shape.

Definitions for Motors

t_{burn} Burning time established between $t_{ignition}$ and the point of maximum rate of change of curvature on the pressure-time record, i.e. tangent bisector method was used to determine the end of web burning time as illustrated in Figure B-12.

$t_{ignition}$ Ignition time, typically 10% P_{max}

t_{total} Total burning time from zero until chamber pressure reaches atmospheric conditions

P_{avg} Average pressure of the interval from time zero until t_{burn}

Pressure Integral (t_{burn})   Integral of the pressure-time curve from time zero until t_{burn}

Pressure Integral (t_{total})   Integral of the pressure-time curve from time zero until t_{total}
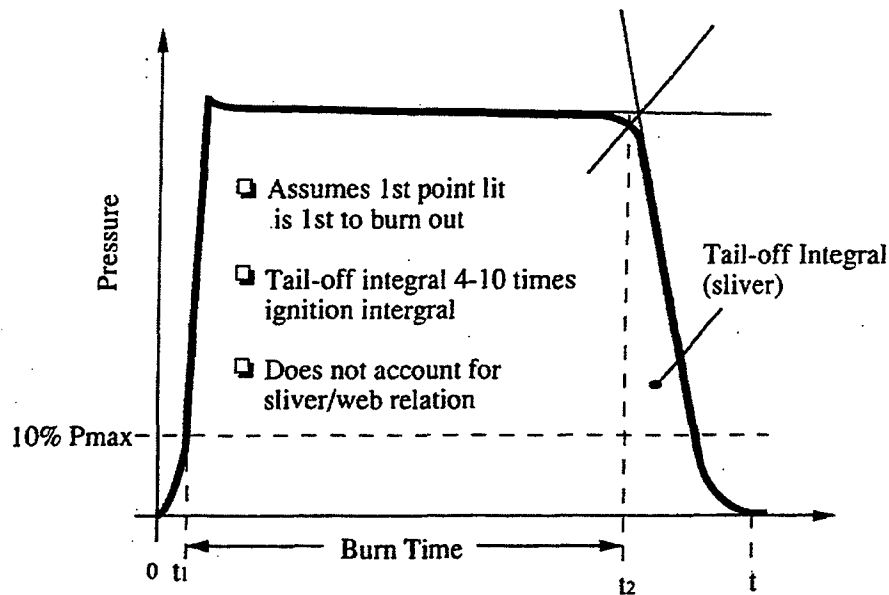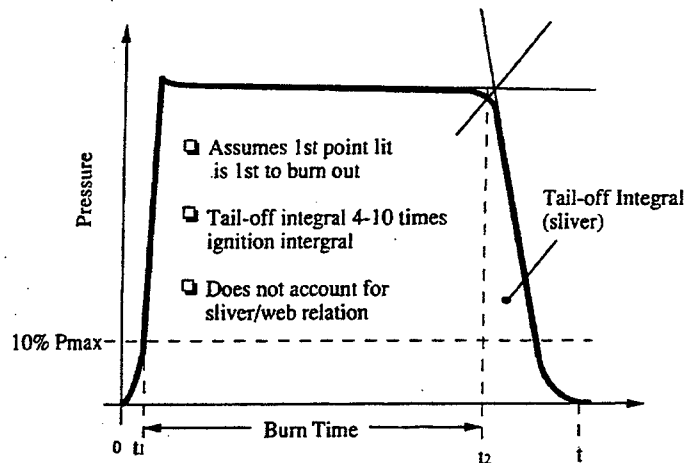

Figure B-12 Definitions of Tangent-Bisector Method

Description of the Motor Method

The fundamental thickness/time burning rate (r_{TOT}) procedure described in APPENDIX B-23 is used.

Definitions for Strands

D	Grain diameter, mm
L	Grain length, mm or inches, measured from end to end in the case of slugs, or from thermocouple center to thermocouple center in the case of strands
P_{1000}	Test pressure, 1000psi nominal
P_{2500}	Test pressure, 2500psi nominal
T_{cham}	Chamber Temperature, 75degF nominal
T_{strand}	Strand temperature
$T/C1$	Thermocouple 1
$T/C2$	Thermocouple 2
t_0	Ignition time, defined as first current in the electric match
t_1	$T/C1$ first indication of temperature rise
t_2	$T/C2$ first indication of temperature rise

Description of Strand Method

SLUGS: Six to 12 sample slugs are formed during batch propellant production. The slugs are compacted to the same density as the production propellant, which is normally in dry-compacted pill form. Standard slug dimensions are 0.50 diameter, by approximately 0.5 inch long.

Each slug is measured for actual dimensions (L, D) then a thermocouple is taped to the center of one end prior to inhibitor application. The inhibitor is a mixture of 5-minute epoxy and titanium dioxide, applied to a minimum thickness of 0.10 inch. The ignition end is left uninhibited, but gets coated with a slurry of BKNO3. An electric match is used to ignite the BKNO3.

Burn time is measured from electric match first current to first temperature rise indicated by the thermocouple. Burn rate is calculated from L/(t2-t1).
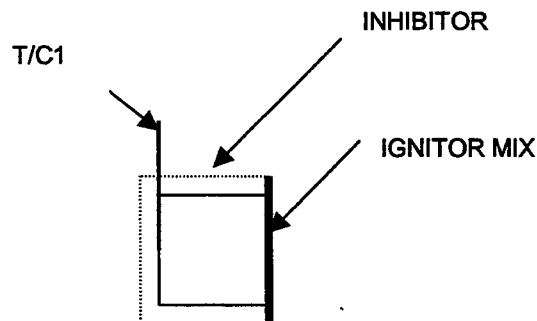
Figure B-13 GD-OTS Strand Method #1

STRANDS: A sample grain is formed during batch propellant production, which is normally in molded or extruded form. The sample grain is formed using the same compaction pressure as the production grains, to obtain a representative density. The sample grain is oven-cured with the rest of the propellant batch, and then is cut into 12 minimum strands 0.50 x 0.50 x 3.5 inches. The same sample grain also yields samples for tensile measurement and Calorimetry.

Two holes are drilled in each test strand 2.000 inches apart, and thermocouples are inserted to the bottoms of the holes prior to application of inhibitor. The strand is then inhibited with a mixture of 5-

minute epoxy and titanium dioxide to a minimum thickness of 0.10 inch. The ignition end is left uninhibited if the strand is to be tested immediately, and gets coated with a slurry of BKNO3. A third thermocouple hole is drilled in the opposite end, immediately prior to testing, to monitor the strand temperature.

Burn rate is calculated from L/(t2 – t1), or (2.000)/(t2 – t1)
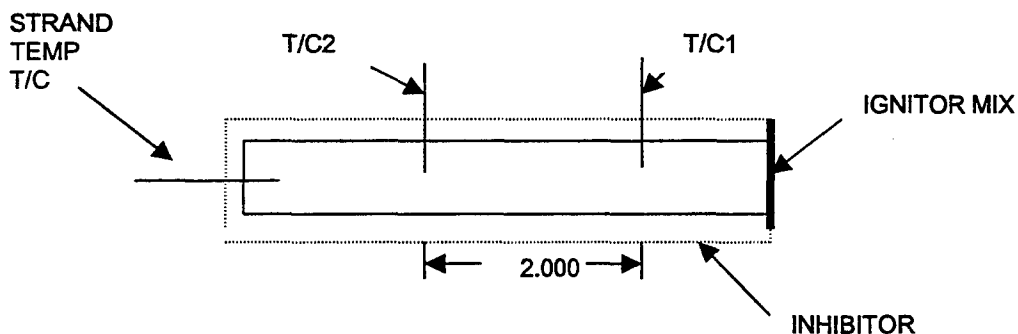
Figure B-14 GD-OTS Strand Method #2

All tests are pressurized using GN2, with the sample at 60-80degF. Pressures are controlled to 1000+/-5psig, and 2500+/-13psig. Actual pressures are used for calculating slope.

The Dixon method is used to test for outliers. The burn rates of set of six samples are arranged in increasing order X1 X2 X3 X4 X5 X6, and the ratios are calculated:

$$R = (X6-X5)/(X6-X1)$$

and

$$R = (X2-X1)/(X6-X1)$$

If the calculated ratio is larger than 0.482, the suspected outlier may be rejected with 90% confidence.

Comments

Much attention has been paid to the influences of ignition delays and thermocouple response times. For the propellants we test, we have determined that these delays are consistent, and of relatively insignificant duration. For very fast burning propellants the ignition delay and thermocouple response could be more significant, but could be treated as a constant factor in burn time calculations. The strand burn rate measurement avoids the ignition transient problem by measuring the flame front passing two thermocouples after it has established itself.

Fast outliers may be caused by inhibitor failure or cracks in the propellant sample that allow the flame to propagate more directly to the thermocouple(s). Unusually slow outliers may be caused by uneven ignition or transverse cracks causing an uneven flame front.

Propellant may occasionally be tested at specific pressures duplicating hardware design points, as a means to verify predictions, but slope exponents and coefficients are necessary to accurately model transients.

Temperature sensitivity (Pi-k) testing has been performed but rarely at temperatures of +100F/+40F. Gas Generator performance at temperature extremes is influenced by many other factors, which combine to outweigh the influence of simple Pi-k.

Introduction

NAWCWD CHINA LAKE uses both the fundamental thickness/time burning rate (r_{TOT}) and the mass balance burning rate (r_{MB}) procedures for calculating solid propellant burning rates.

Definitions

r_b'	reported burning rate, mm/s
w_b	grain web corrected for temperature, mm
P_b	average pressure over burn time (t_b), MPa
P_a	average pressure over action time (t_a), MPa
P_c	motor chamber pressure
t_a	action time (from 30 psia to 30 psia), sec
t_b'	reported burn time (w_b / r_b'), sec
t_b	burn time for determining P_b ($t_{b2} - t_{b1}$), sec
t_{b1}	time where P_c becomes 60% of the action time pressure (P_a) on first sustained rise, sec
t_{b2}	time where d^2P_c/dt^2 is a positive maximum during tail-off, sec (See Figure B-15)
ρ_p	propellant density corrected for temperature, kg/m3
ρ_g	combustion gas density from thermochemistry and (P_b)(MW) / (R)(T_c), kg/m3
MW	molecular weight of the combustion species, kg/kg-mol
T_c	temperature of the combustion species, K , implicitly assumed to be constant
w_b	grain web corrected for temperature, mm

Description of the Method I
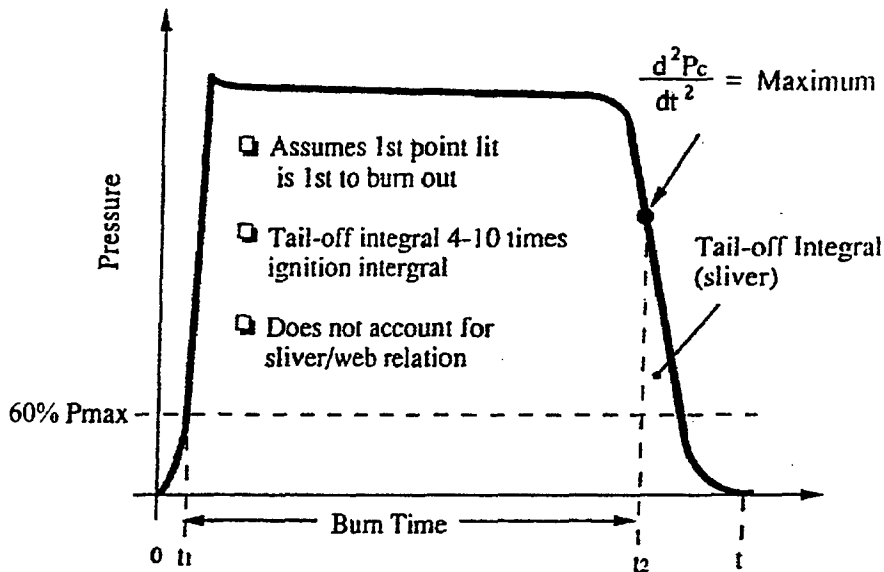
**Figure B-15 NAWCWD Definitions using Brimhall Method
for End of Burn Determination[8]**

Equation 14.1 gives the fundamental thickness/time burning rate (r_{TOT}) method used at NAWCWD CHINA LAKE for determining the motor burning rate of a particular propellant. Burn time is back calculated from Equation 14.2. Burn time commences when the pressure reaches 60% of the

---

[8] Bimhall, K. unpublished, circa 1970. Communication with R.L. Glick stated Brimhall's derivative definition originated from a US Workshop.

average action time pressure (or 60% of the average boost phase action time pressure in the case of a boost-sustain pressure history).

$$r_b' = \frac{w_b}{t_a} \cdot \frac{p_b}{p_a} \cdot \left(\frac{\rho_p}{\rho_p - \rho_g} \right)$$ 14.1

$$t_b' = w_b / r_b'$$ 14.2

$$t_b = t_{b2} - t_{b1}$$ 14.3

Definitions for Method II

A_b	apparent surface burn area
A_t	nozzle throat area
C_d	nozzle discharge coefficient
C_f	nozzle thrust coefficient
F	motor thrust
P_c	motor chamber pressure
P_e	nozzle exit pressure
T_o	ambient temperature
r_b	grain burning rate
ρ_p	propellant density
w_b	grain web corrected for temperature, mm
w_p	propellant mass
ε	nozzle expansion ratio
λ	nozzle divergence factor (correction)
η_T	nozzle thrust efficiency
σ_p	propellant burning rate temperature sensitivity at a constant pressure

Description of the Method II

This section discusses the mass balance burning rate (r_{MB}) procedures used at NAWCWD CHINA LAKE for determining the motor burning rate of a particular propellant.

This method is used to back out burning rate vs. time (pressure). Constraints include burn area vs. web (either theoretical or apparent), throat area vs. time, C^*, propellant weight, density, and etc.

Actual burn areas should be used when using this method for calculating burning rate. Erroneous burning rate values can result if the actual and theoretical burn areas are not the same. This method was applied to the RR II cases.

The method discussed in this paper uses the "apparent" burn area vs. web function. The apparent burn area is a one-dimensional, lumped-sum function calculated from static firing pressure and thrust data. In general, apparent burn area is independent of burn time, pressure, and throat erosion; is nearly independent of temperature (though temperature affects mass flux and the magnitude of erosive burning); is unaffected by nominal perturbations in operating parameters such as initial throat diameter and burning rate; and is fairly insensitive to mix-to-mix variations in burning rate exponent.

Apparent burn area calculated from thrust and pressure is patently dependent upon the grain design, bore geometry, and actual mass flux through the bore. Because the area under the burn area curve is volume and is proportional to propellant mass, deviations in the shape of the curve are caused by alterations to the nominal mass flow rate (i.e., the way the propellant surface regresses). Igniter mass flow, erosive burning, and stagnation pressure drop are lumped into this function; this has proven beneficial for characterizing ignition transients and the magnitude of erosive burning. As the bore in the grain increases with propellant consumption and the pressure drop in the motor diminishes, the apparent burn area converges rapidly with the actual burn area. In practice, the burn area vs. web function is a very useful analytical tool. It is an excellent indicator of motor-to-motor reproducibility

revealing inconsistent machining of radial slots (doughnuts), edge coning, and propellant grain anomalies such as unbonds, cracks, or even anomalous propellant exponent (slope) breaks.

Apparent burn area A_b vs. web data is obtained from pressure and thrust firing data using two iterative steps. In the first step, throat area C_dA_t vs. time data is calculated from pressure and thrust data using Equations 14.4 through 14.7.

$$Z = P_e/P_c \qquad\qquad 14.4$$

$$\varepsilon = f(Z, \gamma) = A_e/C_dA_t \qquad\qquad 14.5$$

$$C_f = f(Z, \gamma, \varepsilon) \qquad\qquad 14.6$$

$$F = P_c(C_dA_t)\,C_f\,\lambda\,\eta_T \qquad\qquad 14.7$$

$$\varepsilon = A_e/C_dA_t \qquad\qquad 14.8$$

Assuming the nozzle exit area (A_e) is constant, the iteration begins with a guess for Z (quotient of nozzle exit pressure and chamber pressure), which produces a value for ε (expansion ratio) through the use of Equation 14.5. These values (Z & ε) are then used to calculate a value for the thrust coefficient C_f, via Equation 14.6. C_dA_t (inseparable product of the throat discharge coefficient and the throat area) is then calculated from Equation 14.7 using the measured pressure and thrust data. Once CdAt is obtained from equation 14.7, the expansion ratio is calculated from Equation 14.8 and compared with the value calculated from Equation 14.5. The procedure is repeated until the two ε values converge at each time increment. Naturally, flow separation in the nozzle must be considered in the process.

Burn area vs. web data are obtained in the second iterative step using Equations 14.9 through 14.12 and C_dA_t vs. time data obtained in the first step. Equation 14.11 is an expression of the unsteady-state mass balance.

$$r_b = f(P_c, \sigma_p, T_o) \qquad\qquad 14.9$$

$$w_b = f(r_b, t, T_o) \qquad\qquad 14.10$$

$$\rho_p = \rho_p(T_o) \qquad\qquad 14.11$$

$$A_b = f(P_c, C_dA_t, r_b, \rho_p, w_p, T_o, w_b) \qquad\qquad 14.12$$

One constraint is imposed upon the burn area vs. web solution. This constraint is a value for burn area at the final web length. To force this constraint upon the solution, the burning rate r_b is adjusted until convergence is attained. The burn rate multiplier (BRM) is the parameter used to adjust the burning rate. The BRM is not as arbitrary as it may appear; if values for the constraints are judiciously chosen and retained as reference or baseline values for subsequent analyses, BRM values will accurately denote mix-to-mix variations in propellant burning rate.

Burn rate is calculated at each time step (Equation 14.9). Web length burned then is calculated using Equation 14.10. Burn surface area as a function of web can then be calculated using Equation 14.12, after the propellant density is corrected for temperature (14.11). The calculated burn area (A_b) at the final web length is compared with the constraint; if high or low the burning rate calculated from Equation 14.9 is multiplied by the BRM, and the process is repeated until convergence is attain.

It must be emphasized that in order for this procedure to work, the burning rate must be known a priori. Therefore, this procedure is best applied to Lot Acceptance Testing (LAT) of production solid rocket motors.

Comments on Method I

While it is a standard in many facilities, experience has shown that 10% of peak pressure may be too soon to start burn time in some test cases. Burn time ends when the 2nd derivative of pressure reaches a relative maximum, however this is a judgment call that is dependent upon the particular motor configuration and firing. Experience also has resulted in the conclusion that burning rate should not be reported for a motor that has an obviously off-center mandrel. This firing should be repeated. Furthermore, a correction for $(V_c)(dP_c/dt)(MW/R.T_c)$ may not really improve the data as it can cause the standard deviation to increase. The d^2P_c/dt^2 definition is an approximation of final burnout, which is not fully correct and will bias results low. The volume change correction will yield higher burning rate results.

Introduction

The Naval Surface Weapons Center, Indian Head uses a basic mass balance burning rate (r_{MB}) procedure for calculating solid propellant burning rates. NSWC/IH also developed a mini slab ballistic test motor that is different from motors typically used for burning rate characterization. Its principal advantage is the ability to measure the burning rate across a wide pressure range. The motor uses small charge weights that allow ballistic characterization of small scale lots and R&D propellant mixes in a rocket motor environment. As grains may be cut from bulk propellant, some of the usual investment in tooling and hardware is avoided. The mini slab motor is schematically represented in Fig. B-16. Figure B-17 shows the pressure vs. time nomenclature.
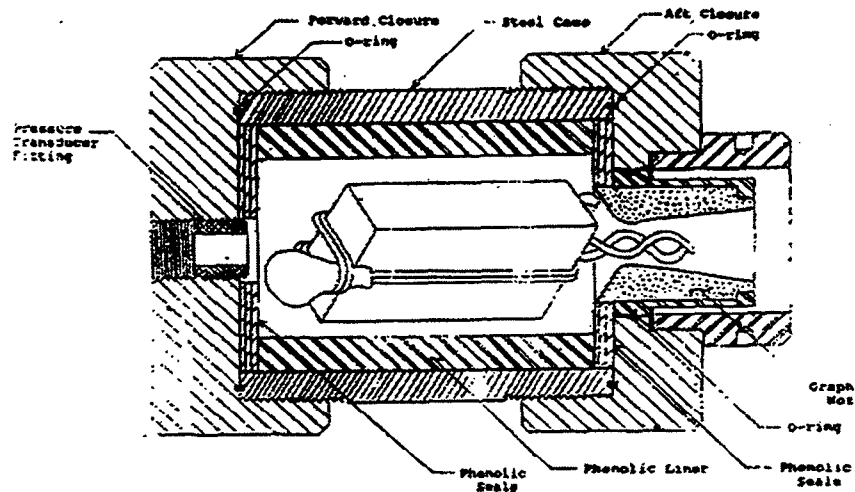
Fig. B-16 Loaded Mini Slab Motor__
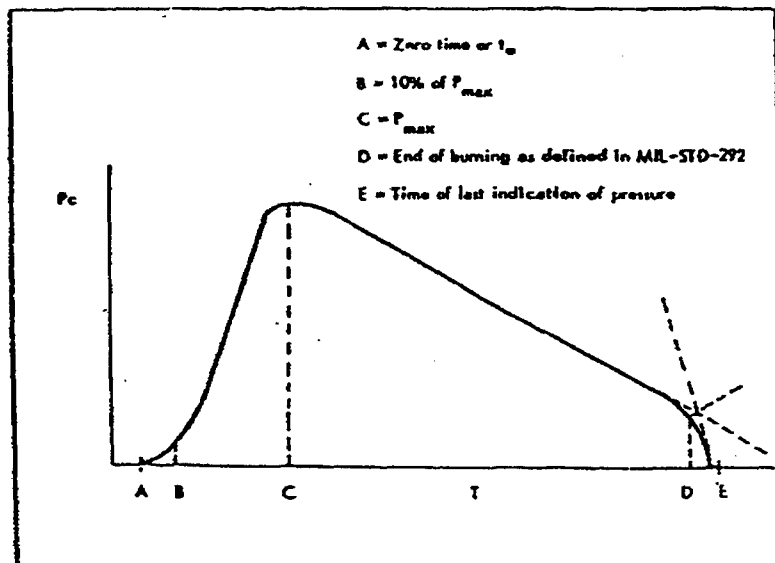
Fig. B-17 Burning Time Definitions

---

[9] US Patent no. 5,419,116 (May 30, 1995) and AIAA paper 92-3046

Definitions

A_t	Nozzle throat cross sectional area
c^*	Characteristic velocity
m_p	propellant mass
r_{avg}	Average burning rate over time interval δt
P_c	Combustion pressure
P_{avg}	Average pressure over time interval δt
P_{max}	Maximum chamber pressure
t_A	Time of first indication of pressure, also optional start of burning time, shown in Fig. B-17
t_B	Start of burning time, typically at 10% P_{max}, shown in Fig. B-17
t_C	Time of P_{max}, shown in Fig. B-17
t_D	Burnout time, defined at the intersection of the linear regression line and the maximum slope tangent line, shown in Fig. B-17
t_E	Time of last indication of pressure, shown in Fig. B-17
V_o	Initial propellant volume
V_p	Propellant volume
Δm_T	Total mass flow through the nozzle, defined by Eq. 15.2
Δm_t	Mass flow through the nozzle at time t, defined by Eq. 15.3
ΔV_t	Propellant volume at time t, defined by Eq. 15.5
ρ_p	Density propellant

Description of the Method

Internal ballistics are calculated based on the following assumptions:

1. The nozzle flow is one dimensional and isentropic,
2. The propellant regresses equally on all slab faces,
3. The nozzle throat area remains constant or changes linearly with time,
4. The perfect gas law applies to the combustion products,
5. The characteristic velocity c^* is assumed constant, which implies a constant temperature assumption.

Remark: For such a motor, the chances of a constant temperature are small because of heat losses to the much larger exposed hardware than occurring with a regular ballistic motor using a centrally perforated grain.

From the mass balance at the nozzle we obtain:

$$m = \frac{p_c . A_t}{c^*}$$

15.1

This equation is integrated to give:

$$\Delta m_T = \frac{1}{c^*} . \int_{t_A}^{t_E} p_c . A_t . dt$$

15.2

Where t_A and t_E are given by Fig. B-9 and Δm_T is the total mass flow through the nozzle. C* is assumed constant over the entire pressure range. The mass flow from t_A to any time t is:

$$\Delta m_t = \frac{1}{c^*} . \int_{t_A}^{t} p_c . A_t . dt$$

15.3

Dividing Eq. 15.3 by Eq. 15.2 we get

$$\frac{\Delta m_t}{\Delta m_T} = \frac{\int_{t_A}^{t} p_c . A_t . dt}{\int_{t_A}^{t_F} p_c . A_t . dt} \qquad 15.4$$

If it is assumed that the mass flow generated by the propellant equals the mass flow through the nozzle (i.e., neglecting mass storage in the motor). Using $m_p = \rho_p V_p$ one obtains:

$$\frac{\Delta V_t}{V_o} = \frac{\int_{t_A}^{t} p_c . A_t . dt}{\int_{t_A}^{t_F} p_c . A_t . dt} \qquad 15.5$$

where V_o is the original propellant volume.

Since V_o, P_c, t and A_t are measured quantities and the geometry of the sample is known, the distance δx that the burning surface regresses in time interval δt can be calculated from

$$r_{avg} = \frac{\delta x}{\delta t} \qquad 15.6$$

r_{avg} is the average burn rate over interval δt. The corresponding average pressure for the time interval is given by

$$P_{avg} = \frac{\int_{\delta t} p_c . dt}{\delta t} \qquad 15.7$$

or can alternatively be given by the rate averaged pressure

$$P_{avg} = \left(\frac{\int_{\delta t} p_c^{n} . dt}{\delta t} \right)^{\frac{1}{n}} \qquad 15.8$$

APPENDIX B-16: UNITED STATES
PRATT & WHITNEY, CHEMICAL SYSTEMS DIVISION (CSD)

Introduction

Pratt & Whitney, CSD (A United Technologies Company) uses a basic mass balance burning rate (r_{MB}) procedure for calculating solid propellant burning rates for two types of ballistic motors.

- TM1 motor, 15.2 cm dia, 6800 g
- 4lb motor, 15.2 cm dia, 1800 g

The data reduction plan allows two alternate definitions for determining the end of burn time. One is based on dp/dt and the other is based on a percentage of the total pressure integral. Until mid 1989 the dp/dt method was used but it frequently gave erroneous data when there was a longer tail-offs due to slight bore offsets. This effect on the data consistency could be minimized using a pressure integral fraction that is less sensitive to curve shape. Different values of pressure integral have been used to define the end of burn time depending on the propellant. This was necessary, at the time of the conversion to the pressure integral method, to provide consistency with the previous database generated with those propellants using the dp/dt method. A value of 0.98 is used for all new propellants for which there are no existing database.

MAXIMUM IGNITION PRESSURE
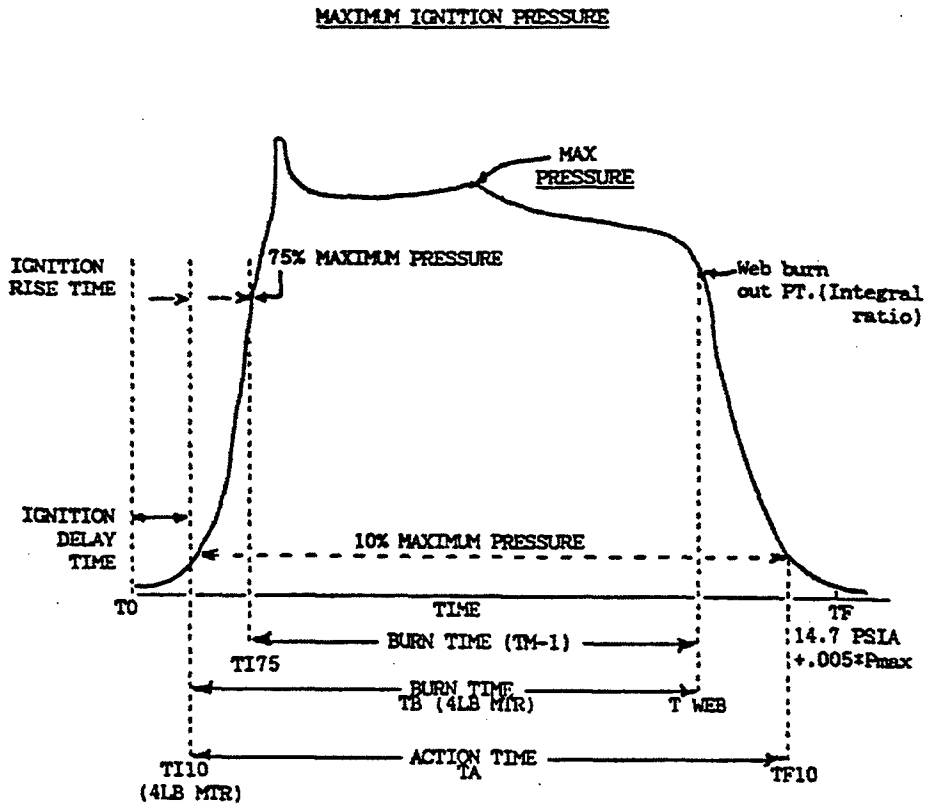
Fig. B-18 Illustration of Ballistic Definitions
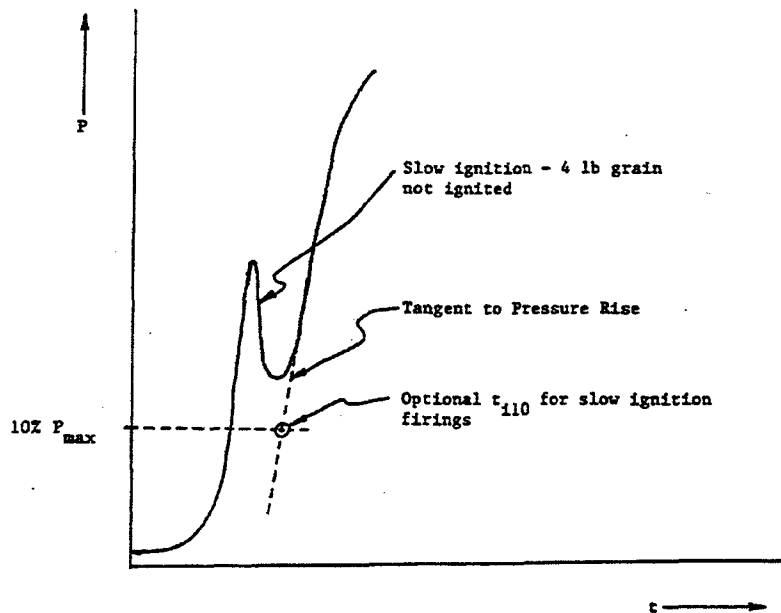
Fig. B-19 Optional Determination of T_{I10} for Slow Ignition Firings

Definitions

A_t	Average throat area. This is calculated measuring throat diameter pre-test and post-test at 3 locations 120 degrees apart and taking the average
I_{PTT}	Total integral of the pressure
I_{PW}	Current value of integral of the pressure at time t_{web}
I_{PI10}	Current value of integral of the pressure at time t_{I10}
IR	Integral Ratio
P_{max}	Maximum pressure
r_b	Burning rate
t_I	Ignition time
t_{I10}	Ignition time when P is 10% of P_{max} during ignition transient

If the ignition transient is not continuous, as illustrated in Fig B-19, but shows evidence of slow ignition, the analyst has the option of disregarding initial portion and may estimate a more appropriate t_{I10} value as illustrated in Fig B-19. This option applies when it is evident that the main grain has not ignited when the transient just exceeds 10% of P_{max}

t_{F10}	Tailoff time when pressure is 10% of P_{max}
t_{I75}	Ignition time when P is 75% of P_{max}
t_{web}	Web burn out time
t_0	Time of first pressure raise
t_F	time when the pressure is 14.7 psia + 0.005 P_{max} during tailoff
t_{burn}	Burning time
T_{PIF}	Tailoff pressure integral factor
W_p	propellant weight
Web_{avg}	average web thickness

Description of Method

The following steps describe the method:

1. Find maximum pressure ($\bar{P}_{max}$) but ignore the ignition spike

2. Find start of burn, defined as

t_{I10}	for a 4lb motor
t_{I75}	for a TM1 motor

3. Find web burnout time (t_{web}) by one of two methods as follows

A. Integral ratio method

Find the t_{web} by locating the time in the integral ratio defined below:

$$\frac{(I_{PW} - I_{PI10})}{I_{PT}} \leq \text{Integral Ratio } (IR), \text{ value set by user (Table B-2) for a specific motor}$$

Typical values of IR for the corresponding motor are provided in the Table B-2. The integral ratio range is approximately, $0.969 \leq IR \leq 0.980$.

B. Derivative method

Find the t_{web} by locating the time in the derivative below:

$$\frac{dP_C}{dt} \leq \text{Pressure Derivative, value set by user (Table B-2) for a specific motor}$$

(Begin at 20% of P_{max} + search backward through the data)

4. Compute ignition time as follows

$t_I = t_{I10} - t_0$ for a 4lb motor
$t_I = t_{I75} - t_0$ for a TM1 motor

5. Compute burn time as follows

$t_{burn} = (t_{web} - t_{I10})$ for a 4lb motor
$t_{burn} = (t_{web} - t_{I75})$ for a TM1 motor

6. Compute Web_{avg} as follows

Measure the distance between the propellant cartridge outside diameter and the propellant inside diameter at four locations representing 0, 90, 180 and 270 degrees for each end. Calculate the propellant web thickness at every location for each end and average the eight web thickness determinations:

$$Web_{avg} = \frac{Web_1 + Web_2 + ... + Web_8}{8}$$ 16.1

Remark: Usually at the centre of grain there is a shrinkage due to pressurization and thermal deformations, so it is possible to improve the calculated Webavg by measuring grain bore and case inside diameter. This will essentially eliminate most of the web bias caused by taking measurement at the grain ends.

7. Compute burn rate as follows

$$r_b = Web_{avg} / t_{burn}$$ 16.2

8. Compute average pressure as follows

$$P_{avg} = \left[\int_{t_0}^{t_{web}} P_C dt - \int_{t_0}^{tI10} P_C dt \right] \Big/ t_{burn}$$ for a 4lb motor   16.3

$$P_{avg} = \left[\int_{t_0}^{t_{web}} P_C dt - \int_{t_0}^{tI75} P_C dt \right] \Big/ t_{burn}$$ for a TM1 motor   16.4

This method allows to calculate others parameters such as C^* and T_{PIF}

$$C^* = A_t \frac{g}{W_p} \int_{t_0}^{t_f} P_C \, dt \qquad W_P \text{ is propellant weight in pound} \qquad 16.5$$

Tailoff Pressure Integral Factor, T_{PIF}, is

$$T_{PIF} = 1 - \frac{\int_{t_0}^{t_{web}} P_C \, dt}{\int_{t_0}^{t_f} P_C \, dt} \qquad \text{for a TM1 motor} \qquad 16.6$$

$$T_{PIF} = 1 - \frac{\int_{t/10}^{t_{web}} P_C \, dt}{\int_{t/10}^{t_f} P_C \, dt} \qquad \text{for a 4 lb motor} \qquad 16.7$$

A number of measurements are then used to determine the coefficients of Vieille's relation $(r = a \, P_C^n)$. The data reduction is done using an interactive computer program.

Comments

Table B-2 Choice for Integral Ratio Depending on Different Known Motor Types

Full-Scale Motor Type	Subscale Motor	Integral Ratio	Derivative pressure [psia/sec]
(Titan	TM1	.98	-1700
commercial)	TM1	.98	-1700
(Titan IV)	TM1	.98	-1700
(ALGOL)	TM1	.978	-1700
(BSM)	4LB	.98	-1700
Titan IV	4LB	.98	-1700
Minuteman	4LB	.967	-1700
Mk111	4LB	*	-1700
MK106	4LB	.969	-1700
IUS	4LB	*	-1700
BLU-106	4LB	.969	-1700
Intelsat	4LB	.965	-1700
AEGIS	4LB	.972	-1700
D5	4LB	.974	-1700
D5 Igniter	4LB	.969	-1700
TOS	4LB	.972	-1700
ORBUS 1	4LB	.98	-1700

Introduction

Mr. Frank Jordan of SNAP used an iterative mass balance burning rate (r_{MBn}) procedure for calculating solid propellant burning rates. While Mr. Jordan is currently not active in the US propulsion industry, his methods nevertheless provided a basis for the procedures used by Atlantic Research Corp, Talley Defense Systems, and Aerojet.

Definitions

A_{bg}	grain geometric burning surface area, in^2
A_{tc}	calculated nozzle throat area, in^2
A_{tm}	average measured nozzle throat area, in^2
A_{em}	measured nozzle exit area, in^2
C^*	characteristic exhaust velocity, ft/s
C^o_F	theoretical thrust coefficient
C^o_{Fvac}	vacuum thrust coefficient
F	measured thrust, lbf
g_o	standard gravity constant, 32.174 ft/s^2
P_a	ambient pressure, psia
P_c	measured motor chamber pressure, psia
P_e	nozzle exit plane pressure, psia
ρ_p	propellant bulk density, lbm/in^3
r_b	burning rate at operating pressure, in/s
w_g	weight flow rate generated, lbm/s
w_s	weight flow rate stored, lbm/s
w_o	weight flow rate out the nozzle, lbm/s
w_p	measured propellant weight, lbm
α	cone half-angle in degrees
γ	ratio of specific heats
λ	cone half angle correction factor
η_T	average nozzle throat efficiency
η_F	average thrust efficiency
$\int P_c dt$	measured pressure integral, psia-s

Description of Method

Frank Jordan has been actively developing solid propellant rocket motor firing analysis procedures over the years. The procedures developed were implemented as computer codes for various different solid propellant rocket motor manufacturing companies. For example at Atlantic Research Corp., a data reduction procedure called Static Firing Analysis (SFA) was developed, at Talley Defense Systems, the procedure was called Talley Rocket Analysis Code (TRAC), while at Aerojet, a procedure called Aerojet Rocket Motor Analysis Code (ARMAC), was written for the Advanced Solid Rocket Motor (ASRM) project. [10, 11, 12]

---

[10] Myers, J.W. and Jordan F.W., "Computerized Static Firing Analysis of Batch Check Motor Firings", Atlantic Research Corp. JANNAF Performance Standardization Subcommittee Meeting, 1982.

[11] Watson T.J., Jordan F.W. and Stóckham L.W., "Accurate Burn Rate Determination for Sub-Scale Test Motors", Aerojet, ASRM Division, Iuka, MS., AIAA 93-2060, Monterey, Ca 1993.

All these computer codes were essentially based on the same analysis procedure, while in addition; some codes had special capabilities that were unique to the company for which they were written. Jordan's method effectively applies a web sliver correction to the common mass balance procedure

$$r_b = \frac{w_b + \varepsilon}{t_b}$$ 17.1

to yield an instantaneous approximation and mean values of burning rate in an iterative procedure

$$\bar{r_b} = \int_t^{tb} \frac{P_c A_{tc} \bar{\eta_t}}{\rho_p A_{bg} C^*} dt$$ 17.2

Jordan's method simultaneously solves for the mass balance (r_{MB}) and thickness/time (r_{TOT}) burning rates, assuming only one burning rate properly defines the propellant, regardless of the method. The method calculates a thickness/time burning rate curve using fractions of the pressure integral for the beginning and ending time definitions. This burning rate curve and the pressure integral fractions at a defined time are used to calculate a mass balance surface versus web burned curve (SW). This SW curve and time-defined fractional pressure integrals are iterated until the calculated SW curve matches the real grain geometry. This surface matching technique assures conservation of mass, and is relatively insensitive to ignition spikes and tail-off anomalies. Demonstrated burning rate accuracy of between 99.77% (coefficient of variation 0.23%) and 99.91% (coefficient of variation of 0.09%) has been demonstrated for a group of 12 high quality motor firings. The procedure holds a twenty-year demonstration record.

Equation 17.3 presents the mass balance relationship used in obtaining the equations for calculating the burn rate as a function of pressure from a single motor firing.

$$\dot{w_g} = \dot{w_s} + \dot{w_o}$$ 17.3

For simplification we will ignore the storage term, since we are not interested in burning rate during ignition and tail-off and the pressure decay rate is too low to be of significance in this development. Therefore, we will limit our mathematical development to the terms in Equation 17.4.

$$\dot{w_g} = \dot{w_o}$$ 17.4

Equation 17.5 presents the source of the weight flow rate generated by grain burning.

$$\dot{w_g} = \rho_p A_{bg} r_b$$ 17.5

Equation 17.6 presents the source of the weight flow rate out the nozzle.

$$\dot{w_o} = \frac{P_c g_o A_{tc} \bar{\eta_T}}{C^*}$$ 17.6

Substituting Equations 17.5 and 17.6 in Equation 17.4 and solving for A_{bg} yields an expression that, when integrated over time, can be used to determine the nozzle throat area history

$$A_{bg} = \frac{P_c g_o A_{tc} \bar{\eta_T}}{\rho_p r_b C^*}$$ 17.7

---

[12] Jordan F.W., Watson T.J. and Stockham L.W., "Propellant Mass Balance Burn Rate and Pressure Exponent", Aerojet ASRM Division, Iuka, MS, AIAA 93-206, Monterey, CA, 1993.

Equation 17.8 presents the source of the average nozzle throat efficiency.

$$\overline{\eta_T} = \frac{w_p\, C^*}{g_o\, \overline{A_{tm}} \displaystyle\int_0^t P_c\, dt}$$

17.8

Equation 17.9 presents the source of the calculated nozzle throat area.

$$A_{tc} = \frac{F}{P_c\, C_F^o\, \overline{\eta_F}}$$

17.9

Equation 17.10 presents the source of the average thrust efficiency.

$$\overline{\eta_F} = \frac{\displaystyle\int_0^t F\, dt}{\overline{A_{tm}}\; \overline{C_F^o} \displaystyle\int_0^t P_c\, dt}$$

17.10

The source of the average and instantaneous thrust coefficients is presented in Equation 17.11.

$$C_F^o = \lambda\, C_{FVac}^o - \frac{P_a\, A_{em}}{P_c\, A_{tm}}$$

17.11

The source of the cone half angle factor is presented in Equation 17.12.

$$\lambda = \frac{1 + \cos\alpha}{2}$$

17.12

The source of the vacuum thrust coefficients is presented in Equation 17.13.

$$C_{FVac}^o = \sqrt{\frac{2\gamma^2}{\gamma - 1}\left(\frac{2}{\gamma + 1}\right)^{(\gamma+1)/(\gamma-1)}\left[1 - \frac{P_e}{P_c}\right]^{(\gamma-1)/\gamma}} + \frac{P_e\, A_{em}}{P_c\, A_{tm}}$$

17.13

Having defined all the parameters needed to calculate the values of the balanced mass flow rates, we now set their substitutions in Equation 17.4 from Equations 17.5 and 17.6 yields Equation 17.14.

$$\rho_p\, A_{bg}\, r_b = \frac{P_c\, g_o\, A_{tc}\, \overline{\eta_T}}{C^*}$$

17.14

Now, solving for burning rate (r_b), we get Equation 17.15.

$$r_b = \frac{P_c\, g_o\, A_{tc}\, \overline{\eta_T}}{\rho_p\, A_{bg}\, C^*}$$

17.15

Solving for burning rate at every point along the measured pressure history (Equation 17.2) permits us to produce a plot of burning rate at pressure versus the pressure. Taking the natural logarithm of the burning rate and pressure permits calculation of a log linear least squares curve fit for the burning rate/pressure function. A few basic assumptions of this method include:

1) The back-calculated rate is insensitive to exponent
2) Mass storage is negligible
3) Burning is sensitive to selection of beginning and end times as are all methods. Burning continues until pressure returns to zero or a selected low pressure.

Prerequisites for Obtaining Accurate Mass Balance Burning Rate

The most critical part of being able to use Equation 17.15 to solve for the burn rate as a function of the measured pressure is the effective nozzle throat area history, which depends on measured thrust. The second most critical part is the elimination of the "hump" or other anomalous burn rate influences. The third most critical part is accounting for bi-directional burning. In addition to these three critical characteristics, the data must be accurate and free from errors.

Thrust Measurement- If measured thrust is not available for calculating the effective nozzle throat area, confidence in the burn rate determined from Equation 17.15 is so low that a pressure exponent calculated from it is practically useless. The pressure exponent is mathematically so sensitive to the actual pressure decay that small errors in pressure make large errors in pressure exponent.

"Hump" Elimination – If the "hump" characteristic is present in the pressure history the ln-rate versus ln-pressure trace will not be linear and will tend to bias the data toward the high end of the pressure history and will tend to result in an "S" shaped ln-rate versus ln-pressure curve.

Bi-directional Burning – Practically all solid propellants exhibit some form of anisotropic or bi-directional burn rate characteristics. Propellants in the double base or composite modified double base group exhibit bi-directional burning as a consequence of the characteristics of burn rate modifiers such as carbon black. Propellants in the polybutadiene group, such as PBAN, CTPB and HTPB exhibit bi-directional and radial variations in burn rate due to casting or flow rheological influences.

When cylindrically perforated grains of polybutadiene propellant are cast with mandrel in place a web-variation in burn rate results called "hump", but with no apparent bi-directional burning rate variation. However, when these propellants are cast into their cases and the core forming mandrel is plunged into the propellant, the "hump" is reduced or eliminated, depending on the relative volumes of the mandrel and case, and bi-directional burning is created.

For the most accuracy in pressure exponent the "hump" must be eliminated and the bi-directional burning must be quantified by motors having a neutral or near neutral pressure history.

Error Isolation – Because the results from the ln-rate versus ln-pressure depend so strongly on the grain and nozzle geometry, it is imperative that no geometry errors be introduced into the data. For this reason a special section of the ROMANS-I does a redundant error isolation analysis. This section of the code uses all measured parameters in all appropriate ballistics equations to isolate data measurement errors. When errors are identified they are corrected and the analysis re-run. It must be noted here that error isolation process does not work well without a minimum of four or five motor firings from the same propellant mix.

Pressure Measurement – Pressure measurement is quite critical to this analysis. The accuracy of the pressure measurement is checked in two ways. First, a plot of the actual pressure histories are over plotted to ensure near absolute agreement between two redundant pressure channels. If two pressure measurements through the same port disagree, one of them is wrong. Next, the error isolation part of ROMANS-I will flag potential pressure measurement errors. This potential is carefully examined to ensure that either there is a probable error or that an error is unlikely. When an error is clearly present, it is corrected and the data re-analyzed.

Nozzle Diameter Measurements – Although the absolute accuracy of the average nozzle throat area is not critical, the relative values of the pre- and post firing nozzle diameter measurements are. The average value of the nozzle throat area is used to calculate the mean nozzle throat efficiency, which is used in Equation 17.15. The average value of the nozzle throat efficiency must be consistent with the average value of the calculated nozzle throat area or there will result a burn rate shift. However, the shift will not affect the accuracy of the pressure exponent or the shape of the ln-rate versus ln- pressure curve but it will result in a burn rate bias.

Grain Dimension Measurements – As can be seen in Equation 17.15, the geometric burning surface area is required to calculate the burn rate. If the grain length, bore diameter or outside diameter are erroneous the burning surface area will not have the proper mean value or progressivity.

An erroneous mean value results in a burn rate bias and an erroneous progressivity (or regressivity) will result in an erroneous pressure exponent.

Comments

The most expanded and complete version of the code could analyze any type of solid propellant rocket motor firing, including:

- Erosive burning
- Spin amplified burning rate
- Boost/sustain
- Multiple grains
- Ablative nozzles
- Dual chambers
- Fuel or oxidizer injected
- Thrust vector controlled
- Special end-burning cylindrical burning rate motors

The code has been used as a burning rate motor analysis tool to:

1. Demonstrate burning rate determination accuracy better than 99.75% (coefficient of variation less than 0.25%)
2. Detect and quantify bi-directional burning in burning rate test motors
3. Quantify acceleration effects on burn rate in spinning motors
4. Determine the effects of casting hysteresis effects on burning rate
5. Determine the erosive burning function for a propellant with a single motor firing
6. Obtain an entire burning rate curve over a given pressure range from a single motor firing
7. Determine a pressure exponent curve as a function of pressure in cases where the pressure exponent varied with pressure

The ARMAC code was a stripped down version of the most elaborate main code. ARMAC was designed to obtain the most accurate burn rate possible from end/internal burning cylinders, including obtaining an entire burn rate curve and pressure exponent from a single motor firing. A more recent version of ARMAC is called Rocket Motor Analysis System I (ROMANS-I). ROMANS-I is now one of the seven parts of the original SFA or TRAC code. Each of the seven parts (ROMANS-I through ROMANS-VII) does one of the above listed tasks that were originally done by SFA, TRAC, ARMAC and others.

ROMANS-I (under the name ARMAC) has demonstrated burning rate accuracy as high as 99.91% (coefficient of variation of 0.09% for 12 motor firings) and a burning rate accuracy as low as 99.77% (coefficient of variation of 0.23% for 12 motor firings) for motors that were all properly made, processed and measured.[13] In addition the ROMANS-I produces: performance parameters and data, graphical presentations of the results, statistical batch information, and an error isolation table.

---

[13] Friedlander, M.P., Jordan, F.W., Hazelette, D.F., "Factors Which Affect The Accuracy of Burn Rate Calculation of Batch Check Motor Firings," Atlantic Research Corp, Cincinnati, OH, AIAA-84-1439, June 1984.

Introduction

Stone Engineering uses an iterated mass balance burning rate (r_{MBn}) procedure for calculating solid propellant burning rates. This technique requires transient pressure traces from the chamber of the burning motor, geometrical measurements of the motor, mass/density measurements of the propellant, and thermo-equilibrium solutions for the propellant formulation.

Definitions

A_t Throat area

$C*$ Characteristic exhaust velocity, $C* = \dfrac{\sqrt{\gamma R T_c}}{\sqrt{(2/\gamma+1)^{(\gamma+1/\gamma-1)}}}$

m Mass flow rate
P Chamber pressure
R Gas constant
ρ_p propellant density
r_b Linear burning rate
S Propellant surface area
T_c Time dependent chamber temperature
T_f Adiabatic flame temperature
V Chamber volume

Definitions and Description of Method

The basis of the Stone Engineering method is exactly the same as the basis of the AMCOM method, namely, the mass continuity equation and the ideal gas equation of state. The Stone Engineering method requires fewer assumptions, however, so it therefore requires more calculation. Irrespective of the vessel in which the propellant burns, one will have the same mass conservation equation

$$\dot{m}_g = \dot{m}_e + \dot{m}_s \qquad\qquad 18.1$$

where e denotes gas exiting through the nozzle, g denotes gas generated, and s denotes gas stored in the motor chamber. The ideal gas equation of state describes the stored gas in terms of measurable quantities through the equation,

$$\dot{m}_s = \frac{V\dot{P}}{RT_c} + \frac{P\dot{V}}{RT_c} \qquad\qquad 18.2$$

Equation 18.2 has an implicit assumption that the chamber temperature is relatively constant with respect to time. If the chamber temperature is a function of time, the ideal gas equation becomes

$$\dot{P}V + \dot{V}P = R(\dot{m}_s T_c + \dot{T}_c m_s) \qquad\qquad 18.3$$

Now add the statement of energy conservation,

$$C_v(\dot{m}_s T_c + \dot{T}_c m_s) = C_p(\dot{m}_g T_g + \dot{m}_e T_c) \qquad\qquad 18.4$$

where C_v, and C_p, are the constant-volume and constant-pressure specific heats, respectively.

Noting the straightforward substitution,

$$\dot{m}_g = \rho_p \dot{V} \qquad\qquad 18.5$$

Equations 18.1, 18.3 and 18.4 now have four unknowns: V, $\dot{m}_e$, $\dot{m}_s$, and T_c. This differs from the

AMCOM method, where T_c is simply the constant adiabatic flame temperature of the propellant.

In order to get more equations, refer to the familiar equation from standard rocket performance predictions for the mass flow exiting through the nozzle

$$\dot{m}_e = \frac{PA_t}{C*}$$

18.6

where $C*$ is *not* a known quantity here. The real characteristic velocity is, by assumption, related to the theoretical characteristic velocity through

$$C* = \eta C_0^* \sqrt{\frac{T_c}{T_f}}$$

18.7

where C_0^* is the theoretical characteristic velocity at the adiabatic flame temperature of the propellant formulation, T_f is the adiabatic flame temperature itself, and η is a constant.

There are now enough equations to solve for $\dot{m}_g$. The procedure is to calculate the mass generation rate, $\dot{m}_g$, and relate it to the linear burning rate at any given point in time through

$$\dot{m}_g = S\rho_p r_b$$

18.8

The total mass expelled must, of course, equal the total mass of the pre-burned propellant, so it is possible to iterate down to η through successive calculations.

Comments

This method is similar to another described in APPENDIX B-10 from U.S. Army Aviation and Missile Command (AMCOM), also located in Huntsville, Alabama. Both methods rely on mass conservation and the ideal gas equation of state to calculate instantaneous mass generation rates. Moreover, they assume that the gas is calorically and thermally perfect, and that the motor is adiabatic. Either method could incorporate an estimated heat transfer without adding too many complications.

The Stone Engineering approach can also estimate bore offsets. The same set of equations define the technique for the bore offset calculations, except that the surface area is now unknown, while the burning rate is known. After solving for the instantaneous surface area, it is possible to integrate to get the web thickness. The difference between this web thickness and the thickness in a non-offset case is the offset.

Introduction

Talley Defense Systems uses the fundamental thickness/time burning rate (r_{TOT}) procedure for calculating solid propellant burning rates.

Definitions

t_{burn} Burning time established between $t_{ignition}$ and the point of maximum rate of change of curvature on the pressure-time record, i.e. tangent bisector method was used to determine the end of web burning time as illustrated in Figure B-20.

$t_{ignition}$ Ignition time, typically 10% P_{max}

t_{total} Total burning time from zero until chamber pressure reaches atmospheric conditions

P_{avg} Average pressure of the interval from time zero until t_{burn}

Pressure Integral (t_{burn})   Integral of the pressure-time curve from time zero until t_{burn}

Pressure Integral (t_{total})   Integral of the pressure-time curve from time zero until t_{total}
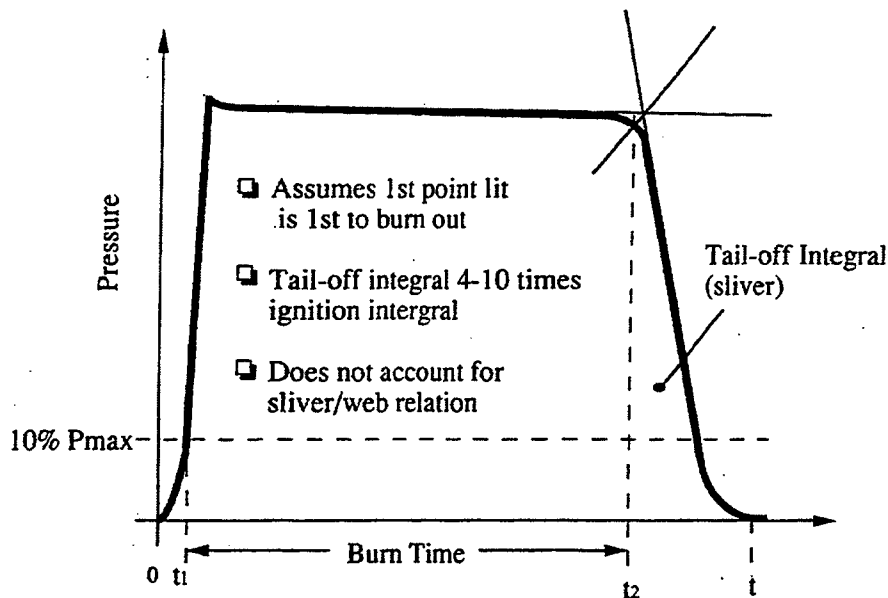
Figure B-20 Definitions of Tangent-Bisector Method

Description of the Method

The burning rate for RR I was found using the fundamental thickness/time burning rate (r_{TOT}) procedure by dividing the given web distance by t_{burn}.

Introduction

Thiokol uses both the fundamental thickness/time burning rate (r_{TOT}) and the mass balance burning rate (r_{MB}) procedures for calculating solid propellant burning rates.

Definitions

t_{burn} Burning time established between $t_{ignition}$ and the point of maximum rate of change of curvature on the pressure-time record, i.e. tangent bisector method was used to determine the end of web burning time as illustrated in Figure B-21.

$t_{ignition}$ Ignition time, typically 10% P_{max} was used at Thiokol / Wasatch, while 50% P_{max} was used at Thiokol / Huntsville when in operation[14]

t_{total} Total burning time from zero until chamber pressure reaches atmospheric conditions

P_{avg} Average pressure of the interval from time zero until t_{burn}

Pressure Integral (t_{burn})   Integral of the pressure-time curve from time zero until t_{burn}

Pressure Integral (t_{total})   Integral of the pressure-time curve from time zero until t_{total}
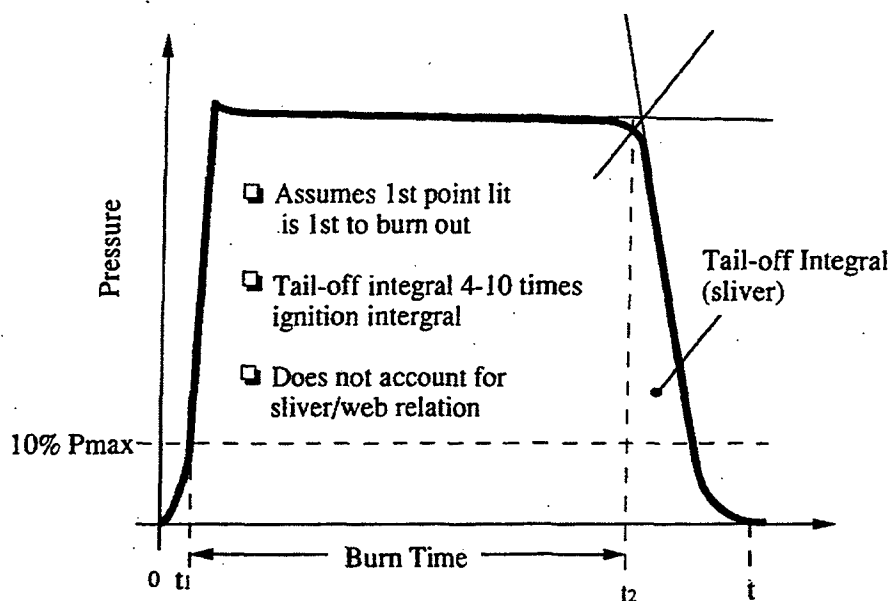
Figure B-21 Definitions of Tangent-Bisector Method

Description of the Method I

The burning rate for RR III, Group 1a (Baseline, concentric bore) was found using the fundamental thickness/time burning rate (r_{TOT}) procedure by dividing the given web distance by t_{burn}.

The burning rate for RR III, Group 2a (Non-concentric or offset bore) was found using the mass balance burning rate (r_{MB}) procedure by dividing a modified web distance by t_{burn}. The modified web

---

[14] Hessler, R.O., communication to WG016 based on experiences while working at Thiokol

distance was computed by multiplying it with the normalized ratio of the pressure integral (t_{burn}) to the pressure integral (t_{total}). The pressure integral ratio for each test was normalized to the corresponding case in the Baseline Group (1a).

The burning rate coefficient and exponent were computed from a linear regression of the burning rate versus pressure data of the combined groups.

Description of the Method II

Thiokol has also used a fundamental mass balance burning rate (r_{MB}) procedure similar to that described in APPENDIX B-25 for calculating solid propellant burning rates.
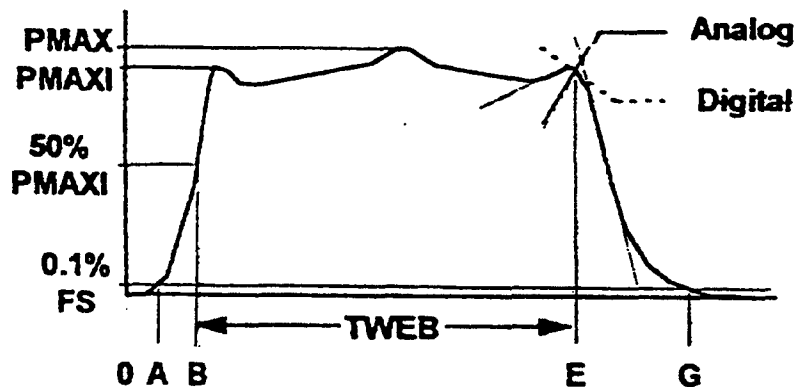
Figure B-22 Thiokol Standard Definitions on Pressure – Time Plot

The Thiokol standard TX3 definitions in use, which were developed during the period 1967 – 1978 are as shown in Figure B-22 and the equations below.

$$TWEB = t_{WEB} = t_E - t_B \qquad \text{20.1}$$

$$r_p = \frac{\int_B^E p\,dt}{\int_A^G p\,dt} \qquad \text{20.2}$$

$$r_b = \frac{0.6415\, r_p - 0.00905}{t_{WEB}} \qquad \text{20.3}$$

$$P_{AVGW} = \frac{\int_B^E p\,dt}{t_{WEB}} \qquad \text{20.4}$$

$$A_b = \frac{V_{drwg}}{0.6415} \qquad \text{20.5}$$

$$A_t = 0.5(A_{ti} + A_{tf}) \qquad \text{20.6}$$

$$K_n = \frac{A_b}{A_t} \qquad \text{20.7}$$

$$r_{bref} = r_b \left(K_{nref} \middle/ K_n \right)^{(nref\,(1-nref))}$$

20.8

$$P_{avgref} = P_{avgw} \left(K_{nref} \middle/ K_n \right)^{\left(1 \middle/ (1-nref) \right)}$$

20.9

And correcting for statistical analysis

$$r_{corr} = r_{bref} \left(m_b \middle/ r_{bmean} \right)$$

20.10

The TX3 definitions shown here were developed by Vellacott c1960. Vellacott was an attendee of the US burning rate workshops of that period. Hessler has examined the mass conservation equations shown, and found that the TX3 definitions of burning rate are basically sound. In particular the web integral r_p of Equation 20.2 arises naturally. The burning rate r_b in Equation 20.3 is determined using the web thickness (0.6415 in) corrected for the fraction of the web burned during the web time (r_p). This definition assumes that C* for the web time and the total time are equal. In application the drawing web thickness is normally used. The web thickness is also adjusted by subtracting a numerical constant (0.00905 in), reflecting a nominal cure shrinkage correction.

Introduction

The Hessler / Glick (HG) method employs an iterated two-point thickness/time burning rate (r_{HG}) procedure for calculating solid propellant burning rates. A discussion of the HG procedure is provided here, while a more detailed explanation of the procedure is available in APPENDIX B-27.

Definitions

See APPENDIX B-27

Description of Method

Virtually all the burning rate measurements depend on one of the two burning rate definitions, r_{TOT} or r_{MB}, with various time point definitions. Well-established industrial procedures are routinely used for both rate definitions. Which definition is better? While r_{TOT} will be in error when burnout is non-instantaneous (as usually observed), r_{MB} will be in error when mass storage is neglected. HG avoids both errors by a modified r_{TOT} procedure explicitly recognizing non-instantaneous burnout. Two r_{TOT} measurements are made using the average web thickness: r_{bi} using the initial burnout time definition t_{Ei}, and r_{bf} using the final burnout time definition t_{Ef}. The two individual measurements, after correction to a common pressure, and iterated with similar motors to determine the proper exponent, will still be in error because W_{avg} is not the web thickness that should be used in either instance. However, the signs of the errors are opposite for the two measurements, so averaging the two tends to eliminate the error. The result of the two-point measurement procedure may be stated as a burning rate definition

$$r_{HG}(p_{nbi}) = \frac{1}{2}\left[r_{TOTi} + r_{TOTf}\left(\frac{p_{nbi}}{p_{nbf}} \right)^n \right]$$

21.1

---

[15] Hessler R.O. and Glick R.L., "Comparison of Burning Rate Calculation Methods," JANNAF Combustion Meeting, West Palm Beach, FL, USA, 27-31 October 1997

[16] Hessler R.O. and Glick R.L., "Behavior of Pressure Derivatives During Burnout of Simulated Rocket Motors," JANNAF Combustion Meeting, West Palm Beach, FL, USA, 27-31 October 1997.

[17] Hessler R.O. and Glick R.L., "Consistent Definition for Burning Rate Measurement in Solid Rocket Motors," Memorandum to WG016, Jan 1998.

[18] Hessler R.O. and Glick R.L., "Consistent Definition for Burning Rate Measurement in Solid Rocket Motors," FGV Fizika Goreniya i Vzryva, Special Issue, Vol. 36, No. 1, Jan-Feb 2000. Presented at the Workshop on "Errors and Noise in Energetic Material Combustion Experiments", Politecnico di Milano, Milan, Italy, 15-16 March 1999.

Introduction

Miller and Barrington reviewed both fundamental thickness/time burning rate (r_{TOT}) and the mass balance burning rate (r_{MB}) procedures for calculating solid propellant burning rates, including several methods for defining the start and end of burning. The mass balance method reviewed was exactly the common Brooks mass balance (r_{MB}) procedure for calculating solid propellant burning rates. Refer to APPENDIX B-9 for a summary of the Brooks analysis procedure.
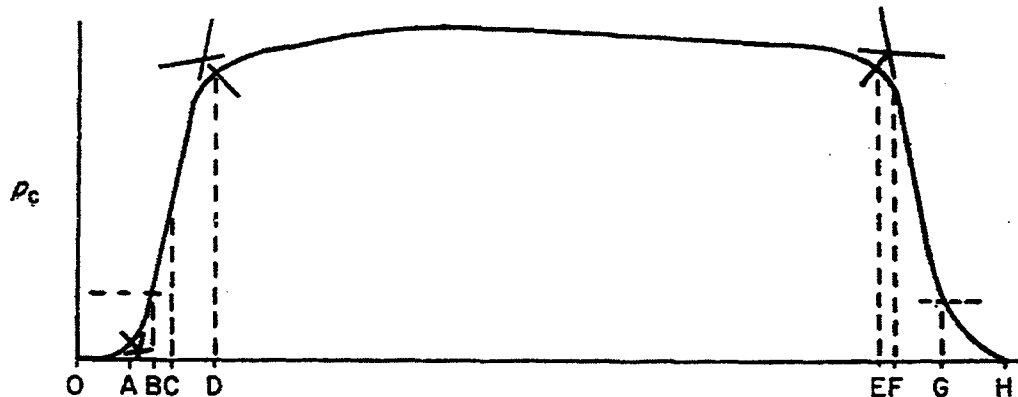
Definitions

Fig. B-23 Miller & Barrington Burning Time Definitions

The surface ignition time may be identified with various points on the primary rise portion of the trace (Fig. B-23):

1. First pressure raise (point O)
2. The inverse tangent bisector (point A),
3. A fixed pressure or a fixed percentage of the average or maximum pressure (point B),
4. The initial inflection (point C),
5. The tangent bi-sector (point D).

The web burnout time may likewise be identified by various points on the pressure decay portion of the trace (Figure B-23):

1. The aft tangent bisector (point E),
2. The point to maximum rate of change of curvature during tail-off (point F),
3. A fixed pressure or fixed percentage of the average or maximum pressure (point G),
4. Point when pressure returns to zero (Point H).

Description of Methods

When Miller and Barrington conducted their review in the late 1960's the fundamental thickness/time burning rate (r_{TOT}) procedure for calculating solid propellant burning rates was the widely held practice. Burning rate was determined by

$$r_b = \frac{w_b}{t_b} \qquad 22.1$$

[19] Miller, W.H. and Barrington, D.K., "A Review of Contemporary Solid Rocket Motor Performance Prediction Techniques," Journal of Spacecraft and Rockets, 7 (3): 225-237, 1970

While web w_b was readily measured, establishment of t_b involves the identification of surface ignition time and web burnout time on the pressure-time trace, as shown in Figure B-23. Miller and Barrington reviewed several techniques, as defined above, but indicated no one method seemed to have proven superior in all applications during the late-1960s.

Miller and Barrington indicated in their review that, based upon data provided by Brooks, using pressure integrals for determining the burning time, such as

$$t_b = (t_E - t_D) \cdot \frac{\int_O^H p_c \cdot dt}{\int_D^E p_c \cdot dt} \qquad 22.2$$

may minimize motor-to-motor variation (e.g. due to sliver or nozzle erosion effects on tail-off). This is of course the rationale for the original development of the mass balance burning rate (r_{MB}) procedures for calculating solid propellant burning rates.

Comments

The latter method for determining burning rate is also recognizable as the common Brook mass balance method. It may be rewritten as:

$$r_{aver} = \frac{w_b \cdot p_{aver}}{I_{pt}} \qquad 22.3$$

The use of tangent bisector is a difficult technique since there are often no regions of constant derivatives on which to base the tangents. Consequently, tangent bisector methods are highly arbitrary and subjective leading to variation between motors and facilities. Moreover, tangent bisector definitions are ad hoc, and generally not tied very closely to the physics of motor operation. Although there is plausible reason for this approximation for initial burnout, the application to the front of the trace is arbitrary.

The Miller and Barrington work[19] was originally presented as AIAA Paper 69-732 at the AIAA 5th Propulsion Joint Specialist Conference, Colorado Springs, CO, June 1969. The work was based on a survey conducted under Contract NAS3-11210 with the NASA Design Criteria Office, Lewis Research Center, during the preparation of a Design Criteria Monograph, which was ultimately published.[20]

---

[20] "Solid Rocket Motor Performance Analysis and Prediction," NASA Space Vehicle Design Criteria (Chemical Propulsion) NASA SP-8039, May 1971.

Introduction

The Thickness/Time burning rate (r_{TOT}) procedure is the simplest and most fundamental burning rate definition and analysis procedure.

Definitions

b burning rate coefficient, constant

n burning rate exponent, constant

p motor pressure

$$p_b = \frac{\int_{t_B}^{t_E} p\, dt}{t_E - t_B}$$ time-averaged pressure, usually associated with a measured burning rate

$$p(r_{meas}) \equiv p_{nb} = \left(\frac{\int_{t_B}^{t_E} p^n\, dt}{t_E - t_B} \right)^{\frac{1}{n}}$$ rate-averaged pressure, which should be associated with measured rates.

For exponent n less than unity, the case for most propellants of engineering interest, rate-averaged pressure is less than time-averaged pressure. Consequently, use of time-averaged pressure p_b results in rates corrected to reference pressure that are low.

p_{ref} reference pressure for reference burning rate

$p(r_{meas})$ pressure associated with the measured burning rate r_{meas}

$$r_{ref} = r_{meas} \left(\frac{p_{ref}}{p(r_{meas})} \right)^n$$ reference burning rate

$$r_{TOT} = \frac{\tau_E - \tau_B}{t_E - t_B} = \frac{\tau_b}{t_b}$$ fundamental thickness/time burning rate definition r_{TOT}

t time

T_i initial temperature

τ_{avg} average web thickness

r_{meas} measured burning rate

t_A start of motor operation, midpoint of the time interval immediately preceding the first perceptible rise in chamber pressure

t_G end of motor operation, midpoint of the time interval immediately preceding the last perceptible decline in chamber pressure

t_b burning time, $t_b = t_E - t_B$

t_B beginning of burning, t_B is the midpoint of the time interval immediately preceding the first perceptible rise in dp/dt on the last sustained pressure rise to equilibrium motor operation, primarily targets the "knee of the curve"

t_E ending of burning

t_{Ei} generally $t_E = t_{Ei}$ for most burning rate analysis methods, with the exception of the HG Method as described in APPENDICIES B-21 and B-27. If used, it is defined as the midpoint of the time interval immediately preceding a negative step to negative value of d^2p/dt^2 during the blowdown period after the end of equilibrium motor operation.

t_{Ef} an additional end of burn time used in an effort to more accurately account for web burned during the pressure tailoff. If used, it is defined as the midpoint of the time interval immediately preceding the positive step to positive value of d^2p/dt^2 at or following the end of equilibrium motor operation

Description of Method

Fig. B-24 Thickness/Time Burning Rate (r_{TOT}) Procedure. This is the simplest and most fundamental burning rate definition and analysis procedure.

Introduction

The iterated thickness/time burning rate (r_{TOTn}) procedure differs from the most commonly used thickness/time rate procedure (APPENDIX B-23) in the use of the rate-averaged pressure p_{nb} as the associated pressure and the iteration to determine exponent n. The iteration typically converges on the fourth iteration.

Definitions

b burning rate coefficient, constant

n_{old} burning rate exponent, old iterated value

n_{new} burning rate exponent, new iterated value

p motor pressure

$$p_b = \frac{\int_{t_B}^{t_E} p \, dt}{t_E - t_B}$$ time-averaged pressure, usually associated with a measured burning rate

$$p(r_{meas}) \equiv p_{nb} = \left(\frac{\int_{t_B}^{t_E} p^n \, dt}{t_E - t_B} \right)^{\frac{1}{n}}$$ rate-averaged pressure, which should be associated with measured rates.

For exponent n less than unity, the case for most propellants of engineering interest, rate-averaged pressure is less than time-averaged pressure. Consequently, use of time-averaged pressure p_b results in rates corrected to reference pressure that are low.

p_{ref} reference pressure for reference burning rate

$p(r_{meas})$ pressure associated with the measured burning rate r_{meas}

$$r_{ref} = r_{meas} \left(\frac{p_{ref}}{p(r_{meas})} \right)^n$$ reference burning rate

$$r_{TOT} = \frac{\tau_E - \tau_B}{t_E - t_B} = \frac{\tau_b}{t_b}$$ fundamental thickness/time burning rate definition r_{TOT}

r_{TOTn} iterated thickness/time burning rate,

t time

T_i initial temperature

τ_{avg} average web thickness

r_{meas} measured burning rate

t_A start of motor operation, midpoint of the time interval immediately preceding the first perceptible rise in chamber pressure

t_G end of motor operation, midpoint of the time interval immediately preceding the last perceptible decline in chamber pressure

t_b burning time, $t_b = t_E - t_B$

t_B beginning of burning, t_B is the midpoint of the time interval immediately preceding the first perceptible rise in dp/dt on the last sustained pressure rise to equilibrium motor operation, primarily targets the "knee of the curve"

t_E ending of burning

t_{Ei} generally $t_E = t_{Ei}$ for most burning rate analysis methods, with the exception of the HG Method as described in APPENDICIES B-21 and B-27. If used, it is defined as the midpoint of the time interval immediately preceding a negative step to negative value of d^2p/dt^2 during the blowdown period after the end of equilibrium motor operation.

t_{Ef} an additional end of burn time used in an effort to more accurately account for web burned during the pressure tailoff. If used, it is defined as the midpoint of the time interval

immediately preceding the positive step to positive value of d^2p/dt^2 at or following the end of equilibrium motor operation
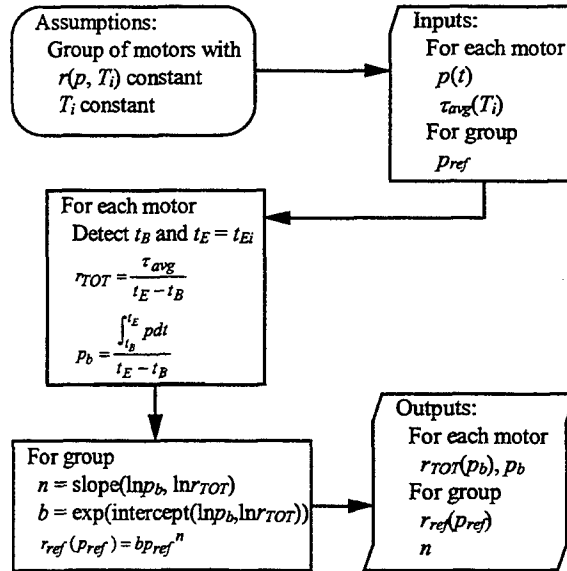

Description of Method

Fig. B-25 Iterated Thickness/Time Burning Rate (r_{TOTn}) Procedure. This procedure differs from the most commonly used Thickness/Time Rate procedure in the use of p_{nb} as the associated pressure and the iteration to determine exponent n. The iteration has typically converged on the fourth iteration.

APPENDIX B-25: REFERENCE
MASS BALANCE RATE (R_{MB})

Introduction

The mass balance burning rate (r_{MB}) procedure differs from the thickness/time rate procedure only in the requirement to detect endpoints of motor operating time and inclusion of the integral ratio in the burning rate definition.

Definitions

α_m interpreted as a correction to either the web thickness, time

b burning rate coefficient, constant

n burning rate exponent, constant

p motor pressure

$$p_b = \frac{\int_{t_B}^{t_E} p\, dt}{t_E - t_B}$$ time-averaged pressure, usually associated with a measured burning rate

$$p(r_{meas}) \equiv p_{nb} = \left(\frac{\int_{t_B}^{t_E} p^n dt}{t_E - t_B} \right)^{\frac{1}{n}}$$ rate-averaged pressure, which should be associated with measured rates.

         For exponent n less than unity, the case for most propellants of engineering interest, rate-averaged pressure is less than time-averaged pressure. Consequently, use of time-averaged pressure p_b results in rates corrected to reference pressure that are low.

p_{ref} reference pressure for reference burning rate

$p(r_{meas})$ pressure associated with the measured burning rate r_{meas}

$$r_{MB} = \frac{(\tau_G - \tau_A)}{(t_E - t_B)} \frac{\int_{t_B}^{t_E} p\, dt}{\int_{t_A}^{t_G} p\, dt} = \frac{\tau_{avg}}{t_b} \alpha_m$$ fundamental mass balance burning rate, r_{MB}, neglecting mass storage

$$r_{ref} = r_{meas} \left(\frac{p_{ref}}{p(r_{meas})} \right)^n$$ reference burning rate

t time

T_i initial temperature

τ_{avg} average web thickness

r_{meas} measured burning rate

t_A start of motor operation, midpoint of the time interval immediately preceding the first perceptible rise in chamber pressure

t_G end of motor operation, midpoint of the time interval immediately preceding the last perceptible decline in chamber pressure

t_b burning time, $t_b = t_E - t_B$

t_B beginning of burning, t_B is the midpoint of the time interval immediately preceding the first perceptible rise in dp/dt on the last sustained pressure rise to equilibrium motor operation, primarily targets the "knee of the curve"

t_E ending of burning

t_{Ei} generally $t_E = t_{Ei}$ for most burning rate analysis methods, with the exception of the HG Method as described in APPENDICIES B-21 and B-27. If used, it is defined as the midpoint of the time interval immediately preceding a negative step to negative value of d^2p/dt^2 during the blowdown period after the end of equilibrium motor operation.

t_{Ef} an additional end of burn time used in an effort to more accurately account for web burned during the pressure tailoff. If used, it is defined as the midpoint of the time interval

immediately preceding the positive step to positive value of d^2p/dt^2 at or following the end of equilibrium motor operation
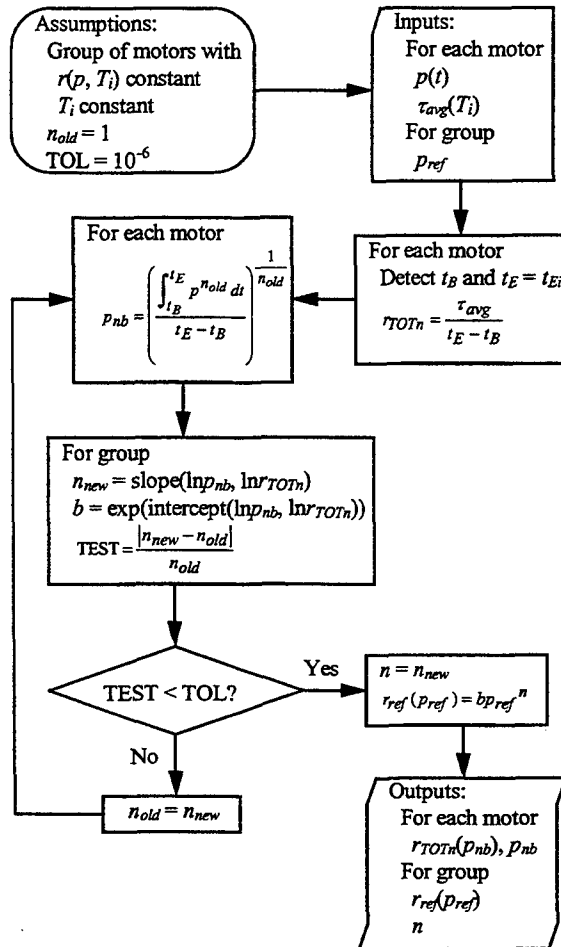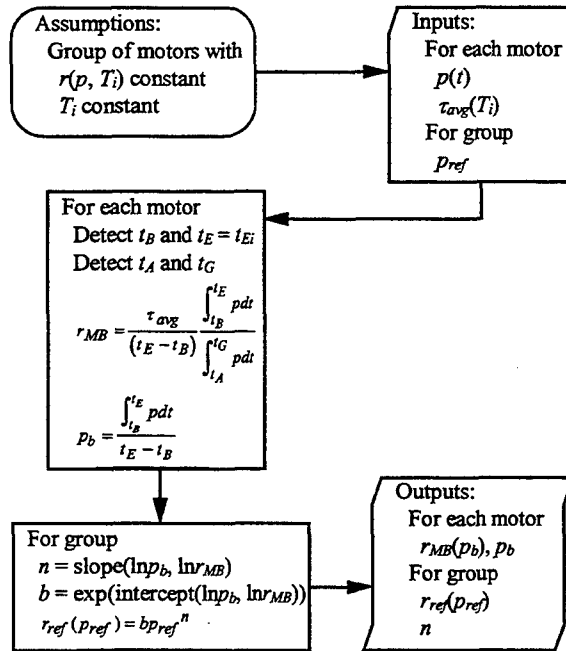
Description of Method

Fig. B-26 Mass Balance Burning Rate (r_{MB}) Procedure. This procedure differs from the Thickness/Time Rate procedure only in the requirement to detect endpoints of motor operating time and inclusion of the integral ratio in the burning rate definition.

APPENDIX B-26: REFERENCE
ITERATED MASS BALANCE RATE (R_{MBn})

Introduction

The iterated mass balance burning rate (r_{MBn}) procedure differs from the common mass balance rate procedure (APPENDIX B-25) in the use of the rate-averaged pressure p_{nb} as the associated pressure and the iteration to determine exponent n.

Definitions

α_m interpreted as a correction to either the web thickness, time

b burning rate coefficient, constant

n_{old} burning rate exponent, old iterated value

n_{new} burning rate exponent, new iterated value

p motor pressure

$$p_b = \frac{\int_{t_B}^{t_E} p\, dt}{t_E - t_B}$$ time-averaged pressure, usually associated with a measured burning rate

$$p(r_{meas}) \equiv p_{nb} = \left(\frac{\int_{t_B}^{t_E} p^n\, dt}{t_E - t_B} \right)^{\frac{1}{n}}$$ rate-averaged pressure, which should be associated with measured rates.

For exponent n less than unity, the case for most propellants of engineering interest, rate-averaged pressure is less than time-averaged pressure. Consequently, use of time-averaged pressure p_b results in rates corrected to reference pressure that are low.

p_{ref} reference pressure for reference burning rate

$p(r_{meas})$ pressure associated with the measured burning rate r_{meas}

$$r_{MBn} = \frac{\tau_{avg} \int_{t_B}^{t_E} p\, dt}{(t_E - t_B) \int_{t_A}^{t_G} p\, dt} = \frac{\tau_{avg}}{t_b} \alpha_m$$ iterated mass balance burning rate, r_{MBn}, neglecting mass storage

$$r_{ref} = r_{meas} \left(\frac{p_{ref}}{p(r_{meas})} \right)^n$$ reference burning rate

t time

T_i initial temperature

τ_{avg} average web thickness

r_{meas} measured burning rate

t_A start of motor operation, midpoint of the time interval immediately preceding the first perceptible rise in chamber pressure

t_G end of motor operation, midpoint of the time interval immediately preceding the last perceptible decline in chamber pressure

t_b burning time, $t_b = t_E - t_B$

t_B beginning of burning, t_B is the midpoint of the time interval immediately preceding the first perceptible rise in dp/dt on the last sustained pressure rise to equilibrium motor operation, primarily targets the "knee of the curve"

t_E ending of burning

t_{Ei} generally $t_E = t_{Ei}$ for most burning rate analysis methods, with the exception of the HG Method as described in APPENDICIES B-21 and B-27. If used, it is defined as the midpoint of the time interval immediately preceding a negative step to negative value of d^2p/dt^2 during the blowdown period after the end of equilibrium motor operation.

t_{Ef} an additional end of burn time used in an effort to more accurately account for web burned during the pressure tailoff. If used, it is defined as the midpoint of the time interval

immediately preceding the positive step to positive value of d^2p/dt^2 at or following the end of equilibrium motor operation

Description of Method

Assumptions:
Group of motors with
$r(p, T_i)$ constant
T_i constant
$n_{old} = 1$
TOL $= 10^{-6}$

Inputs:
For each motor
$p(t)$
$\tau_{avg}(T_i)$
For group
p_{ref}

For each motor
Detect t_B and $t_E = t_{Ei}$
Detect t_A and t_G

$$r_{MBn} = \frac{\tau_{avg}}{(t_E - t_B)} \frac{\int_{t_B}^{t_E} p\,dt}{\int_{t_A}^{t_G} p\,dt}$$

For each motor

$$p_{nb} = \left(\frac{\int_{t_B}^{t_E} p^{n_{old}}\,dt}{t_E - t_B} \right)^{\frac{1}{n_{old}}}$$

For group
$n_{new} = \text{slope}(\ln p_{nb}, \ln r_{MBn})$
$b = \exp(\text{intercept}(\ln p_{nb}, \ln r_{MBn}))$
$$\text{TEST} = \frac{|n_{new} - n_{old}|}{n_{old}}$$

TEST < TOL?

Yes

$n = n_{new}$
$r_{ref}(p_{ref}) = b p_{ref}{}^n$

No

$n_{old} = n_{new}$

Outputs:
For each motor
$r_{MBn}(p_{nb}), p_{nb}$
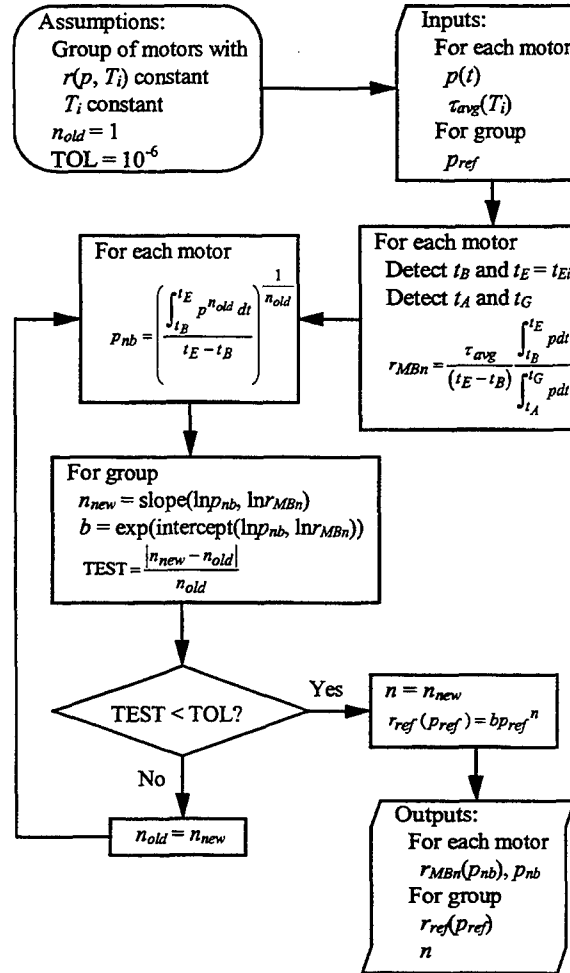For group
$r_{ref}(p_{ref})$
n

Fig. B-27 Iterated Mass Balance Burning Rate (r_{MBn}) Procedure. This procedure differs from the common Mass Balance rate procedure in the use of p_{nb} as the associated pressure and the iteration to determine exponent n.

APPENDIX B-27: REFERENCE
ITERATED TWO-POINT THICKNESS/TIME RATE (R$_{HG}$)

Introduction

The iterated two-point thickness/time burning rate (r_{HG}) differs from the iterated thickness/time rate (r_{TOTn}) procedure (APPENDIX B-24) by inclusion of a second measurement based on final burnout time t_{Ef} and in the use of an intermediate correction of the second measurement to the rate-averaged pressure p_{nb}.

Definitions

b burning rate coefficient, constant

n_{old} burning rate exponent, old iterated value

n_{new} burning rate exponent, new iterated value

p motor pressure

$p_b = \dfrac{\int_{t_B}^{t_E} p\,dt}{t_E - t_B}$ time-averaged pressure, usually associated with a measured burning rate

$p(r_{meas}) \equiv p_{nb} = \left(\dfrac{\int_{t_B}^{t_E} p^n\,dt}{t_E - t_B}\right)^{\frac{1}{n}}$ rate-averaged pressure, which should be associated with measured rates.

             For exponent n less than unity, the case for most propellants of engineering interest, rate-averaged pressure is less than time-averaged pressure. Consequently, use of time-averaged pressure p_b results in rates corrected to reference pressure that are low.

p_{nbi} $p_{nbi} = \left(\dfrac{\int_{t_B}^{t_{Ei}} p^{n_{old}}\,dt}{t_{Ei} - t_B}\right)^{\frac{1}{n_{old}}}$ rate-averaged pressure at the initial burnout time t_{Ei},

p_{nbi} $p_{nbf} = \left(\dfrac{\int_{t_B}^{t_{Ef}} p^{n_{old}}\,dt}{t_{Ef} - t_B}\right)^{\frac{1}{n_{old}}}$ rate-averaged pressure at the final burnout time t_{Ei}

p_{ref} reference pressure for reference burning rate

$p(r_{meas})$ pressure associated with the measured burning rate r_{meas}

$r_{HG}(p_{nbi}) = \dfrac{1}{2}\left(r_{TOTi} + r_{TOTf}\left(\dfrac{p_{nbi}}{p_{nbf}}\right)^n\right)$ two-point measurement procedure burning rate definition

$r_{ref} = r_{meas}\left(\dfrac{p_{ref}}{p(r_{meas})}\right)^n$ reference burning rate

$r_{TOT} = \dfrac{\tau_E - \tau_B}{t_E - t_B} = \dfrac{\tau_b}{t_b}$ fundamental thickness/time burning rate definition r_{TOT}

r_{TOTi} $r_{TOTi} = \dfrac{\tau_{avg}}{t_{Ei} - t_B}$,   thickness/time burning rate using τ_{avg} and the initial burnout time t_{Ei}

r_{TOTf} $r_{TOTf} = \dfrac{\tau_{avg}}{t_{Ef} - t_B}$,   thickness/time burning rate using τ_{avg} and the final burnout time t_{Ei}

t time

T_i initial temperature

τ_{avg} average web thickness

r_{meas} measured burning rate

t_A start of motor operation, midpoint of the time interval immediately preceding the first perceptible rise in chamber pressure

t_G end of motor operation, midpoint of the time interval immediately preceding the last perceptible decline in chamber pressure

t_b burning time, $t_b = t_E - t_B$

t_B beginning of burning, t_B is the midpoint of the time interval immediately preceding the first perceptible rise in dp/dt on the last sustained pressure rise to equilibrium motor operation, primarily targets the "knee of the curve"

t_E ending of burning

t_{Ei} midpoint of the time interval immediately preceding a negative step to negative value of d^2p/dt^2 during the blowdown period after the end of equilibrium motor operation.

t_{Ef} midpoint of the time interval immediately preceding the positive step to positive value of d^2p/dt^2 at or following the end of equilibrium motor operation

Description of Method

Assumptions:
Group of motors with
$r(p, T_i)$ constant
T_i constant
$n_{old} = 1$
$TOL = 10^{-6}$

Inputs:
For each motor
$p(t)$
$\tau_{avg}(T_i)$
For group
p_{ref}

For each motor

$$p_{nbi} = \left(\frac{\int_{t_B}^{t_{Ei}} p^{n_{old}} dt}{t_{Ei} - t_B} \right)^{\frac{1}{n_{old}}}$$

$$p_{nbf} = \left(\frac{\int_{t_B}^{t_{Ef}} p^{n_{old}} dt}{t_{Ef} - t_B} \right)^{\frac{1}{n_{old}}}$$

For each motor
Detect t_B, t_{Ei}, and t_{Ef}

$$r_{TOTi} = \frac{\tau_{avg}}{t_{Ei} - t_B}$$

$$r_{TOTf} = \frac{\tau_{avg}}{t_{Ef} - t_B}$$

For each motor

$$r_{HG}(p_{nbi}) = \frac{1}{2}\left(r_{TOTi} + r_{TOTf}\left(\frac{p_{nbi}}{p_{nbf}}\right)^n \right)$$

For group
$n_{new} = \text{slope}(\ln p_{nbi}, \ln r_{HG})$
$b = \exp(\text{intercept}(\ln p_{nbi}, \ln r_{HG}))$

$$TEST = \frac{|n_{new} - n_{old}|}{n_{old}}$$

TEST < TOL?

Yes → $n = n_{new}$
$r_{ref}(p_{ref}) = b p_{ref}^{\,n}$

No → $n_{old} = n_{new}$

Outputs:
For each motor
$r_{HG}(p_{nbi})$, p_{nbi}
For group
$r_{ref}(p_{ref})$
n
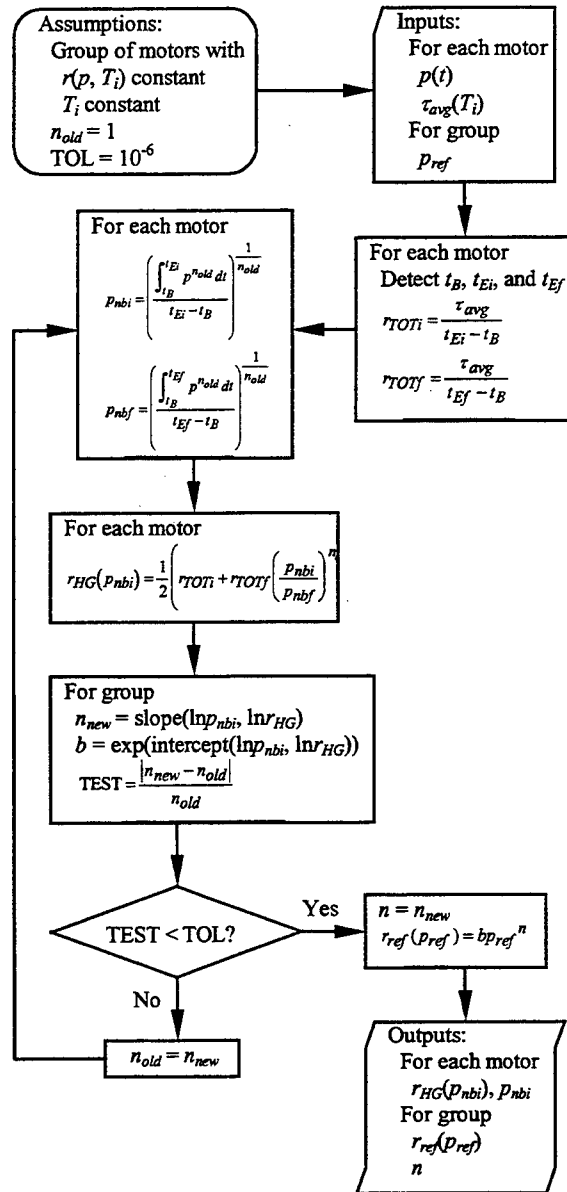
Fig. B-28 Iterated Two-Point Thickness/Time Burning Rate (r_{HG}) Procedure. This procedure differs from the Iterated Thickness/Time Rate (r_{TOTn}) procedure by inclusion of a second measurement based on final burnout time t_{Ef} and in the use of an intermediate correction of the second measurement to p_{nb}.

APPENDIX C

SIMULATED MOTOR DATA
ROUND ROBIN DESIGNS

APPENDIX C
Simulated Motor Data Round Robin Designs

TABLE OF CONTENTS

Appendicies C-1 through C-4 provide details of the design of the simulated pressure-time motor data used as a basis for assessing the burning rate analysis methods. A brief summary of some of the methods was provided in Sections 3 and 4. Table 9 of Section 5 lists those methods applied to the Round Robin (RR) exercises.

APPENDIX C-1: ROUND ROBIN #1

SIMPLE END-BURNER GRAIN / FREDERICK CODE

Introduction

Round Robin #1 is based on GasGen Version 2.0 ('93). GasGen is a spreadsheet program based on a relatively straightforward simulation logic developed by WG016 member Dr. Robert Frederick at UAH, US. A simple end-burning grain as shown in Figure C-1 was simulated.
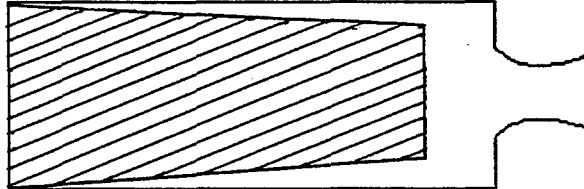

Figure C-1 RR #1 End-Burner Grain

Conditions of the Motor Configuration[1]

Range of expected pressure exponent	0.3 – 0.6
Propellant density	1.74 gm/cc
Propellant C*	1500 m/sec
Sampling rate range	1000 Hz
Pressure range – nominal	10 MPa (absolute)
Burning rate range – nominal	20 mm/sec
K ratio	200
Abnormality of pressure trace	> 10%
Nozzle throat diameter	5.0 mm
Burning time – nominal	5 sec
Grain web – nominal	100 mm
Pressure accuracy	3.6 KPa (arrived at by 15 MPa/4096 Hz sampling) Or +0.5% Full Scale (15 MPa)

Cases Examined [2]

Propellant burning rate and other propellant data, and propellant geometry data form the input. RR#1 consisted of pressure versus time data generated for the cases listed in Table C-1.

Table C-1 RR #1 Small Motor Ballistic Simulations Examined

Group	Cases	Perturbation
1	1	Neutral - Baseline
	2	Progressive
	3	Regressive
	4	Progressive with noise added

Pressure-time curves for these cases are shown in Chapter 4, Figure 4.6. All four cases used the same burning rate equation.

---

[1] Fry, R.S., Letter: "AGARD/PEP Working Group #27, Burning Rate Measurement Analysis Round Robin," 12 Jun 1997, and Enclosure 1 (3 pages): "AGARD/PEP ANALYSIS ROUND ROBIN Problem Definition."

[2] Fry, R.S., and Frederick, R., Diskette: "AGARD/PEP WG #27 Analysis Round Robin Data Cases 1-4," June 1997.

Results Obtained

Table C-2 presents the reduced data from the RR #1 simulations using a standard thickness/time method and several different start burn time definitions. Data tabulated for each simulation includes burn time, burning rate, and time-averaged and rate-averaged pressures. Primary data is taken from the "P'min > Web" entry for each simulation. The end of burning time t_E for a simulation equals its Burn Time for the "0% > Web" definition; beginning of burning time t_B may be calculated for each Burn Time definition by subtracting that Burn Time from t_E.

Table C-2 Reduced Data:
NATO RTO/AVT WG016 RR#1 Simulations[3]

CASE 1 - Neutral

Burn Time Definition	Burn Time	Rate	Pavg \<Time>	Pavg \<Rate>
P'min > Web	5.142	19.62548	9.96271	9.92309
0% > Web	5.142	19.62548	9.96271	9.92345
10% > Web	5.120	19.70980	10.00384	9.98540
50% > Web	5.078	19.87282	10.06188	10.05822

CASE 2 - Progressive

Burn Time Definition	Burn Time	Rate	Pavg \<Time>	Pavg \<Rate>
P'min > Web	5.002	20.17477	10.42713	10.37940
0% > Web	5.002	20.17477	10.42713	10.37983
10% > Web	4.978	20.27204	10.47536	10.45237
50% > Web	4.929	20.47356	10.54639	10.54068

CASE 3 - Regressive

Burn Time Definition	Burn Time	Rate	Pavg \<Time>	Pavg \<Rate>
P'min > Web	5.290	19.07641	9.50695	9.47047
0% > Web	5.290	19.07641	9.50695	9.47080
10% > Web	5.268	19.15607	9.54501	9.52800
50% > Web	5.226	19.31003	9.59775	9.59373

CASE 4 – Progressive with Noise Added

Burn Time Definition	Burn Time	Rate	Pavg \<Time>	Pavg \<Rate>
P'min > Web	5.783	17.45015	8.19181	8.11169
0% > Web	5.833	17.30057	8.12253	8.00393
10% > Web	5.734	17.59927	8.25834	8.21027
50% > Web	5.605	18.00432	8.37441	8.34877

---

[3] Hessler, R.O., "An Analysis of Burning Rate Round Robin Data", JANNAF Combustion Meeting, West Palm Beach, CPIA Pub 662, Vol I, PP 521-526, October 1997.

APPENDIX C-2: ROUND ROBIN #2

2 x 4 CYLINDRICAL PERFORATED (CP) GRAIN / SPP CODE

Introduction

Round Robin #2 is based on the Solid Performance Program (SPP) Version 7.0. The method of approach used by the SPP is to predict solid rocket motor performance by calculating deviations from ideal performance using a series of independent efficiency models.[4] The SPP analysis consists of two parts: nozzle performance and motor performance. The motor performance module, which was used to generate the RR #2 data, contains different design modules (for axisymmetric (2D) and 3D grains) and uses an internal ballistics module.

Conditions of Motor Configuration

The simulated motors have a cylindrically perforated (CP) propellant grain with 2-inch outer diameter, 1-inch inside diameter, and 3.75 inches long.[5] This particular design is commonly referred to as a "2-by-4" motor, a 2C1-3.75 motor, or a 2C1-4 motor. It is used at several facilities for burning rate measurements. The simple 2x4 motor grain as shown in Figure C-2 was simulated.
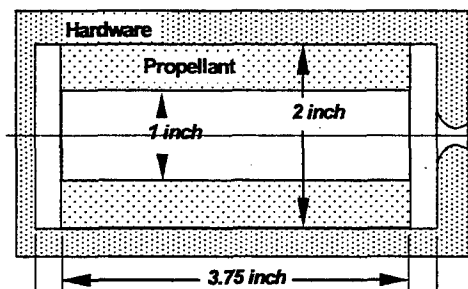

Figure C-2 Schematic of 2x4-Inch Test Motor Geometry

High pressure cases used a throat diameter of d_t = 0.30 in, while the low pressure cases used d_t = 0.50 in.

Propellant reactants (SPP Input) included

C 7.332	H 10.982	O 0.058	15%	-2970	298.15F	0.8070
N 1.	H 4.	O 4.	85%	-70690	298.15 F	1.9500

Propellant density: Cases 1-8   0.06206 lb/cu in
                        Cases 9-12   0.06365 lb/cu in

Cases Examined

Twelve different simulated pressures-time traces were generated using the Solid Performance Program (SPP) Version 7.0 for Round Robin #2. Table C-3 summarizes the design of the data cases.

The test cases are grouped in pairs, with one each at nominally 1.5 and 9 MPa, as shown in Fig. 1. The six pairs were designed to establish a baseline and to examine the effects of perturbations of variables in the simulations. Differences between pairs result from designed perturbations of L*, ignition, erosive burning, distortion of the cylindrical burning surface into a barrel shape by cure shrinkage and thermal stresses, and offset misalignment of the barrel-shaped bore. The most obvious differences among the pairs in this dataset are for Cases 9 through 12, which involve grain distortion

---

[4] SPP 2X4-inch ballistic simulations provided courtesy D. Coates, Science Engineering Applications.

[5] Fry, R.S., Letter: "NATO Research and Technology Organization (RTO) Working Group #27, Burning Rate Measurement Analysis Round Robin II," 12 June 1998, and Enclosure3 (6 pages): "Summary of Round Robin II Data Cases and Data Request."

and misalignment. The burn surface versus web thickness data as shown in Table C-4 was supplied to the participants.

Table C-3 RR#2 Small Motor Ballistic Simulations Examined

Case	Description	L*	Pmax	Ignition	Erosive Burning	Nozzle Erosion	Off-Axis Bore
1	Baseline	Low	Low				
2	Baseline	Low	High				
3	Baseline w/ Increased L*	High	Low				
4	Baseline w/ Increased L*	High	High				
5	Baseline w/ Igniter Effect	Low	Low	X			
6	Baseline w/ Igniter Effect	Low	High	X			
7	Baseline w/ Igniter Effect and Erosive Burning	Low	Low	X	X		
8	Baseline w/ Igniter Effect and Erosive Burning	Low	High	X	X		
9	Baseline w/ Igniter Effect, Erosive Burning and Nozzle Erosion	Low	Low	X	X	X	
10	Baseline w/ Igniter Effect, Erosive Burning and Nozzle Erosion	Low	High	X	X	X	
11	Baseline w/ Igniter Effect, Erosive Burning, Nozzle Erosion, and Off-Axis Bore	Low	Low	X	X	X	X
12	Baseline w/ Igniter Effect, Erosive Burning, Nozzle Erosion, and Off-Axis Bore	Low	High	X	X	X	X

Table C-4 Burn Surface versus Web Thickness for RR#2 Data Cases

	Cases 1-8	Cases 9-10	Cases 11-12
Burn Distance	Surface Area	Surface Area	Surface Area
0.00	16.4934	17.5156	17.6747
0.05	16.9960	17.9828	18.1417
0.10	17.4044	18.3532	18.5119
0.15	17.7186	18.6270	18.7855
0.20	17.9385	18.8041	18.9624
0.25	18.0642	18.8845	19.0426
0.30	18.0956	18.8682	19.0260
0.35	18.0327	18.7552	18.9128
0.40	17.8757	18.5455	18.7029
0.45	17.6243	6.2135	10.9855
0.50	0.0000	0.0000	0.0000

Round Robin #2 case results are examined more closely below:

Results Obtained

The stated objectives of the round robin were to clarify distinctions among several existing burning rate measurement analysis methods and to determine the causes of differences between them. The

RR #2 dataset contains several flaws, some of which are sufficient to severely obstruct attainment of the stated objectives. While flaws in the simulated dataset hamper definitive discrimination among timepoint definitions and among burning rate definitions, some general trends are suggested.

Any measurement of burning rate based on the interpretation of a motor pressure-time history depends upon several layers of definitions:

- Timepoint definitions for the beginning and ending(s) of burning,
- Burning rate definition (Thickness/Time, Mass Balance, or the Average Burnout modification of the Thickness/Time method),
- Definition of the associated (Rate- or Time-Averaged) pressure, and
- Correction to reference conditions

The following flaws in the RR #2 dataset are discussed in detail below

- An instantaneous initial pressure rise time
- Uncertainty in the web thickness burned
- Influence of reference pressure used due to other flaws

Instantaneous Initial Pressure Rise

All cases show a very steep pressure rise at ignition as compared in Figure C-3. Such a steep pressure rise is normally not observed in actual firings but is inherent to the ignition simulation subroutine implemented in the SPP code. The pressure vs. time traces for case 4 is much less steep due to a larger initial L* value (i.e. larger initial chamber volume).
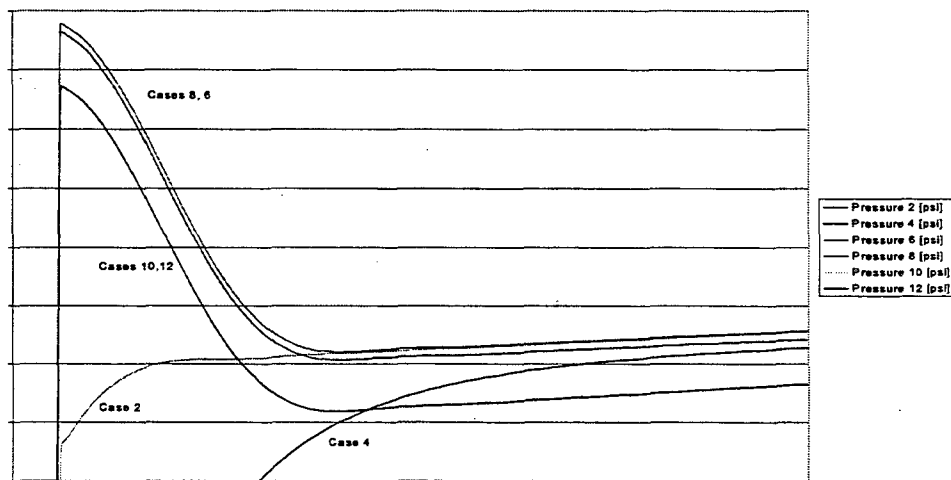

Figure C-3 RR#2 High Pressure (odd numbered) Cases at Ignition

The effect of erosive burning is very mild. Moreover, it represents negative erosion (Robillard-Lenoir relation). The effect of the eroding nozzle (Case 10) is clearly visible from the pressure vs. time trace as a reduced pressure during the test. The influence of a bore offset is not visible from the ignition transient of the test but can be seem from the prolonged tail-off part (Case 11 in Figure C-4).
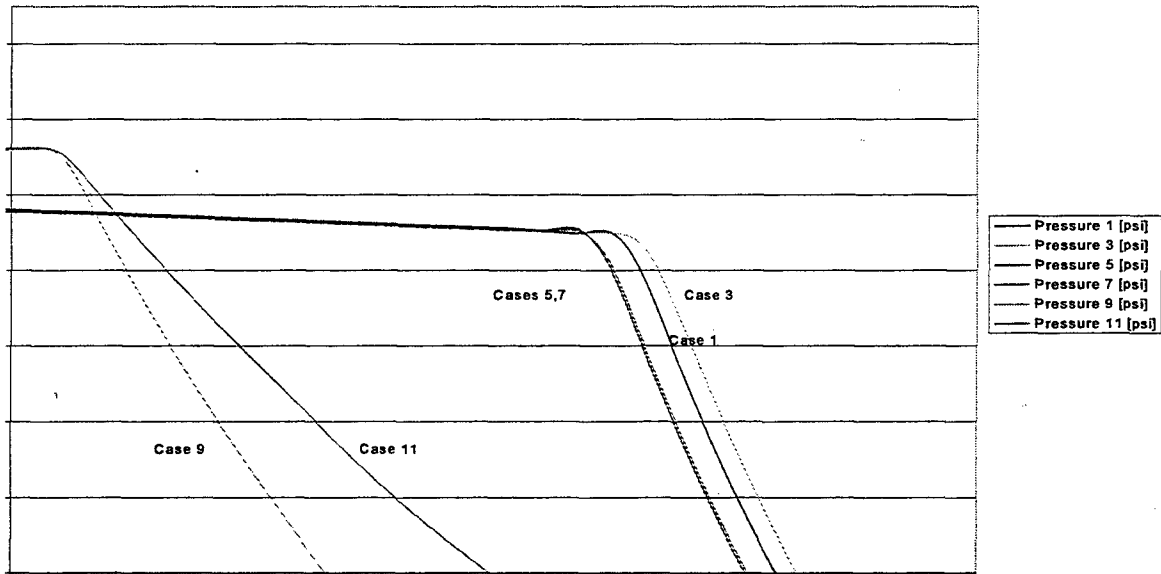
Figure C-4 RR#2 Low Pressure (even numbered) Cases at Tail-off

The high L* case experiences a tail-off later in the firing due to pressurization of the combustion chamber during the ignition transient. The igniter operation effectively reduces the burning time. The cases 1 through 7 show a similar behavior at tail-off. Peculiar is the slight upswing in the pressure at the unset of tail-off. This could be due to the so-called Friedman curl, however, SPP does not actually account for this. The Friedman curl accounts for liner effects on burning rate. When the burning propellant web approaches the liner (or casing) the burning rate will increase (decrease) as heat conducted into the propellant is accumulating (dissipated into the metal wall).
The source of the upswing might be the Spline functions used in correcting the SSP output data with a lower than 1 kHz sample rate to data with a sample rate of 1 kHz. Spline functions tend to have difficulty with gradients.

Moreover, due to a 'peculiarity' of the SPP code, the onset and end of burning occurred at pressures higher than zero pressure (30 psi equivalent to 0.2 MPa). The data cannot easily be corrected for this, which makes the application of certain methods (e.g. the method relying on 10 % P_{max}) more difficult.

Instantaneous initial pressure rise prevents discrimination among definitions for beginning of burning. All burnout definitions based on the "knee of the curve" will give the same timepoint within fundamental timescale resolution.[6] Interpolation to improve timescale resolution filters out the discontinuity at the initial burnout event, obviating the derivative-based definition for initial burnout. The final burnout event appears to occur well past the final timepoint, obviating the derivative-based final burnout definition. Consequently, the round robin results will be unable to discriminate between most timepoint definitions.

Burned Web Evaluation

For the data reduction all parties contributing to RR#2 used a web thickness of 12.7 mm (0.5 inch.). The web actually burned during the test may be different from this value. This will negatively affect the results and effectively will reduce the burning rate.

---

[6] This is inescapable until the simulation includes spatially varying pressure and rate, thermal discontinuities at the wall (Friedman Curl/Uncurl), formulation gradient at the wall, and external temperature gradients, all in combination with deformed geometry.

The pressure-time trace and the reference burning rate relation were used to back-calculate the web actually burned during each test. In Table C-5, the results are given showing the web consumed and the percentage of the total web burned. In interpreting these data, it should be realized that the curves used were not full curves in that they did not commence and finish at zero pressure but at about 2 bar. The effect will be negligible for the ignition transient, but will have an effect at the tail-off that is difficult to quantify.

Table C-5 RR #2 - Calculated Burned Web

Case Description	Case Number	Time at End of Burning [s]	Web Consumed[1] [mm]	Web Burned [%]	Web Remaining [%]
Baseline	1	1.766	12.301	96.86	3.14
	2	0.936	12.535	98.70	1.30
Large L*	3	1.766	12.318	96.99	3.01
	4	0.946	12.645	99.57	0.43
Ignition	5	1.756	12.275	96.65	3.35
	6	0.926	12.482	98.28	1.72
Erosive Burning	7	1.756	12.274	96.65	3.35
	8	0.936	12.500	98.43	1.57
Nozzle Erosion	9	1.716	11.608	91.40	8.60
	10	0.996	12.229	96.29	3.71
Off-Axis Bore	11	1.776	12.054	94.91	5.09
	12	0.966	12.396	97.61	2.39

[1] The available web is 12.7 mm (0.5 inch).

From the table it is clear that the assumption of a fully consumed web (using a thickness over time method) yields an error that depends on the particular test and on the definition used for the time points to determine the burning time. The web burned is less for the low-pressure cases as compared to the high-pressure cases. This would mean a relatively larger error for low-pressure tests as compared to the large pressure tests. Burning rates will be predicted too high with a larger deviation at the lower pressures than at the higher pressures. This results in a lower exponent.

Comparison of the furnished web thickness with the furnished surface-web tables makes it immediately clear that the furnished web thickness is the thickness at final burnout. However, the simulations appear to have ended before final burnout was reached.

Thickness/Time rate requires the thickness at initial burnout, and Mass Balance rate and Average Burnout rate require the average web thickness. Problems arise when one considers what values will be used.

Some participants may accept and use the furnished web thickness, thinking that it is the usually available design web thickness. Those who do so will get results that are in error by 5% to 15% because it isn't the web thickness they require, plus some unknown and variable additional error of order 5% because simulations stopped before complete burnout.
Some or all of the participants simply used the surface-web table and selected the value they needed with possibly varying degrees of accuracy. Those who did obtained results that were fairly close to the input rate, if they recognized and accounted for the premature ending of the simulations.

The availability of the surface-web tables for individual motors has created an artificial environment in which all burning rate definitions will produce almost identical results. At least within the fundamental timescale resolution at initial burnout, which appears to be 0.6% to 1.2%. However, this is just about the difference between the burning rate definitions when the appropriate web thickness is used, so the round robin results would seem unable to discriminate between rate definitions with much certainty.

Correction to Reference Pressure

Results for the different cases show varying degrees of bias as a result of the various perturbations and because of choice of associated pressure. Clarifying this point in future round robin results is possible, and would be a positive result.

The correction to reference pressure, itself, is well founded and generally accepted. The error for the round robin cases is dominated by the choice of associated pressure because of the extended tailoff of all cases, and is largely resolved by the associated pressure determination.

APPENDIX C-3: ROUND ROBIN #3

2 x 4 CYLINDRICAL PERFORATED (CP) GRAIN / HESSLER-GLICK CODE / Baseline Cases

Introduction

Round Robin #3 is based on a computer program, created by R.O. Hessler and R. Glick in support of the WG 016, to generate simulated motor data for research into burning rate measurement methods.[7] The cylindrical geometry, equilibrium burning, and bulk mode operation were chosen for study of the performance of burning rate measurement methods under known ideal conditions. The program also permits offset of the circular bore to study the effect of non-instantaneous burnout upon burning rate measurements. This model of a small motor ballistic behavior performed very well as a tool for understanding burning rate analysis methods as discussed further in Section 4.3.3. Simulations compared with of a group of real motors indicate general agreement, but more refinement of the simulation is needed to improve match during pressure rise and fall as discussed in connection with the results below.

The computer program based on the bulk equations of change generates simulated motor data that has the same overall character as real motors:
- An exponential pressure rise asymptotically approaching level operation,
- A period of level operation having gradual pressure changes consistent with the surface-web relation,
- An extended burnout process if web thickness variations are permitted, and
- An exponential pressure decay asymptotically approaching atmospheric pressure after final burnout.

Description of Simulation Code

The simulation program discussed here was developed for the specific purpose of exploring the effect of non-instantaneous burnout upon analysis procedures in otherwise "ideal" motors in support of the NATO RTO/AVT WG 016 objectives. Eccentricity (bore offset or off-axis bore) is used as a general analog for non-uniform web thickness. An abbreviated discussion of the prediction program[7] is provided here, highlighting the general assumptions and equations involving the mass generation and mass discharge rates. A description is included of a modeled case-bonded, eccentrically perforated cylindrical grain.

The following general assumptions were made:
- Hardware is rigid and stationary,
- Spatial gradients are negligible,
- Heat losses are negligible,
- Combustion products are a perfect gas,
- Thermochemical properties are constant, and
- Gases initially in the free volume are combustion products at initial propellant grain temperature.

With these assumptions, the conservation equations reduce to the bulk equations of change for the mass and energy contained in the chamber gas volume. The resulting system of equations is reduced to a set of four differential equations in four unknowns, chamber pressure p, gas temperature T, chamber volume V, and distance burned x. These equations with the mass generation and discharge expressions, summarized below, form the basis for the prediction.

The rate of gas generation at the burning surface is the product of the propellant density ρ_c, the burning rate r, and the burning surface area A_s.

---

[7] R.O. Hessler and R.L. Glick, "A Ballistic Prediction for Burning Rate Motors and Non-Instantaneous Burnout," memorandum in support of NATO RTO/AVT WG016, October 1998.

The propellant density is constant by assumption of constant thermochemical properties. Burning rate assumptions include:

- Propellant is homogeneous and at uniform temperature,
- Equilibrium burning begins at an ignition event, and
- Equilibrium burning continues until the burning surface goes to zero.

The propellant assumptions preclude formulation gradients and thermal gradients. Assumption of equilibrium burning rate neglects thermal wave and surface texture development, modified thermal wave near thermal property discontinuities (Friedman Curl/Uncurl), dynamic burning, and burning extinction.

Burning surface assumptions include:

- Propellant grain is a case-bonded right circular cylinder with eccentrically located circular perforation,
- Propellant grain is undeformed by cure or thermal shrinkage,
- Propellant burns on ends and interior cylindrical surface, and
- Ignition is simultaneous over the entire surface.

Mass is discharged through an ideal convergent-divergent nozzle. The nozzle throat area A_n is constant. The characteristic velocity C^* is the *chamber* C^*, dependent upon chamber temperature T, which is *not* the theoretical propellant C^*_f at flame temperature T_f.

Nozzle flow assumptions include:

- Fluid is a perfect gas,
- Flow is adiabatic and frictionless,
- Velocity is constant across any cross-section, and
- Sonic plane is at minimum area.

The uniform velocity assumption precludes flow separation or reversal at low pressures. The nozzle flow regime coefficient, K_d, is defined for three cases, sonic, sub-sonic, and no flow.

The final set of equations was solved numerically, using a standard fourth-order Runge-Kutta integrator routine with step size control.[8, 9] In the Mathcad 6+ implementation used here, the accuracy of the numerical integration is controlled by the background convergence tolerance, which was set to 10^{-6}, corresponding roughly to 6-digit accuracy in the calculations. In other implementations, there is likely a similar convergence tolerance.

Conditions of Motor Configuration

Motor Geometry
A typical 2x4-inch small motor with a cylindrically perforated (CP) propellant grain, commonly referred to as a 2C1-3.75 motor, or a 2C1-4 motor was again used for burning rate simulations as shown schematically in Fig. C-5. Cylindrical geometry is used to minimize web thickness variation. Transverse sections of the motor with the cylindrical perforation misaligned are shown in Fig. C-6. The section at the left in Fig. C-6 shows the geometry before-ignition, from which the maximum and minimum propellant web thicknesses are seen to depend on the degree of eccentricity ε.

[8] Press, W.H., Flannery, B.P., Teukolsky, S.A., and Vetterling, W.T., *Numerical Recipes, The Art of Scientific Computing*, Cambridge, Eng., UK, Cambridge University Press, 1989
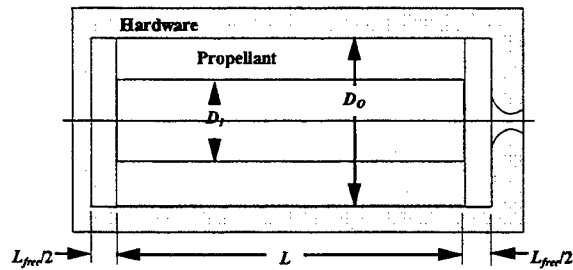[9] MathSoft, Inc., *Mathcad PLUS 6.0*, Cambridge, MA, USA, MathSoft, Inc., 1995

Fig. C-5 Schematic of 2X4-inch Test Motor Geometry Simulated[10]
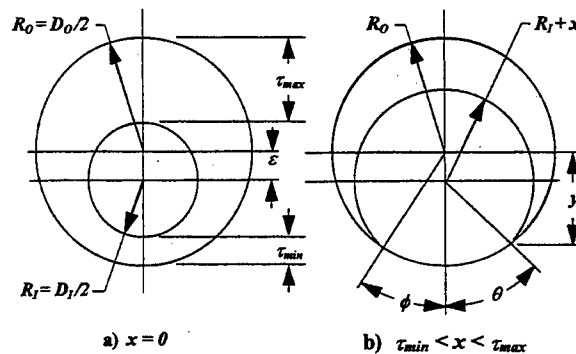

a) $x = 0$ b) $\tau_{min} < x < \tau_{max}$

**Fig. C-6 Section of Eccentrically Perforated Propellant Grain Simulation
a) Before Ignition, b) During Burnout. (Eccentricity greatly exaggerated.)**[10]

The beginning of burnout occurs when the distance burned x equals the minimum web τ_{min}. Burnout is complete when x equals the maximum web τ_{max}. These two events, initial and final burnout, define the ends of the burnout process.

Dimensions at temperature T_i = 294.22 K are:

     D_O = 50.80 mm D_i = 25.40 mm

     L = 95.25 mm L_{free} = 31.928 mm

The nozzle diameters were different for each motor in a group, and were included in the data files.

Propellant Properties
The propellant is homogeneous and at constant initial temperature T_i = 294.22 K. Arbitrary propellant properties have been used, and do not vary with pressure:

Density	1.72944 g/cc	C*	1566.0 m/s
Specific heat ratio:	1.1742		
Adiabatic flame temperature:	3121.67 K		
Molecular weight:	25.560 kg/kmole		

Burning Rate
The bulk equilibrium burning rate has the form $r = b\,p^n$, where b and n are constants. Values were not furnished to the participants.

Simulation Resolution
The simulation employs an adaptive Runge-Kutta procedure with convergence tolerance corresponding to 10^{-6}. The pressure values were subsequently truncated to a minimum of five

---

[10] Hessler R.O. and Glick R.L., "Behavior of Pressure Derivatives During Burnout of Simulated Rocket Motors," JANNAF Combustion Meeting, West Palm Beach, FL, USA, 27-31 October 1997.

significant figures, so pressure resolution is of order 0.003% or better. The sampling rate used for the simulation was 10kHz. With the minimum burning time about 0.8 sec, time resolution is 0.012% or better.

Cases Examined

Simulated pressure-time histories of two groups of motors shown in Table C-6 were distributed to the RR #3, Groups 1 & 2 participants as listed in Table 4.8. Group 1 was a group of five ideal motors to serve as a baseline against which the effects of various motor parameter variations upon burning rate measurement procedures could be compared. Group 2 was a perturbation of bore offset to simulate non-instantaneous burnout.

Table C-6 RR #3 Small Motor Ballistic Simulations Examined

Group	Cases	Perturbation
1	1-5	Baseline
2	6-10	Bore offset

Each group contains five motors, equally spaced in log pressure. The only difference between motors within a group is the nozzle size 10.5435, 9.3650, 8.3160, 7.3863, and 6.5608. The only difference between the two groups is the degree of eccentricity or offset of the cylindrical bore.

The two groups of simulated motors are simulated (Figures 4.18, 4.19 and 4.20), with nominal pressures of 3.5, 5, 7, 10, and 14 MPa. For motors having the same nozzle size in the two groups, the data is identical until the burnout process begins. After initial burnout, the tailoff is appreciably different.

The motor cavity is a right circular cylinder with a convergent nozzle at one end (Figure C-5). The propellant grain is a case-bonded right circular cylinder with a cylindrical bore or perforation. The bore centerline is coincident with case centerline in Group 1, but translated or offset a small amount in Group 2 (Figure C-6). Data reduced from real motors of the design dimensions provided indicates non-instantaneous burnout corresponding to 0.3 to 0.9% of web thickness. An intermediate bore offset was used in the simulations. The offset value is zero for Group 1, and is the same for all motors in Group 2. The value is not furnished.

The nozzle diameters are repeated from group to group, so the first motor in Group 1 (Case 1) has the same nozzle as the first motor in Group 2 (Case 6).

The simulation employs an adaptive Runge-Kutta procedure with convergence tolerance corresponding to 10^{-6}. The pressure values were subsequently truncated to a minimum of five significant figures, so pressure resolution is of order 0.003% or better. The sampling rate used for the simulation was 10kHz. With the minimum burning time about 0.8 sec, time resolution is 0.012% or better.

Results Obtained

Burning rate data reduced from the simulated motor data can be used to examine two specific questions considered critical to understanding of burning rate measurements:

- What is the bias (scale factor) and precision (non-reproducibility) of a given analysis procedure when applied to an ideal motor with perfect instrumentation?
- What is the effect of non-instantaneous burnout upon that analysis procedure?

The detailed analysis results are reviewed in detail in Chapter 4, Section 4.3.3.

A computer program based on the bulk equations of change was used to generate simulated motor data that has the same overall character as real motors. This model of a small motor ballistic behavior performed very well as a tool for understanding burning rate analysis methods as discussed further in

Section 4.3.3. The following simulation limitations were identified, which if mitigated can improve the model utility:

- The initial pressurization and final decay predicted by the simulation are appreciably more rapid than observed in real motors. This is believed due to heat losses to the hardware, which is not included in the simulation.
- The simulation does not predict the initial and final peaks often observed in real motors. These peaks are believed due to temporary modifications of burning rate caused by formulation gradients and/or non-equilibrium burning, which are not included in the simulation.
- The simulation does not predict the smoothly rounded "knee of the curve" at initial burnout usually observed in real motors; pressure in this region changes very abruptly. The rounded curve is believed due to temporary modifications of burning rate caused by formulation gradients and/or non-equilibrium burning, which are not included in the simulation.
- The simulation does not predict the mid-run "hump" usually observed in real motors. The mid-run "hump" is believed due to local modification of burning rate caused by formulation gradients caused by the propellant flow during casting, which is not included in the simulation.
- Analyses of real motor data indicate that burning rates are depressed significantly during the burnout process. This is suspected to be due to non-equilibrium burning and/or heat losses, which are not included in the simulation.

Some of these effects are illustrated by Hessler[11] in Figures C-7 and C-8.
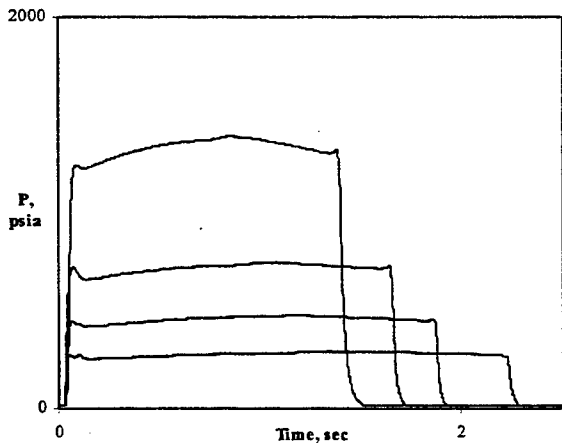

Figure C-7 Pressure-Time Histories of Real 2C1-3.75 Motors.

Four motors from one mix of an unspecified propellant, tested at the same initial propellant temperature.
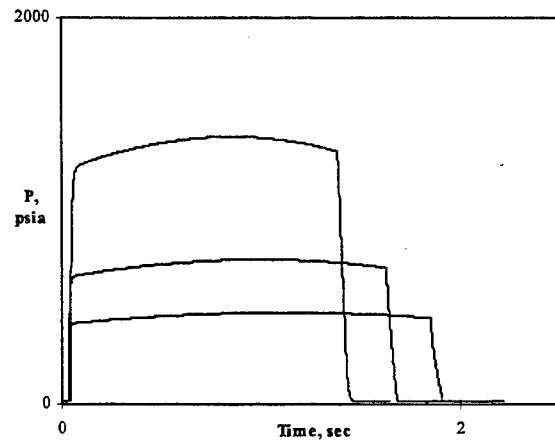

Figure C-8 Simulated 2C1-3.75 Pressure-Time Histories.

The higher-pressure motors of Figure C-7 were simulated, using arbitrary thermochemical properties. The low-pressure motor, for which the rate fell below the fitted rate-pressure line, was not simulated. Assumptions of propellant homogeneity and equilibrium burning rate exclude phenomena that cause the initial peak and the slight peak at initial burnout.

APPENDIX C-4: ROUND ROBIN #3X

2 x 4 CYLINDRICAL PERFORATED (CP) GRAIN / HESSLER-GLICK CODE / Expanded Cases

Introduction

Round Robin #3X is also based on the computer program, created by R.O. Hessler and R. Glick in support of the WG 016, to generate simulated motor data for research into burning rate measurement methods.[11] Motor and propellant information is examined for eight additional groups of simulated rocket motors beyond those examined in RR #3. These groups are designed to examine the effects of non-neutrality, L-star, further bore offset perturbations, and of higher rate, pressure, and exponent. Data typically unknown, such as the burning rate equation, bore offset, and randomized parameters were withheld from the participants.

Conditions of Motor Configuration

The original groups were designed to determine the intrinsic error of analysis procedures at modest rate and pressure, and to assess the effects of non-instantaneous burnout. The purpose of the present groups is to expand the non-instantaneous burnout perturbations, and add additional perturbations of non-neutrality, L-star, and of the rate-pressure regime. The perturbations and the resulting simulations are discussed below.

Motor Geometry
The motor cavity is a right circular cylinder with a convergent nozzle at one end as shown previously in Figure C-5. The propellant grain is a case-bonded right circular cylinder with a cylindrical bore or perforation. This geometry approximates 2C1-3.75 or "2x4" motors used at several US facilities. The geometry results in pressure-time histories that are nearly constant pressure (neutral), but are slightly convex, with a smooth maximum near mid-burn. The sampling rate was 10 kHz for all the groups except for group 9.

Nominal dimensions at temperature T_i = 294.22 K are:

D_O	50.80 mm	All groups
D_I	25.40 mm	All groups
L	95.25 mm	Groups 1-2, 5-10
	120.65 mm	Group 3
	69.85 mm	Group 4
L_{free}	31.928 mm	Groups 1-6, 9-10
	158.75 mm	Group 7
	Random	Group 8 (values withheld)

The different grain lengths of Groups 3 and 4 were selected to cause appreciable progressivity and regressivity, respectively. The free length for Group 7 is unrealistically large, but was necessary to match slower ignition rise rates observed in real motors with comparable rates, believed caused by heat losses, which are not included in the simulations.[11] The random free lengths of Group 8 approximate variations of thread engagement for motors with pipe threads.

Bore Offset
The centerline of the central perforation, or bore, is offset from case centerline for all groups to cause non-instantaneous burnout. Groups 3-4 and 7-8 have the same constant bore offset value as Group 2. Groups 5 and 9 have a different constant bore offset. The random bore offsets of Groups 6 and 10 approximate tailoff variations in real motors.[12] Values are not furnished.

---

[11] R.O. Hessler and R.L. Glick, "A Ballistic Prediction for Burning Rate Motors and Non-Instantaneous Burnout," memorandum in support of NATO RTO/AVT WG016, October 1998.

[12] Hessler, R.O., Glick, R.L., Jordan, F.W., and Fry, R.S. "Burning Rate Measurement in Batch Test Motors," JANNAF Combustion Meeting, Monterey, November 1996.

Nozzle Sizes

The nozzle diameters are different for each motor in a group, and are included in the data files. The nozzle diameters are repeated from group to group, where possible, but the diameters are different for Groups 3, 4, and 9. Nozzle sizes were selected to provide nominal pressures of 3.5, 5, 7, 10, and 14 MPa for all groups but Group 9. Nozzles for Group 9, which also has a higher rate, were set to provide nominal pressures of 3.5, 7, 14, 28, and 56 MPa.

Propellant

The propellant is homogeneous and at constant initial temperature T_i = 294.22 K. Arbitrary propellant properties have been used, and do not vary with pressure:

Density	1.72944 g/cc
Specific heat ratio:	1.1742
Adiabatic flame temperature:	3121.67 K
Molecular weight:	25.560

Burning Rate

The bulk equilibrium burning rate has the form $r = b\,p^n$, where b and n are constants. Values of the constants are not furnished. The burning rate for Group 9 is much higher than for the other groups.

Simulations

The data above was used to predict the pressure-time histories for each of the cases (Figures 4- and 4-), using a simulation program that does not consider heat losses, transient burning, or formulation gtradients.[11] Pressure values were truncated to a minimum of five significant figures at average pressure to provide resolution of order 0.003% or better. Time resolution was 0.012% or better for all groups. The sampling rate was increased above the 10kHz used for other groups to maintain time resolution with the higher rate of Groups 9 and 10.

Cases Examined

The present simulated motor data consists of 40 additional cases, arranged in groups of five, labeled Groups 3 through 10. These additional groups are mainly perturbations of the original Group 2, which had constant bore offset. The exception is Group 9, which is a perturbation from Group 5. The primary perturbations are listed in Table C-7 below.

Table C-7 RR #3X Small Motor Ballistic Simulations Examined

Group	Cases	Perturbation
3	11-15	Non-neutral trace shape (Progressive)
4	16-20	Non-neutral trace shape (Regressive)
5	21-25	Different constant bore offset
6	26-30	Random bore offset
7	31-35	Different constant L*
8	36-40	Random L*
9	41-45	Different rate equation and bore offset
10	46-50	Additional random bore offset

Results Obtained

Burning rate data reduced from the simulated motor data can be used to examine two specific questions considered critical to understanding of burning rate measurements:

- What is the bias (scale factor) and precision (non-reproducibility) of a given analysis procedure when applied to an ideal motor with perfect instrumentation?
- What is the effect of non-instantaneous burnout upon that analysis procedure?

The detailed analysis results are reviewed in Chapter 4, Section 4.3.4.

APPENDIX D

UNCERTAINTY AND ERROR ANALYSIS

APPENDIX D
Uncertainty and Error Analysis

TABLE OF CONTENTS

This Appendix provides details of uncertainty concepts as may be applied to analysis of experimental data. The principle reference for this Appendix is the "JANNAF Rocket Engine Performance Test Data Acquisition and Interpretation Manual," CPIA Pub 245, April 1975. This appendix supports discussions in Section 7 on Small Motor Data Quality.

APPENDIX D-1: UNCERTAINTY CONCEPTS

STATISTICAL BASIS OF UNCERTAINITY CONCEPTS

> The treatment of uncertainty in testing is based on established statistical methods.

For a measured value (or a calculated value), the first reaction is always - "that's the number." However, if the question is asked - "Are you 100 percent confident or would you rather take a small band around the value and say the true value lies in the band?" - most people would prefer to take the band. The wider the band is, the more confident we become that the true answer is within the band, but the less information we gain. For example, a band wide enough to enclose the true measured burning rate of most motors may provide useless information. Thus, there are two opposing constraints on the size of the band. The first is that the larger the band, the greater the confidence that we have included the real value. The second constraint is that the narrower the band, the more useful is the information for those using it. Statistical procedures provide guidance for specifying the size of the band to be placed around a given measurement.

If a motor were tested under identical conditions an infinite number of times and the burning rate found precisely, a distribution of rates would be recorded as shown in Figure D-1 because of slight variations in valve positions, internal temperatures, and other nonrepeatable effects. If the same motor were run on a static test stand an infinite number of times, the values measured would also form a distribution. The center of this distribution could be displaced from the center of the true motor distribution by some amount (Figure D-2) called the test stand bias. In addition, the shape of the distribution (indicated by the standard deviation, σ) may be quite different since instrumentation variations and errors also add to the spread of measured numbers (note that the full-scale motor testing was assumed to be determined with perfect instruments).

For a single test (Figure D-2), a value will be measured that may fall anywhere on the test distribution, and this value will correspond to some true value on the full-scale motor distribution. However, the test value could be anywhere on the distribution of values that could have been measured depending on the particular random instrumentation errors occurring.

The distribution of values that could be measured depending on instrumentation errors can be estimated based on knowledge of the instruments. If a point is then selected corresponding to twice the estimate of the real instrumentation-caused standard deviation (precision, S), the probability is only 5% that the measured value is farther away from the true value than $B_{TEST}^{\pm} \pm t_{95} S_{TEST} = U_{TEST}^{\pm}$. Where t_{95} is the tabularized Student's distribution and approaches 2 for a large (>30) number of observations (degrees of freedom). Stated in another way, the probability (or confidence) is 95% that the true value and measured value are closer than $B_{TEST}^{\pm} + t_{95} S_{TEST}$ if the bias estimate is accurate.

For a production run of motors, manufacturing tolerances introduce motor-to-motor variations as well as run-to-run variations (Figure D-4). In this discussion, the treatment will be directed primarily toward the single-test situation (Figure D-3) and the multiple-test situation (Figure D-2). Motor-to-motor effects will be treated in future updates to this manual. For a full-scale motor, the overall uncertainty based on a single test of a different motor of the same type is:

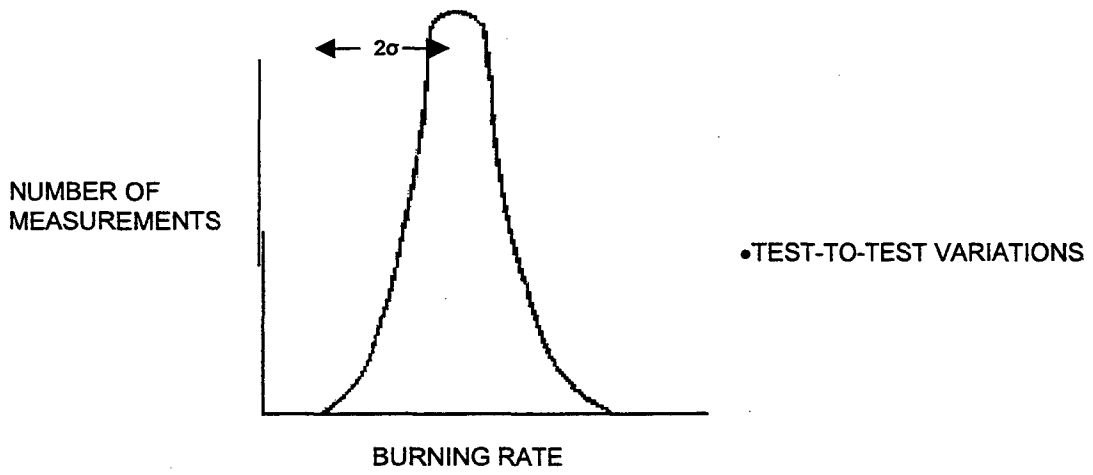$$U_{full-scale}^{\pm} = B_{test}^{\pm} \pm t_{95} \sqrt{\left[S_{test}^{2} + S_{motor-to-motor}^{2} + S_{run-to-run}^{2} \right]} \qquad \text{D-1}$$

NUMBER OF
MEASUREMENTS

•TEST-TO-TEST VARIATIONS

BURNING RATE

Figure D-1 Performance Distribution of Motor Burning Rate Tests No. 0 TO ∞

NUMBER OF
MEASUREMENTS

•RUN-TO-RUN VARIATION
•   INSTRUMENTATION
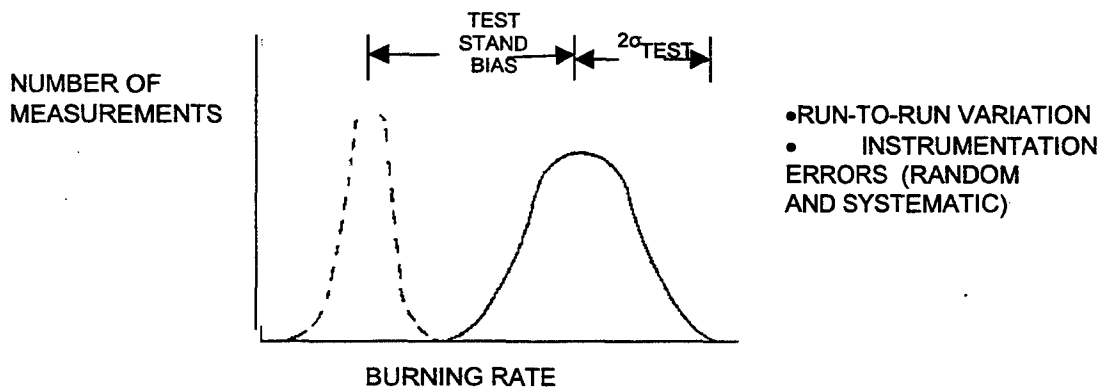ERRORS (RANDOM
AND SYSTEMATIC)

BURNING RATE

**Figure D-2 Comparison of Full-Scale Motor with Subscale Static Test
Performance Distributions**
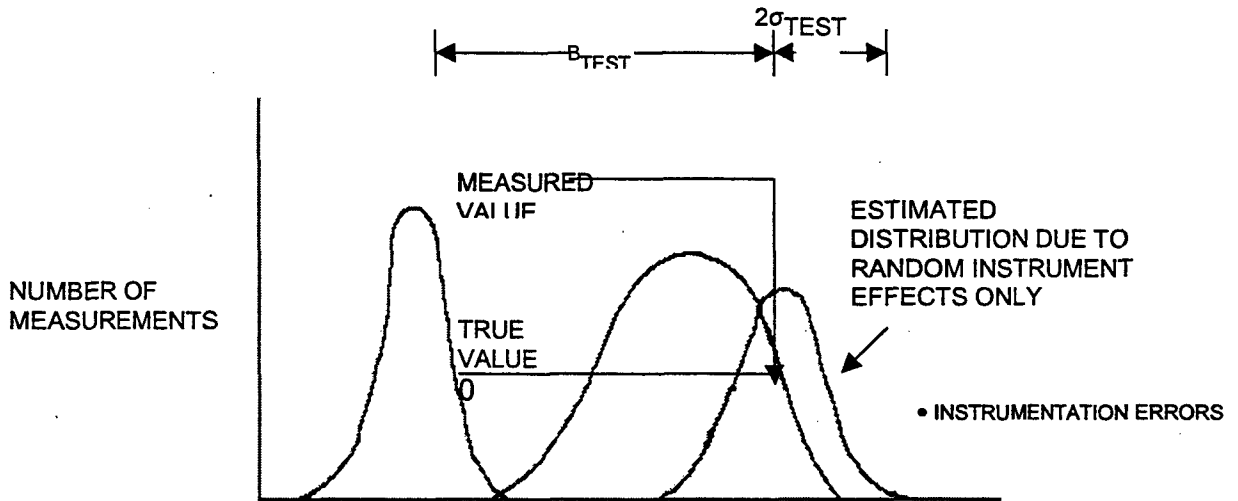
Figure D-3 Single Test Variations
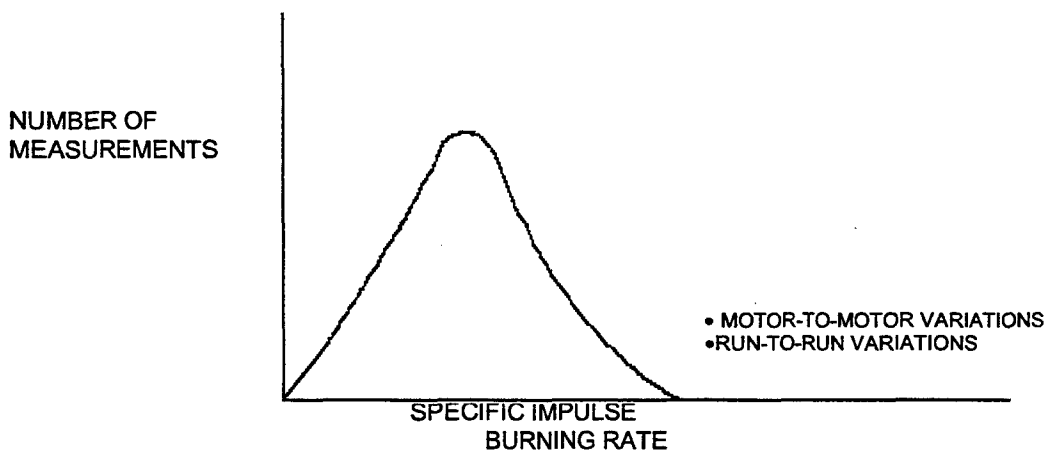

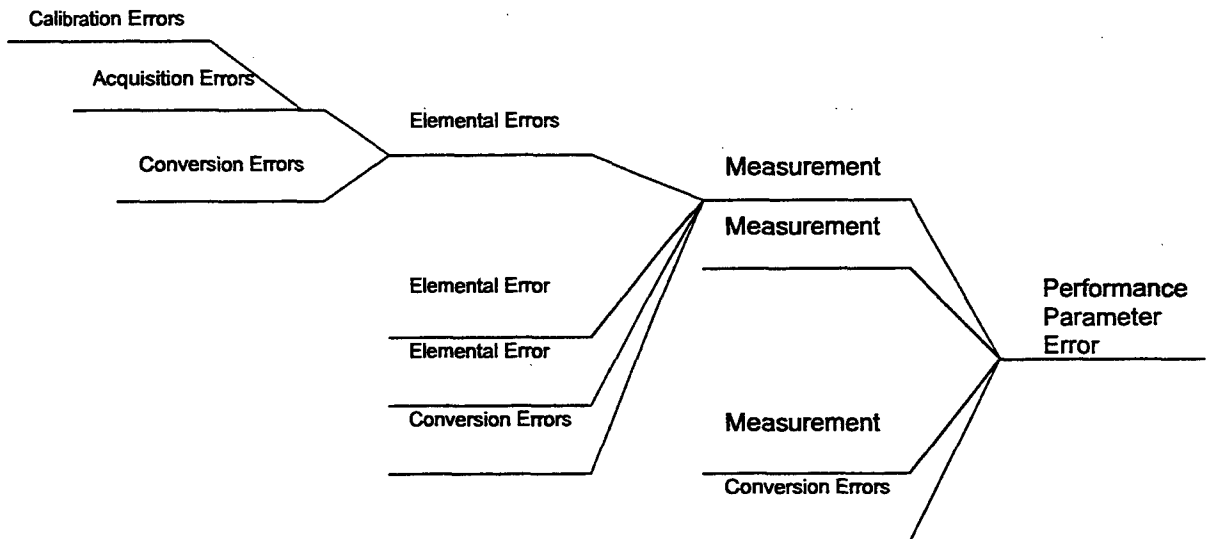**Figure D-4 Motor and Run Variations**

TRACEABILITY OF ERROR

> At every stage in the tracing of measurement back to an absolute standard (National Bureau of Standards), additional error is introduced and must be included in uncertainty

Every performance parameter (ISP, C*, etc.) can be traced to absolute standards at the National Bureau of Standards. This tracing starts initially when an interlaboratory standard (e.g., proving ring, standard turbine flowmeter) is matched (calibrated) to the NBS standard. In the calibration process, the Interlab Standard (ILS) is matched to the NBS standard in a series of checks. This series of checks has some random error. The following stages are transfer standard (TS), working standard (WS) and, finally, the calibration of the measurement instrument (MI).

When the measurement instrument is used to acquire data, a series of data acquisition errors is possible. When the direct reading (e.g., voltage, resistance) is recorded and converted to a meaningful parameter (e.g., pressure, temperature), additional errors are introduced. The errors introduced in proceeding from the NBS standard to the usable parameter derived directly from the measurement instrument are referred to as elemental errors. These elemental errors have both a bias (fixed error) and a precision (random error).

When instrument parameters are combined into measured parameters of interest (e.g., mass flowrate), the elemental errors of each of the parameters must be combined. Additional error may be introduced by the use of inexact computational procedures (e.g., incompressible flow as an approximation to real fluid flow) and by errors in tabularized constants (e.g., density, specific heat).

A. Error Propagation
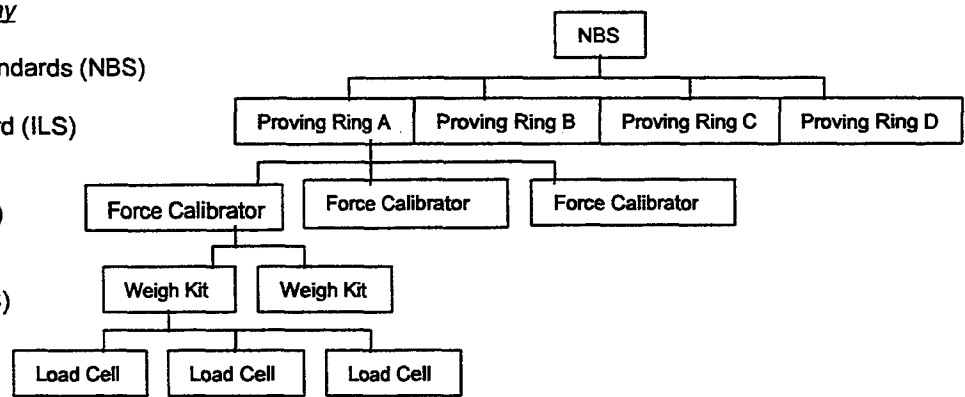

B. Calibration Hierarchy

C. Error Sources

Calibration Hierarchy Error Sources			
Calibration	Bias Limit	Precision Index	Degrees of Freedom
NBS-ILS	b_{11}	s_{11}	ν_{11}
ILS-TS	b_{21}	s_{21}	ν_{21}
TS-WS	b_{31}	s_{31}	ν_{31}
WS-MI	b_{41}	s_{41}	ν_{41}

Data Acquisition Error Sources			
Error Source	Bias Limit	Precision Index	Degrees of Freedom
Excitation Voltage	b_{12}	s_{12}	ν_{12}
Electrical Simulation	b_{22}	s_{22}	ν_{22}
Signal Conditioning	b_{32}	s_{32}	ν_{32}
Recording Device	b_{42}	s_{42}	ν_{42}
Force Transducer	b_{52}	s_{52}	ν_{52}
Thrust Bed Mechanics	b_{62}	s_{62}	ν_{62}
Environmental Effects	b_{72}	s_{72}	ν_{72}

Elemental Data Conversion Error Sources			
Error Source	Bias Limit	Precision Index	Degrees of Freedom
Calibration Curve Fit	b_{13}	s_{13}	ν_{13}
Computer Resolution	b_{23}	s_{23}	ν_{23}

Measurement and Performance Parameter Conversion Error Sources			
Error Source	Bias Limit	Precision Index	Degrees of Freedom
Defining Relationships	B_1	S_1	ν_1
Input Constants	B_2	S_2	ν_2
Computer Relationship	B_3	S_3	ν_3

CALCULATION OF PRECISION

> Precision of the measurement is a degree of mutual agreement of
> repeated independent values for controlled conditions. Precision is a
> measure of the repeatability and is a function of the dispersion about

If a measurement were made an infinite number of times, the values of this measurement would form a distribution about some mean with measurements far from the mean becoming less and less numerous with distance from the mean (assuming the errors in measurement to be random). The distribution would be an essentially normal distribution with the number density (frequency distribution, probability distribution) given by:

$$\frac{n(x)}{n(o)} = f(x) = \frac{1}{\sqrt{2\pi\sigma^2}} e^{-(x-\mu)^2/2\sigma^2} \qquad \text{D-2}$$

where n is the number of occurrences, σ is the standard deviation, and μ is the mean. The standard deviation of any distribution is given by:

$$\sigma = \sqrt{\int_{-\infty}^{\infty}\left[x - \left(\int_{-\infty}^{\infty} xf(x)dx\right)\right]^2 f(x)dx} \qquad \text{D-3}$$

where f(x) is the probability distribution of the variable x.

In practice, an infinite number of measurements and continuous probability distributions are impractical to obtain. Therefore, the standard deviation must be estimated from the available measurements. This estimate is the precision. The precision is given by the expression:

$$S = \sqrt{\frac{\sum\limits_{i=1}^{N}(x_i-\bar{x})^2}{N-1}} \quad \text{with } \nu = N - 1 \text{ degrees of freedom} \qquad \text{D-4}$$

Where $\bar{x}$ is the average (or mean) of the measured values.

The precision of a performance parameter stems from the entire chain of random errors starting with the initial calibration against the NBS standard.

CALCULATION OF BIAS

> The bias that remains after calibration is made up of three components: small, known bias too small to easily remove by calibration; small bias having known direction but unknown magnitude; and small, completely unknown biases.

The treatment of bias differs from the treatment of precision in that bias remaining after calibration is preliminarily unknown and unknowable. Therefore, judgment must be used in estimating the largest potential bias or bias limit. This bias limit corresponds to the 95-percent confidence band on all possible values of potential bias that could be estimated. In some cases (e.g., calibration curve extrapolation), a bias band can be placed around a value using limiting procedures (straight line, exponential). In other cases, additional experimentation may aid in determining bias (e.g., dipping temperature bulb in ice-water mixture). In some cases, a value must be based purely on engineering judgment.

The elemental instrument bias is made up of three components after calibration:

- $b^{\pm}_{ij_{KNOWN}}$ - Bias having known direction and magnitude. The b^{+} are those values that would give higher readings than the mean while b^{-} would give lower values. b^{+} and b^{-} may have different magnitudes.

- $b^{\pm}_{ij_{UNKNOWN}}$ - Bias having known direction but unknown magnitude.

- $b^{u}_{ij_{UNKNOWN}}$ - Bias having unknown direction and unknown magnitude.

Measurement and parameter bias are based on combinations of these elemental biases.


CALCULATION OF UNCERTAINTY

> The uncertainty interval around a parameter is intended to be the region within which 95 percent of all measurements (including the true value) of that parameter will fall. The uncertainty is a statistical combination of bias and precision.

For presentation, a single measure of error called the uncertainty has been chosen by the JANNAF Working Group. The uncertainty is made up of the bias and the precision and represents the interval for a parameter within which 95 percent of all measurements and the true value will lie. In other words, the region is to have a 95-percent probability of enclosing the true value and all other measurements of the value as shown in Figure D-5.

The uncertainty is not a rigorous statistic since an estimated bias term is included. Therefore, the bias, precision, and degrees of freedom should always be available for any uncertainty quotation.

The upper limit of the uncertainty interval is defined by the upper limit of the bias interval (B^+). The lower limit is defined by the lower limit of the bias interval (B^-).
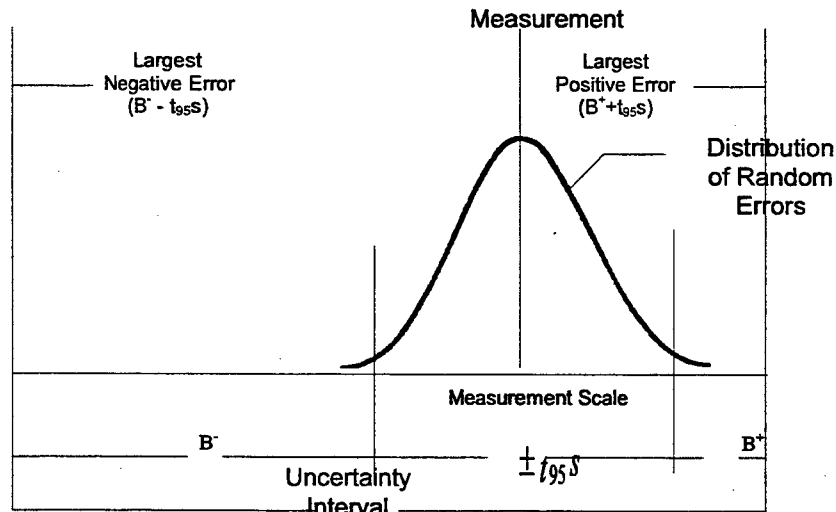
(The True Value is expected to fall within this interval at 95 confidence.)

Figure D-5 Measurement Uncertainty Behavior

The uncertainty interval U is $U^- = B^- - t_{95}S$ to $U^+ = B^+ + t_{95}S$.

Any instrument reading, measurement value, or derived parameter should be quoted as: "value + U^+ - U^-".

In many cases, only an uncertainty is available from a previous step without the associated bias, precision, and degrees of freedom. In this case, the entire uncertainty can be assumed to be precision with greater than 30 degrees of freedom unless a better judgmental resolution between bias and precision components is available. That is, the simplified method for all calibrations $\sum S^2 \approx U^2$ up to the current must be employed. The further combining of bias and precision would then continue from this point. This procedure results in a larger uncertainty than the rigorous procedure since prior bias components are multiplied by t_{95} rather than unity.

DETERMINATION OF FULL-SCALE UNCERTAINTY FROM SUBSCALE TEST DATA

> Every motor intended for flight use must have a minimum performance level specified for use in payload and propellant planning or for rejection purposes.

There are two situations for which a flight uncertainty must be determined based upon ground testing:

- Flight uncertainty for a given motor based on ground testing of that motor

- Flight uncertainty for a given motor based on ground testing of the same model

For the first situation, the ability of the motor to reproduce identical conditions for the same command must be taken into account. This repeatability for a given motor is referred to as run-to-run variation. In the second situation, still another source of uncertainty must be included. This additional source is the manufacturing repeatability from motor to motor. The determination of run-to-run and motor-to-motor errors is made difficult because of instrumentation error. For a large production run having many tests of many motors, all effects may be determined at once and not separated.

TREND STATISTICS

> Trend statistics can be used to test the randomness of measurement system data. The trend ratio statistic can indicate non-randomness, but cannot certify randomness.

Long-term trends are characterized by a steady average increase or decrease of the observed data with respect to observation order or another controlling variable. Trends that show a periodic increase and decrease of the observed data are a characteristic of nonrandomness. The trend ratio statistic, sometimes termed the mean square successive difference statistic, is effective in determining the trend types of nonrandomness.

Consider the sample of size N to be analyzed. The data are arranged in the order of the observation so that X_i is the value of the ith observation where X_1 is the first observation, X_2 the second, etc. If the sample is a random sample, the data treated as ordered by observation should exhibit a random distribution.

Let the trend ratio (η) be defined as: $\eta = \delta^2 / S^2$
where

$$\delta^2 = \sum_{i=1}^{N-1} \left(X_{(i+1)} - X_i \right)^2 / {}^2(N-1)$$ D-5

N = number of data samples

The quantity δ^2 measures the mean squared difference between successive observations. If either steady or periodic trends exist, successive values will be closer to one another than if the observations were random. Therefore, the value of δ^2 will be less when trend exists than when the observations are random. The value of S^2 is unaltered by data order. Small values of η are indicative of trend. If the trend does not exist by this test, the test does not imply randomness. When trend is a suspect, then additional testing should be undertaken.

OUTLIER DETECTION

> Outliers or wild observations in the data may introduce bias. The rejection of outlier data must consider whether the data are true samples of the process and what problems are in the measurement process that can produce the maverick data.

Measurement systems may produce wild data points. These points may be caused by temporary or intermittent malfunctions of the measurement system, or they may represent actual variations in the measurement. Errors of this type cannot be estimated as part of the uncertainty of the measurement. The points are out-of-control points for the system and are meaningless as steady-state data as illustrated in Figure D-6, and should be discarded.
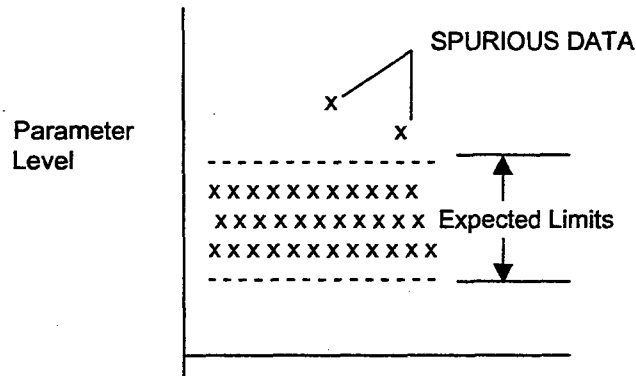

Figure D-6 Outliers Outside the Range of Acceptable Data

All data should be inspected for wild data points as a continuing quality control check on the measurement process. Identification criteria should be based on engineering analysis of instrumentation, thermodynamics, flow profiles, and past history with similar data. To ease the burden of scanning large masses of data, a computerized routine is available to scan steady-state data and indicate suspected outliers. The indicated points should then be subjected to a comprehensive engineering analysis.

This routine[1] is intended of use in scanning small samples of data from a large number of parameters at many time slices. The work of paging through volumes of data can be reduced to a manageable job with this approach. The computer will scan the data and flag suspect points. The engineer, relieved of the burden of scanning the data, can closely examine each suspected wild point.

Several general-purpose outlier techniques were reviewed and discussed elsewhere.[2] The U.S. Air Force Arnold Engineering Development Center (AEDC) developed a technique to indicate outliers in small or moderately sized samples of data. The AEDC method, as compared with the Thompson's Tau method, detects a larger proportion of the outliers in the data and, when no outliers are present, it indicates fewer good points. The AEDC method is useful for computer routines since it is fast and requires little core storage. The method discriminates between good data and outliers by examining how far each point lies from the average value.

UNCERTAINTY OF EXTRAPOLATION

> Some measurement systems are used beyond the ranges calibrated. An increase in uncertainty is needed to account for extrapolation.

Calibration of an instrument or measurement system for the range of use is always desirable. When an instrument is used out of the range of calibration, the measurement system uncertainty must reflect the larger risk. A procedure is presented for:

A. The normal calibration where the instrument being calibrated has less precision than the calibration process:

$$S' = \sqrt{S^2\left(\frac{n+1}{n}\right) - S_{i-1}^2\left(\frac{1}{n}\right) + \left(\frac{1}{n-1}\right)\left(\frac{X-\overline{X}}{S}\right)^2 \left(S^2 - S_{i-1}^2\right)}$$ D-6

Where

S' = precision adjusted for an extrapolation
S = the precision for the calibration range
S_{i-1} = precision of the next higher calibration hierarchy
n = number of observations in the calibration
X = abscissa to which the curve is extrapolated
$\overline{X}$ = mean value of the abscissa values of the calibration

B. The instrument being calibrated can be shown to be more precise than the calibration process:

$$S' = \sqrt{S^2 + \frac{n}{n-1}\left(\frac{X-\overline{X}}{S}\right)^2 \left(S^2 - S_{i-1}^2\right)}$$ D-7

where all symbols are defined as above.

In addition to an increased precision, the bias must also be adjusted. Often this adjustment can be made by examination of the calibration curve being extrapolated, as illustrated in Figure D-7.
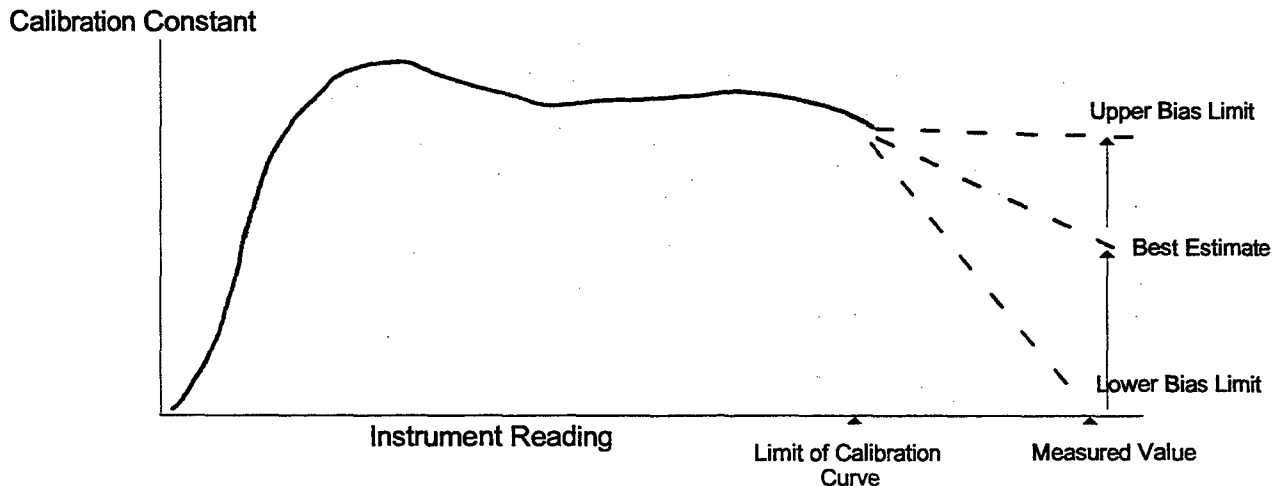

Figure D-7 Bias Derived from Uncertainty of Extrapolation

TRACEABILITY CONCEPTS

> The hierarchy levels of calibration from the measuring instrument to the National Bureau of Standards are recorded and statistically evaluated. Documented evaluation of the calibration hierarchy of each measurement system used is traceability.

Each contractor establishes extensive hierarchies of measurement process calibrations. The National Bureau of Standards is the ultimate reference for the standards laboratories used by the contractors. At each level of the hierarchy, there are formal calibration procedures. These procedures not only define the calibration methods and the frequency for calibration, but specify the information to be recorded for permanent documentation. The observations and the adjustment procedures are recorded. Also recorded are the manufacture numbers, identification (serial) numbers, date, personnel, and other data pertinent to the measurement.

When any level is recalibrated, the prior data are not destroyed but provide an historical analysis for each level and the measurement process. These data are essential in the determination of bias.

The precision of the measurement process can be determined by knowing the consistency of the data samples. Uncertainty can be measured only against the true value traceable to NBS standards. A process of calibrating is the determination of output for a known or absolute standard input. Additional uncertainty is introduced at each level of the calibration hierarchy so that the known input is known only to within the uncertainty limits at the using level. NBS provides an uncertainty limit (and the calibration data) for the calibrations (certification) performed.

NBS certifies a total set of mass standards at one time. Normal comparisons are on a double pan balance. The balance is calibrated to indicate an observed difference in weight between the two pans to a high level of accuracy. Multiple weightings and clusters of weights at each weighing are combined by a preweighing design. Each weight is involved in more than one weighing, the data are least square fit, and the weight values are known to a better precision than when calibrated singly.

A mass standard certification provides data to eight or more significant figures. The uncertainty limits are quoted for a 99-percent confidence interval. The confidence interval includes the uncertainties with NBS standards.

Proving rings which measure force values by deflection are commonly used. The deflection is read in terms of an arbitrary scale inscribed by the face of the micrometer dial. These proving rings are calibrated by the NBS using dead weights and comparison rings. An entire calibration consists of three sets of loads at 10 intervals ranging from 10 to 100 percent of full load. A quadratic equation is fit to the data and, generally, the dispersion of data at each load is consistent and large deviations indicate problems. The uncertainty is reported as precision and an absolute band but, by special request, the data are available for user evaluation.

Standards of temperature are based on the electrical and mechanical properties of materials commonly determined using thermocouples. NBS-produced tables for standard thermocouple wire are available. Certification of thermocouples by NBS is available, but statistical limits are largely judgment.

Electrical standards of resistance and voltage are critical measurement system calibrations. NBS-calibrated resistors are calibrated with the Thomas-type, 1-ohm, and oil-immersed resistors in a Wenner bridge. Resistors above 1,000,000 ohms are air calibrated with a Wheatstone bridge. Uncertainty tests are given and represent three times the standard deviation plus an estimated systematic error. Standards of voltage are estimated with a similar procedure using voltage dividers and potentiometers with standard cells.

Other standards of volume, length, time, and frequency are available through NBS. As a measurement process is established, the traceability of each contribution must be documented.

TREATMENT OF REDUNDANT MEASUREMENTS

> Redundant measurements can be used to reduce the uncertainty in a value, if the measurements are both representative of the value.

Redundant instruments can be used for measurement of thrust, and chamber pressure. Use of the average value from such measurements should effectively reduce the uncertainty if all measurements are within acceptable limits.

First, a test is applied to determine whether the measured values truly represent the same value. In this case, each measurement is compared to the average to determine whether it is outside the estimated population range.

Using the Student's t tables for nondirectional tests, a measurement beyond the 95-percent range is rejected as no longer belonging to the same population.

After eliminating outliers, the precision of the resulting average measurement value is given by:

$$S = \sqrt{\sum_{i=1}^{N} \frac{S_i^2}{\upsilon_i}}$$

D-8

Where N is the number of redundant instruments used in calculating the mean value.

Sometimes, redundancy is not direct as when a flow is measured, split, and the split portions measured. In this case, the sum of the split portions would be found and the combined uncertainty (RMS) calculated. This combined measurement would then be used as a single instrument.

APPENDIX D-2: SOURCES OF ERROR

UNCERTAINTY OF CALIBRATION

> Data of the mean value and uncertainty interval for a measurement are no better than the calibration. Traceability with complete documentation is required to establish the contributions of calibration to the final value of uncertainty.

The calibration of the measurement process is a comparison to a standard or an instrument traceable to a standard to establish a relationship between the value measured by the process and the true value and uncertainty in the relationship.

All calibration measuring and test equipment, whether within the immediate control of a contractor or not, shall be subject to a control, as necessary, to ensure conformance. This control will provide for methods of checking to ensure a ready detection of deficiencies and timely positive action for the correction of discovered calibration compromises and biases. Traceability documentation and checking procedures of the measurement system will provide the objective evidence to stated conformance. These records will be available so that Government representatives, as required, may review them.

The calibration process requires control of the type of instruments and system (adequacy of standards), environmental factors (temperature, humidity, vibration and cleanliness), and the procedures to establish consistent practices and intervals between calibrations. Changes and adjustments require substantiation and statistical evaluation (as applicable) of the measurement system effects.

When one standard is calibrated from another (e.g., Reference Standard from Interlab Standard or Working Standard from Reference Standard), and when the actual test instrument is calibrated, random or systematic errors occur. As shown in Figure D-8, most calibration curves are the average of several calibration runs. In general, enough runs should be made to obtain a good statistical representation of the distribution of calibrations about the mean.
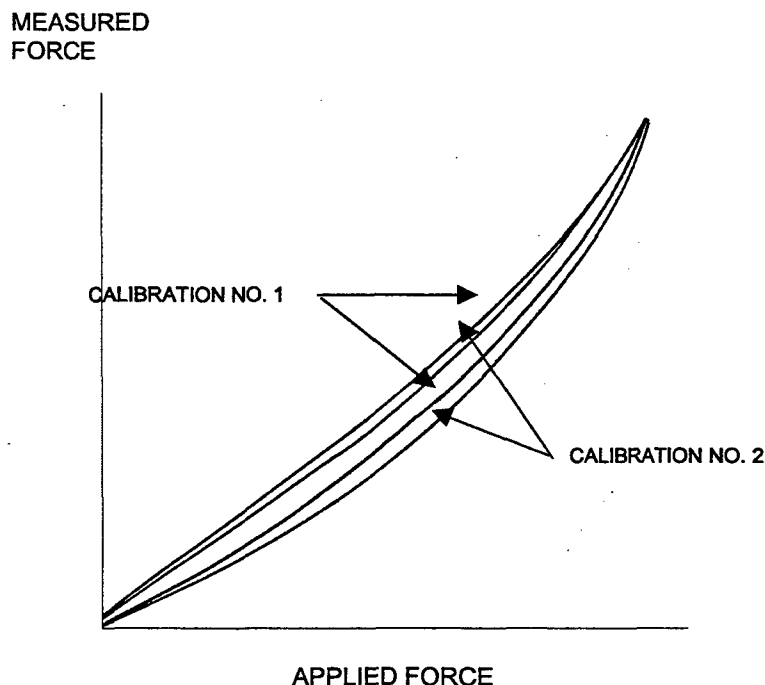

Figure D-8 Bias Derived from Uncertainty of Calibration

UNCERTAINTY OF ACQUISITION

> Installation and use effects cause uncertainty of acquisition.

A particular instrument such as a pressure transducer will have a certain bias and precision independent of use stemming from calibration and calibration hierarchy. In addition, the specific use of the instrument may contribute to the uncertainty. For example, a pressure transducer may be installed in such a way that aspiration occurs at the point pressure must be measured. This aspiration effect may be estimated, but some additional uncertainty will be introduced. The sources of acquisition error were summarized in APPENDIX D-1.

Environmental effects that may increase the uncertainty of an installed instrument beyond the basic uncertainty are:
- Temperature effects (flowmeters, pressure gages, thrust gages, areas, lengths)
- Heat transfer effects (temperature gages)
- Pressure effects (temperature gages, thrust gages)
- Flow effects (temperature gages, thrust gages, pressure gages)

Often, the additional uncertainty can be best treated as an additional bias in the instrument. However, sometimes the effect also has a random portion that must be included in the precision in the standard manner.

Since the measuring instruments must have voltage sources and resulting voltages must be measured, another potential source of error lies in the electrical subsidiary equipment, connectors, and leads. Connector resistance can reduce signal, and inductance effects in unshielded wires can produce erroneous readings. The electrical system should be checked out periodically with the instrumentation to avoid problems.

The estimation of errors stemming from installation or electrical equipment can be difficult. However, some attempt should be made to determine the magnitude of the errors and include the effect in the overall uncertainty calculation for the measurement. Even if the term is small or zero, this estimate should appear explicitly in the uncertainty calculation.

Recording is not only a convenience but also a necessity so that statistical properties can be evaluated. Detailed review of recording methods should include:

Physical Characteristic:
- What is the output resolution and readability?
- What are the effects of nonlinearity and hysteresis on the uncertainty?
- What are the long- and short-term precisions? Are there drifts, noise etc., that cause increased uncertainty?
- What degree of dynamic frequency response properties is determinable?

Data Availability:
- What observer information shall be recorded?
- What portions of the recording procedure can be comprised or eliminated?
- What frequency response will be evaluated?
- What data storage limitations will reduce the statistical evaluation?
- What is the data delay time? (The delay time is from the recording until data reduction and presentation.)

A discussion of the characteristics of the many recording systems available for calibration and use of the test facilities is not practical. Many digital systems (analog-to-digital) are currently being used to test recording. In general, these systems have a high reliability, good resolution, and good short-and long-term stability, handle several hundred measurements, and exclude the many human operator influences. These systems, in general, are not significant contributors to the measurement system uncertainty. Other recording methods may include one or more areas, which can comprise the final

uncertainty. There is a need for technique and careful selection to satisfactorily attain the required uncertainty.

The major error potentials in digital systems are the signal treatment and averaging over the noncontinuous signals. Both of these effects are small. In other systems, particularly those requiring visual judgment, errors can be noticeable. For example, determination of flowmeter speed by visually counting the signal on an oscillograph can lead to a bias in the flowrate. Direct-inking graphic recorder charts have potential errors of mechanical pen lag and of visual interpretation.

For all recording methods, estimates of the errors should be made and included in the measurement uncertainty.

UNCERTAINTY OF CALCULATIONS

> The calculation of a desired parameter from raw measurement often requires intermediate assumptions or computational steps introducing uncertainty.

The calculation of a factor such as heat flux from an actual measurement such as temperature history requires application of an analytical relationship. Certain assumptions may have been made in deriving this relationship (such as infinite flat plate with no external heat flow) that are not strictly exact and which introduce an uncertainty into the resulting value over and above the uncertainty of the constituent measurements.

Examples of such uncertain calculations are:
- Heat flux from temperature history
- Chamber pressure
- Ambient pressure thrust
- Throat area change due to thermal and pressure effects
- Physical shape and size changes with heat and pressure
- Physical properties of mixtures

In each case, the assumptions going into the calculation must be examined, and an estimate made of the magnitude of the potential error. For example, with chamber pressure, an estimate should be made of the potential error of using the simplified procedure rather than the rigorous procedure, and a further estimate made using perfect gas constant flow rather than real gas flow. The uncertainty introduced is generally directional (for example, ignoring heat loss from a heat flux probe can result in an error of underestimation only) and, therefore, can be treated as a bias rather than a precision.

As with all biases, some degree of judgment must be used in determining the bias. In the case of chamber pressure, for example, a rigorous computational procedure may not be available for comparison (otherwise, why use the simplified procedure). Therefore, an estimate must be made on the basis of past cases or on limit procedures. In using a limit procedure, the most opposite set of assumptions or calculations is used and the difference between this value and the value obtained from the calculation used is the maximum error that could result. An example is shown in Figure D-9.
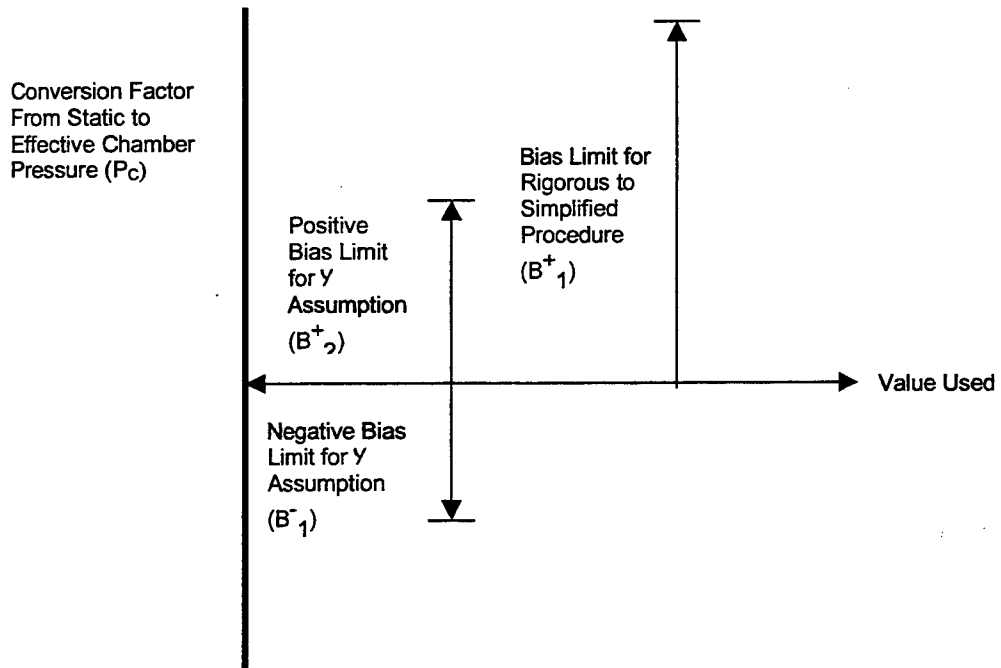
Figure D-9 Bias Derived from Uncertainty of Calculations

APPENDIX D-3: COMPARISON OF TEST DATA WITH PREDICTIONS

UNCERTAINTY TREATMENT OF SIMULTANEOUS DATA AND PREDICTION

> The correlation of test data with predicted values must be
> based on statistical concepts since both the measurements
> and predictions contain uncertainties.

The question of when a predicted value and a measured value match (within the best of our ability to determine that both are equally valued representations of the true value) is essentially the same as the question of when two independent sets of tests have given the same result. The prediction procedures can be thought of as an independent set of tests using different data and different computational procedures to arrive at the same conclusion.

If a large number of (uncertain) sets of measurements were made, each using different procedures, the differences in the means of these measurements would form a normal distribution when all errors are essentially random. Using this real distribution of differences between means as a basis, the probability of the means of two sets of measurements being within a certain range of each other from purely random effects is given by the area under the probability distribution between two values. As shown in Figure D-10, the shaded area gives the probability of two means being within a range of 0 to $\pm Z$ standard deviations, where Z is the actual difference between the means divided by the standard deviation[3].

To make the probability that the closeness of agreement is real and not chance equal to or greater than 95 percent (the correlation, Ω, is larger than 0.95), the normalized difference observed, Z, must be less than 0.06, as illustrated below using data taken from Figure 4.40.

$$\text{Probability (z is not by chance)} = 2\,[1 - F(z)] = \Omega$$

$$= 2\,[1 - (\,F(z) \text{ for } Z=0.06)]$$

$$= 2\,[1 - (.5239222)]$$

$$= 2\,[.4760778]$$

$$= 0.9521556$$

Since a large number of sets of independent tests is impossible, the standard deviation of the distribution of differences in means must be estimated based on the uncertainties of the two distributions (note that the predicted values is really an estimate of the mean of the distribution of possible predicted values, as discussed in the following sections).
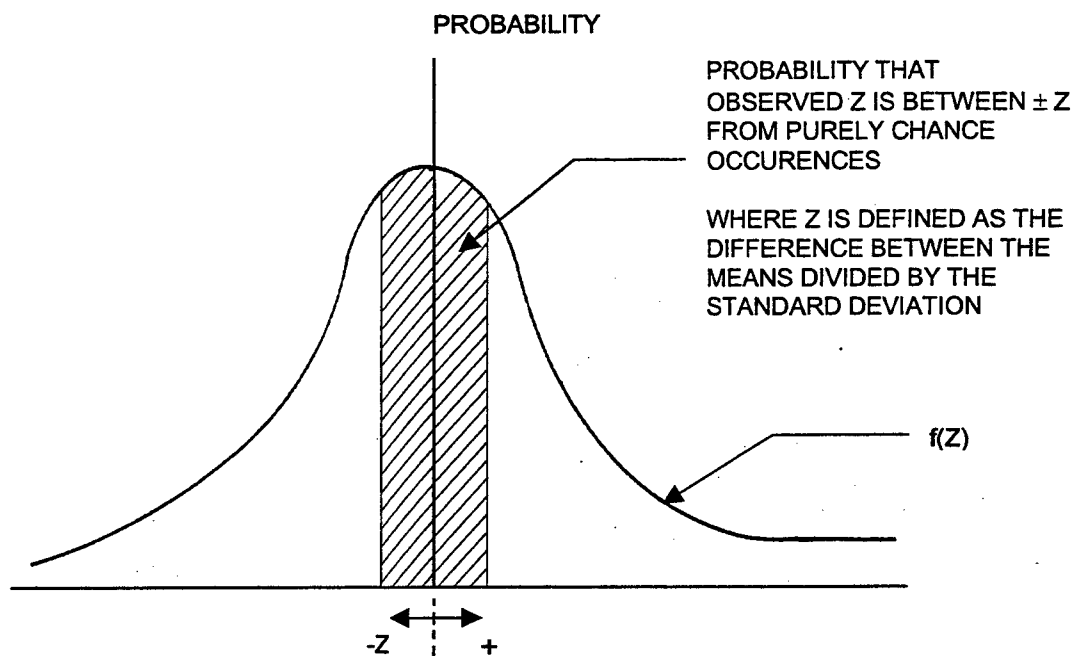
PROBABILITY

PROBABILITY THAT
OBSERVED Z IS BETWEEN ± Z
FROM PURELY CHANCE
OCCURENCES

WHERE Z IS DEFINED AS THE
DIFFERENCE BETWEEN THE
MEANS DIVIDED BY THE
STANDARD DEVIATION

f(Z)

-Z   +

Figure D-10 Probability Two Means are Within the Range 0 to ± Z

UNCERTAINTY OF PREDICTION PROCEDURE

> The Evaluation Procedures can be thought of as an independent measuring
> procedure using a different set of measured data (reaction rates, enthalpies, etc.).
> The predicted value is then the mean of a distribution of possible predicted values.

For each input, built-in datum, and built-in correlation in the Evaluation Procedures, there is a range or distribution of possible values about the value actually used. As an example, the exit area can be measured numerous times and the resulting measurements will form a normal distribution, with increasingly large errors from the mean correspondingly less likely. For other logically chosen data, the same effect also would hold. A change in a specific input or built-in value will cause a corresponding change in specific impulse.

If all the inputs were exercised over their entire probability ranges and the results weighted by the probability of that difference in input, a probability range for a specific test parameter (e.g. burning rate) could be developed. This distribution will approach a normal distribution almost exactly because of the large number of inputs and built-in information, as shown below.
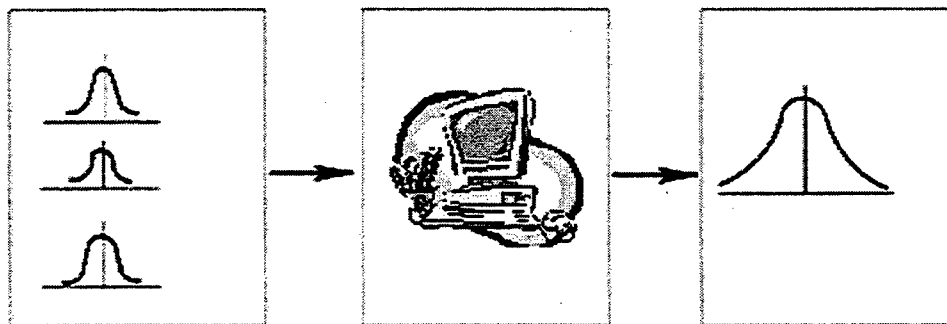

Figure D-11 The Distribution of the Desired Test Parameter will Approach a Normal Distribution If All Inputs are Handled Properly

The cost of actually developing the distribution for a specific case is almost prohibitive. Therefore, an estimate of the distribution can be made based on the major components of the calculation. The relationship is:

$$U^{\pm}_{PRED} = t_{95}\sqrt{\sum_{i=1}^{N} S_i^{\,2}} \pm \sqrt{\sum_{i=1}^{N}\left(B_i^{\pm}\right)^2} \qquad \text{D-9}$$

Where N in the total number of major or equally important components of the calculation

For the rigorous procedure, the major components are the inviscid thrust, the boundary layer thrust decrement, the propulsive damp thrust, and the net flowrate. For the simplified procedure, the efficiencies (vaporization, mixing, heat loss, reaction kinetics, two-dimensional, and boundary layer) become the major components. The problem is then reduced to estimating the uncertainty in these combined effects rather than in each item of input data.

Alternatively, an uncertainty goal can be established and the allowable uncertainty in each of the constituent components can be found. For example, if the goal of the rigorous procedure is 1 percent, and there are no biases:

$$S_i \leq \frac{(0.01)(\Pr edictedValue)}{\sqrt{ZN}} \leq \frac{(0.01)(\Pr edictedValue)}{\sqrt{8}} \qquad \text{D-10}$$

If one of the constituent uncertainties is known to be higher or lower than allowable, the others must be made more stringent or can be relaxed, accordingly.

Estimates of the uncertainty caused by input data can be made by developing sensitivity coefficients of the form:

$$\frac{\Delta ISP_i}{\Delta Input_i} \qquad \text{D-11}$$

And estimating the 2S level for the input. The procedure is time consuming and may not be worth the extra effort required.

UNCERTAINTIES IN INDIVIDUAL PERFORMANCE LOSSES

> The uncertainty incurred in trying to isolate a specific performance loss is a combination of the test uncertainty and the uncertainty of the other loss predictions.

In many cases, the performance analyst wants to isolate a specific performance effect such as mixing or vaporization. To accomplish this isolation, the other effects must be assumed to be accurately predicted. These other factors are then used to calculate the desired factor from test data. However, both the test data and the predicted factors have some uncertainty associated with them, resulting in an uncertainty in the isolated loss.

The effects of joint test and prediction uncertainty can be handled straightforwardly using the same procedures already developed (note that the uncertainty in derived test parameters such as ISP may already include joint measurements and prediction uncertainties). The method of combining uncertainties is:

$$U^{\pm}_x = \pm t_{95}\sqrt{S_{test}^{\,2} + \sum_{i=1}^{N} S_{pred}^{\,2}} \pm \sqrt{\left(B^{\pm}_{test}\right)^2 + \left(B^{\pm}_{pred}\right)^2} \qquad \text{D-12}$$

Where the factors must be in the proper form.

As an example, the C* energy release efficiency is given by (simplified definition):

$$\eta_{C^*_{ER}} = \frac{C^*_{TEST}}{\eta_{C^*_{KIN}}\,\eta_{C^*_{TD}}\,\eta_{C^*_{BL}}\,\eta_{C^*_{HL}}\,\eta_{ODE_{AVGMP}}} \qquad \text{D-13}$$

The corresponding uncertainty is

$$U^{\pm}_{\eta_{C^*_{ER}}} = \pm t_{95}\sqrt{S_{C^*_{ER}}{}^2_{TEST} + S_{C^*_{ER}}{}^2_{KIN} + S_{C^*_{ER}}{}^2_{TD} + S_{C^*_{ER}}{}^2_{BL} + S_{C^*_{ER}}{}^2_{HL} + S_{C^*_{ER}}{}^2_{ODE}} \qquad \text{D-14}$$

Each of the S factors is the change in $\eta_{C^*_{ER}}$ caused by a change of S in the specific factor. That is, the S for C^*_{TEST} is expressed in m/s. This S factor is added to the C^*_{TEST} and a new $\eta_{C^*_{ER}}$ calculated. The difference is the $\eta_{C^*_{ER}}$ values in the S factor for test uncertainty. Symbolically:

$$S_{C^*_{ER\,TEST}} = \frac{C^*_{TEST} + S_{C^*_{TEST}} - C^*_{TEST}}{\eta_{C^*_{KIN}}\,\eta_{C^*_{TD}}\,\eta_{C^*_{BL}}\,\eta_{C^*_{HL}}\,C^*_{ODE_{AVGMR}}} \qquad \text{D-15}$$

References

[1] "Handbook – Uncertainty in Gas Turbine Measurements," ADEC-TR-73-5, February 1973.

[2] "ICRPG Handbook for Estimating the Uncertainty in Measurements Made with Liquid Propellant Rocket Engine Systems," CPIA Pub 180, April 1969.

[3] W. L. Hays, Statistics, Hold, Rinehart, Winston, New York, N.Y., 1963.

APPENDIX E

CHEMICAL PROPULSION TECHNOLOGY REVIEWS ISSUED BY JHU/CPIA

CHEMICAL PROPULSION TECHNOLOGY REVIEWS (CPTR)

CPTR 74   SOLID PROPELLANT SUBSCALE BURNING RATE TEST TECHNIQUES AND
               HARDWARE FOR U.S. AND SELECTED NATO FACILITIES (U-A)

CPTR 73   SOLID PROPELLANT TEST MOTOR SCALING (U-A)

CPTR 72   SUBSCALE FAST COOKOFF TESTING AND MODELING FOR THE HAZARD
               ASSESSMENT OF LARGE ROCKET MOTORS (U-A)

CPTR 70   OVERVIEW OF PULSE DETONATION PROPULSION TECHNOLOGY (U-A)

PUB. 688   INSENSITIVE EXPLOSIVES FOR FRAGMENTATION WARHEADS (U-E)

CPTR 99-69   BURNING RATES OF STANDARD SOLID PROPELLANTS FOR GUN APPLICATIONS (U-C)

CPTR 98-68   REUSABLE LAUNCH VEHICLE PROPULSION SYSTEMS (U-C)

PUB. 664   PROVEN GEL PROPULSION SYSTEM CAPABILITIES TO MEET ADVANCED
               TACTICAL AND INTERCEPTOR END-GAME MISSILE REQUIREMENTS -
               RESPONSE TO CPIA REPORT NO. CPTR 96-63, MAY 1996 (U-B)

PUB. 661   FIRE AND EXPLOSION HAZARDS OF LIQUID PROPELLANTS AND RELATED
               MATERIALS - AN ACCIDENT REVIEW (U-B)

CPTR 97-66   EXPENDABLE LAUNCH VEHICLE PROPULSION TECHNOLOGY (U-C)

CPTR 97-65   ELECTRIC THRUSTER SYSTEMS (U-A)

CPTR 96-64   ELECTRIC PROPULSION FOR SPACECRAFT (U-A)

CPTR 96-63   REVIEW OF PROPELLANT CANDIDATES FOR NEAR-TERM THEATER DEFENSE DIVERT
               ATTITUDE CONTROL SYSTEMS (U-B)

CPTR 96-62   NATIONAL ASSETS FOR HYPERSONIC FLOW & PROPULSION SYSTEM
               TESTING (U-E)

CPTR 95-60   PULSE MOTOR TECHNOLOGY (U-D)

CPTR 95-58   ENVIRONMENTALLY BENIGN CLEANING AND DEGREASING METHODS FOR THE SOLID
               ROCKET MOTOR INDUSTRY (U-A)

CPTR 95-57   COMBUSTION STABILITY OF INTERCEPTOR ROCKET MOTORS: A PRACTICAL
               APPROACH TO MANAGING INSTABILITY PROBLEMS (U-C)
               (This publication has a Confidential Appendix-not automatically mailed out)

CPTR 94-56   ROCKET MOTOR SERVICE LIFE PREDICTION METHODOLOGY (U-B)

CPTR 94-55   VARIABLE FLOW DUCTED ROCKET TECHNOLOGY (U) (C-E)

CPTR 94-54   EARTH-STORABLE GELLED BIPROPELLANT TECHNOLOGY (U-C)

CPTR 93-53   SOLID ROCKET MOTOR COMPONENTS FOR INSENSITIVE MUNITIONS (U-D)

CPTR 93-52   NEW HIGH-ENERGY OXIDIZERS (U-C)

CPTR 92-50   LO₂/LH₂ LIQUID ROCKET ENGINE CYCLES (U-C)

CPTR 91-48   AMMONIUM NITRATE PROPELLANTS (U-C)

CPTR 91-47   NEW SOLID PROPELLANT PROCESSING TECHNIQUES (U-C)

CPTR 89-46   STANDARD EXHAUST PLUME MODELS (U-C)

CPTR 89-45   DISPOSAL OF SOLID ROCKET MOTOR PROPELLANTS (U-C)

CPTR 88-44   GAP MINIMUM-/REDUCED-SMOKE PROPELLANTS (U) (C-C)

CPTR 88-43   ELECTROSTATIC DISCHARGE TEST METHODOLOGIES FOR SOLID
              ROCKET PROPELLANTS (U-C)

CPTR 87-42   NEW SOLID ROCKET PROPELLANT POLYMER BINDER MATERIALS (U-D)

CPTR 87-41   COMBUSTION INSTABILITY: INSTRUMENTATION AND DATA ANALYSIS
              METHODS FOR MOTORS AND LABORATORY DEVICES (U-C)

CPTR 87-40   ANALYSIS OF TRANSPORTATION-INDUCED STRESSES IN SOLID
              ROCKET MOTORS (U-B)

CPTR 86-39   DISPOSAL AND RECLAMATION OF PEP MATERIALS (U-B)

CPTR 86-38   CANTED AND SCARFED NOZZLES (U-C)

CPTR 86-37   CONSOLIDATED CHARGES FOR LARGE-CALIBER GUNS (U-D)

CPTR 86-36   LABORATORY METHODS FOR MEASURING COMBUSTION RESPONSE
              FUNCTIONS (U-A)

CPTR 85-35   STRIP LAMINATE ROCKET MOTOR CASES (U-D)

CPTR 85-34   MOISTURE AND DAMAGE EFFECTS ON COMPOSITE MOTOR CASES (U-C)

CPTR 85-33   THERMAL REACTIVITY OF TACTICAL ORDNANCE (U-D)

CPTR 85-32   HYDRAZINE COMPATIBILITY (U-C)

CPTR 85-31   COMPUTER PROGRAMS FOR PROPULSION SYSTEM COST ESTIMATION (U-D)

CPTR 85-30   BURNING RATE ENHANCEMENT BY PHYSICAL METHODS (U) (C-B)

CPTR 84-29   MOISTURE EFFECTS ON MECHANICAL PROPERTIES OF SOLID PROPELLANTS (U-C)

CPTR 84-28   INFORMATION SOURCES FOR COMPOSITE ROCKET MOTOR CASES (U-C)

CPTR 84-27   VULNERABILITY OF LOVA PROPELLANTS (U)(C-B)

CPTR 84-26   GLYCIDYL AZIDE POLYMER (GAP) (U-B)

CPTR 84-25   PLUME ELECTROMAGNETIC EFFECTS (U) (C--B)

CPTR 83-24   NOZZLELESS MOTOR TECHNOLOGY (U) (C-D)

CPTR 83-23   SOLID PROPELLANT ROCKET MOTOR THRUST TERMINATION (U-B)

UNDERWATER ROCKET PROPULSION (U)
SOME RECENT DEVELOPMENTS IN LIQUID PROPULSION GUN TECHNOLOGY (U)
HIGH DENSITY SOLID ROCKET PROPELLANTS (U)
MISSILES AND SPACE PROPULSION TECHNOLOGY
ELECTROMAGNETIC PROPULSION
MUZZLE FLASH SUPPRESSION
EXTENDIBLE EXIT CONES
PARTICLE SIZE ANALYSIS
ARMY MISSILE PROPULSION TECHNOLOGY

CPTR-2   CPIA PUB. 305 (C-B)
BURN RATE CONTROL OF HMX/RDX MINIMUM SMOKE PROPELLANTS (U)
LOW SMOKE MOTOR DEVELOPMENT (U)
GUN BARREL EROSION REDUCTION
LIQUID ENGINE PERFORMANCE PREDICTION TECHNOLOGY
HYDRAZINE COMPATIBILITY
THE SPACE SHUTTLE ORBITER PROPULSION UNITS

CPTR-1   CPIA PUB. 301 (C-B)
HIGH ENERGY TOUGH PROPELLANTS (U)
SYNTHESIS OF ENERGETIC PLASTICIZERS (U)
CONTROL OF BURN RATE PRESSURE EXPONENT IN AP/HTPB COMPOSITE
PROPELLANTS (U)
REVIEW OF THRUST VECTOR CONTROL FOR HIGHLY MANEUVERABLE TACTICAL
MISSILES (U)
INTEGRAL ROCKET RAMJET COMBUSTOR DEVELOPMENT PROGRAMS (U)
EXHAUST PLUME SMOKE PREDICTION AND MEASUREMENT
CPIA INFORMATION STORAGE AND RETRIEVAL

APPENDIX F

INITIAL DISTRIBUTION

INITIAL DISTRIBUTION

- ARMY -

ARMY AVIATION AND MISSILE
COMD/REDSTONE ARSENAL
    1 BEN F. WILSON
    1 DOCUMENTS, AMSMI-RD-CS-R
    1 DR. JAMES G. CARVER
    1 DR. WILLIAM MELVIN
    1 MR. J. MICHAEL LYON
    1 TERRY L. VANDIVER

ARMY RESEARCH LAB/ABERDEEN
    1 LOUISE LETENDRE

ARMY TANK AUTOMOTIVE & ARMAMENT
COMD/PICATINNY
    1 PATRICIA AYS

US ARMY RESEARCH OFFICE/RSCH
TRIANGLE PK
    1 D. M. MANN

- NAVY -

NAVAL AIR WARFARE CTR/CHINA LAKE
    1 CHRIS TOFTNER
    1 DR. FRED S. BLOMSHIELD
    1 DR. GEOFFREY A. LINDSAY
    1 DR. JAMES HOOVER
    1 DR. MAY L. CHAN
    1 HOWARD BOWMAN
    1 JACK M. PAKULAK
    1 JAMES A. GROSS
    1 JAMES A. LOUNDAGIN
    1 JAMES C. BALDWIN
    1 MARY S. PAKULAK
    1 STUART R. BLASHILL
    1 TECH LIB/P. BACKES
    1 THERESE ATIENZAMOORE
    1 THOMAS L. BOGGS

NAVAL SURFACE WARFARE CTR/INDIAN
HEAD
    1 MICHAEL P. SIKORA

- AIR FORCE -

AFRL/EDWARDS AFB
    1 DR. LAWRENCE P. QUINN
    1 JEANNIE PATON
    1 JOHN H. CLARK
    1 ROBERT C. CORLEY

AFRL/WPAFB
    1 W. LEE BAIN

NATL AIR INTEL CTR/WPAFB
    1 BEVERLY BRINK

- NASA -

NASA AEROSPACE INFO CTR/HANOVER
    1 ACQUISITIONS DEPT

NASA GLENN RSCH CTR/CLEVELAND
    1 SCOTT MEYER
    1 WOODROW WHITLOW

NASA JOHNSON SPACE CTR/HOUSTON
    1 BARRY WITTSCHEN
    1 GERALD SANDERS

NASA JSC WSTF/LAS CRUCES
    1 LURLENE FORD/ET.AL.

NASA LANGLEY/HAMPTON
    1 MR. MELVIN LUCY
    1 S. MILLER/MS-185 TECH LIB

NASA/MARSHALL SPACE FLIGHT CTR
    1 CN22/LIBRARY
    1 DR. TERRY F. GREENWOOD

NASA/WASHINGTON, DC
    1 DAVID STONE
    1 W. R. FRAZIER, CODE QS

- OTHER GOV'T. -

DEF TECH INFO CTR/FT BELVOIR
    2 DTIC-OCC

DTRA/ARLINGTON
    1 FRANK TRACESKI

- NON-GOV'T. -

AEROJET/SACRAMENTO
    1 AEROJET-TIC

AEROSPACE/LOS ANGELES
    1 BENITA CAMPBELL, M1-199

ALLIANT AEROSPACE COMPANY/MAGNA
    1 LIBRARY, M/S H

ATK TACTICAL SYSTEMS COMPANY
LLC//ROCKET CENTER
    1 DOTTIE LYON

ATLANTIC RESEARCH CORP/GAINESVILLE
    1 TECHNICAL INF CTR

BOEING COMPANY/CANOGA PARK
    1 H. E. SNELL, TIC BA29

BOEING/SEATTLE
    1 LIB ACQ

GENERAL DYNAMICS OTS (AEROSPACE)
INC/REDMOND
    1 JAMES GURLEY

LLNL/LIVERMORE
    1 BETTE MOORE

PACIFIC SCIENTIFIC ENERGETIC
MATERIALS CO/CHANDLER
    1 SMALLWOOD/KORCSMAROS

PENNSYLVANIA STATE UNIV/STATE
COLLEGE
    1 DR. DANIEL KIELY

RAYTHEON COMPANY/TUCSON
    1 SHANNON MACK

SANDIA NATIONAL LABS/ALBUQUERQUE
    1 DIV 2554/M. GRUBELICH
    1 O-4916/S. LANDENBERGER

TALLEY/MESA
    1 SECURITY OFFICE

THIOKOL PROPULSION/ELKTON
    1   THOMAS HOLMAN

THIOKOL/BRIGHAM CITY
    1 ELLEN WAGSTAFF

UNITED TECHNOLOGIES/SAN JOSE
    1 TECHNICAL LIBRARY

UNIVERSAL PROPULSION COMPANY INC/PHOENIX
    1 JAMES J. BAKER

Total No. 100

September 20, 2001